



National Library
of Canada

Acquisitions and
Bibliographic Services Branch

395 Wellington Street
Ottawa, Ontario
K1A 0N4

Bibliothèque nationale
du Canada

Direction des acquisitions et
des services bibliographiques

395, rue Wellington
Ottawa (Ontario)
K1A 0N4

Your file - Votre référence

Our file - Notre référence

NOTICE

The quality of this microform is heavily dependent upon the quality of the original thesis submitted for microfilming. Every effort has been made to ensure the highest quality of reproduction possible.

If pages are missing, contact the university which granted the degree.

Some pages may have indistinct print especially if the original pages were typed with a poor typewriter ribbon or if the university sent us an inferior photocopy.

Reproduction in full or in part of this microform is governed by the Canadian Copyright Act, R.S.C. 1970, c. C-30, and subsequent amendments.

AVIS

La qualité de cette microforme dépend grandement de la qualité de la thèse soumise au microfilmage. Nous avons tout fait pour assurer une qualité supérieure de reproduction.

S'il manque des pages, veuillez communiquer avec l'université qui a conféré le grade.

La qualité d'impression de certaines pages peut laisser à désirer, surtout si les pages originales ont été dactylographiées à l'aide d'un ruban usé ou si l'université nous a fait parvenir une photocopie de qualité inférieure.

La reproduction, même partielle, de cette microforme est soumise à la Loi canadienne sur le droit d'auteur, SRC 1970, c. C-30, et ses amendements subséquents.

Canada

UNIVERSITY OF ALBERTA

**Acoustic Variable Order Infinite Elements for Wave
Envelope and Multi-domain Boundary Element
Modelling.**

by

Luc Cremers



A thesis submitted to the Faculty of Graduate Studies and Research in partial fulfilment
of the requirements for the degree of **Doctor of Philosophy**.

Department of Mechanical Engineering

Edmonton, Alberta

Fall 1994



National Library
of Canada

Acquisitions and
Bibliographic Services Branch

395 Wellington Street
Ottawa, Ontario
K1A 0N4

Bibliothèque nationale
du Canada

Direction des acquisitions et
des services bibliographiques

395, rue Wellington
Ottawa (Ontario)
K1A 0N4

Your file - Votre référence

Car file - Notre référence

The author has granted an irrevocable non-exclusive licence allowing the National Library of Canada to reproduce, loan, distribute or sell copies of his/her thesis by any means and in any form or format, making this thesis available to interested persons.

L'auteur a accordé une licence irrévocable et non exclusive permettant à la Bibliothèque nationale du Canada de reproduire, prêter, distribuer ou vendre des copies de sa thèse de quelque manière et sous quelque forme que ce soit pour mettre des exemplaires de cette thèse à la disposition des personnes intéressées.

The author retains ownership of the copyright in his/her thesis. Neither the thesis nor substantial extracts from it may be printed or otherwise reproduced without his/her permission.

L'auteur conserve la propriété du droit d'auteur qui protège sa thèse. Ni la thèse ni des extraits substantiels de celle-ci ne doivent être imprimés ou autrement reproduits sans son autorisation.

ISBN 0-315-95168-0

Canada

Name LUC CREMERS

Dissertation Abstracts International is arranged by broad, general subject categories. Please select the one subject which most nearly describes the content of your dissertation. Enter the corresponding four-digit code in the spaces provided.

MECHANICAL ENGINEERING

SUBJECT TERM

0548

SUBJECT CODE

U·M·I

Subject Categories

THE HUMANITIES AND SOCIAL SCIENCES

COMMUNICATIONS AND THE ARTS

Architecture 0729
Art History 0377
Cinema 0900
Dance 0378
Fine Arts 0357
Information Science 0723
Journalism 0391
Library Science 0399
Mass Communications 0708
Music 0413
Speech Communication 0459
Theater 0465

EDUCATION

General 0515
Administration 0514
Adult and Continuing 0516
Agricultural 0517
Art 0273
Bilingual and Multicultural 0282
Business 0688
Community College 0275
Curriculum and Instruction 0727
Early Childhood 0518
Elementary 0524
Finance 0277
Guidance and Counseling 0519
Health 0680
Higher 0745
History of 0520
Home Economics 0278
Industrial 0521
Language and Literature 0279
Mathematics 0280
Music 0522
Philosophy of 0998
Physical 0523

Psychology 0525
Reading 0535
Religious 0527
Sciences 0714
Secondary 0533
Social Sciences 0534
Sociology of 0340
Special 0529
Teacher Training 0530
Technology 0710
Tests and Measurements 0288
Vocational 0747

LANGUAGE, LITERATURE AND LINGUISTICS

Language 0679
 Ancient 0289
 Linguistics 0290
 Modern 0291
Literature 0401
 General 0294
 Classical 0295
 Comparative 0297
 Medieval 0298
 Modern 0316
 African 0591
 American 0305
 Asian 0352
 Canadian (English) 0355
 Canadian (French) 0593
 English 0311
 Germanic 0312
 Latin American 0315
 Middle Eastern 0313
 Romance 0314
 Slavic and East European

PHILOSOPHY, RELIGION AND THEOLOGY

Philosophy 0422
Religion 0318
 General 0321
 Biblical Studies 0319
 Clergy 0320
 History of 0322
 Philosophy of 0469
Theology

SOCIAL SCIENCES

American Studies 0323
Anthropology 0324
 Archaeology 0326
 Cultural 0327
 Physical 0327
Business Administration 0310
 General 0272
 Accounting 0770
 Banking 0454
 Management 0338
 Marketing 0385
Canadian Studies 0501
Economics 0503
 General 0505
 Agricultural 0508
 Commerce-Business 0509
 Finance 0510
 History 0511
 Labor 0358
 Theory 0366
Folklore 0351
Geography 0578
Gerontology
History
 General

Ancient 0579
Medieval 0581
Modern 0582
Black 0328
African 0331
Asia, Australia and Oceania 0332
Canadian 0334
European 0335
Latin American 0336
Middle Eastern 0333
United States 0337
History of Science 0585
Law 0398
Political Science 0615
 General 0616
 International Law and Relations 0617
 Public Administration 0814
Recreation 0452
Social Work 0626
Sociology 0627
 General 0938
 Criminology and Penology 0631
 Demography 0628
 Ethnic and Racial Studies 0629
 Individual and Family Studies 0630
 Industrial and Labor Relations 0700
 Public and Social Welfare 0344
 Social Structure and Development 0709
 Theory and Methods 0999
Transportation 0453
Urban and Regional Planning
Women's Studies

THE SCIENCES AND ENGINEERING

BIOLOGICAL SCIENCES

Agriculture 0473
 General 0285
 Agronomy 0475
 Animal Culture and Nutrition 0476
 Animal Pathology 0359
 Food Science and Technology 0478
 Forestry and Wildlife 0479
 Plant Culture 0480
 Plant Pathology 0817
 Plant Physiology 0777
 Range Management 0746
 Wood Technology 0306
Biology 0287
 General 0308
 Anatomy 0309
 Biostatistics 0379
 Botany 0329
 Cell 0353
 Ecology 0369
 Entomology 0793
 Genetics 0410
 Limnology 0307
 Microbiology 0317
 Molecular 0416
 Neuroscience 0433
 Oceanography 0821
 Physiology 0778
 Radiation 0472
 Veterinary Science 0786
 Zoology 0760
Biophysics
 General
 Medical

Geodesy 0370
Geology 0372
Geophysics 0373
Hydrology 0388
Mineralogy 0411
Paleobotany 0345
Paleoecology 0426
Paleontology 0418
Paleozoology 0985
Palynology 0427
Physical Geography 0368
Physical Oceanography 0415

HEALTH AND ENVIRONMENTAL SCIENCES

Environmental Sciences 0768
Health Sciences 0566
 General 0300
 Audiology 0992
 Chemotherapy 0567
 Dentistry 0350
 Education 0769
 Hospital Management 0758
 Human Development 0982
 Immunology 0564
 Medicine and Surgery 0347
 Mental Health 0569
 Nursing 0570
 Nutrition 0380
 Obstetrics and Gynecology
 Occupational Health and Therapy 0354
 Ophthalmology 0381
 Pathology 0571
 Pharmacology 0419
 Pharmacy 0572
 Physical Therapy 0382
 Public Health 0573
 Radiology 0574
 Recreation 0575

Speech Pathology 0460
Toxicology 0383
Home Economics 0386

PHYSICAL SCIENCES

Pure Sciences
Chemistry 0485
 General 0749
 Agricultural 0486
 Analytical 0487
 Biochemistry 0488
 Inorganic 0738
 Nuclear 0490
 Organic 0491
 Pharmaceutical 0494
 Physical 0495
 Polymer 0754
 Radiation 0405
Mathematics 0605
Physics 0986
 General 0606
 Acoustics 0608
 Astronomy and Astrophysics 0608
 Atmospheric Science 0748
 Atomic 0607
 Electronics and Electricity
 Elementary Particles and High Energy 0798
 Fluid and Plasma 0759
 Molecular 0609
 Nuclear 0610
 Optics 0752
 Radiation 0756
 Solid State 0611
Statistics 0463
Applied Sciences
Applied Mechanics 0346
Computer Science 0934

Engineering 0537
 General 0538
 Aerospace 0539
 Agricultural 0540
 Automotive 0541
 Biomedical 0542
 Chemical 0543
 Civil 0544
 Electronics and Electrical 0548
 Heat and Thermodynamics 0545
 Hydraulic 0546
 Industrial 0547
 Marine 0794
 Materials Science 0548
 Mechanical 0743
 Metallurgy 0551
 Mining 0552
 Nuclear 0549
 Packaging 0765
 Petroleum 0554
 Sanitary and Municipal 0790
 System Science 0428
Geotechnology 0796
Operations Research 0795
Plastics Technology 0994
Textile Technology

PSYCHOLOGY

General 0621
Behavioral 0384
Clinical 0622
Developmental 0620
Experimental 0623
Industrial 0624
Personality 0625
Physiological 0989
Psychobiology 0349
Psychometrics 0632
Social 0451



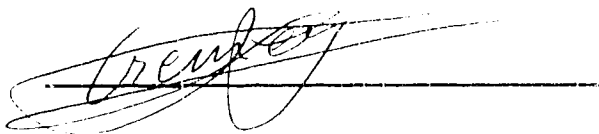
UNIVERSITY OF ALBERTA

RELEASE FORM

Name of Author: **Luc Cremers**
Title of Thesis: **Acoustic Variable Order Infinite Elements for Wave Envelope and Multi-domain Boundary Element Modelling.**
Degree: **Doctor of Philosophy**
Year this degree granted: **1994**

Permission is hereby granted to the University of Alberta Library to reproduce single copies of this thesis and to lend or sell copies for private, scholarly or scientific research purposes only.

The author reserves all other publication and other rights in association with the copyright in the thesis, and except as hereinbefore provided neither the thesis nor any substantial portion thereof may be printed or otherwise reproduced in any material form whatever without the author's prior written permission.

A handwritten signature in dark ink, appearing to read 'Cremers', is written over a horizontal line.

Luc Cremers

Venlosesteenweg 167

B-3680 Maaseik

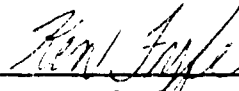
Belgium

Date: Sept 22nd 1994

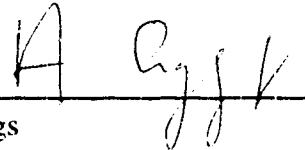
UNIVERSITY OF ALBERTA

Faculty of Graduate Studies and Research

The undersigned certify that they have read, and recommend to the Faculty of Graduate Studies and Research for acceptance, a thesis entitled **Acoustic Variable Order Infinite Elements for Wave Envelope and Multi-domain Boundary Element Modelling** submitted by **Luc Cremers** in partial fulfilment of the requirements for the degree of **Doctor of Philosophy**.



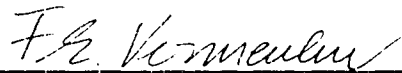
Dr. K. R. Fyfe (Supervisor)



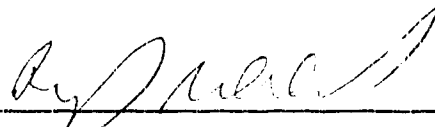
Dr. A. Craggs



Dr. M. G. Faulkner



Dr. F. Vermeulen



Dr. R. J. Bernhard

Date: 22-09-94



Dr. M. Zuo

To my family,

for their encouragement and support during the preparation of this thesis.

ABSTRACT

The formulation and testing of a variable order infinite wave envelope element and a direct collocation *multi-domain* boundary element method for analyzing acoustic radiation and scattering problems in an unbounded domain are presented. These methods have been developed to provide efficient numerical modelling tools, in terms of computation time and computer data-storage requirements, compared to existing finite element and boundary element methods.

The variable order infinite wave envelope element is based on a finite to infinite geometry mapping and a wavelike representation within the element shape function. It allows for the specification of an arbitrary number of acoustic degrees of freedom in the radial infinite direction, yielding a $1/r^n$ expansion for the proper modelling of the amplitude decay. The element can be incorporated into a standard finite element scheme, yielding computationally efficient banded system matrices. Both two-dimensional and axisymmetric problems are presented to show the use, accuracy and limitations of the element. In addition to this, different acoustic modelling aspects are focussed upon. These include the modelling of acoustic wave propagation above infinite homogeneous impedance planes, different methods to prescribe acoustic sources and alternative postprocessing procedures. Special attention is given to limitations encountered for this finite element based modelling of wave propagation in unbounded domains. The limitations are assessed by analyzing the higher order multi-poles of an infinitely long oscillating rigid cylinder and an axisymmetric pulsating rigid sphere.

A direct collocation multi-domain boundary element method for acoustic radiation and scattering problems in unbounded domains is introduced. For effective modelling of the acoustic field variables along the infinite interfaces of adjacent subdomains, a new variable order infinite boundary element is formulated. The element is based on the variable order infinite wave envelope element, and thus features a finite to infinite geometry mapping and a special shape function, combining an appropriate amplitude decay and wavelike variation. Both two-dimensional and axisymmetric modelling of acoustic radiation and scattering problems are presented, indicating the use, the advantages and the limitations of the method. The benefits of this multi-domain boundary element method include banded system matrices, for better computational efficiency, and the elimination of singularities, due to the non-uniqueness problem, common for conventional boundary integral methods.

ACKNOWLEDGEMENTS

I would like to thank my supervisor, Dr. Ken R. Fyfe, for his assistance and guidance throughout my work at the Department of Mechanical Engineering of the University of Alberta.

I would like to express my appreciation to Dr. A. Craggs, Dr. M. G. Faulkner, Dr. J. P. Coyette (N.I.T., Leuven, Belgium) and Dr. R. J. Astley (University of Canterbury, Christchurch, New Zealand) for valuable discussions in the preparation of this work.

Special thanks are extended to Dr. W. Van Petegem for meticulous proofreading of this document.

My sincere thanks also go to my fellow graduate students, for their assistance and friendship, and to all my other friends, for creating a great atmosphere during my stay here in Edmonton. Thanks to Bill and Darrell for the numerous relaxing coffee breaks and our traditional rendezvous at the *Old Power Plant Bar* on Fridays.

I am grateful for the financial support of the Natural Sciences and Engineering Research Council of Canada and the Canada Mortgage and Housing Corporation in completing this work. I would also like to acknowledge the financial support provided by the Professor R. Snoeys and the Jean-Jacques Barbason foundation of Belgium.

Above all, I am indebted to my parents, my sister Carla, my sister Marie-Josée, her husband Ludo and my little nephews Bram and Tom, for their continued encouragement and support, which make it possible to see the completion of this work today.

TABLE OF CONTENTS

CHAPTER	Page
1. INTRODUCTION	1
References	8
 2. A VARIABLE ORDER INFINITE ACOUSTIC WAVE ENVELOPE ELEMENT	 11
2.1. Introduction	11
2.2. Theory	14
2.2.1. Governing equations and boundary conditions	14
2.2.2. Weighted residual formulation	15
2.2.3. Variable order infinite wave envelope element	17
2.2.3.1. <i>Infinite geometry mapping</i>	17
2.2.3.2. <i>Shape functions</i>	19
A. <i>Amplitude decay</i>	19
B. <i>Wavelike variation</i>	23
2.2.3.3. <i>Weighting functions</i>	24
2.2.3.4. <i>Element system matrices</i>	25
2.3. Practical implementation	27
2.3.1. Acoustic node connectivity	27
2.3.2. Sparse solver	28
2.3.3. Post-processing	29
2.4. Discussion of results	29
2.4.1. Infinite cylinder	30
2.4.1.1. <i>Analytical solutions</i>	30
2.4.1.2. <i>Geometry mesh with exact source location</i>	31
A. <i>Acoustic radiation: dipole and quadrupole</i>	31
B. <i>Acoustic scattering</i>	32

2.4.1.3. <i>Geometry mesh with combined use of conventional and infinite wave envelope elements</i>	32
2.4.1.4. <i>Geometry mesh with random source location</i>	33
2.4.1.5. <i>Geometry mesh with shift of source location</i>	33
2.4.2. <i>Sphere</i>	34
2.4.2.1. <i>Analytical solutions</i>	34
2.4.2.2. <i>Geometry mesh with exact source location</i>	35
<i>A. Acoustic radiation: monopole</i>	35
<i>B. Acoustic scattering</i>	35
2.4.3. <i>Scattering by a double barrier</i>	36
2.5. <i>Conclusions</i>	36
<i>Figures</i>	39
<i>References</i>	62

3. ON THE USE OF VARIABLE ORDER INFINITE WAVE ENVELOPE ELEMENTS FOR ACOUSTIC RADIATION AND SCATTERING	66
3.1. <i>Introduction</i>	66
3.2. <i>Theory</i>	68
3.2.1. <i>Governing equations and boundary conditions</i>	68
3.2.2. <i>Finite element system matrices</i>	69
3.2.3. <i>Variable order infinite wave envelope element</i>	70
3.2.3.1. <i>Infinite geometry mapping</i>	71
3.2.3.2. <i>Shape functions</i>	72
3.2.3.3. <i>Weighting functions</i>	73
3.2.4. <i>Modelling of impedance planes</i>	74
3.2.5. <i>Application of sources</i>	74
3.2.5.1. <i>Superposition of scattered and incident acoustic pressure fields</i>	75
3.2.5.2. <i>Nodal source application</i>	75
3.2.6. <i>Post-processing of results</i>	78

3.3. Discussion of results	78
3.3.1. Limitations of the variable order infinite wave envelope element modelling	78
3.3.1.1. <i>Axisymmetric oscillating sphere</i>	80
3.3.1.2. <i>Infinitely long oscillating cylinder</i>	82
3.3.1.3. <i>Scattering from a rigid body</i>	83
3.3.2. Modelling of a coherent monofrequency line source above a homogeneous impedance plane	85
3.3.3. Modelling of acoustic scattering of a cylindrical source from a double barrier configuration	86
3.4. Conclusions	88
Figures	91
References	128

4. A VARIABLE ORDER INFINITE ELEMENT FOR MULTI- DOMAIN BOUNDARY ELEMENT MODELLING OF ACOUSTIC RADIATION AND SCATTERING	131
4.1. Introduction	131
4.2. Theory	134
4.2.1. Governing equations and boundary conditions	134
4.2.2. The direct boundary element method	135
4.2.2.1. <i>Surface Helmholtz integral equation</i>	136
4.2.2.2. <i>Two-dimensional numerical implementation</i>	137
4.2.2.3. <i>Axisymmetric numerical implementation</i>	140
4.2.3. The multi-domain concept	141
4.2.4. Variable order infinite boundary element	144
4.2.4.1. <i>Infinite geometry mapping</i>	145
4.2.4.2. <i>Shape function</i>	146
A. <i>Amplitude decay</i>	146
B. <i>Wavelike variation</i>	148

4.2.4.3. Numerical integration	149
4.2.5. Post-processing of results	151
4.3. Discussion of results	151
4.3.1. Simple acoustic radiation and scattering examples	151
4.3.1.1. Acoustic monopole radiation by an infinitely long rigid cylinder	152
4.3.1.2. Acoustic monopole radiation by an axisymmetric rigid sphere	154
4.3.1.3. Acoustic plane wave scattering from an infinitely long rigid cylinder	155
4.3.2. Limitations of the multi-domain boundary element modelling .	157
4.3.3. Cylindrical source scattering from a single rigid barrier	161
4.4. Conclusions	163
Figures	166
References	202
 5. CONCLUSIONS AND FUTURE RESEARCH	 206
5.1. Summary	206
5.2. Conclusions	210
5.3. Recommendations for future research	213
 APPENDIX 2-A	
Finite element weighted residual formulation for exterior radiation	214
 APPENDIX 2-B	
Derivative of the radial shape function	216
 APPENDIX 2-C	
Inverse geometry mapping	217

APPENDIX 2-D

Effect of source shift	219
----------------------------------	-----

APPENDIX 3-A

Modelling of a coherent monofrequency line source above a homogeneous impedance plane.	221
--	-----

APPENDIX 4-A

The Helmholtz integral equation	224
---	-----

APPENDIX 4-B

Efficient numerical integration of the singular boundary element integrals .	229
--	-----

LIST OF TABLES

	Page
Table 2.D.1 Modelling of a reciprocal decay by an n^{th} order infinite element . .	220

LIST OF FIGURES

	Page
Figure 2.1	39
Radiating body in an infinite domain.	
Figure 2.2	40
One-dimensional infinite geometry mapping	
Figure 2.3	41
Two-dimensional infinite geometry mapping.	
Figure 2.4	42
One-dimensional mapping of shape functions.	
Figure 2.5	43
Lagrangian shape function.	
Figure 2.6	44
Cylinder: Two-dimensional geometry mesh (30 lwe)	
Exact source at origin.	
Figure 2.7	45
Cylinder: Two-dimensional geometry mesh (30 * (6 cfe + 1 lwe)).	
Exact source at origin.	
Figure 2.8	46
Cylinder: Two-dimensional geometry mesh (30 lwe).	
Random source.	
Figure 2.9	47
Cylinder: Two-dimensional geometry mesh (30 lwe).	
Source shift.	
Figure 2.10	48
Cylinder: Two-dimensional postprocessing mesh (630 field points).	

Figure 2.11	49
Acoustic radiation by a vibrating cylinder ($kR = \pi$).	
Contour lines of radiated acoustic pressure amplitude.	
1. Dipole - Analytical; 2. Dipole - 2 nd order lwe; 3. Quadrupole - Analytical;	
4. Quadrupole - 2 nd order lwe	
(A=0 B=.04 C=.08 D=.12 E=.16 F=.20 G=.24 H=.28 I=.32 J=.36 K=.40).	
Figure 2.12	50
Scattering of an acoustic plane wave from a rigid cylinder ($kR = \pi$).	
Contour lines of scattered acoustic pressure amplitude $ P_s / P_i $.	
Geometry mesh with exact source location.	
1. Analytical; 2. 2 nd order lwe; 3. 3 rd order lwe; 4. 4 th order lwe	
(A=0 B=.15 C=.30 D=.45 E=.60 F=.75 G=.90 H=1.05 I=1.20 J=1.35 K=1.50)	
Figure 2.13	51
Scattering of an acoustic plane wave from a rigid cylinder ($kR = \pi$).	
Contour lines of scattered acoustic pressure amplitude $ P_s / P_i $.	
Geometry mesh with combined use of conventional finite elements and infinite wave envelope elements.	
1. Analytical; 2. 1 st order lwe; 3. 2 nd order lwe 4. 3 rd order lwe	
(A=0 B=.15 C=.30 D=.45 E=.60 F=.75 G=.90 H=1.05 I=1.20 J=1.35 K=1.50)	
Figure 2.14	52
Scattering of an acoustic plane wave from a rigid cylinder ($kR = \pi$).	
Contour lines of scattered acoustic pressure amplitude $ P_s / P_i $.	
Geometry mesh with random source location.	
1. Analytical; 2. 2 nd order lwe; 3. 3 rd order lwe; 4. 4 th order lwe	
(A=0 B=.15 C=.30 D=.45 E=.60 F=.75 G=.90 H=1.05 I=1.20 J=1.35 K=1.50)	
Figure 2.15	53
Acoustic quadrupole radiation by a vibrating cylinder ($kR = \pi$).	
Contour lines of radiated acoustic pressure amplitude.	
Geometry mesh with shift of source location.	
1. Analytical; 2. 1 st order lwe; 3. 2 nd order lwe; 4. 3 rd order lwe	
(A=0 B=.04 C=.08 D=.12 E=.16 F=.20 G=.24 H=.28 I=.32 J=.36 K=.40)	

Figure 2.16	54
Acoustic radiation by a sphere - monopole.	
Frequency response function of the amplitude of the radiated acoustic pressure at $r = 5R$.	
Figure 2.17	55
Scattering of a plane acoustic wave from a rigid sphere ($kR = 1$).	
$ P_s / P_i $ at $r = 5R$.	
Figure 2.18	56
Scattering of a plane acoustic wave from a rigid sphere ($kR = 2$).	
$ P_s / P_i $ at $r = 5R$.	
Figure 2.19	57
Scattering of a plane acoustic wave from a rigid sphere ($kR = 4$).	
$ P_s / P_i $ at $r = 5R$.	
Figure 2.20	58
Scattering of a plane acoustic wave from a rigid sphere ($kR = 8$).	
$ P_s / P_i $ at $r = 5R$.	
Figure 2.21	59
Double barrier: Two-dimensional geometry mesh (100 cfe and 30 lwe).	
Source at origin.	
Figure 2.22	60
Double barrier: Two-dimensional postprocessing mesh (542 field points).	
Figure 2.23	61
Scattering of an acoustic plane wave from a double barrier ($kW = 3\pi$).	
Contour lines of total acoustic pressure amplitude $ P_t $. ($ P_i = 1$).	
1. bem; 2. 1 st order lwe; 3. 2 nd order lwe; 4. 5 th order lwe	
(A=0 B=.24 C=.48 D=.72 E=.96 F=1.20 G=1.44 H=1.68 I=1.92 J=2.16 K=2.40)	
Figure 3.1	91
Modelling an infinite acoustic domain using conventional finite elements and variable order infinite wave envelope elements.	
Figure 3.2	92

The use of image sources in acoustic scattering problems above a hard plane.	
Figure 3.3	93
Applying a two-dimensional cylindrical source at an acoustic degree of freedom.	
Figure 3.4	94
The boundary element postprocessing concept.	
Figure 3.5	95
A single layer of 75 quadratic infinite wave envelope elements for two-dimensional modelling of acoustic radiation or scattering from a cylinder.	
Figure 3.6	96
Acoustic radiation by a sphere - monopole.	
Geometry mesh used: 90 lwe.	
Frequency response function of the amplitude of the radiated acoustic pressure at $r = 5R$.	
Figure 3.7	97
Acoustic radiation by a sphere - monopole.	
Geometry mesh used: 45 qwe.	
Frequency response function of the amplitude of the radiated acoustic pressure at $r = 5R$.	
Figure 3.8	98
Spherical multi-pole of order 1.	
Geometry mesh used: 75 qwe.	
Polar plot ($0 < \theta < 90$) of the amplitude of the radiated acoustic pressure at $r = 5R$ for $kR = 20$.	
Figure 3.9	99
Spherical multi-pole of order 2.	
Geometry mesh used: 75 qwe.	
Polar plot ($0 < \theta < 90$) of the amplitude of the radiated acoustic pressure at $r = 5R$ for $kR = 20$.	
Figure 3.10	100
Spherical multi-pole of order 10.	
Geometry mesh used: 75 qwe.	

<p>Polar plot ($0 < \theta < 90$) of the amplitude of the radiated acoustic pressure at $r = 5R$ for $kR = 20$.</p> <p>Figure 3.11</p> <p>Spherical multi-pole of order 20.</p> <p>Geometry mesh used: 75 qwe.</p> <p>Polar plot ($0 < \theta < 90$) of the amplitude of the radiated acoustic pressure at $r = 5R$ for $kR = 20$.</p> <p>Figure 3.12</p> <p>Spherical multi-pole of order 20.</p> <p>Different angular discretization in geometry mesh.</p> <p>Polar plot ($0 < \theta < 90$) of the amplitude of the radiated acoustic pressure at $r = 5R$ for $kR = 20$.</p> <p>Figure 3.13</p> <p>Spherical multi-pole of order 1.</p> <p>Geometry mesh used: 75 qwe.</p> <p>Frequency response function of the amplitude of the radiated acoustic pressure at $x = 0$; $y = 5R$.</p> <p>Figure 3.14</p> <p>Spherical multi-pole of order 2.</p> <p>Geometry mesh used: 75 qwe.</p> <p>Frequency response function of the amplitude of the radiated acoustic pressure at $x = 0$; $y = 5R$.</p> <p>Figure 3.15</p> <p>Spherical multi-pole of order 10.</p> <p>Geometry mesh used: 75 qwe.</p> <p>Frequency response function of the amplitude of the radiated acoustic pressure at $x = 0$; $y = 5R$.</p> <p>Figure 3.16</p> <p>Spherical multi-pole of order 20.</p> <p>Geometry mesh used: 75 qwe.</p> <p>Frequency response function of the amplitude of the radiated acoustic pressure at</p>	<p>101</p> <p>102</p> <p>103</p> <p>104</p> <p>105</p> <p>106</p>
--	---

$x = 0; y = 5R.$

Figure 3.17 107

Cylindrical multi-pole of order 1.

Geometry mesh used: 75 qwe.

Polar plot ($0 < \theta < 90$) of the amplitude of the radiated acoustic pressure at $r = 5R$ for $kR = 20$.

Figure 3.18 108

Cylindrical multi-pole of order 2.

Geometry mesh used: 75 qwe.

Polar plot ($0 < \theta < 90$) of the amplitude of the radiated acoustic pressure at $r = 5R$ for $kR = 20$.

Figure 3.19 109

Cylindrical multi-pole of order 10.

Geometry mesh used: 75 qwe.

Polar plot ($0 < \theta < 90$) of the amplitude of the radiated acoustic pressure at $r = 5R$ for $kR = 20$.

Figure 3.20 110

Cylindrical multi-pole of order 20.

Geometry mesh used: 75 qwe.

Polar plot ($0 < \theta < 90$) of the amplitude of the radiated acoustic pressure at $r = 5R$ for $kR = 20$.

Figure 3.21 111

Cylindrical multi-pole of order 1.

Geometry mesh used: 75 qwe.

Frequency response function of the amplitude of the radiated acoustic pressure at $x = 5R; y = 0$.

Figure 3.22 112

Cylindrical multi-pole of order 2.

Geometry mesh used: 75 qwe.

Frequency response function of the amplitude of the radiated acoustic pressure at $x = 5R; y = 0$.

Figure 3.23	113
Cylindrical multi-pole of order 10.	
Geometry mesh used: 75 qwe.	
Frequency response function of the amplitude of the radiated acoustic pressure at $x = 5R$; $y = 0$.	
Figure 3.24	114
Cylindrical multi-pole of order 20.	
Geometry mesh used: 75 qwe.	
Frequency response function of the amplitude of the radiated acoustic pressure at $x = 5R$; $y = 0$.	
Figure 3.25	115
Scattering of an acoustic plane wave ($\rightarrow +x$) from a rigid cylinder.	
Geometry mesh used: 75 qwe.	
Frequency response function of the amplitude of the scattered acoustic pressure $ P_s / P_i $ at $x = -5R$; $y = 0$.	
Figure 3.26	116
Scattering of an acoustic plane wave ($\rightarrow +x$) from a rigid cylinder.	
Geometry mesh used: 75 qwe.	
Polar plot ($0 < \theta < 180$) of the amplitude of the scattered acoustic pressure $ P_s / P_i $ at $r = 5R$ for $kR = 20$.	
Figure 3.27	117
Scattering of an acoustic plane wave ($\downarrow -z$) from a rigid sphere.	
Geometry mesh used: 75 qwe.	
Frequency response function of the amplitude of the scattered acoustic pressure $ P_s / P_i $ at $x = 0$; $y = 5R$.	
Figure 3.28	118
Scattering of an acoustic plane wave ($\downarrow -z$) from a rigid sphere.	
Geometry mesh used: 75 qwe.	
Polar plot ($-90 < \theta < 90$) of the amplitude of the scattered acoustic pressure $ P_s / P_i $ at $r = 5R$ for $kR = 20$.	
Figure 3.29	119

Cylindrical source above a homogeneous impedance plane: Configuration sketch.

Figure 3.30 120

Modelling of a cylindrical source, at $x = 0$; $y = 0.25$, above a homogeneous impedance plane ($\beta = 0.005$).

Geometry mesh used: 58 cfe and 16 qwe.

Frequency response function of the amplitude of the acoustic pressure at $x = 10$; $y = 0.25$.

Figure 3.31 121

Modelling of a cylindrical source, at $x = 0$; $y = 0.25$, above a homogeneous impedance plane ($\beta = 0.1$).

Geometry mesh used: 58 cfe and 16 qwe.

Frequency response function of the amplitude of the acoustic pressure at $x = 10$; $y = 0.25$.

Figure 3.32 122

Modelling of a cylindrical source, at $x = 0$; $y = 0.25$, above a homogeneous impedance plane ($\beta = 0.5$).

Geometry mesh used: 58 cfe and 16 qwe.

Frequency response function of the amplitude of the acoustic pressure at $x = 10$; $y = 0.25$.

Figure 3.33 123

Modelling of a cylindrical source, at $x = 0$; $y = 0.25$, above a hard plane ($\beta = 0$). (1) G_β -solution; (2) 2nd order infinite wave envelope element modelling.

Geometry mesh used: 58 cfe and 16 qwe.

Contour plot of the amplitude of the acoustic pressure for $k = 10$.

Figure 3.34 124

Modelling of a cylindrical source, at $x = 0$; $y = 0.25$, above a homogeneous impedance plane ($\beta = 0.5$).

(1) G_β -solution; (2) 5th order infinite wave envelope element modelling.

Geometry mesh used: 58 cfe and 16 qwe.

Contour plot of the amplitude of the acoustic pressure for $k = 10$.

Figure 3.35 125

Geometry mesh for the modelling of a double barrier configuration: 30 conventional finite elements (cfe) and 20 qwe.	
Figure 3.36	126
Scattering from a double barrier with rigid platform ($\beta = 0$). Cylindrical source at $x = 0$; $y = 0.2W$. Geometry mesh used: 30 cfe and 20 qwe (order 8). Frequency response function of the amplitude (dB) of the acoustic pressure at $x = 5W$; $y = 0.15W$.	
Figure 3.37	127
Scattering from a double barrier with soft platform ($\beta = 0.5$). Cylindrical source at $x = 0$; $y = 0.2W$. Geometry mesh used: 30 cfe and 20 qwe (order 8). Frequency response function of the amplitude (dB) of the acoustic pressure at $x = 5W$; $y = 0.15W$.	
Figure 4.1	166
Radiating body in an infinite domain: geometric configuration for boundary integral formulations.	
Figure 4.2	167
Multi-domain boundary element configuration.	
Figure 4.3	168
Infinite boundary element geometry mapping.	
Figure 4.4	169
Variable order infinite boundary element.	
Figure 4.5	170
Sample subdomain boundary element discretisation.	
Figure 4.6	171
Sample two-dimensional multi-domain mesh for an infinitely long rigid cylinder.	
Figure 4.7	172
Sample axisymmetric multi-domain mesh for a rigid sphere.	
Figure 4.8	173

Acoustic radiation by a rigid cylinder - monopole.

Frequency response function of the amplitude of the radiated acoustic pressure
at $r = 5R$.

Figure 4.9 174

Acoustic radiation by a rigid sphere - monopole.

Frequency response function of the amplitude of the radiated acoustic pressure
at $r = 5R$.

Figure 4.10 175

Scattering of an acoustic plane wave ($\rightarrow +x$) from a rigid cylinder.

Polar plot ($0 < \theta < 180$) of the amplitude of the scattered acoustic pressure $|P_s|/|P_i|$
at $r = 5R$ for $kR = 2.405$.

Figure 4.11 176

Scattering of an acoustic plane wave ($\rightarrow +x$) from a rigid cylinder.

Polar plot ($0 < \theta < 180$) of the amplitude of the scattered acoustic pressure $|P_s|/|P_i|$
at $r = 5R$ for $kR = 8.654$.

Figure 4.12 177

Scattering of an acoustic plane wave ($\rightarrow +x$) from a rigid cylinder.

Frequency response function of the amplitude of the scattered acoustic pressure
 $|P_s|/|P_i|$ at $x = 1.1R$; $y = 0$ (Near field - forward scattering).

Figure 4.13 178

Scattering of an acoustic plane wave ($\rightarrow +x$) from a rigid cylinder.

Frequency response function of the amplitude of the scattered acoustic pressure
 $|P_s|/|P_i|$ at $x = 0$; $y = 1.1R$ (Near field - sideward scattering).

Figure 4.14 179

Scattering of an acoustic plane wave ($\rightarrow +x$) from a rigid cylinder.

Frequency response function of the amplitude of the scattered acoustic pressure
 $|P_s|/|P_i|$ at $x = -1.1R$; $y = 0$ (Near field - backward scattering).

Figure 4.15 180

Scattering of an acoustic plane wave ($\rightarrow +x$) from a rigid cylinder.

Frequency response function of the amplitude of the scattered acoustic pressure
 $|P_s|/|P_i|$ at $x = 100R$; $y = 0$ (Far field - forward scattering).

Figure 4.16	181
Scattering of an acoustic plane wave ($\rightarrow +x$) from a rigid cylinder.	
Frequency response function of the amplitude of the scattered acoustic pressure $ P_s / P_i $ at $x = 0$; $y = 100R$ (Far field - sideward scattering).	
Figure 4.17	182
Scattering of an acoustic plane wave ($\rightarrow +x$) from a rigid cylinder.	
Frequency response function of the amplitude of the scattered acoustic pressure $ P_s / P_i $ at $x = -100R$; $y = 0$ (Far field - backward scattering).	
Figure 4.18	183
Scattering of an acoustic plane wave ($\rightarrow +x$) from a rigid cylinder.	
Frequency response function of the amplitude of the scattered acoustic pressure $ P_s / P_i $ at $x = 0$; $y = 5R$.	
Results obtained for infinite boundary elements of order 1, while varying the degree of subdomaining.	
Figure 4.19	184
Scattering of an acoustic plane wave ($\rightarrow +x$) from a rigid cylinder.	
Frequency response function of the amplitude of the scattered acoustic pressure $ P_s / P_i $ at $x = 0$; $y = 5R$.	
Results obtained for infinite boundary elements of order 2, while varying the degree of subdomaining.	
Figure 4.20	185
Scattering of an acoustic plane wave ($\rightarrow +x$) from a rigid cylinder.	
Frequency response function of the amplitude of the scattered acoustic pressure $ P_s / P_i $ at $x = 0$; $y = 5R$.	
Results obtained for infinite boundary elements of order 3, while varying the degree of subdomaining.	
Figure 4.21	186
Scattering of an acoustic plane wave ($\rightarrow +x$) from a rigid cylinder.	
Frequency response function of the amplitude of the scattered acoustic pressure $ P_s / P_i $ at $x = 0$; $y = 5R$.	
Results obtained for infinite boundary elements of order 4, while varying the degree	

of subdomaining.

Figure 4.22 187

Scattering of an acoustic plane wave ($\rightarrow +x$) from a rigid cylinder.

Frequency response function of the amplitude of the scattered acoustic pressure $|P_s|/|P_i|$ at $x = 0$; $y = 5R$.

Results obtained for a mesh with 2 subdomains, while varying the order of the infinite boundary element.

Figure 4.23 188

Scattering of an acoustic plane wave ($\rightarrow +x$) from a rigid cylinder.

Frequency response function of the amplitude of the scattered acoustic pressure $|P_s|/|P_i|$ at $x = 0$; $y = 5R$.

Results obtained for a mesh with 4 subdomains, while varying the order of the infinite boundary element.

Figure 4.24 189

Scattering of an acoustic plane wave ($\rightarrow +x$) from a rigid cylinder.

Frequency response function of the amplitude of the scattered acoustic pressure $|P_s|/|P_i|$ at $x = 0$; $y = 5R$.

Results obtained for a mesh with 12 subdomains, while varying the order of the infinite boundary element.

Figure 4.25 190

Scattering of an acoustic plane wave ($\rightarrow +x$) from a rigid cylinder.

Frequency response function of the amplitude of the scattered acoustic pressure $|P_s|/|P_i|$ at $x = 0$; $y = 5R$.

Results obtained for a mesh with 20 subdomains, while varying the order of the infinite boundary element.

Figure 4.26 191

Cylindrical multi-pole of order 5.

Polar plot ($0 < \theta < 90$) of the amplitude of the radiated acoustic pressure at $r = 5R$ for $kR = 20$.

Figure 4.27 192

Cylindrical multi-pole of order 15.

Polar plot ($0 < \theta < 90$) of the amplitude of the radiated acoustic pressure at $r = 5R$ for $kR = 20$.	
Figure 4.28	193
Cylindrical multi-pole of order 25. Polar plot ($0 < \theta < 90$) of the amplitude of the radiated acoustic pressure at $r = 5R$ for $kR = 20$.	
Figure 4.29	194
Cylindrical multi-pole of order 25. Polar plot ($0 < \theta < 90$) of the amplitude of the radiated acoustic pressure at $r = 5R$ for $kR = 20$. Effect of degree of subdomaining.	
Figure 4.30	195
Cylindrical multi-pole of order 10. Contour plot of the amplitude of the acoustic pressure for $kR = 5$. Example of a poor radiator.	
Figure 4.31	196
Cylindrical multi-pole of order 10. Contour plot of the amplitude of the acoustic pressure for $kR = 15$. Example of a good radiator.	
Figure 4.32	197
Cylindrical multi-pole of order 25. Polar plot ($0 < \theta < 90$) of the amplitude of the radiated acoustic pressure at $r = 5R$ for $kR = 20$. Effect of the use of conventional interface boundary elements in the acoustic near field.	
Figure 4.33	198
Scattering of a two-dimensional cylindrical source from a single rigid barrier. (source @ $x = -1.5H$; $y = 0.15$) Contour plot of the amplitude of the total acoustic pressure for $kH = 5$. (Contour levels ranging from 0 to 2.0 with a step of 0.1)	

Figure 4.34 199

Scattering of a two-dimensional cylindrical source from a single rigid barrier.

(source @ $x = -1.5H$; $y = 0.15$)

Frequency response function of the amplitude of the total acoustic pressure at
 $x = 5H$; $y = 0.1H$.

Figure 4.35 200

Scattering of a two-dimensional cylindrical source from a single rigid barrier.

(source @ $x = -1.5H$; $y = 0.15$)

Frequency response function of the amplitude of the total acoustic pressure at
 $x = 5H$; $y = 0.1H$.

Effect of local resonances.

Figure 4.36 201

Scattering of a two-dimensional cylindrical source from a single rigid barrier.

(source @ $x = -1.5H$; $y = 0.15$)

Frequency response function of the insertion loss at $x = 5H$; $y = 0.1H$.

NOMENCLATURE

a, a_i	acoustic source distance
a_{m_i}	component of boundary element pressure influence matrix
\overline{A}_n	prescribed admittance boundary condition
A_{ij}	component of finite element damping matrix
$[A]$	finite element damping matrix
	boundary element pressure influence matrix
b_{m_i}	component of boundary element velocity influence matrix
$[B]$	boundary element velocity influence matrix
c	acoustic wave propagation velocity
C_n, S_n, U_n, V_n	Stenzel functions of order n
$C(P)$	Helmholtz integral constant (solid angle factor)
$erfc(x)$	complementary error function
f	frequency of vibration
$f_n(\theta, \phi)$	three-dimensional radiation patterns
F_i	component of acoustic loading vector
$\{F\}$	acoustic loading vector
$F_n(\theta), G_n(\theta)$	two-dimensional radiation patterns
G	free-space Green's function
G_β	approximate analytical solution for a two-dimensional mono-frequency source above a homogeneous impedance plane
G_w	geometric weighting function
G_0	Green's function for a rigid half plane
H	height of barrier
$H_n^{(2)}$	n^{th} order Hankel function of the second kind
IL	insertion loss (dB)
j_n	spherical Bessel function of the first kind of integer order n
J	Jacobian of geometry transformation
J_n	Bessel function of the first kind of integer order n

J_ν	Bessel function of the first kind of fractional order ν
k	acoustic wave number
k_c	critical wave number (transition from poor to good radiator)
k_{nq}	q^{th} critical frequency for multi-pole of order n
K_1^A, K_1^B	non-singular parts of angular integral of free-space Green's function
K_2^A, K_2^B	singular parts of angular integral of free-space Green's function
K_{ij}	component of finite element stiffness matrix
$[K]$	finite element stiffness matrix
M_i	geometry mapping function
M_{ij}	component of finite element mass matrix
$[M]$	finite element mass matrix
n	order of element
$\underline{n}_0, \underline{n}_\infty, \dots$	unit normal pointing into the acoustic domain
N_i	element shape function
N_i^n	element shape function of order n
N_n	Bessel function of the second kind of integer order n
p	acoustic pressure
\bar{p}	prescribed acoustic pressure
p_s	scattered acoustic pressure
p_i	incident acoustic pressure
p_t	total acoustic pressure
p'	trial function of acoustic pressure
P	observation point
P_0	pressure amplitude
P_n	Legendre polynomial of zeroth order and degree n
P_β	correction term for G_0 to obtain G_β
Q	volume source strength
	radiating point
r, θ, z	polar coordinates
r_∞	semi-infinite distance
R	characteristic radius

$R(x)$	distance from source to field point
R_a	radial distance to axisymmetric axis
R_i^n	\sqrt{r} -factor for two-dimensional radial shape function
$ R_p - R_q $	distance between field point P and Q
s, t	local coordinates
S	surface
S_0	surface of radiating body
S_p	surface with prescribed pressure boundary condition
S_{imp}	surface with prescribed impedance boundary condition
S_{vel}	surface with prescribed velocity boundary condition
S_∞	surface at infinity
S_i	angular shape function
t	time
T_i^n	radial shape function of order n
$\{\bar{v}\}$	prescribed particle velocity vector
$\overline{v_n}$	prescribed normal surface velocity
$\overline{v_{n_s}}$	scattered prescribed normal surface velocity
$\overline{v_{n_i}}$	incident prescribed normal surface velocity
$\overline{v_{n_t}}$	total prescribed normal surface velocity
V	volume
$\overline{V_n}$	velocity amplitude of n^{th} order multi-pole
W	characteristic distance between two barriers
W_i	weighting function
W_i^n	weighting function of order n
x, y, z	Cartesian coordinates
x_0, x_n, x_{II}	one-dimensional geometry positions determining the finite to infinite geometry mapping
\underline{x}	position vector
$\overline{Z_n}$	prescribed normal impedance

Greek Symbols

α_{B_n}	q^{th} root of the n^{th} order Bessel function of the first kind
β	relative normal surface admittance
Γ	boundary
Γ^h	hard plane boundary
Γ^o	boundary of radiating body
Γ^i	interface boundary
ϵ_n	Neumann function
θ, ϕ	angular measures
λ	acoustic wavelength
$\mu(s, t)$	phase function
ρ	density of acoustic medium
ω	acoustic circular frequency

Other Symbols

δ, d	partial and total derivative
e	natural logarithm base
i	imaginary number $\sqrt{-1}$
Im	imaginary part
Π	product operator
Σ	summation operator
∇	gradient operator
∇^2	Laplacian operator
$*$	complex conjugate
$/$	derivative
$\ \quad \ $	determinant

Matrix Notation

$\{x\}$ vector (one-dimensional array)

$\{x\} = \{x\}^T$ transposed vector

$[A]$ matrix ($n \times m$)

$[A]^T$ transposed matrix

$\begin{bmatrix} x_i \\ y_i \end{bmatrix}$ matrix ($2 \times n$)

$\langle x_i \ y_i \rangle = \begin{bmatrix} x_i \\ y_i \end{bmatrix}^T$ transposed matrix ($2 \times n$)

CHAPTER 1

INTRODUCTION

Noise control engineering has become an important aspect of mechanical design. A great deal of research effort is devoted towards the dynamic analysis of structures to improve the acoustic performance of the product. The analysis is not only focussed upon the improvement of existing structures, but moreover, upon the optimization of new products in the early stages of the design process. Guidelines for this design optimization include noise control regulations, limiting the allowable noise levels emitted by the product, e.g. for appliances, car and aircraft industry, and prescribed desired sound radiation patterns for products such as hifi speakers and ultra-sound detection probes. In all cases, the acoustic pressure field, interior or exterior to the vibrating structure, has to be evaluated.

Over the years, a large number of modelling tools have been developed for analyzing these dynamic structural-acoustic problems. In general, a structural-acoustic model comprises three parts, i.e. the model of the structure, the acoustic field modelling and the coupling between the two models. The elasto-acoustic coupling effect can be omitted in many cases, when the radiation loading of the acoustic medium on the vibrating structure is negligible. The acoustic response can then be evaluated within the acoustic model itself, based on boundary conditions, e.g. prescribed surface velocity patterns, obtained from the structural model.

The research conducted for this thesis involves the harmonic acoustic modelling of radiation and scattering from a vibrating surface within an infinite domain. This type of problem is governed by the classical Helmholtz equation with prescribed boundary conditions on the radiating surface and a suitable radiation condition, simulating an infinite acoustic domain [1.1-1.3]. Sommerfeld stipulated that, in order to have a well-posed radiation problem in an infinite domain, it is not sufficient to only satisfy a condition of finiteness, as is the case in static potential problems, but in addition, a radiation condition has to be specified, only permitting outgoing travelling waves into infinity. The finiteness and radiation conditions are combined into the so-called Sommerfeld radiation condition. In general, the application of the latter condition in mathematical models is not an easy task.

Closed-form analytical solutions to the acoustic radiation problem are only available for a limited number of special cases. These involve radiation and scattering problems from simple geometries such as spheres and cylinders, where the technique of separation of variables is applicable. Various textbooks on acoustics [1.4-1.10] give detailed analyses of these classic solutions.

For the analysis of radiation problems from vibrating bodies of arbitrary geometry and boundary conditions, a more general solution method is necessary. A variety of numerical methods have been developed, ranging from approximate analytical solutions to boundary integral and finite element based methods. An overview of these different methods is given in References [1.11-1.13].

Boundary integral methods are very well-suited for the modelling of infinite domains from a theoretical point of view. Through the use of the free-space Green's function and Green's theorem, the problem can be reduced to the solution of the Helmholtz surface integral equation on the boundary of the acoustic domain. The Sommerfeld radiation condition is inherently satisfied within the Green's kernel and the number of dimensions of the problem is reduced by one. Boundary integral methods in general consist of two phases. In a first phase, the acoustic variables on the surface are solved for using the surface Helmholtz integral equation. Secondly, the acoustic field variables at an arbitrary field point can be determined by evaluating the Helmholtz

boundary integral, based on the calculated surface field variables.

A wide range of numerical implementations of these boundary integral methods have been developed. These are the so-called Boundary Element Methods (BEM). In these formulations, a discretized Helmholtz integral equation is solved. Both direct and indirect formulations of the boundary element method have been developed. The direct formulation solves for the field variables of interest, i.e. acoustic pressure and particle velocity, on the surface directly, while the indirect approach solves for the acoustic pressure and velocity jumps, the double and single layer potentials. All these boundary element methods are well documented in the literature [1.14-1.17].

A well-known problem of the boundary integral methods is the non-uniqueness problem. The surface Helmholtz integral formulation does not have a unique solution at certain frequencies. These critical frequencies correspond to the eigenfrequencies of the corresponding interior problem [1.18-1.20]. Different formulations have been proposed for solving this problem. Schenck proposed a combined Helmholtz integral equation formulation [1.18], where both the surface and the interior Helmholtz integral equation are discretized, to calculate the field variables on the surface. The resulting over-determined system of equations is then solved by a least-squares method to obtain the unique solution. The problem for this method lies in the choice of the interior over-determination points. Points chosen on the nodal lines of the interior modes do not aid in reducing the singularity. An adequate choice of these over-determination points can therefore be difficult at high frequencies where the modal density of the interior problem becomes very high. Another method is proposed by Burton and Miller [1.20]. They suggest a combination of the surface Helmholtz integral equation and its derivative for solving the non-uniqueness problem.

Another practical problem for the boundary element methods is the fact that the formulation is non-local. This means that every unknown acoustic field variable is coupled to every other unknown of the system. The system matrices are thus fully populated complex matrices. This is in contrast with finite element based methods, where the system matrices are banded, due to element interconnectivity. Therefore, despite the fact that only the radiating surface has to be discretized, computer data storage can

quickly become a problem, resulting in excessive computation times for the solution phase of the method.

In an effort to obtain a more local application of the Sommerfeld radiation condition, researchers have been developing finite element based methods for acoustic radiation in an infinite domain. A straightforward implementation is the simple truncation of a conventional finite element mesh by the pc-impedance condition, at a finite but distant boundary from the radiating body, stipulating local outgoing travelling waves. This quickly leads to a very large number of acoustic degrees of freedom, because a large region surrounding the radiator or scatterer must be meshed, according to the discretization rule of thumb of seven degrees of freedom per wavelength. Moreover, it should be noted that spurious reflections occur due to the finite implementation of the pc-impedance condition. This can lead to large errors, since acoustic waves are allowed to flow back towards the radiating body, possibly establishing standing wave patterns in the acoustic near-field. Higher order boundary conditions have been developed to improve the application of a radiation condition at a finite distance. These boundary dampers have been described by Bayliss, Gunzberger and Turkel [1.21] and more recently implemented by Assaad, Bossut and Decarpigny [1.22-1.23]. Their mono- and dipolar damping elements are capable of absorbing, respectively, the first and the first two contributions of the asymptotic expansion of the outgoing acoustic waves, reducing the size of the conventional finite element near-field mesh to some degree.

Another finite element based method is the implementation of so-called infinite elements by the group of Zienkiewicz and Bettess [1.24-1.26]. These infinite elements span as a single layer around the acoustic near-field of the radiating body, extending the domain into infinity. An appropriate $(1/r)$ amplitude decay and wavelike variation is built into the element shape functions for adequate modelling of the outgoing acoustic waves. The difficulty in the implementation of these elements lies in the integration involved in the calculation of the element contributions to the system matrices, due to the complex exponential in the integrand, used to model the wavelike variation. Special integration procedures have to be used, rather than the conventional Gauss-Legendre quadrature rules.

Astley and Coyette [1.27] introduced the wave envelope principle to the formulation of the latter infinite elements. The wave envelope principle involves a finite element procedure, whereby the complex conjugates of the shape functions are used as weighting functions in a modified Galerkin weighted residual scheme. This particular choice of weighting functions leads to the cancellation of the complex exponentials in the integrand of the element system matrices. All harmonic spatial variations have therefore been removed from the integrand allowing for simple Gauss quadrature integration. In essence, these infinite wave envelope elements only model the envelope of the outgoing travelling waves. The resulting assembled system matrices are no longer symmetric, but still reveal a banded form, due to the element connectivity. This results in a reduced need for computer data-storage as compared to the global boundary element methods. Both infinite elements and infinite wave envelope elements are matched to a conventional finite element mesh, modelling the acoustic near-field. Again, in order to avoid spurious reflections of the outgoing acoustic waves, the near-field mesh has to extend sufficiently into the acoustic domain, before the infinite elements can properly be matched to it.

The first part of this thesis is focussed on an extension of the infinite wave envelope element formulation, in an effort to be able to move the infinite wave envelope elements closer to the radiating body and, therefore, drastically reducing the size of the conventional near-field finite element mesh. Wilcox [1.3] formulated a generalization of the theorems of Rellich and Atkinson on acoustic radiation, which states that, in general, an arbitrary radiation function for the region exterior to a sphere of finite radius can be written as an infinite series of radiation patterns of increasing order. In order to adequately model all the subsequent radiation patterns by a single layer of infinite elements, not only the angular discretization has to be sufficient, but also, an adequate number of terms in the $(1/r)^n$ -expansion have to be present for modelling the amplitude decay. Therefore a variable order infinite wave envelope element is proposed, allowing for a flexible choice of the number of acoustic degrees of freedom along the radial edges of the element extending out to infinity. In general, this more powerful infinite wave envelope element is able to model the acoustic radiation more accurately. The need for a conventional finite element mesh for the acoustic near-field can be minimized and in

some cases even omitted.

The formulation of the variable order infinite wave envelope element is introduced in Chapter 2. Special Lagrangian type shape functions for the amplitude decay modelling are developed, along with an explanation of the other important aspects of the element, such as the finite to infinite geometry mapping, the wavelike variation and the wave envelope principle for the modified weighted residual scheme. Furthermore, the implementation of an inverse geometry mapping routine is introduced, used in a post-processing routine to evaluate the acoustic field variables at an arbitrary point in the acoustic domain. Examples of two-dimensional and axisymmetric radiation and scattering problems are shown to illustrate the use and the performance of the variable order infinite wave envelope element.

Chapter 3 is devoted to a thorough investigation into the use and the limitations of the variable order infinite wave envelope element. A systematic study of the modelling of higher order cylindrical and spherical multi-poles is performed, revealing limitations of the variable order infinite wave envelope element modelling due to the local implementation of the Sommerfeld radiation condition. In the same chapter, different methods of acoustic source application for modelling scattering problems from rigid bodies are explained. An alternative post-processing method, based on the Helmholtz boundary integral equation, is also introduced. In addition, special radiation applications are studied, such as the modelling of acoustic sources above homogeneous impedance planes.

In Chapter 4, a multi-domain boundary element procedure is developed in an effort to merge the accurate modelling of the Sommerfeld radiation condition of the boundary integral methods with the computational efficiency of the finite element based methods. Zeng et al. [1.28] introduced a variational multi-domain boundary element method for two-dimensional modelling of acoustic radiation and scattering problems. Within their formulation, the infinite interfaces between the different subdomains, along which continuity of the acoustic field variables is prescribed, are modelled using a finite number of conventional interface boundary elements, followed by a single infinite interface boundary element. The formulation of the latter infinite element is based on the infinite

element of Zienkiewicz et al. [1.24-1.26]. In this chapter, a direct collocation multi-domain boundary element method is developed for two-dimensional and axisymmetric acoustic radiation and scattering. A special variable order infinite interface boundary element is created for accurate modelling of the infinite subdomain interfaces. The infinite boundary element is based on the formulation of the variable order infinite wave envelope element, discussed earlier. An arbitrary number of acoustic degrees of freedom can be chosen along the interface, rendering a more powerful element and thus reducing the need for conventional interface boundary elements in the acoustic near-field. Again, the performance of the multi-domain boundary method is tested, analyzing higher orders of multi-pole radiation patterns. The effects of the degree of subdomaining and the order of the infinite interface elements on the accuracy of the method are studied. Advantages and limitations of the method are discussed.

Finally, Chapter 5 contains conclusions for this work, summarizing the advantages and limitations of both the variable order infinite wave envelope element and multi-domain boundary element modelling. Suggestions for future research within the area are also included.

The following Chapters 2, 3 and 4 have all been written as separate stand-alone papers, that have either been published or submitted for publication. At the end of the thesis a number of appendices are given with more detail on certain topics. Appendix 2-A details the finite element weighted residual formulation for exterior radiation. A closed form of the derivative of the radial shape function of the variable order infinite wave envelope element is given in Appendix 2-B. The inverse geometry mapping is explained in Appendix 2-C, while a study on the effect of acoustic source shift of the variable order infinite wave envelope element is included in Appendix 2-D. In Appendix 3-A, a summary of the derivation of an approximate analytical solution for the modelling of a mono-frequency line source above an homogeneous impedance plane is given. Finally, Appendix 4-A outlines the derivation of the surface Helmholtz integral equation and an efficient numerical integration procedure for the evaluation of the singular boundary element integrals is presented in Appendix 4-B.

REFERENCES

- 1.1. F. V. ATKINSON, "On Sommerfeld's radiation condition," *The Philosophical Magazine* **40**, 645-651 (1949).
- 1.2. A. BAYLISS, M. GUNZBURGER and E. TURKEL, "Boundary conditions for the numerical solution of elliptic equations in exterior regions," ICASE Report No. 80/1, NASA Langley, 1980.
- 1.3. C. H. WILCOX, "A generalization of theorems of Rellich and Atkinson," *Proceedings of the American Mathematical Society*, 271-276 (1956).
- 1.4. L. L. BERANEK, *Noise and Vibration Control*, (McGraw Hill, New York, 1971).
- 1.5. L. CREMER, M. HECKL and E. E. UNGAR, *Structure-Borne Sound*, (Springer Verlag, Berlin, 1973).
- 1.6. M. C. JUNGER and D. FEIT, *Sound, Structures and their Interaction*, (M.I.T. Press, Cambridge, Massachusetts, 1972).
- 1.7. P. M. MORSE and K. U. INGARD, *Theoretical Acoustics*, (McGraw Hill, New York, 1968).
- 1.8. A. D. PIERCE, *ACOUSTICS: An Introduction to its Physical Principles and Applications* (Published by the Acoustical Society of America, New-York, 1991).
- 1.9. E. SKUDRZYK, *The Foundations of Acoustics* (Springer-Verlag, Vienna, New-York, 1971).
- 1.10. F. FAHY, *Sound and Structural Vibration: Radiation, Transmission and Response*, (Academic Press, London, 1985).
- 1.11. O. C. ZIENKIEWICZ, D. W. KELLY and P. BETTESS, "The Sommerfeld (radiation) condition on infinite domains and its modelling in numerical procedures," *Computing Methods in Applied Sciences and Engineering, Third International Symposium, IRIA Laboria, Lect. in Math. V 704*, 169-192 (1977).
- 1.12. O. C. ZIENKIEWICZ, P. BETTESS, T. C. CHIAM and C. EMSON, "Numerical methods for unbounded field problems and a new infinite element formulation", *Computational Methods for Infinite Domain Media-Structure Interaction AMD 46*,

- 115-147 (1981).
- 1.13. **R. J. BERNHARD, B. K. GARDNER and D. C. SMITH**, "Alternative Methods for Computing Sound Radiation from Vibrating Surfaces", Proceedings of the 5th International Modal Analysis Conference, Schenectady, NY: Union College, 343-349, (1987).
 - 1.14. "Boundary element methods in acoustics", Eds. **R. D. Ciskowski and C. A. Brebbia**, Boston, Computational Mechanics Publications (1991).
 - 1.15. **B. SOENARKO**, "An advanced boundary element formulation for acoustic radiation and scattering in three dimensions", Ph.D. dissertation, University of Kentucky (1983).
 - 1.16. **K. R. FYFE**, "An Investigation of the acoustic properties of vibrating finite cylinders using the boundary element method," Ph.D dissertation, University of Waterloo (1986).
 - 1.17. **A. F. SEYBERT**, "Review of the boundary element method in acoustics," Noise Control Foundation, New York, NY, USA 2532, 25-32 (1991).
 - 1.18. **H. A. SCHENCK**, "Improved integral formulation for acoustic radiation problems", Journal of the Acoustical Society of America **44**, 41-58 (1967).
 - 1.19. **L. G. COPLEY**, "Fundamental results concerning integral representations in acoustic radiation", Journal of the Acoustical Society of America **44**, 28-32 (1968).
 - 1.20. **A. J. BURTON and G. F. MILLER**, "The application of integral equation methods to the numerical solution of some exterior boundary value problems", Proceedings of the Royal Society of London **A323**, 201-210 (1971).
 - 1.21. **A. BAYLISS, M. GUNZBURGER and E. TURKEL**, "Boundary conditions for the numerical solution of elliptic equations in exterior regions," ICASE Report No. 80/1, NASA Langley, 1980.
 - 1.22. **R. BOSSUT and J.-N. DECARPIGNY**, "Finite element modelling of radiating structures using dipolar damping elements," Journal of the Acoustical Society of America **86**, 1234-1244 (1989).
 - 1.23. **J. ASSAAD, J.-N. DECARPIGNY, C. BRUNEEL, R. BOSSUT and B. HAMONIC**, "Application of the finite element method to two-dimensional

- radiation problems," *Journal of the Acoustical Society of America* **94**, 562-573 (1993).
- 1.24. P. BETTESS and O. C. ZIENKIEWICZ, "Diffraction and refraction of surface waves using finite and infinite elements", *International Journal for Numerical Methods in Engineering* **11**, 1271-1290 (1977).
 - 1.25. P. BETTESS, "Infinite elements", *International Journal for Numerical Methods in Engineering* **11**, 53-64 (1977).
 - 1.26. P. BETTESS, "More on infinite elements", *International Journal for Numerical Methods in Engineering* **15**, 1613-1626 (1980).
 - 1.27. R. J. ASTLEY, J. P. COYETTE, G. J. MACAULAY, "Mapped wave envelope elements for acoustical radiation and scattering," *Journal of Sound and Vibration* **170**, 97-118 (1994).
 - 1.28. X. ZENG, L. F. KALLIVOKAS AND J. BIELAK, "Stable localized symmetric integral equation method for acoustic scattering problems," *Journal of the Acoustical Society of America* **91**, 2510-2518 (1992).

CHAPTER 2

A VARIABLE ORDER INFINITE ACOUSTIC WAVE ENVELOPE ELEMENT¹

2.1. INTRODUCTION

Infinite physical domains are commonly assumed when developing mathematical models for engineering problems, where the region to be analyzed is of very small dimensions compared to those of the surrounding medium. One example is the calculation of the acoustic properties of radiating bodies in an unbounded field.

In the past, these wave propagation problems have been analyzed by different numerical methods. Using the finite element (FEM) method, an obvious way to deal with an infinite domain is simply to truncate the finite element model at an arbitrary distance and to apply a suitable boundary condition, such as the Sommerfeld radiation condition [2.1,2.2], at the distant boundary. In general, this will yield a huge number of acoustic degrees of freedom, considering the acoustic finite element rule of thumb requirement of

¹A version of this chapter has been published in *Journal of Sound and Vibration* (1994) **171**(4), 483-508.

approximately seven nodes per wavelength. Other methods involve the matching of an analytical far field solution onto a finite element near field model, boundary element (BE) methods and so-called infinite element methods. A paper by Zienkiewicz, Bettess, Chiam and Emson [2.3] gives a concise overview of all these methods.

In recent years, much research effort has been put into the development of different boundary element formulations [2.3-2.6]. This formulation is well-suited to model infinite domains from a theoretical point of view, because it is inherently based on a boundary integral representation that takes into account the Sommerfeld radiation boundary condition. The related discrete boundary element method only requires a discretization of the sound radiating surface and enables one to solve, first, for the acoustic variables on the surface and, then, at an arbitrary field point using surface results. A disadvantage, from a practical point of view, is that the formulation yields full, complex system matrices which can lead to computer data storage problems, although the dimensionality of the problem has been reduced by the boundary element process. Another difficulty is the so-called non-uniqueness problem that occurs at certain critical frequencies. Different methods to overcome this problem have been suggested. Some of these are inexpensive [2.7], but require the appropriate selection of over-determination points, while others are more reliable, but tend to be computationally costly [2.8].

Simultaneously, research has been done to try to accommodate the infinite boundary within finite element analysis [2.1,2.2,2.9-2.20]. The idea is to model the acoustic near field, i.e., the immediate surroundings of the radiating body, by conventional finite elements (CFE) and to match a single layer of special elements, which stretch out to infinity, to model the acoustic far field. The radiation condition not only requires zero acoustic pressure conditions at large distances, but also the existence of outgoing travelling waves exclusively, such that all acoustic energy is radiated outward. Therefore, an appropriate asymptotic amplitude decay and wavelike variation has to be incorporated within the infinite element. Different strategies have been used in an attempt to extend the finite element method (FEM) in this way. Both exponential and reciprocal decaying shape functions have been adopted in conjunction with a wavelike variation $\exp(-ikr)$. In all these infinite element formulations, special numerical integration techniques, other than

the conveniently used Gauss-Legendre quadrature formulae, have to be used in order to deal with the complex exponential in the integrand of the system matrices. These infinite elements do not introduce a large number of acoustic degrees of freedom, and can easily be incorporated in a standard finite element program by matching the infinite element mesh, modelling the acoustic far field, onto the conventional finite element mesh, modelling the acoustic near field.

Recently, a new infinite wave envelope element has been developed by Astley and Coyette [2.21]. A finite to infinite geometry mapping is used in combination with a reciprocal decaying wavelike variation in the shape function, along with the wave envelope approach [2.22-2.29] in a modified Galerkin weighted residual procedure for evaluating the system matrices. This involves the choice of the complex conjugate of the shape function as the weighting function, which eliminates the complex exponential factors in the integrands, resulting in simple integration of the acoustic mass, stiffness and damping matrices. They also suggested the use of a geometric weighting factor ($\sim 1/r^2$) to make sure that all integrals in calculating the system contributions are finite. With these modifications, the symmetry of the element matrices is lost, but the banded nature of the global system matrices is preserved due to the element connectivity.

The element developed in this chapter uses the latter infinite wave envelope element as a basis. Because of the finite to infinite geometry mapping present in the infinite wave envelope element derivation, an n^{th} order polynomial in the parent finite element will yield an expansion of the form $a_1/r + a_2/r^2 + \dots + a_n/r^n$ in the radial infinite direction of the real infinite element. This created the idea of a powerful element for modelling acoustic radiation. By the use of Lagrangian polynomials as shape functions in the parent element, an arbitrary number of terms in the $1/r$ expansion can be generated for modelling the amplitude decay of the outgoing travelling wave. The implementation of the element as such allows a flexible choice in the number of acoustic degrees of freedom in the radial infinite direction. The infinite wave envelope elements, discussed above, require several layers of conventional finite elements for appropriate modelling of the acoustic near field. The move to higher order elements however, will allow the

infinite wave envelope element to model the acoustic near field better, and, in some cases, the need for conventional finite elements is totally eliminated.

In the following, the formulation and implementation of the variable order infinite wave envelope element (LWE; where L denotes a linear discretization in the angular direction of the element) will be presented. Results of different acoustic radiation and scattering problems, both two-dimensional and axisymmetric, will be shown and compared with boundary element and, if possible, with analytical solutions.

2.2. THEORY

2.2.1. GOVERNING EQUATIONS AND BOUNDARY CONDITIONS

The acoustic pressure field generated by a rigid vibrating body in an infinite domain can be described by the classical linear acoustic wave equation, given as

$$\nabla^2 p(\underline{x}, t) = \frac{1}{c^2} \frac{\partial^2 p(\underline{x}, t)}{\partial t^2} \quad \underline{x} \in V \quad (2.1)$$

where $p(\underline{x}, t)$ denotes the acoustic pressure and c the speed of sound in the acoustic medium. If only harmonic steady-state conditions are considered, the pressure $p(\underline{x}, t)$ can be written as $p(\underline{x}, t) = p(\underline{x}) e^{i\omega t}$, where ω is the circular frequency. Substitution into the classical wave equation (Equation (2.1)) yields the Helmholtz equation

$$\nabla^2 p(\underline{x}) + k^2 p(\underline{x}) = 0 \quad \underline{x} \in V \quad (2.2)$$

where $k = \omega / c$ is the acoustic wave number.

Suitable boundary conditions include prescribed acoustic pressure, velocity or acoustic impedance on the surface S_0 of the body and a radiation condition at a surface at infinity S_∞ (Figure 2.1). For example, a commonly applied prescribed velocity profile on the radiating body is given as

$$\nabla p \cdot \underline{n}_o = -i \rho \omega \overline{v}_n \quad \underline{x} \in S_o \quad (2.3)$$

where \underline{n}_o is the unit normal on the surface S_o , ρ the density of the acoustic medium and \overline{v}_n the prescribed normal surface velocity.

An appropriate radiation condition is given by the Sommerfeld radiation condition,

$$\lim_{r \rightarrow \infty} r^\alpha \left(\frac{\partial p}{\partial r} + i k p \right) = 0 \quad (2.4)$$

where $\alpha = 1$ for three-dimensional and $\alpha = 1/2$ for two-dimensional problems, simulating an unbounded acoustic field (r is the radial coordinate). This is equivalent to stipulating the pc-impedance condition at a boundary at infinity,

$$\nabla p \cdot \underline{n}_\infty = -i k p \quad \underline{x} \in S_\infty \quad (2.5)$$

prescribing outward travelling plane waves at infinity.

2.2.2. WEIGHTED RESIDUAL FORMULATION

Application of the weighted residual formulation to the Helmholtz equation, as given in detail in Appendix 2-A, yields

$$\int_V \nabla W_i \cdot \nabla p' dV - \omega^2 \int_V \frac{1}{c^2} W_i p' dV - \int_S W_i \frac{\partial p'}{\partial n} dS = 0 \quad (2.6)$$

where p' denotes a trial function for the acoustic pressure and W_i a weighting function. In general, the surface integral in Equation (2.5) consists of two parts, one on the radiating body and one on a surface at infinity. This is depicted as

$$\int_S W_i \frac{\partial p'}{\partial n} dS = \int_{S_o} W_i \frac{\partial p'}{\partial n} dS + \int_{S_\infty} W_i \frac{\partial p'}{\partial n} dS \quad (2.7)$$

By applying the boundary conditions of Equation (2.3) and (2.5), we can write

$$\int_S W_i \frac{\partial p'}{\partial n} dS = -i\omega \int_{S_0} \rho W_i \bar{v}_n dS - i\omega \int_{S_0} \frac{1}{c} W_i p' dS \quad (2.8)$$

Since $p' \rightarrow 0$, as $S_0 \rightarrow \infty$, will be prescribed by a suitable choice of shape functions, the damping term in Equation (2.8) at S_0 will vanish. As a result, a set of simultaneous equations can be formulated in the form

$$[[K] - \omega^2 [M]] \{p\} = \{F\} \quad (2.9)$$

where related coefficients are given as

$$K_{ij} = \int_V \nabla W_i \cdot \nabla N_j dV \quad (2.10)$$

$$M_{ij} = \int_V \frac{1}{c^2} W_i N_j dV \quad (2.11)$$

$$F_i = -i\omega \int_{S_0} \rho W_i \bar{v}_n dS \quad (2.12)$$

In Equation (2.9), $[K]$ and $[M]$ are the acoustic stiffness and mass matrices. $\{F\}$ is the acoustic forcing vector corresponding to the prescribed velocity input on the sound radiating body, while $\{p\}$ are the unknown nodal pressure values to be solved for.

2.2.3. VARIABLE ORDER INFINITE WAVE ENVELOPE ELEMENT

The variable order infinite wave envelope element is based on the infinite wave envelope element developed by Astley and Coyette [2.21]. The formulation of the element involves three main aspects that will be discussed individually, i.e., the infinite geometry mapping, the special shape functions and the weighting functions, followed by the actual derivation of the element system matrices. Only the formulation of a two-dimensional and axisymmetric element is presented in this chapter. Implementation of a three-dimensional element is conceptually the same.

2.2.3.1. Infinite geometry mapping

The infinite geometry mapping can be best explained by observing the one-dimensional case. The mapping is obtained from the general *one* to *one* transformation

$$x(t) = c_1 + \frac{c_2}{1 - t} \quad (2.13)$$

with

$$\begin{aligned} t = -1 &\rightarrow x = x_I \\ t = 0 &\rightarrow x = x_{II} \end{aligned} \quad (2.14)$$

These conditions define the coefficients c_1 and c_2 in Equation (2.13). The infinite domain of the element is mapped onto a unit parent element by this infinite geometry mapping, as illustrated in Figure 2.2 [2.14]. The element mapping is completely defined once the position of node 1, x_I , at the finite-infinite boundary interface, and node 2, x_{II} , are specified. The position of this node 2, x_{II} , sets the parameter x_0 , defined by

$$x_0 = 2x_I - x_{II} \quad (2.15)$$

and is the pole of the inverse transformation, which will also be referred to as the source.

The mapping of local to global coordinates can then be written as

$$x(t) = \sum_{i=1}^n M_i(t) x_i \quad (2.16)$$

with the mapping functions M_i defined as

$$\begin{aligned} M_I(t) &= \frac{-2t}{1-t} \\ M_{II}(t) &= \frac{1+t}{1-t} \end{aligned} \quad (2.17)$$

Independency of the choice of origin of the coordinate system is preserved, given that

$$M_I(t) + M_{II}(t) = 1 \quad (2.18)$$

Solving for t in Equation (2.16) gives the inverse mapping

$$t = 1 - 2 \frac{a}{r} \quad (2.19)$$

where $a = x_{II} - x_I = x_I - x_0$. The parameter a denotes the distance from the source to the finite boundary of the element, while r is the distance to an arbitrary point in the element from the source at x_0 . On examining these mapping functions, it is apparent that the local coordinates $t = -1, 0, +1$ correspond to the global coordinates $x = x_I, x_{II}, \infty$, respectively.

This infinite geometry mapping can readily be extended to two- and three-dimensional geometries. The infinite mapping in the radial infinite direction, as in the one-dimensional geometry above, is combined with a linear mapping in the angular finite direction, as shown in Figure 2.3. The mapping functions are obtained by multiplying the respective shape functions, yielding [2.14]

$$\begin{aligned} M_I(s,t) &= \frac{-t(1+s)}{1-t} & M_{III}(s,t) &= \frac{(1+t)(1-s)}{2(1-t)} \\ M_{II}(s,t) &= \frac{-t(1-s)}{1-t} & M_N(s,t) &= \frac{(1+t)(1+s)}{2(1-t)} \end{aligned} \quad (2.20)$$

The mapping from local to global coordinates can then be written as

$$x(s,t) = \sum_{i=I}^{IV} M_i(s,t) x_i \quad y(s,t) = \sum_{i=I}^{IV} M_i(s,t) y_i \quad (2.21)$$

The domain of the two-dimensional infinite element is, thus, defined by the position of the four geometry nodes (I to IV), as shown in Figure 2.3. Care must be taken in defining these four geometry nodes, such that the radial infinite edges (1 and 2 as in Figure 2.3) are divergent. From a mathematical point of view, these radial diverging edges ensure that uniqueness of the infinite geometry mapping is preserved. But, moreover, it is apparent that, from the physics of the problem, the geometry of the element should agree with the ray paths and constant phase surfaces of the solution.

Note that independency of the origin of the coordinate system is preserved, i.e.,

$$\sum_{i=I}^{IV} M_i(s,t) = 1 \quad (2.22)$$

and that the inverse infinite mapping along each infinite edge is again of the form

$$t = 1 - 2 \frac{a_i}{r} \quad (2.23)$$

2.2.3.2. Shape functions

The shape functions of the infinite wave envelope element involve both the modelling of an appropriate amplitude decay and a wavelike variation of the field variable p .

A. Amplitude decay

The geometry mapping, discussed in Section 2.2.3.1., can also be applied to the modelling of the field variable p . An interpolation, using standard finite element polynomial shape functions of the pressure p in the parent element, will yield a $1/r^n$ expansion in the real element, as a result of the infinite geometry mapping. This can easily be shown by considering a one-dimensional example, as in Figure 2.4.

In the local three-noded element, the field variable is interpolated using second order shape functions, which gives

$$p = \sum_{i=1}^3 N_i p_i = \frac{t(t-1)}{2} p_1 + (1-t^2) p_2 + \frac{t(t+1)}{2} p_3 \quad (2.24)$$

The inverse infinite geometry mapping for this one-dimensional case is given in Equation (2.19). Therefore, substituting Equation (2.19) into Equation (2.24) yields an expansion of the pressure p in terms of the global coordinate r , resulting in

$$p = p_3 + (-p_1 + 4p_2 - 3p_3) \frac{a}{r} + (2p_1 - 4p_2 + 2p_3) \frac{a^2}{r^2} \quad (2.25)$$

It is seen that the value of the pressure p asymptotically approaches the nodal value of node 3, p_3 , which is mapped to infinity. Note the importance that the source location, specified by the distance a , has on the rate of decay of the field variable p . It represents the pole of the reciprocal expansion, used in modelling the amplitude decay of the outgoing travelling wave. From a physical point of view, it can thus be interpreted as its acoustic source.

The boundary condition of the problem at hand stipulates a zero pressure value at infinity. This can be satisfied by only including the contributions by the finite nodes in Equation (2.24) or (2.25), i.e., nodes 1 and 2. In general, for an n^{th} order approximation, only the contributions of the n finite nodes will be considered through their respective shape functions, which all tend to zero at infinity. The value of the $n+1^{\text{th}}$ node, at infinity, is assumed to be zero.

An n^{th} order polynomial approximation of the pressure p , using n degrees of freedom, in the parent element will yield an expansion of the form $1/r^n$ in the real element, as in

$$\begin{aligned} & a_0 + a_1 t + a_2 t^2 + \dots + a_n t^n \\ & \quad \quad \quad \uparrow \\ & b_1 \left(\frac{1}{r} \right) + b_2 \left(\frac{1}{r} \right)^2 + \dots + b_n \left(\frac{1}{r} \right)^n \end{aligned} \quad (2.26)$$

Therefore, in using n^{th} order polynomial shape functions in the radial infinite r direction of the element, an appropriate amplitude decay for the field variable p can be achieved.

A flexible way for specifying an n^{th} order polynomial in the parent element is through the use of Lagrangian polynomials. The n^{th} order Lagrangian polynomial is determined by n acoustic nodes equally spaced between the finite geometry nodes, as shown in Figures 2.3 and 2.5. The $n+1^{\text{th}}$ acoustic node at infinity is prescribed to zero. The n shape functions in the radial infinite r direction can therefore be written as

$$T_i^n(t) = \frac{\pi(t)}{\pi'(t_i) (t-t_i)} \quad 1 \leq i \leq n \quad (2.27)$$

with

$$\pi(t) = \prod_{i=1}^{n+1} (t-t_i) \quad (2.28)$$

By using the local mapping $t = t_1 + \tau h = \tau / (n-1) - 1$ as in Figure 2.5, where $h = 1/(n-1)$ and $t_1 = -1$, the radial shape functions can be rewritten in the form,

$$\begin{aligned} T_i^n(\tau) &= C_i^n \tau(\tau-1)(\tau-2) \dots (\tau-(i-2))(\tau-i) \dots (\tau-(n-1))(\tau-2(n-1)) \\ &= C_i^n \left(\prod_{\substack{j=0 \\ j \neq i-1}}^{n-1} (\tau-j) \right) (\tau-2(n-1)) \end{aligned} \quad (2.29)$$

with,

$$C_i^n = \frac{(-1)^{n-i}}{(i-1)! (n-i)! (i-2n+1)} \quad (2.30)$$

The radial shape functions for the fifth order element are shown in Figure 2.5. Again, it should be noted that the shape function for the $n+1^{th}$ node at infinity, i.e., node 6, is not considered, since its nodal value is prescribed to be zero.

As previously mentioned, the use of these radial shape functions in the parent element yields a $1/r$ expansion in the real element, which is a suitable amplitude decay modelling for three-dimensional and axisymmetric acoustic wave propagation problems. In two-dimensional problems however, the amplitude decays approximately as $1/\sqrt{r}$. This can be shown by observing the monopole solution to the Helmholtz equation (Equation (2.2)), i.e., the zeroth order Hankel function of the second kind $H_0^{(2)}(kr)$, with wave number k and radial coordinate r , for large values of r . It can be shown that [2.4,2.19]

$$\lim_{r \rightarrow \infty} H_0^{(2)}(kr) \sim \frac{1}{\sqrt{r}} e^{-ikr} \quad (2.31)$$

Therefore, an appropriate shape function for two-dimensional problems can be achieved by multiplying the radial shape functions T_i^n by a \sqrt{r} factor, in order to achieve a $1/\sqrt{r}$ expansion. This is equivalent to a $\sqrt{(1-t_i)/(1-t)}$ factor in the parent element. For the two-dimensional radial shape functions we obtain

$$\begin{aligned} T_i^{n,2D}(\tau) &= R_i^n(\tau) C_i^n \tau(\tau-1)(\tau-2) \dots (\tau-(i-2))(\tau-i) \dots (\tau-(n-1))(\tau-2(n-1)) \\ &= R_i^n(\tau) C_i^n \left(\prod_{j=i-1}^{n-1} (\tau-j) \right) (\tau-2(n-1)) \end{aligned} \quad (2.32)$$

with

$$R_i^n(\tau) = \sqrt{\frac{2(n-1)-(i-1)}{2(n-1)-\tau}} \quad (2.33)$$

Note that the \sqrt{r} factor is normalized in order to preserve a unit absolute value at the

acoustic node at hand.

The shape functions in the angular finite s direction are chosen to be linear, i.e.,

$$\begin{aligned} S_1(s) &= \frac{1+s}{2} \\ S_2(s) &= \frac{1-s}{2} \end{aligned} \quad (2.34)$$

depending on which edge (1 or 2) of the element the acoustic nodes are located at, as in Figure 2.3.

B. Wavelike variation

To account for the wavelike variation, a periodic component of the form $\exp(-ikr)$ is introduced into the shape function. One should note that in order to maintain compatibility between the shape functions of the conventional finite elements in the near field and the infinite wave envelope elements of the far field, the phase must be set to zero at the finite-infinite element interface at $t = -1$. The wavelike variation in local coordinates is, therefore,

$$e^{-ik(r-a)} = e^{-ik\mu(s,t)} = e^{-ika(s)\frac{1+t}{1-t}} \quad (2.35)$$

The phase function $\mu(s,t)$ in Equation (2.35) uses an interpolated source location $a(s)$, given by

$$a(s) = \frac{1+s}{2} a_1 + \frac{1-s}{2} a_2 \quad (2.36)$$

indicating that the outward travelling wave is emanating from a source, located in the near field, at a distance $a(s)$ away from the finite-infinite element interface, as shown in Figure 2.3.

Finally, combining the modelling of the amplitude decay and the wavelike

variation, the following form of shape function is obtained for the $2n$ acoustic degrees of freedom,

$$N_i^n(s,t) = T_i^n(t) S_1(s) e^{-ik\mu(s,t)} \quad 1 \leq i \leq n \quad (\text{edge1}) \quad (2.37)$$

$$N_{n+i}^n(s,t) = T_i^n(t) S_2(s) e^{-ik\mu(s,t)} \quad 1 \leq i \leq n \quad (\text{edge2}) \quad (2.38)$$

where the radial part T^n is either taken from Equation (2.29) for axisymmetric problems or Equation (2.32) for two-dimensional problems.

2.2.3.3. Weighting functions

In conventional finite element analysis, the shape functions are chosen as weighting functions in the weighted residual formulation, the so-called Galerkin method. The great advantage of this method is that symmetric system matrices are obtained. The Galerkin method in the formulation of the infinite elements yields complex exponentials in the integrands involved in the evaluation of the system matrices, which complicates the numerical integration a great deal. The conveniently used Gauss quadrature formulae are no longer applicable and special quadrature rules (Gauss-Laguerre for example) have to be used but require more sampling points.

The wave envelope approach uses the complex conjugate of the shape functions as weighting functions in a modified Galerkin procedure [2.21]. Due to this particular choice, the complex exponential factors in the integrands of the system matrix formulation will cancel out. Therefore, Gauss quadrature numerical integration can be used for the evaluation of the system matrices. It should be noted that the number of Gauss points will depend solely on the order of the interpolating polynomial of the shape function, and not on the wave number k of the travelling wave, since all harmonic spatial variations have been removed from the integrals.

In order to deal with the infinite diverging element geometry, Astley and Coyette [2.21] suggested the use of a $(a/r)^2$ geometric weighting factor to ensure finiteness of the integrals involved in the evaluation of the system matrices. This particular choice of

geometric weighting function is based on the observation that, for a three-dimensional element, the element domain, over which the residual is weighted, expands proportional to r^2 . The addition of this geometric weighting factor, therefore, provides a better balance between near and far field weighting.

The weighting functions for the modified Galerkin formulation can, therefore, be written as

$$W^n(s,t) = G_w(t) N^n(s,t) = G_w(t) T^n(t) S(s) e^{+ik\mu(s,t)} \quad (2.39)$$

where the geometric weighting factor in local coordinates is given by

$$G_w(t) = \left(\frac{1-t}{2}\right)^2 \quad \Rightarrow \quad G_w(\tau) = \left(1 - \frac{\tau}{2(n-1)}\right)^2 \quad (2.40)$$

2.2.3.4. Element system matrices

Based on Equation (2.10), the characteristic stiffness coefficient for a two-dimensional variable order infinite wave envelope element is

$$K_{ij}^e = \int_{-1}^1 \int_{-1}^1 \left\langle \frac{\partial W_i^n}{\partial s} \quad \frac{\partial W_j^n}{\partial t} \right\rangle [J^{-1}]^T [J^{-1}] \begin{bmatrix} \frac{\partial N_i^n}{\partial s} \\ \frac{\partial N_j^n}{\partial t} \end{bmatrix} \|J\| ds dt \quad (2.41)$$

where J denotes the Jacobian of the geometry transformation from global to local coordinates.

The local derivatives of the weighting and shape functions, respectively, defined in Equations (2.39), (2.37) and (2.38) can be worked out as follows

$$\frac{\partial W_i^n}{\partial s} = \left(G_w T_i^n \frac{dS_i}{ds} + ik G_w T_i^n S_i \frac{\partial \mu}{\partial s} \right) e^{+ik\mu} \quad (2.42)$$

$$\frac{\partial W^n_i}{\partial t} = \left(\frac{dG_w}{dt} T^n_i S_i + G_w \frac{dT^n_i}{dt} S_i + ik G_w T^n_i S_i \frac{\partial \mu}{\partial t} \right) e^{-ik\mu} \quad (2.43)$$

$$\frac{\partial N^n_j}{\partial s} = \left(T^n_j \frac{dS_j}{ds} - ik T^n_j S_j \frac{\partial \mu}{\partial s} \right) e^{-ik\mu} \quad (2.44)$$

$$\frac{\partial N^n_j}{\partial t} = \left(\frac{dT^n_j}{dt} S_j - ik T^n_j S_j \frac{\partial \mu}{\partial t} \right) e^{-ik\mu} \quad (2.45)$$

The derivatives in these equations can easily be evaluated. Appendix 2-B deals with the derivative of the radial part of the shape function. Substituting the expressions from Equations (2.42) to (2.45) into Equation (2.41) yields

$$\begin{aligned} [K_e] = \int_{-1}^1 \int_{-1}^1 & \left(G_w T^n_i \frac{dS_i}{ds} + ik G_w T^n_i S_i \frac{\partial \mu}{\partial s} - \frac{dG_w}{dt} T^n_i S_i + G_w \frac{dT^n_i}{dt} S_i + ik G_w T^n_i S_i \frac{\partial \mu}{\partial t} \right) \\ & \times [J^{-1}]^T [J^{-1}] \begin{bmatrix} T^n_j \frac{dS_j}{ds} - ik T^n_j S_j \frac{\partial \mu}{\partial s} \\ \frac{dT^n_j}{dt} S_j - ik T^n_j S_j \frac{\partial \mu}{\partial t} \end{bmatrix} \|J\| ds dt \end{aligned} \quad (2.46)$$

In a similar way, the characteristic mass coefficients of the variable order infinite wave envelope element can be determined as

$$M^e_{ij} = \int_{-1}^1 \int_{-1}^1 \frac{1}{c^2} \{ G_w T^n_i S_i \} [T^n_j S_j] \|J\| ds dt \quad (2.47)$$

based on Equation (2.11).

In both element matrices, the complex exponential has been removed from the integrand. Gauss quadrature numerical integration can be used. The element interpolation

functions consist of a linear variation in the finite angular direction and an n^{th} order variation in the infinite radial direction. $n+1$ Gauss-Legendre integration points are needed in the radial direction for convergence of the system matrix coefficients.

The element stiffness matrix, obtained through this modified Galerkin procedure, is no longer symmetric and has complex coefficients; although, after the element assembly, the sparsity of the global system matrices is preserved because of the element connectivity. A special sparse complex solver is used to take full advantage of this sparsity.

2.3. PRACTICAL IMPLEMENTATION

Infinite elements can easily be incorporated in a conventional finite element program. In the following, different aspects involved in the implementation of the variable order infinite wave envelope element will be explained, such as the use of geometry and acoustic node connectivity, the sparse full complex solver and the post-processing of the results.

2.3.1. ACOUSTIC NODE CONNECTIVITY

The variable order infinite wave envelope element is completely defined by its four geometry nodes and the specification of the order of the radial shape function. In order to have the flexibility of changing the order of the element while keeping the same initial geometry mesh, the acoustic node connectivity is determined within the program. Based on the geometry connectivity and the specified order n , acoustic degrees of freedom are inserted along the infinite edges between the geometry nodes *I* and *IV*, and *II* and *III*, as depicted in Figure 2.3. The strategy of this routine is as follows. The geometry connectivity, based on internal node numbering (i.e., 1 to # of nodes), is copied into the acoustic connectivity (i.e., all geometry nodes become acoustic nodes). Then, all geometry nodes that are on the finite-infinite element interface are determined (i.e., position *I* or *II*). For all these interface nodes, $n - 2$ acoustic degrees of freedom are

inserted along the infinite edge of the wave envelope element. The global dimension of the problem is updated by adding the total number of inserted acoustic degrees of freedom.

Note that this renumbering scheme is only required for subparametric infinite wave envelope elements, i.e., order higher than 2. Special cases involve the isoparametric second order infinite wave envelope element, in which case the geometry nodes coincide with the acoustic degrees of freedom, and the superparametric first order infinite wave envelope element, where only the geometry nodes at the finite-infinite element interface are taken to be acoustic degrees of freedom.

2.3.2. SPARSE SOLVER

As a result of the element formulation, the element stiffness matrix is no longer symmetric and consists of fully complex coefficients. The global system matrix, after assembly of all the element contributions, will therefore no longer have the familiar banded symmetric form, characteristic of finite element models. However, sparsity is preserved through the acoustic element connectivity.

Although a complex non-symmetric banded solver can be used for solving the system of equations, a special full complex solver has been chosen, i.e., the CSPSLV routine from the NSWCL library [2.33]. This solver only requires the storage of the non-zero elements of the matrix in a single complex one-dimensional array (Yale storage format). Two integer arrays are used to store the information regarding the position of the different non-zero elements in the original global matrix.

The use of this solver ensures minimal data storage requirements. Also, there is no longer concern about the size of the maximum bandwidth, which can quickly become large, due to the number of acoustic degrees of freedom connected in higher order elements.

2.3.3. POST-PROCESSING

Post-processing of the results includes contour line plots of the acoustic pressure, using a field point mesh of the field of interest, polar plots of the acoustic pressure at a certain radial distance from the sound radiating body and frequency response functions of the acoustic pressure at specific field points. The field point mesh for generating contour line plots is a linear grid of field points. Example meshes are shown later in Figures 2.10 and 2.22, which can be processed by a conventional FEM post-processor. In general, the discretization of the post-processing mesh will be much finer than the geometry mesh, in order to give a proper representation of the pressure field obtained by using the higher order infinite wave envelope elements. Care must be taken that all field points lie within the modelled acoustic domain.

Pressure values are assigned to these field points by determining the element of the acoustic finite element model within which limits they are located and by then interpolating among the acoustic degrees of freedom of that element, using the element shape functions. To determine whether or not a field point is situated within a certain element, the inverse geometry mapping is performed on the global coordinates of the field point, as explained in Appendix 2-C. If the field point lies in the element, the local coordinates will fall within the unit limits of the parent element (i.e. $-1 \leq s \leq 1$ and $-1 \leq t \leq 1$).

2.4. DISCUSSION OF RESULTS

In what follows, different examples of acoustic radiation and scattering from a rigid body are presented to illustrate the use of the variable order infinite wave envelope element. Both two-dimensional and axisymmetric models are used to calculate acoustic pressure fields generated by the radiation or scattering of an infinitely long cylinder or sphere. A two-dimensional model of scattering of an acoustic plane wave by a double barrier configuration is also investigated. Results are presented in the form of contour line plots of the pressure field, polar plots and frequency response functions. Numerical results

are compared with analytical (if available) or boundary element solutions. The boundary element calculations have been done using the direct/collocation option available in SYSNOISE software [2.4]. In all examples, the acoustic medium is air with density $\rho = 1.21 \text{ kg/m}^3$ and speed of sound $c = 340 \text{ m/s}$.

2.4.1. INFINITE CYLINDER

The acoustic field around an infinite cylinder of radius $R = 1$ is modelled using different geometry meshes, shown in Figures 2.6 to 2.9. All meshes assume symmetry with respect to the x -axis. The meshes differ in the choice of source location and whether or not conventional acoustic finite elements are used. It is apparent that the source, for the modelling of a vibrating cylinder or sphere, should be located at the centre for symmetry reasons. However, in general, the location of the source is not known. The sensitivity of the solution to changes in source location is therefore investigated. In order to easily compare numerical results, a single post-processing mesh is used, as shown in Figure 2.10. The effects of using higher order infinite wave envelope elements and their sensitivity to the geometry mesh, i.e., source location, is studied.

2.4.1.1. Analytical solutions

The analytical solutions for the pressure fields of two-dimensional monopole, dipole and quadrupole acoustic radiation are given in cylindrical coordinates as [2.30]

$$p(r, \theta) = -i \rho c \bar{V}_n \frac{H_n^{(2)}(kr)}{H_n^{(2)}(kR)} \cos(n\theta) \quad (2.48)$$

where $H_n^{(2)}$ is the n^{th} order cylindrical Hankel function of the second kind, and $n = 0, 1, 2$ for monopole, dipole and quadrupole radiation, respectively.

The corresponding normal velocity distribution on the vibrating surface of the infinite cylinder is

$$\overline{V}_n(\theta) = \overline{V}_n \cos(n\theta) \quad \overline{V}_n \ll R \quad (2.49)$$

where \overline{V}_n is the velocity amplitude.

The scattered acoustic pressure generated by the scattering of an acoustic plane wave $p_i(x) = P_0 \exp(-ikx)$, travelling along the symmetry axis (x-axis), by an infinite cylinder can be analytically evaluated as [2.30]

$$p_s(r, \theta) = -P_0 \sum_{n=0}^{\infty} \epsilon_n i^n \frac{J'_n(kR) H_n^{(2)}(kr)}{H_n^{(2)}(kR)} \cos(n\theta) \quad (2.50)$$

where J_n is the n^{th} order Bessel function of the first kind, ϵ_n is the Neumann function ($\epsilon_n = 1$ if $n = 0$ and $\epsilon_n = 2$ if $n > 0$), P_0 is the amplitude of the incident plane wave and θ is measured from the direction of the incoming plane wave. The summation converges rapidly and was truncated after ten terms for the results in this chapter.

2.4.1.2. Geometry mesh with exact source location

In Figure 2.6, the geometry mesh with exact source location is shown. Only infinite wave envelope elements are used for modelling the acoustic domain. The source location is located at the centre of the cylinder (the origin of the coordinate system) for symmetry reasons. All elements are therefore aligned radially. The discretization in the angular direction is directed by the classical rule of thumb of seven acoustic degrees of freedom per wavelength.

A. Acoustic radiation: dipole and quadrupole

The amplitude of the acoustic pressure field due to dipole and quadrupole radiation for $kR = \pi$ is shown in Figure 2.11. The acoustic wave number is chosen such that the diameter of the cylinder corresponds to exactly one wavelength. Normal velocity boundary conditions are imposed according to Equation (2.49), with $\overline{V}_n = 0.001$ m/s. Both pressure patterns can be accurately modelled using second order infinite wave

envelope elements. Only two degrees of freedom are needed in the radial direction, yielding two terms in the $1/\sqrt{r}$ expansion.

B. Acoustic scattering

Next, the modelling of scattering of an acoustic plane wave, travelling in the positive x-direction, by a rigid cylinder is considered. The scattered acoustic pressure field can be calculated by reformulating the problem as an equivalent radiation problem. The normal scattered velocities $\overline{v_{n_s}}$ on the surface of the body are prescribed, based on the normal component of the particle velocity $\overline{v_{n_i}}$ of the incident plane wave, such that the rigid body condition, $\overline{v_{n_t}} = \overline{v_{n_i}} + \overline{v_{n_s}} = 0$, of the total field is satisfied on the body. Contour lines of the amplitude of the scattered acoustic pressure field, normalized to the amplitude $P_0 = |P_i|$ of the incident plane wave, for $kR = \pi$ are shown in Figure 2.12. As can be seen from the comparison with the analytical solution, at least three degrees of freedom in the radial direction are needed to model the pressure pattern adequately.

2.4.1.3. Geometry mesh with combined use of conventional and infinite wave envelope elements

For the modelling of arbitrary geometries, the use of conventional finite elements (CFE) is required, due to the geometry restrictions of the infinite wave envelope element. In general, the acoustic medium between concave-shaped structures has to be modelled using conventional elements, such that a single layer of diverging infinite wave envelope elements can be matched onto it. In the following, the combined use of these elements is tested. The geometry mesh used, shown in Figure 2.7, consists of a single layer of infinite wave envelope elements matched on six layers of conventional acoustic finite elements. Again, the scattering of an acoustic plane wave from a rigid cylinder for $kR = \pi$ is modelled. Contour lines of the normalized amplitude of the scattered acoustic pressure field are shown in Figure 2.13. A third order infinite wave envelope element is needed to provide an accurate modelling. The use of lower order elements results in spurious

reflections into the near field, indicating an improper impedance match at the finite-infinite element interface.

2.4.1.4. Geometry mesh with random source location

In general, for an arbitrary sound-radiating body, the position of the acoustic source is not apparent. Therefore, sensitivity of the infinite wave envelope element to the source location is investigated. In this example, a geometry mesh is chosen with a single layer of infinite wave envelope elements, radially aligned through the origin (exact source), but with a random source location for each separate element, as shown in Figure 2.8. The acoustic scattered pressure fields of the normalized amplitude for $kR = \pi$, evaluated using second, third and fourth order infinite wave envelope elements, are shown in Figure 2.14. For this random source location, a fourth order infinite wave envelope element is necessary for adequate modelling of the scattered pressure field, whereas only a third order element was required for the exact source location.

2.4.1.5. Geometry mesh with shift of source location

The geometry mesh, shown in Figure 2.9, has a single acoustic source for all infinite wave envelope elements shifted half the radius in the positive x -direction from the exact source location at the origin. The amplitude of the acoustic pressure field is observed for quadrupole radiation for $kR = \pi$ and $\overline{V}_n = 0.001$ m/s. From the results, shown in Figure 2.15, it can be seen that the symmetry, destroyed by the geometry mesh, is gradually restored by going to higher order infinite wave envelope elements.

The results shown in Sections 2.4.1.4. and 2.4.1.5. indicate that the inaccuracy in acoustic source location can be accounted for by adding more acoustic degrees of freedom in the infinite radial direction of the infinite wave envelope element. A simple one-dimensional example, given in Appendix 2-D, shows a similar tendency.

2.4.2. SPHERE

The acoustic field around a rigid sphere of radius $R = 1$ is now considered, using an axisymmetric model. Both radiation and scattering problems are investigated.

2.4.2.1. Analytical solutions

The acoustic pressure generated by monopole radiation of a rigid sphere can be written analytically as

$$p(r) = \rho c \overline{V}_0 \left(\frac{R}{r} \right) \frac{ikR}{1 + ikR} e^{-ik(r-R)} \quad (2.51)$$

where \overline{V}_0 is the velocity amplitude.

The scattered acoustic pressure caused by the scattering of an acoustic plane wave, travelling along the symmetry axis (z -axis), by a rigid sphere can be analytically evaluated as [2.30]

$$p_s(r, \theta) = -P_0 \sum_{n=0}^{\infty} \frac{(2n+1) i^n P_n(\cos(\theta)) U_n(kR)}{kr [U_n(kR) + i V_n(kR)]} [S_n(kr) + i C_n(kr)] \quad (2.52)$$

where P_n is a Legendre polynomial of zeroth order and degree n . The Stenzel functions S_n , C_n , U_n and V_n in Equation (2.52) are defined as follows [2.30]

$$\begin{aligned} S_n(kr) &= \sqrt{\frac{\pi kr}{2}} J_{n+\frac{1}{2}}(kr) \\ C_n(kr) &= -\sqrt{\frac{\pi kr}{2}} N_{n+\frac{1}{2}}(kr) \end{aligned} \quad (2.53)$$

and

$$\begin{aligned} U_n(kr) &= kr S_{n+1}(kr) - n S_n(kr) \\ V_n(kr) &= kr C_{n+1}(kr) - n C_n(kr) \end{aligned} \quad (2.54)$$

where J_n and N_n are the n^{th} order Bessel function of the first and second kind, respectively. Again, the infinite series was truncated after ten to fifteen terms.

2.4.2.2. Geometry mesh with exact source location

A. Acoustic radiation: monopole

A frequency response function ($0 < kR < 6\pi$) for the amplitude of the acoustic pressure for a field point, at $r = 5R$, is shown in Figure 2.16. The axisymmetric geometry mesh used consists of a single layer of sixty variable order infinite wave envelope elements (LWE) with an exact acoustic source location. The infinite wave envelope solution is compared to the boundary element collocation method solution (60 linear BE). The latter shows the characteristic singularity problems at the critical frequencies, $kR = n\pi$ ($n = 1, 2, \dots$). The infinite wave envelope solution is obtained only using a first order element. This provides virtually the exact solution, since the required $1/r$ decay can be modelled. Note that no singularity problems are present for the infinite wave envelope element modelling.

B. Acoustic scattering

For the following results, an axisymmetric geometry mesh of thirty variable order infinite wave envelope elements is used with an exact acoustic source location at the origin. The scattering of an acoustic plane wave, travelling in the negative z -direction, from a rigid sphere is evaluated at different wave numbers, i.e., $kR = 1, 2, 4$ and 8 . Results are presented in the form of a polar plot of the normalized scattered pressure amplitude at $r = 5R$. From the comparison with the analytical solution, shown in Figures 2.17 to 2.20, it can be seen how the numerical solution improves by going to higher order elements. At least three to five acoustic degrees of freedom are needed in

the infinite radial direction to accurately model the scattered pressure pattern. The case of $kR = 8$ required an increased angular resolution of fifty variable order infinite wave envelope elements for appropriate modelling of the boundary conditions of the scattered acoustic pressure field.

2.4.3. SCATTERING BY A DOUBLE BARRIER

The last example presented consists of a two-dimensional configuration of two barriers of height $h = 0.3W$, a distance $W = 1$ apart. The geometry mesh used is shown in Figure 2.21 and the post-processing mesh in Figure 2.22. The geometry mesh consists of a single layer of thirty variable order infinite wave envelope elements, with their acoustic source located at the origin, matched on a conventional finite element mesh, modelling the concave region in between the two barriers. The two-dimensional scattering of an acoustic plane wave, travelling in the positive x -direction, is modelled at $kW = 3\pi$. Since no analytical solution is available for this type of problem, the infinite wave envelope element solution is compared with the boundary element collocation solution. The amplitude of the total acoustic pressure field is shown in Figure 2.23.

The numerical solution, obtained using the infinite wave envelope elements, gradually improves by going to higher order elements. The fifth order element modelling provides good comparison with the boundary element solution. Great calculation speed is observed for the infinite wave envelope modelling, being virtually five times faster than the boundary element solution (total solution and post-processing time). Even though the dimensionality of the infinite wave envelope element model is greater than that of the boundary element model, where only the boundary is being discretized, great speed advantage is obtained due to the sparsity of the element system matrices due to the global element connectivity.

2.5. CONCLUSIONS

The two-dimensional and axisymmetric formulation and implementation of a new

variable order infinite wave envelope element for acoustic radiation and scattering problems have been presented. The infinite geometry mapping, the special shape functions, modelling a reciprocal wavelike variation, and weighting functions, used in the wave envelope approach, have been discussed.

The geometry of the element is defined by the geometry nodes at the finite-infinite element interface and the location of the acoustic sources, resulting in a divergent infinite element domain. An arbitrary number of acoustic degrees of freedom can be specified on the radial infinite edges in order to accurately model the amplitude decay of the propagating acoustic waves.

Different two-dimensional and axisymmetric acoustic radiation and scattering problems have been presented to show the use and accuracy of the variable order infinite wave envelope element. Results were evaluated by comparing contour plots of acoustic pressure fields, polar plots and frequency response functions at specific field points with their analytical or boundary element solutions.

From the formulation of the element, it can be seen that the geometry of the element, i.e., the acoustic source location and the direction of the infinite edges, are of great importance. Ideally, the element geometry should correspond to the ray paths and constant phase surfaces of the solution. It was shown that uncertainty in the acoustic source location can be accounted for by using higher order elements. The addition of extra acoustic degrees of freedom allows an adequate modelling of the amplitude decay.

Conventional elements can be used for modelling the acoustic near field. A single layer of diverging infinite wave envelope elements is fitted onto the conventional finite element mesh. The order of the infinite wave envelope element has to be sufficiently high in order to avoid spurious reflections into the acoustic near field. The results of this work have shown that the use of higher order infinite wave envelope elements restricts the need for conventional elements to fill concave regions of the radiating or scattering body.

It is shown that the infinite wave envelope element method provides a great alternative for the boundary element method for modelling exterior acoustic problems. The non-uniqueness problems occurring at critical frequencies are non-existent in the infinite wave envelope problem. The method also shows a great calculation speed

advantage, due to sparsity of the system matrices, as opposed to the full, complex matrices involved in the boundary element formulation. Furthermore, the variable order infinite acoustic wave envelope element can be incorporated in a finite element scheme for elasto-acoustic coupling [2.31,2.32].

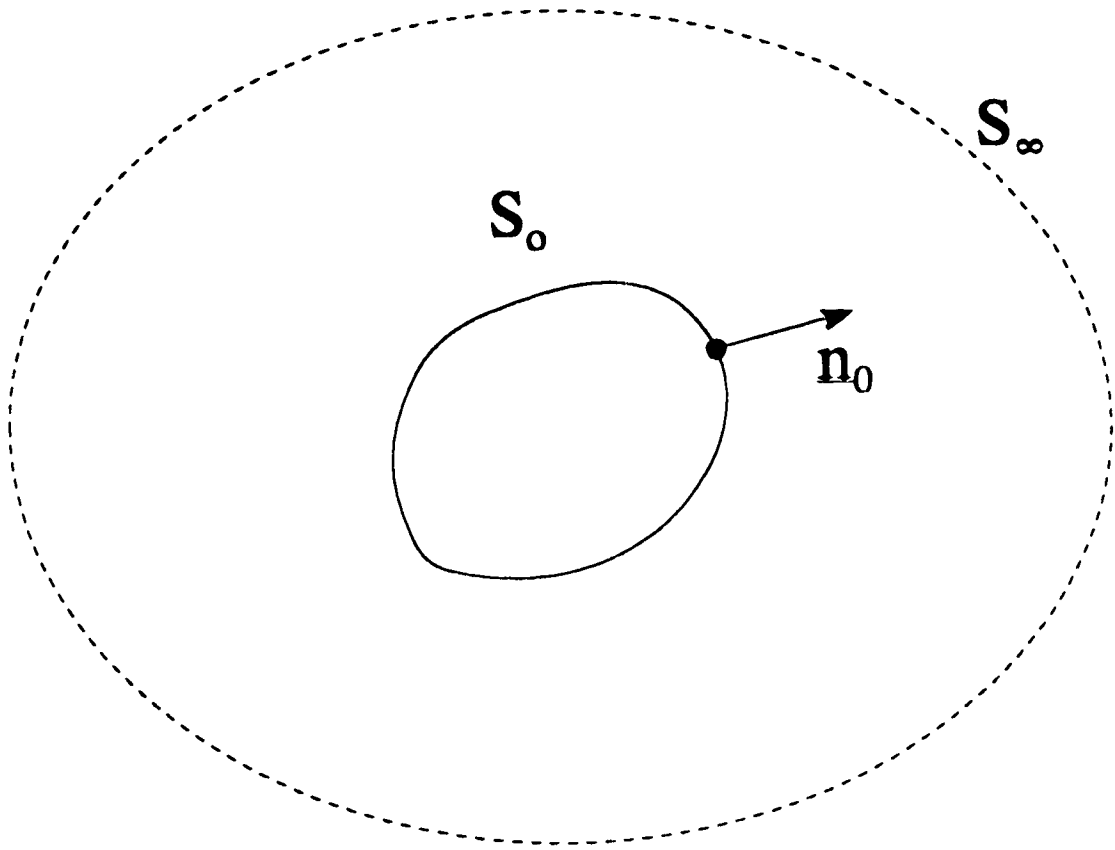


Figure 2.1 Radiating body in an infinite domain.

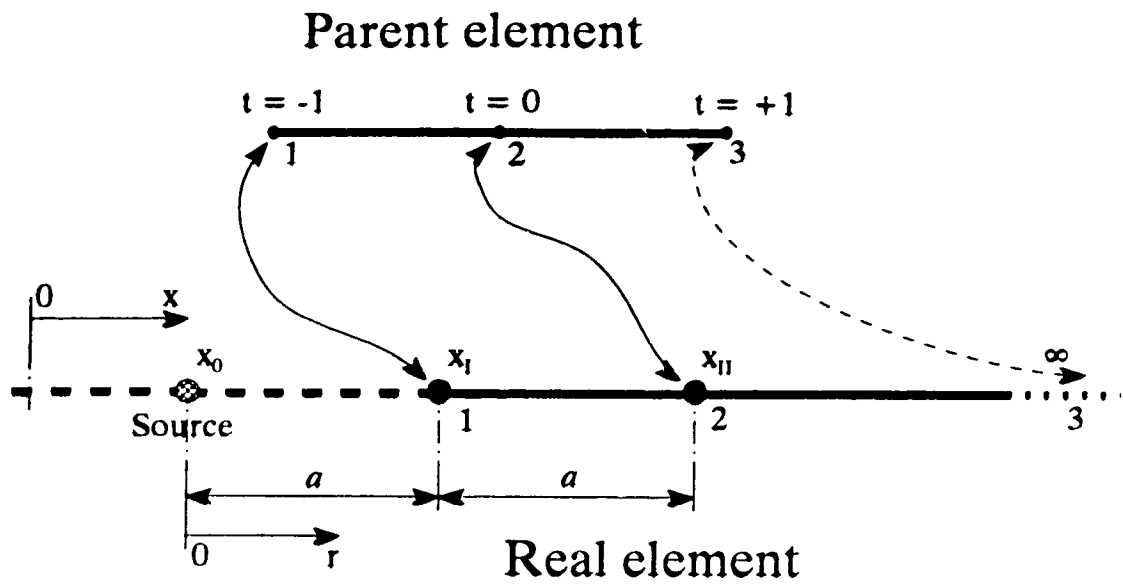


Figure 2.2 One-dimensional infinite geometry mapping.

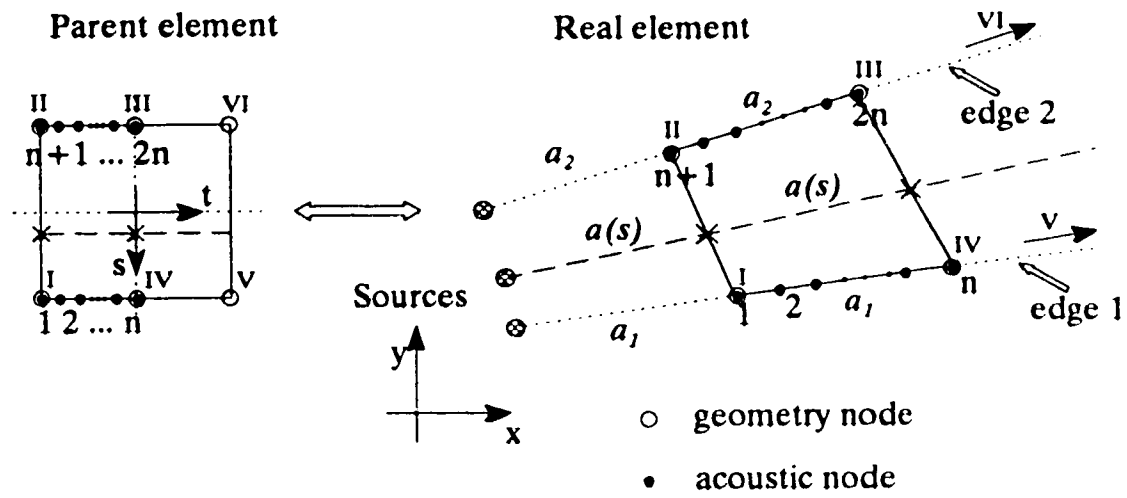


Figure 2.3 Two-dimensional infinite geometry mapping.

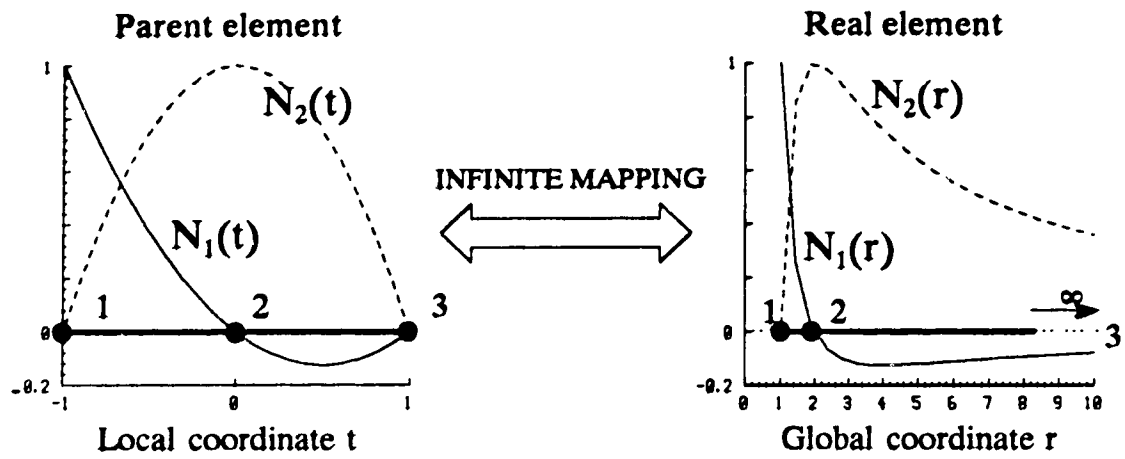


Figure 2.4 One-dimensional mapping of shape functions.

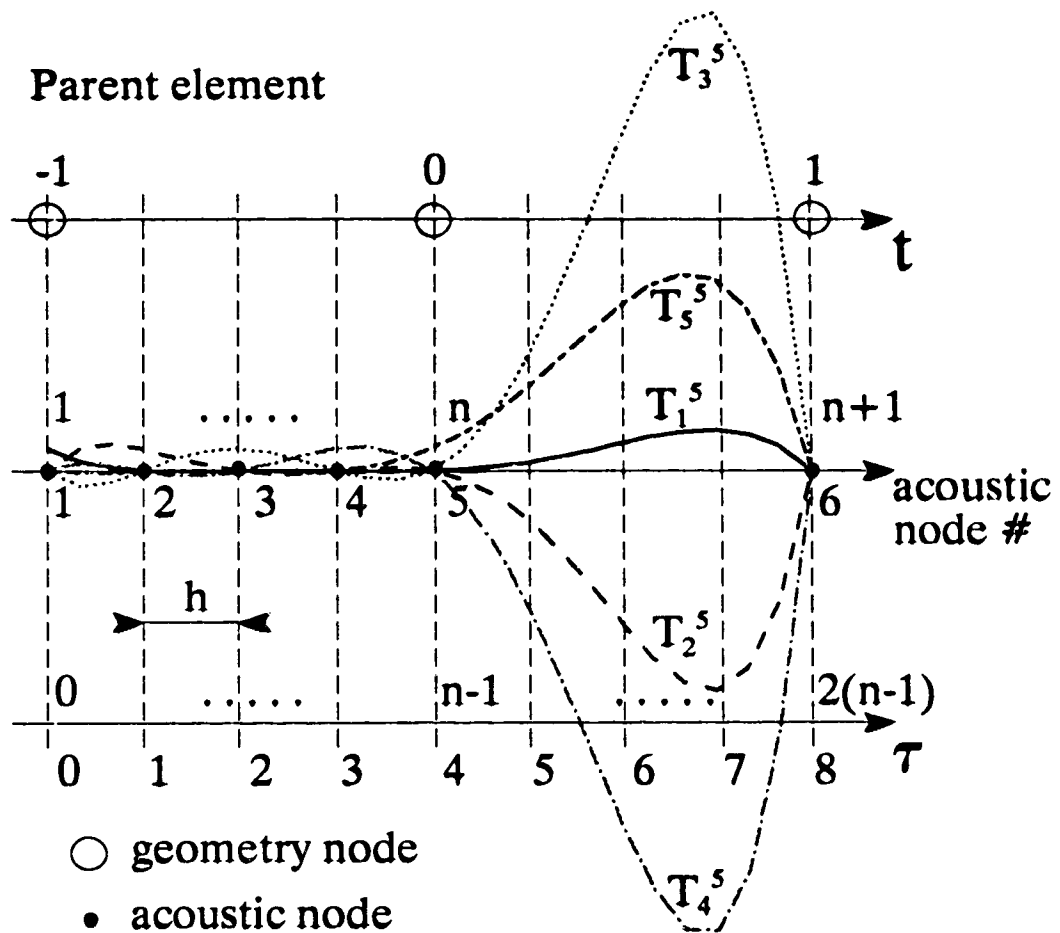


Figure 2.5 Lagrangian shape function.

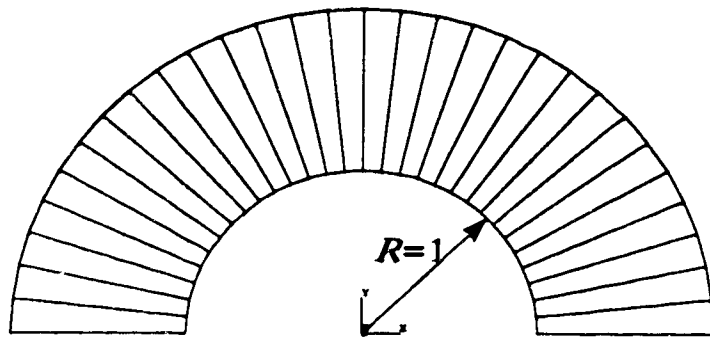


Figure 2.6 Cylinder: Two-dimensional geometry mesh (30 lwe).
Exact source at origin.

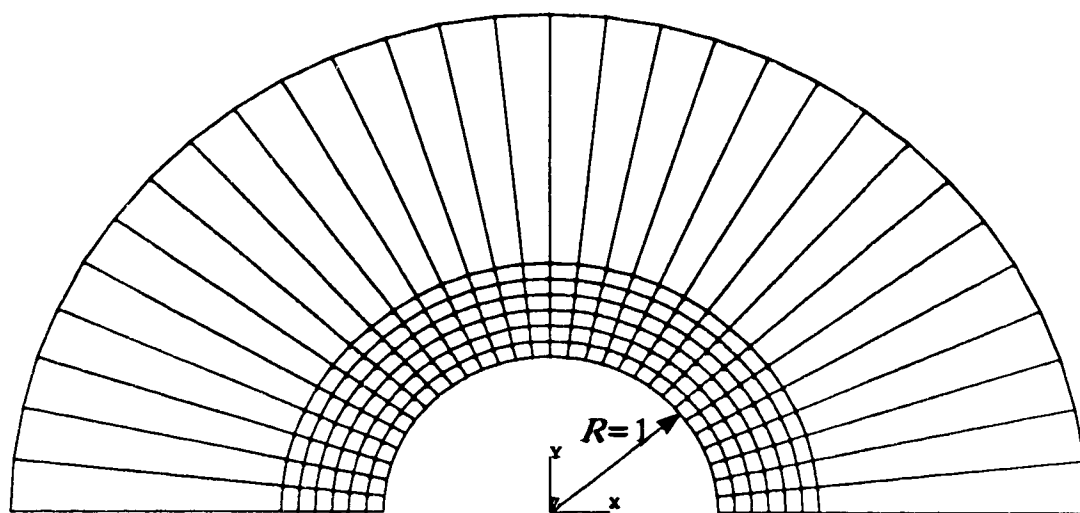


Figure 2.7 Cylinder: Two-dimensional geometry mesh (30 * (6 cfe + 1 lwe)).
Exact source at origin.

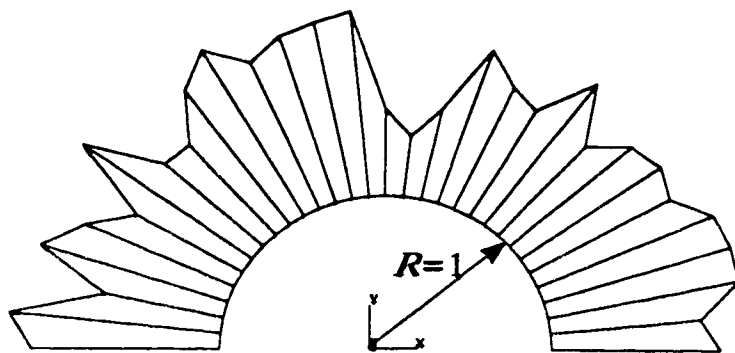


Figure 2.8 Cylinder: Two-dimensional geometry mesh (30 lwe).
Random source.

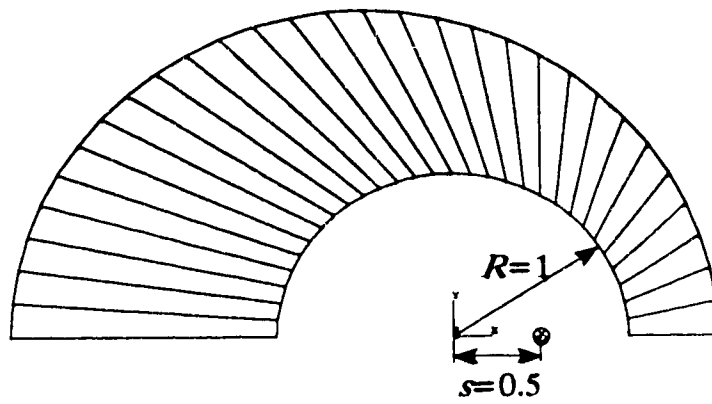


Figure 2.9 Cylinder: Two-dimensional geometry mesh (30 lwe).
Source shift.

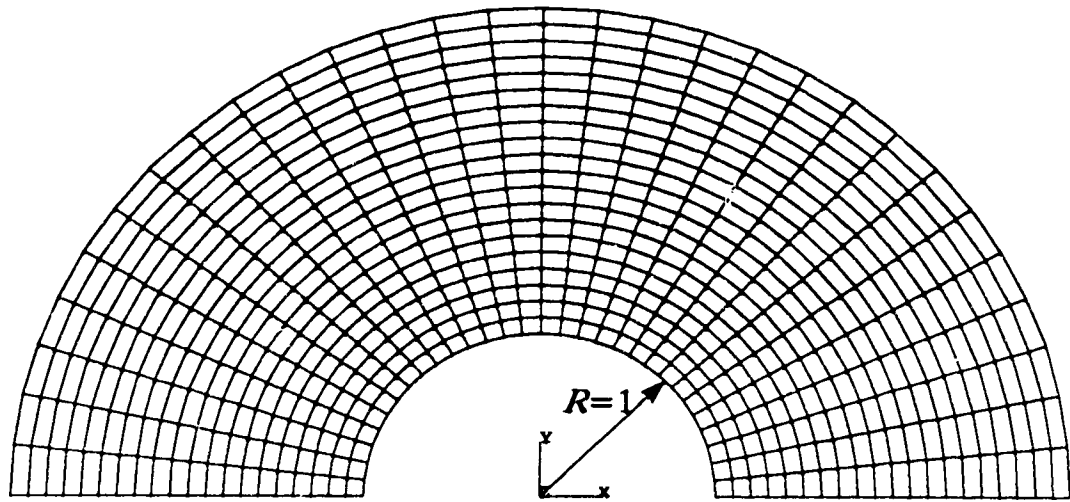


Figure 2.10 Cylinder: Two-dimensional post-processing mesh (630 field points).

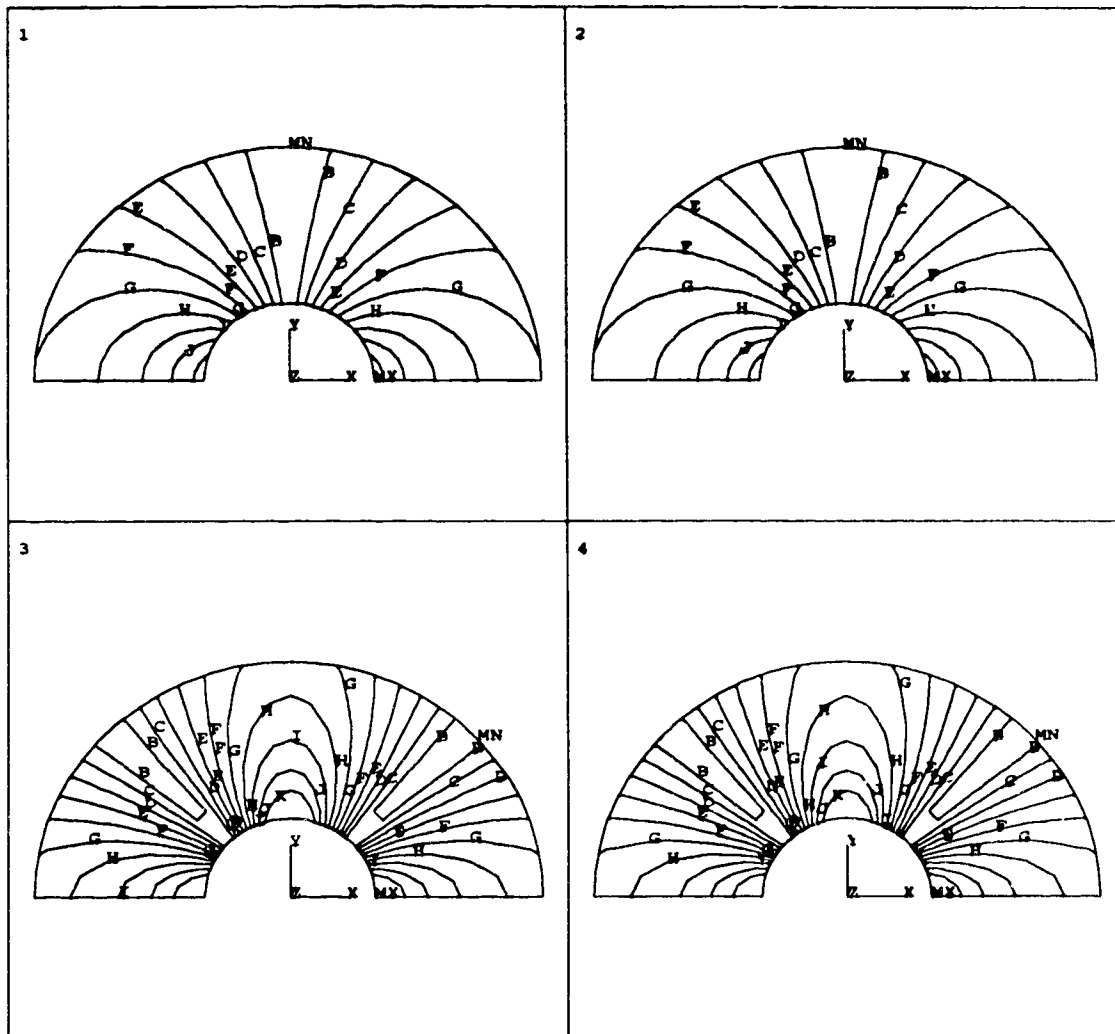


Figure 2.11 Acoustic radiation by a vibrating cylinder ($kR = \pi$).
 Contour lines of radiated acoustic pressure amplitude.
 1. Dipole - Analytical; 2. Dipole - 2nd order lwe; 3. Quadrupole -
 Analytical; 4. Quadrupole - 2nd order lwe
 (A=0 P=.04 C=.08 D=.12 E=.16 F=.20 G=.24 H=.28 I=.32 J=.36
 K=.40)

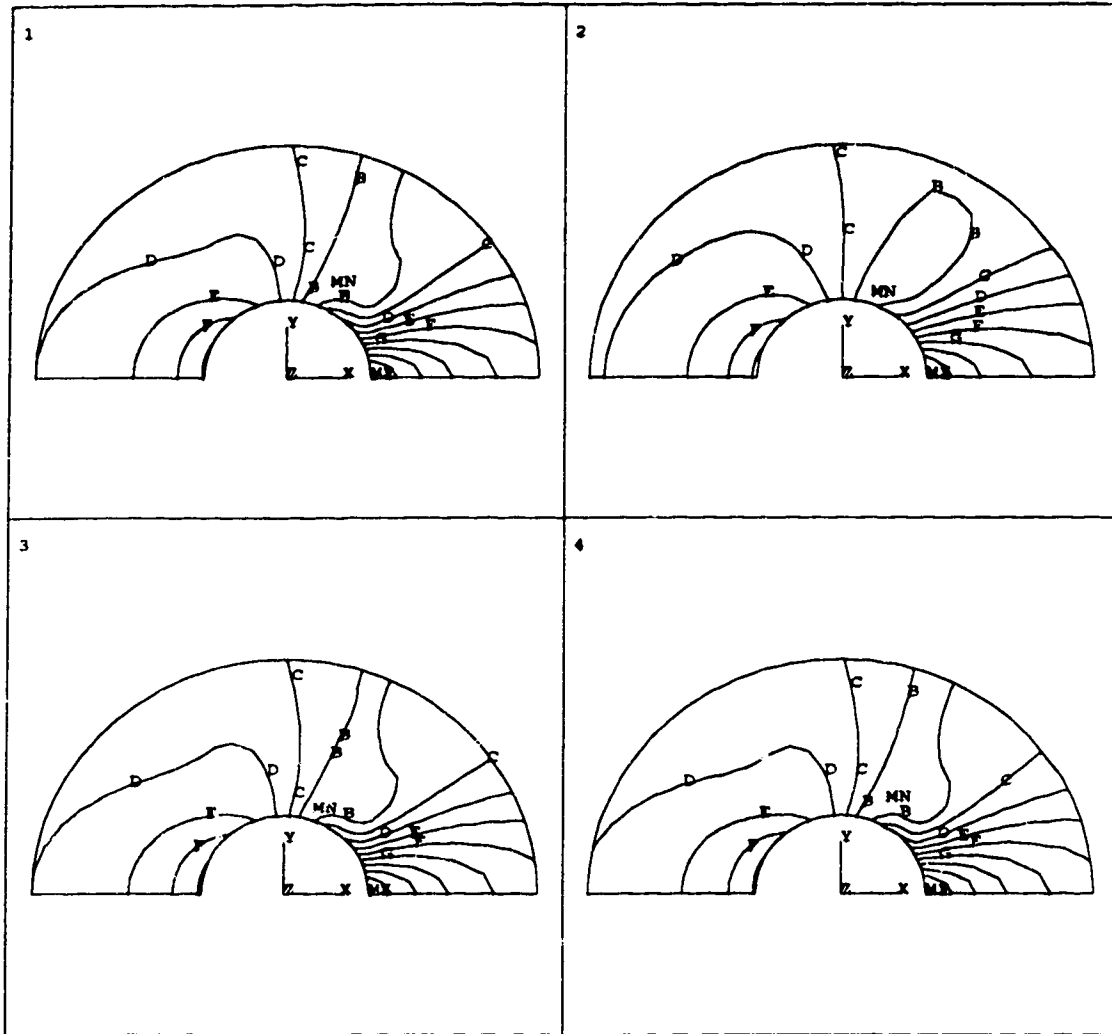


Figure 2.12 Scattering of an acoustic plane wave from a rigid cylinder ($kR = \pi$). Contour lines of scattered acoustic pressure amplitude $|P_s|/|P_i|$. Geometry mesh with exact source location.
 1. Analytical; 2. 2nd order lwe; 3. 3rd order lwe; 4. 4th order lwe
 (A=0 B=.15 C=.30 D=.45 E=.60 F=.75 G=.90 H=1.05 I=1.20 J=1.35 K=1.50)

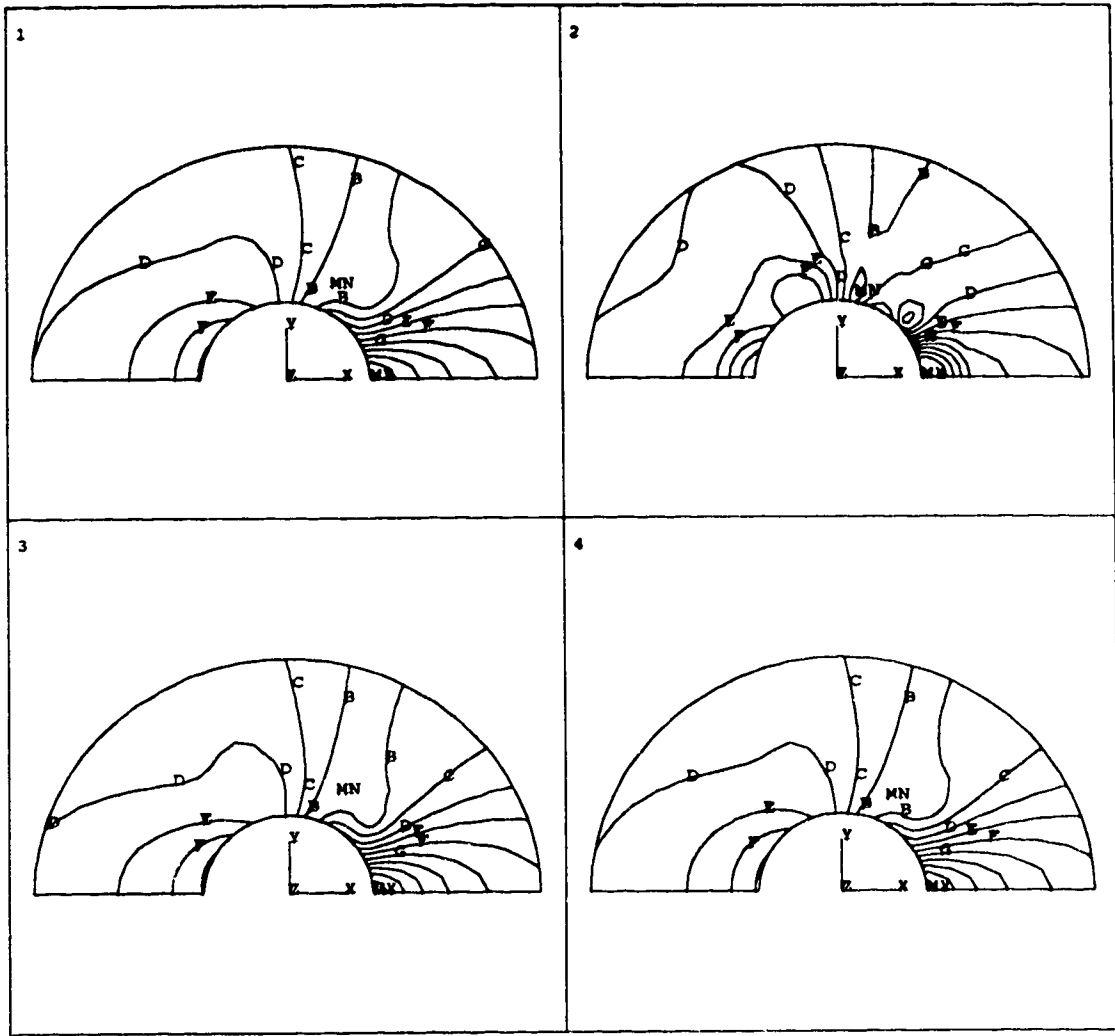


Figure 2.13 Scattering of an acoustic plane wave from a rigid cylinder ($kR = \pi$). Contour lines of scattered acoustic pressure amplitude $|P_s|/|P_i|$. Geometry mesh with combined use of conventional finite elements and infinite wave envelope elements.
 1. Analytical; 2. 1st order lwe; 3. 2nd order lwe 4. 3rd order lwe
 (A=0 B=.15 C=.30 D=.45 E=.60 F=.75 G=.90 H=1.05 I=1.20 J=1.35 K=1.50)

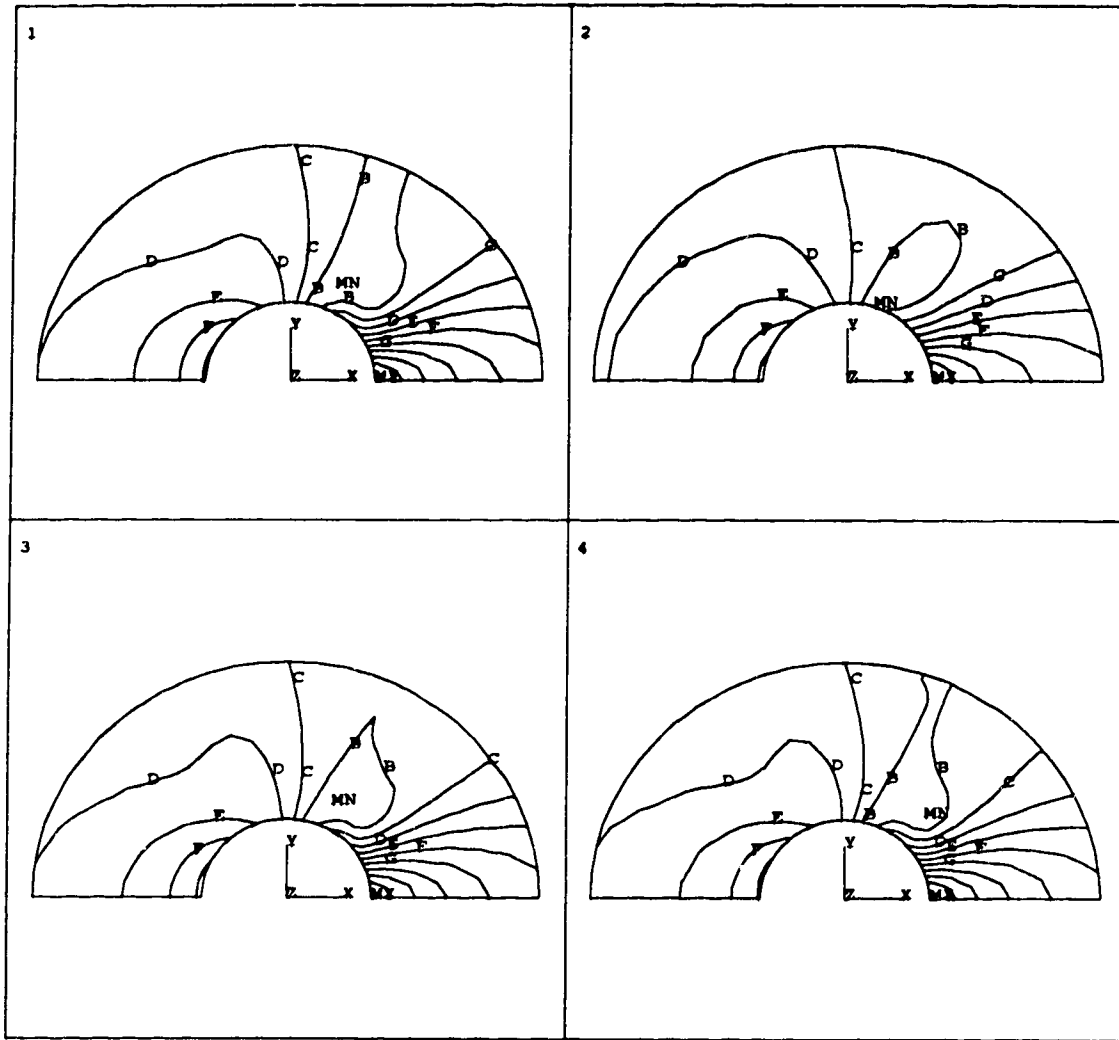


Figure 2.14 Scattering of an acoustic plane wave from a rigid cylinder ($kR = \pi$). Contour lines of scattered acoustic pressure amplitude $|P_s|/|P_i|$. Geometry mesh with random source location.
 1. Analytical; 2. 2nd order lwe; 3. 3rd order lwe; 4. 4th order lwe
 (A=0 B=.15 C=.30 D=.45 E=.60 F=.75 G=.90 H=1.05 I=1.20 J=1.35 K=1.50)

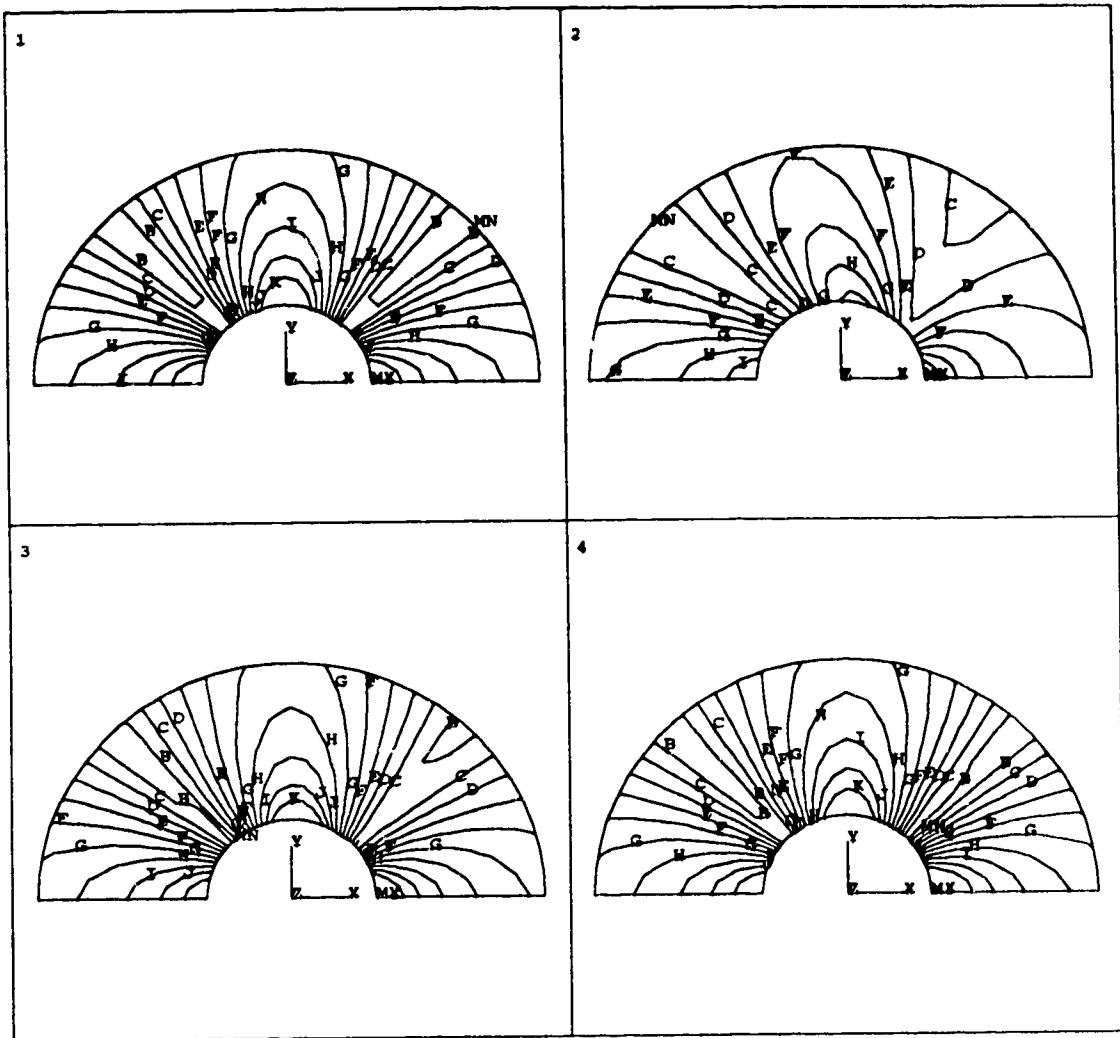


Figure 2.15 Acoustic quadrupole radiation by a vibrating cylinder ($kR = \pi$).
 Contour lines of radiated acoustic pressure amplitude.
 Geometry mesh with shift of source location.
 1. Analytical; 2. 1st order lwe; 3. 2nd order lwe; 4. 3rd order lwe
 ($A=0$ $B=.04$ $C=.08$ $D=.12$ $E=.16$ $F=.20$ $G=.24$ $H=.28$ $I=.32$ $J=.36$
 $K=.40$)

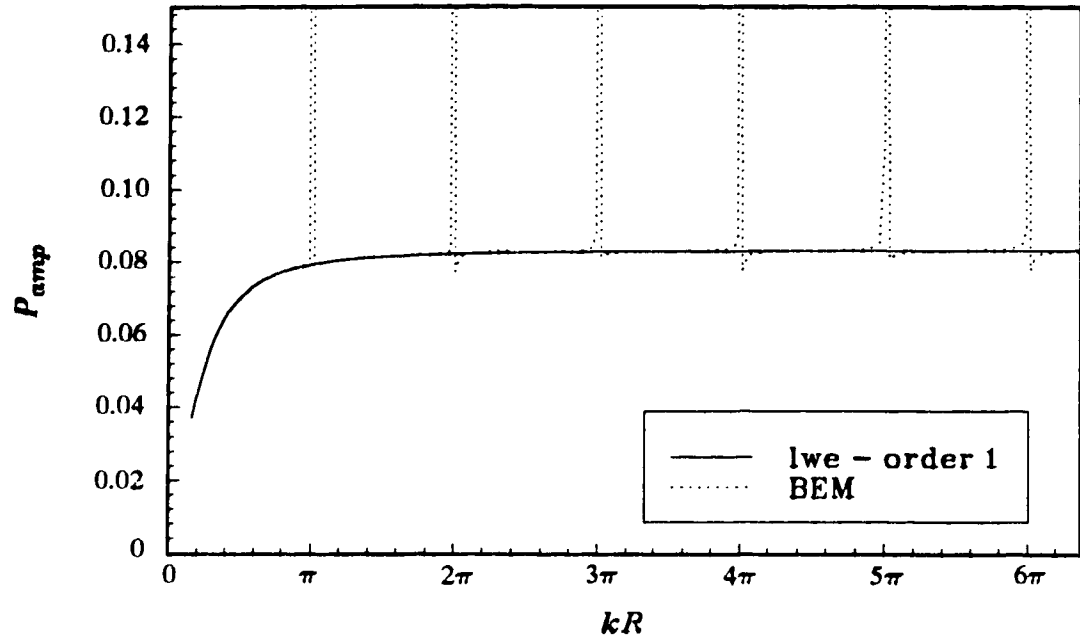


Figure 2.16 Acoustic radiation by a sphere - monopole.
Frequency response function of the amplitude of the radiated acoustic pressure at $r = 5R$.

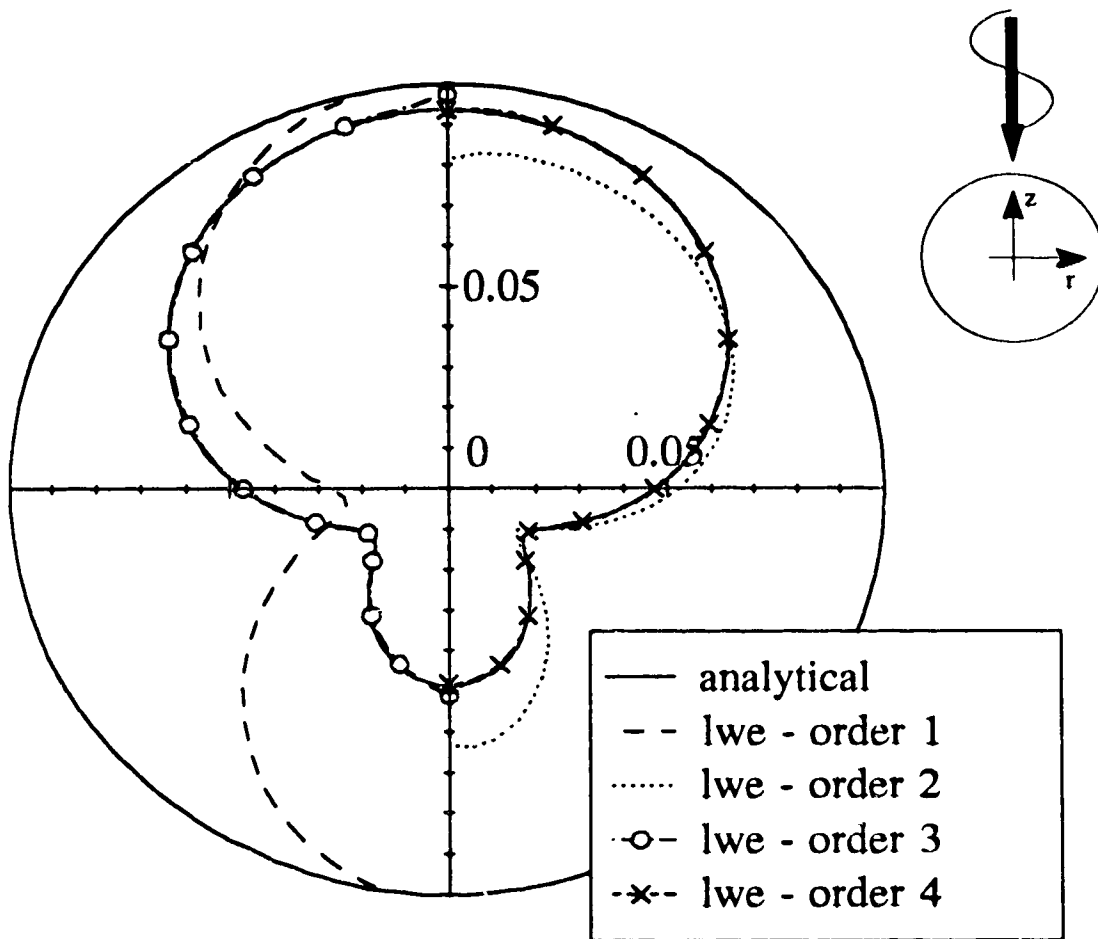


Figure 2.17 Scattering of a plane acoustic wave from a rigid sphere ($kR = 1$). $|P_s|/|P_i|$ at $r = 5R$.

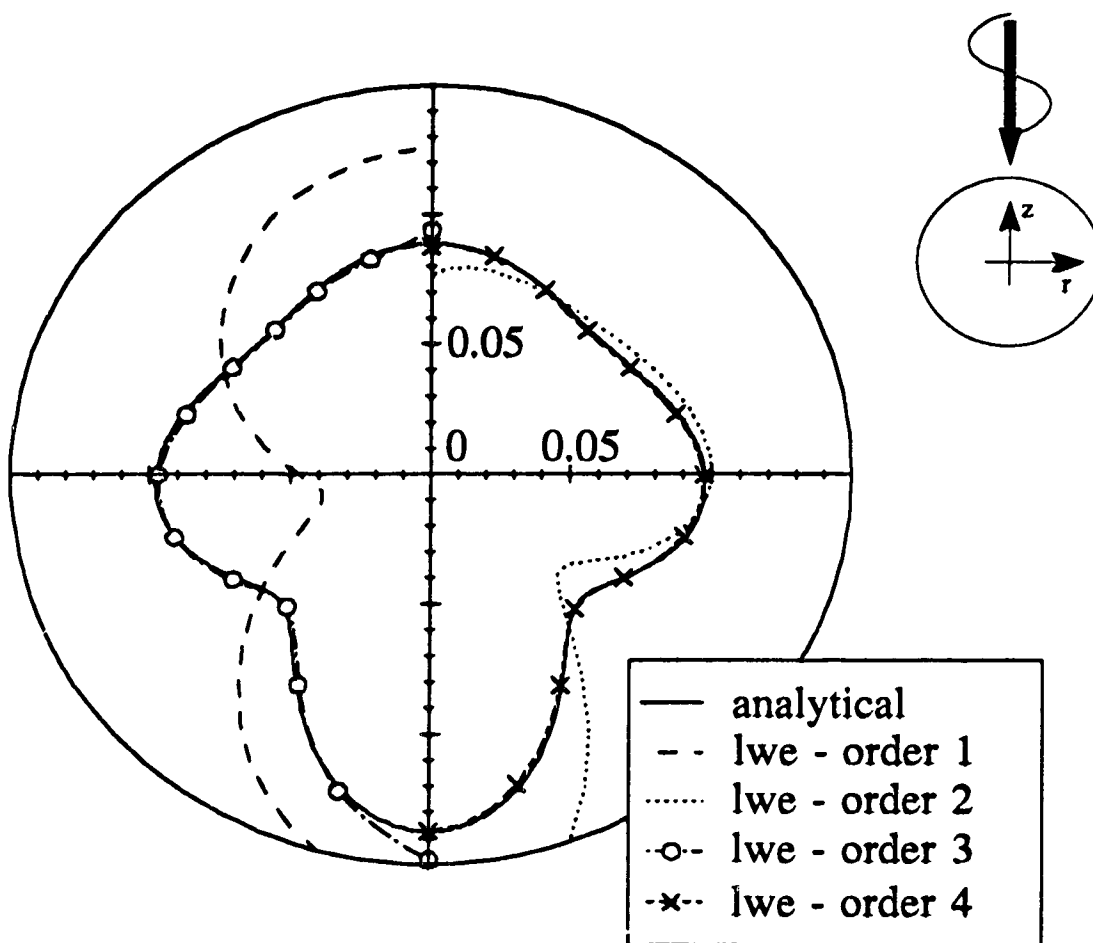


Figure 2.18 Scattering of a plane acoustic wave from a rigid sphere ($kR = 2$). $|P_s|/|P_i|$ at $r = 5R$.

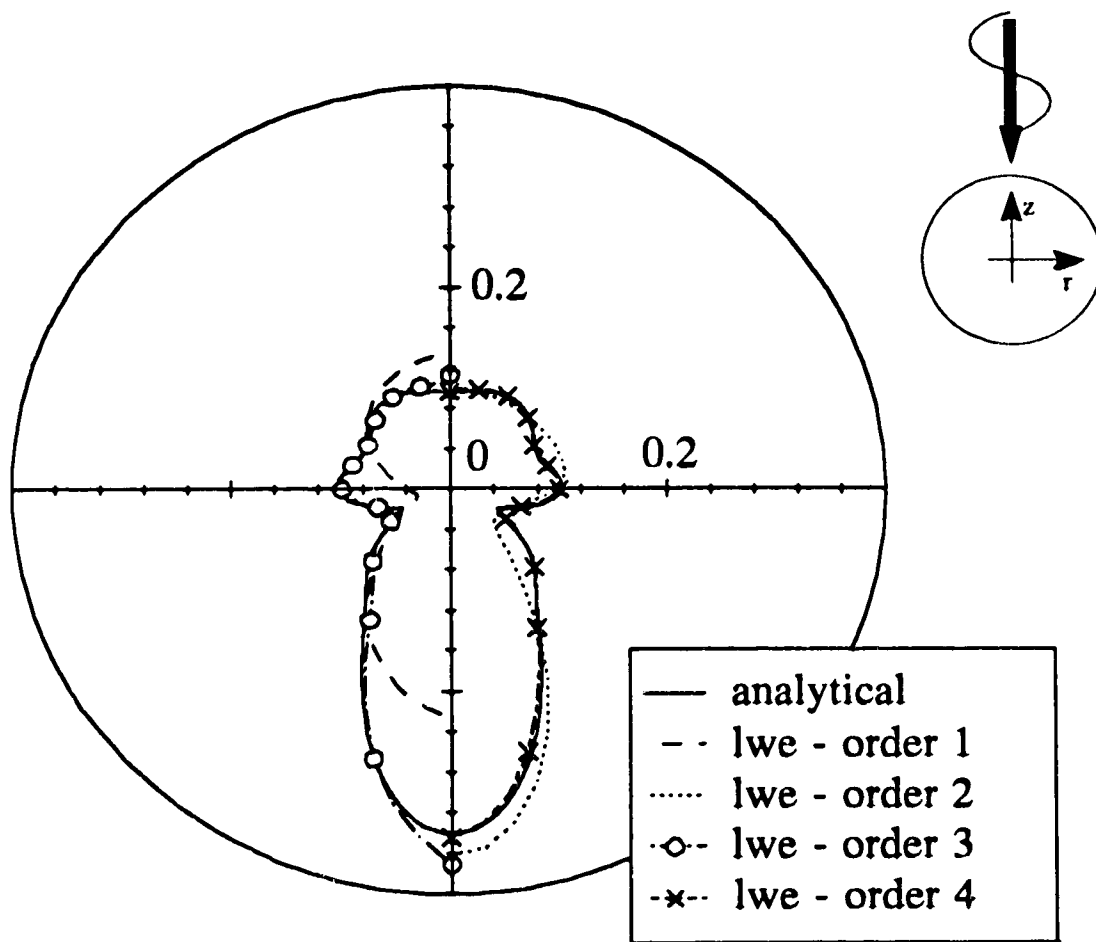


Figure 2.19 Scattering of a plane acoustic wave from a rigid sphere ($kR = 4$). $|P_s|/|P_i|$ at $r = 5R$.

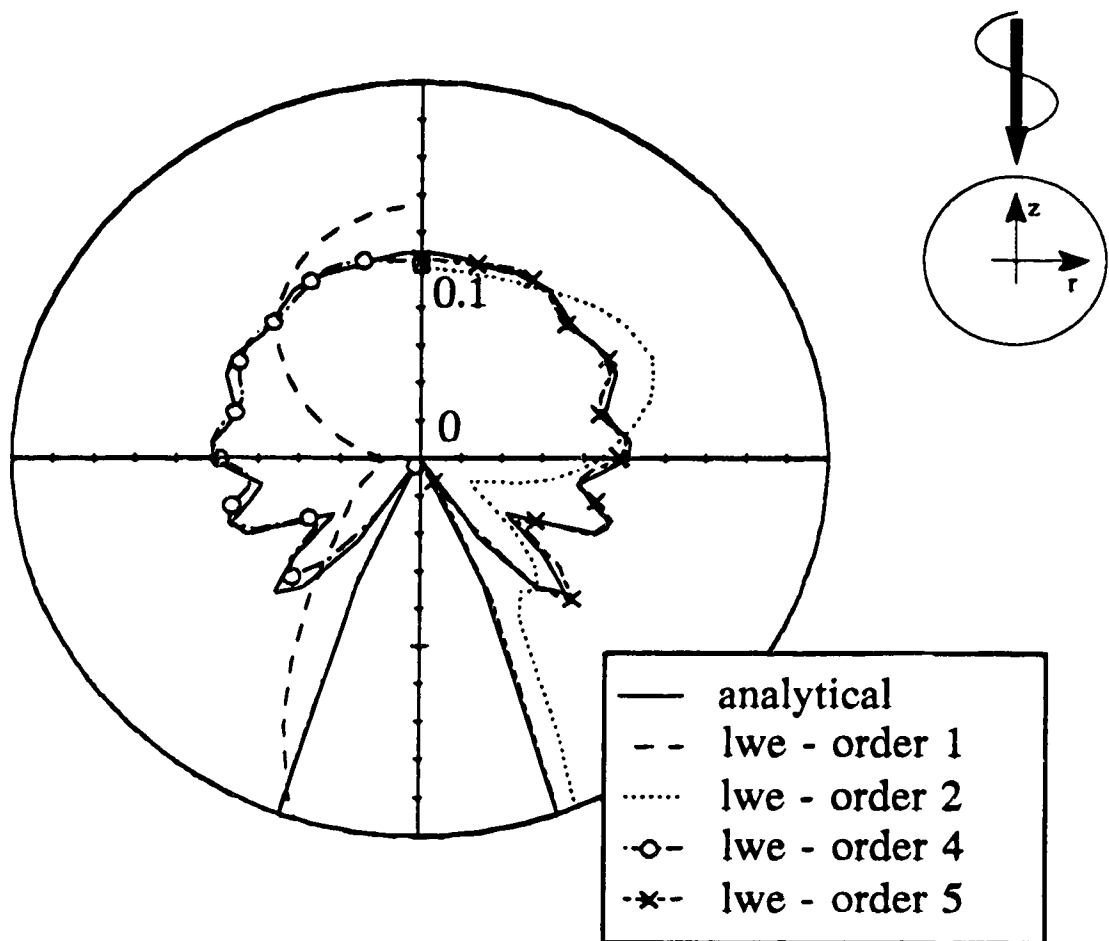


Figure 2.20 Scattering of a plane acoustic wave from a rigid sphere ($kR = 8$). $|P_s|/|P_i|$ at $r = 5R$.

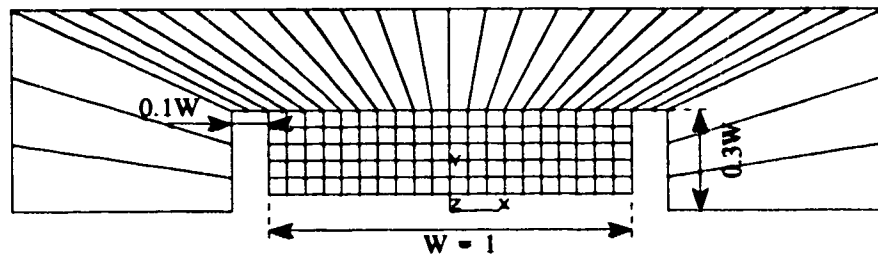


Figure 2.21 Double barrier: Two-dimensional geometry mesh (100 cfe and 30 lwe). Source at origin.

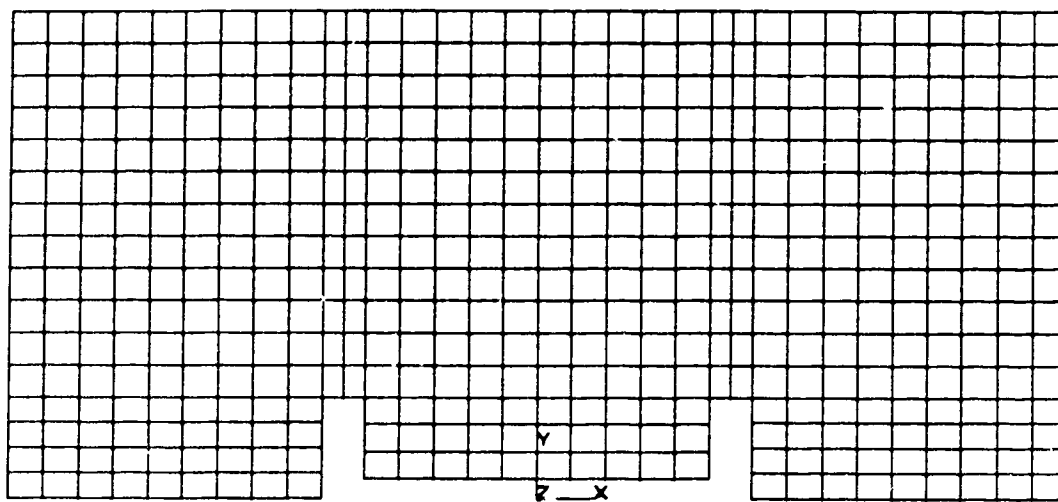


Figure 2.22 Double barrier: Two-dimensional post-processing mesh (542 field points).

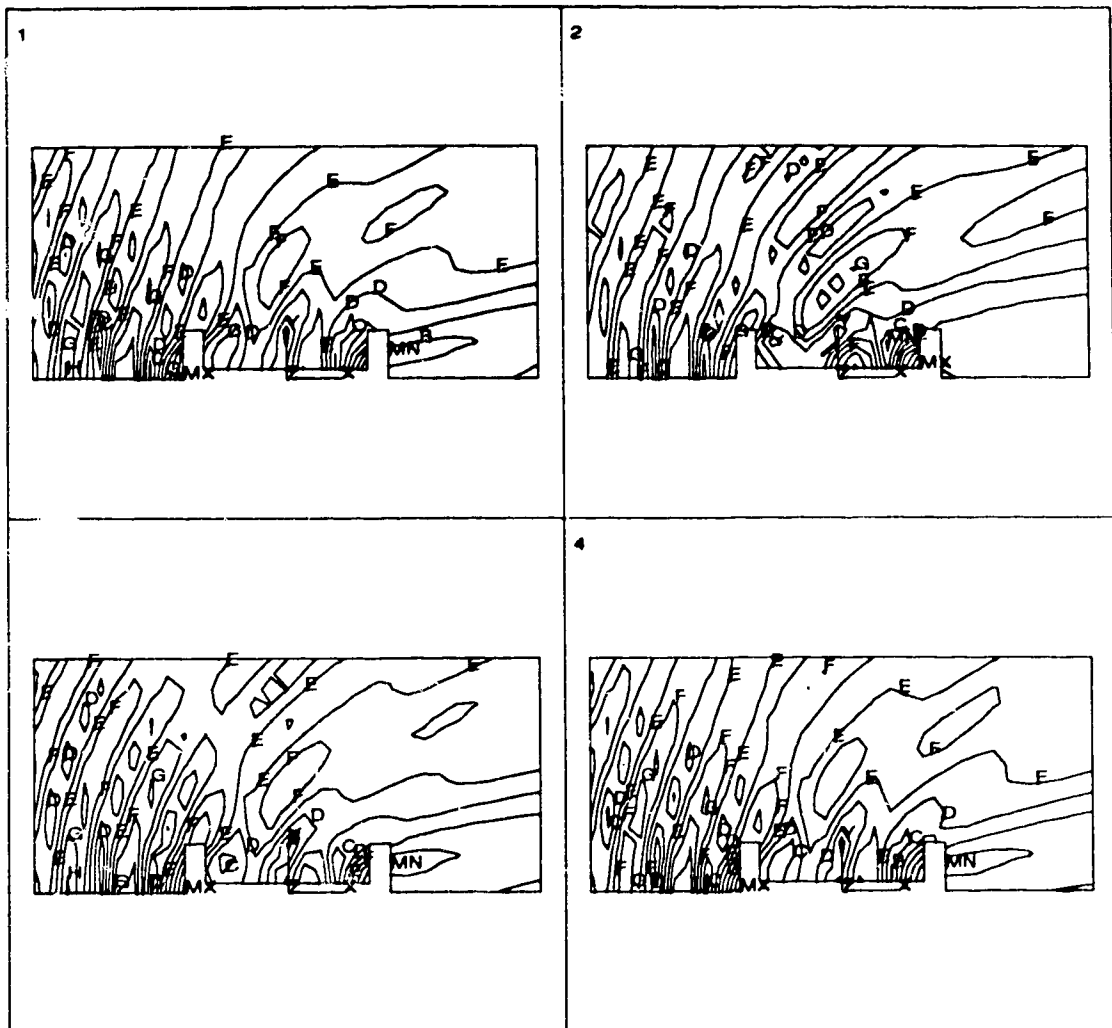


Figure 2.23 Scattering of an acoustic plane wave from a double barrier ($kW = 3\pi$). Contour lines of total acoustic pressure amplitude $|P_t|$. ($|P_i| = 1$).
 1. bem; 2. 1st order lwe; 3. 2nd order lwe; 4. 5th order lwe
 (A=0 B=.24 C=.48 D=.72 E=.96 F=1.20 G=1.44 H=1.68 I=1.92 J=2.16 K=2.40)

REFERENCES

- 2.1. O. C. ZIENKIEWICZ, D. W. KELLY and P. BETTESS, "The Sommerfeld (radiation) condition on infinite domains and its modelling in numerical procedures", *Computing Methods in Applied Sciences and Engineering, Third International Symposium, IRIA Laboria, Lectures in Mathematics V* **704**, 169-192 (1977).
- 2.2. R. J. ASTLEY and W. EVERSMAN, "Finite element formulations for acoustical radiation", *Journal of Sound and Vibration* **88**, 47-64 (1983).
- 2.3. O. C. ZIENKIEWICZ, P. BETTESS, T. C. CHIAM and C. EMSON, "Numerical methods for unbounded field problems and a new infinite element formulation", *Computational Methods for Infinite Domain Media-Structure Interaction* **AMD 46**, 115-147 (1981).
- 2.4. *SYSNOISE User's Manual* 1992 Version 4.4, Numerical Integration Technologies, Leuven, Belgium.
- 2.5. K. R. FYFE and F. ISMAIL, "Investigation of the acoustic properties of vibrating finite cylinders", *Journal of Sound and Vibration* **128**, 361-376 (1989).
- 2.6. A. F. SEYBERT, B. SOENARKO, F. J. RIZZO and D. J. SHIPPY, "An advanced computational method for radiation and scattering of acoustic waves in three dimensions", *Journal of the Acoustical Society of America* **77**, 362-386 (1985).
- 2.7. H. A. SCHENCK, "Improved integral formulation for acoustic radiation problems", *Journal of the Acoustical Society of America* **44**, 41-58 (1967).
- 2.8. A. J. BURTON and G. F. MILLER, "The application of integral equation methods to the numerical solution of some exterior boundary value problems", *Proceedings of the Royal Society of London* **A323**, 201-210 (1971).
- 2.9. P. BETTESS and O. C. ZIENKIEWICZ, "Diffraction and refraction of surface waves using finite and infinite elements", *International Journal for Numerical Methods in Engineering* **11**, 1271-1290 (1977).
- 2.10. P. BETTESS, "Infinite elements", *International Journal for Numerical Methods in Engineering* **11**, 53-64 (1977).

- 2.11. P. BETTESS, "More on infinite elements", *International Journal for Numerical Methods in Engineering* **15**, 1613-1626 (1980).
- 2.12. G. BEER and J. L. MEEK, "Infinite domain elements", *International Journal for Numerical Methods in Engineering* **17**, 43-52 (1981).
- 2.13. P. P. LYNN and H. A. HADID, "Infinite elements with $1/r^n$ type decay", *International Journal for Numerical Methods in Engineering* **17**, 347-355 (1981).
- 2.14. J. M. M. C. MARQUES and D. R. J. OWEN, "Infinite elements in quasi-static materially nonlinear problems", *Computers and Structures* **18**, 739-751 (1984).
- 2.15. O. C. ZIENKIEWICZ, C. EMSON and P. BETTESS, "A novel boundary infinite element", *International Journal for Numerical Methods in Engineering* **19**, 393-404 (1983).
- 2.16. S. PISSANETZKY, "An infinite element and a formula for numerical quadrature over an infinite interval", *International Journal for Numerical Methods in Engineering* **19**, 913-927 (1983).
- 2.17. P. BETTESS and J. A. BETTESS, "Infinite elements for static problems", *Engineering Computations* **1**, 4-16 (1984).
- 2.18. P. BETTESS, C. EMSON, T. C. CHIAM, "A new infinite element for exterior wave problems", *Numerical Methods in Coupled Systems* 489-504. Chichester: John Wiley (1984).
- 2.19. O. C. ZIENKIEWICZ, K. BANDO, P. BETTESS, C. EMSON and T. C. CHIAM, "Mapped infinite elements for exterior wave problems", *International Journal for Numerical Methods in Engineering* **21**, 1229-1251 (1985).
- 2.20. J. P. E. GORANSSON and C. F. DAVIDSSON, "A three dimensional infinite element for wave propagation", *Journal of Sound and Vibration* **115**, 556-559 (1987).
- 2.21. R. J. ASTLEY, J. P. COYETTE, G. J. MACAULAY, "Mapped wave envelope elements for acoustical radiation and scattering", *Journal of Sound and Vibration* **170**, 97-118 (1994).
- 2.22. K. J. BAUMEISTER, "Analysis of sound propagation in ducts using the wave envelope concept", NASA Technical note D-7719, 1-37 (1974).

- 2.23. R. J. ASTLEY and W. EVERSMAN, "A note on the utility of a wave envelope approach in finite element duct transmission studies", *Journal of Sound and Vibration* **76**, 595-601 (1981).
- 2.24. R. J. ASTLEY, "Wave envelope and infinite elements for acoustical radiation", *International Journal for Numerical Methods in Fluids* **3**, 507-526 (1983).
- 2.25. R. J. ASTLEY and W. EVERSMAN, "Wave envelope and infinite element schemes for fan noise radiation from turbofan inlets", *American Institute of Aeronautics and Astronautics Journal* **22**, 1719-1726 (1984).
- 2.26. R. J. ASTLEY, "Finite element, wave envelope formulation for acoustical radiation in moving flows", *Journal of Sound and Vibration* **103**, 471-485 (1985).
- 2.27. A. V. PARRETT and W. EVERSMAN, "Wave envelope and finite element approximations for turbofan noise radiation in flight", *American Institute of Aeronautics and Astronautics Journal* **24**, 753-760 (1986).
- 2.28. P. BETTESS, "A simple wave envelope element example", *Communications in Applied Numerical Methods* **3**, 77-80 (1987).
- 2.29. A. V. PARRETT, "Application of finite and wave envelope element approximations to acoustic radiation from turbofan engine inlets in flight", Ph.D. Thesis, Department of Mechanical Engineering, University of Missouri-Rolla (1984).
- 2.30. E. SKUDRZYK, "The Foundations of Acoustics", New York: Springer-Verlag (1971).
- 2.31. J. P. COYETTE, "Modelling radiation from submerged structures: a comparison of boundary element and finite element techniques", *Second International Congress on Recent Developments in Air- and Structure-borne Sound and Vibration*, March 4-6, Auburn University **2**, 1027-1035 (1992).
- 2.32. J. P. COYETTE, "Validation of a new wave envelope formulation for handling exterior acoustic and elasto-acoustic problems in the frequency domain", *DGLR/AIAA 14th Aeroacoustics Conference*, 11-14 May, Aachen, **1**, 421-427 (1992).

- 2.33. *NSWC library of mathematics subroutines* 1993, Naval Surface Warfare Center, Dahlgren Division, Dahlgren, Virginia.

CHAPTER 3

ON THE USE OF VARIABLE ORDER INFINITE WAVE ENVELOPE ELEMENTS FOR ACOUSTIC RADIATION AND SCATTERING¹

3.1. INTRODUCTION

The modelling of acoustic radiation and scattering in unbounded domains is of great interest in many areas of acoustic research and design. Some of the main research fields involve the modelling of sound barriers for attenuating outdoor sound propagation, noise control of jet engine turbines and speaker design, to name a few. Different mathematical modelling tools have been developed to help solve these acoustic wave propagation problems, ranging from pure analytical methods, restricted to special geometry cases, to more generally applicable numerical methods such as finite element (FE) and boundary element (BE) methods.

The ability of various analytical and numerical methods to model acoustic

¹A version of this chapter has been submitted to *Journal of the Acoustical Society of America* for publication

radiation and scattering problems depends largely on how well the Sommerfeld radiation condition is satisfied [3.1-3.4]. It is a well-known fact that in order to obtain a unique solution for wave propagation problems in infinite fields, the condition of *finiteness* at infinity is not sufficient, as is the case in static problems. In addition, a *radiation* condition is necessary, ensuring that all acoustic energy is radiating outward, by only allowing outgoing propagating waves. The latter condition is very important, since failure of complying to it, causes an energy built-up within the region yielding erratic results.

Applying the Sommerfeld radiation condition accurately in discrete numerical methods is a difficult task. Only the so-called boundary integral methods [3.5,3.6] can satisfy the conditions at infinity exactly, through the use of kernels that inherently fulfil the governing equations for infinite domains. The down side of these methods is that full system matrices result from the formulation, due to the *global* application of the radiation condition. Data storage and calculation time quickly become a problem.

The finite element based methods employ a *local* approach in applying the radiation condition, in an effort to preserve the advantages of finite element modelling, i.e. banded system matrices. One of the methods applies a radiation condition at a distant but finite boundary, using mono- or dipolar damping elements [3.7-3.9]. These damping elements are designed to filter the monopolar or dipolar components of the radiation function. They will only perform well as long as only those lower order multi-poles are present in the radiation function at the finite boundary. In order to accomplish this, the finite boundary often has to be moved a substantial distance away from the radiating body, resulting again in large system matrices due to the great number of acoustic degrees of freedom needed to model the near-field.

Another method of locally applying the radiation condition is the infinite element approach and the use of the variable order infinite wave envelope elements [3.10-3.17]. These elements span the whole infinite acoustic domain and model the outgoing propagating waves by including an appropriate amplitude decay and wavelike variation in the trial functions. The wave envelope elements differ from the standard infinite elements by the choice of weighting functions in a modified Galerkin weighted residual formulation. This wave envelope approach [3.12-3.15] permits the use of standard Gauss

quadrature integration in the evaluation of the element system matrices.

In this chapter, the modelling possibilities and limitations of the variable order infinite wave envelope element for acoustic radiation and scattering problems are investigated. The limitations of the variable order infinite wave envelope modelling are addressed by investigating the higher order multi-poles of the infinitely long radiating rigid cylinder, for two-dimensional modelling, and the axisymmetric oscillating rigid sphere, for axisymmetric three-dimensional acoustic modelling. Then, the possibility of modelling infinite homogeneous impedance planes is analyzed and compared to an approximate analytical solution. Different methods for applying acoustic sources are proposed, i.e. the superposition of scattered and incident fields and the direct nodal source application. Finally, an alternative post-processing method, based on the boundary integral method, is introduced.

3.2. THEORY

3.2.1. GOVERNING EQUATIONS AND BOUNDARY CONDITIONS

Harmonic, steady-state acoustic radiation and scattering in an infinite medium, with speed of sound c and density ρ , is governed by the Helmholtz equation, given as

$$\nabla^2 p(\underline{x}) + k^2 p(\underline{x}) = 0 \quad \underline{x} \in V \quad (3.1)$$

where $k = \omega/c$ is the acoustic wave number.

Appropriate boundary conditions involve prescribing acoustic pressure ($p = \bar{p}$ on S_p), normal velocity ($v_n = \bar{v}_n$ on S_{vel}) or impedance ($\bar{Z}_n = 1/\bar{A}_n = \bar{p}/\bar{v}_n$ on S_{imp}) conditions on the surface of the radiating body and stipulating the Sommerfeld radiation condition at a surface at infinity S_∞ , as [3.14,3.15]

$$\nabla p(\underline{x}) \cdot \underline{n}_\infty = -ikp(\underline{x}) \quad \underline{x} \in S_\infty \quad (3.2)$$

for modelling local outward travelling plane waves.

3.2.2. FINITE ELEMENT SYSTEM MATRICES

Applying standard finite element procedures, results in a set of simultaneous equations that can be written in the form [3.15]

$$[[K] - \omega^2 [M] - i \omega [A]] \{p\} = i \omega \{F\} \quad (3.3)$$

with related coefficients

$$K_{ij} = \int_V \nabla W_i \cdot \nabla N_j dV \quad (3.4)$$

$$M_{ij} = \int_V \frac{1}{c^2} W_i N_j dV \quad (3.5)$$

$$A_{ij} = \int_{S_{\text{imp}}} \rho \overline{A_n} W_i N_j dS \quad (3.6)$$

$$F_i = \int_{S_{\text{out}}} \rho W_i \bar{v} dS \quad (3.7)$$

$[K]$, $[M]$ and $[A]$ are the acoustic stiffness, mass and damping matrix respectively in Equation (3.3), while $\{F\}$ is the acoustic forcing vector and $\{p\}$ the unknown nodal pressure values. The weighting functions and shape functions are indicated as W_i and N_j , respectively.

3.2.3. VARIABLE ORDER INFINITE WAVE ENVELOPE ELEMENT

The development of the variable order infinite wave envelope element stems from the observation that a three-dimensional radiation function $p(r)$, for the region exterior to a sphere $|r - r_0| = R$, can be written as an infinite series of the form [3.3]

$$p(kr) = \frac{e^{-ikr}}{r} \sum_{n=0}^{\infty} \frac{f_n(\theta, \phi)}{r^n} \quad (3.8)$$

where (r, θ, ϕ) are spherical coordinates relative to the origin r_0 . The infinite series converges absolutely and uniformly in r , θ and ϕ in any region $r \geq R + \epsilon > R$. The coefficients $f_n(\theta, \phi)$ for $n > 0$ can be determined from the radiation pattern $f_0(\theta, \phi)$ by the recursion formula

$$2ikn f_n = n(n-1)f_{n-1} + Df_{n-1} \quad n = 1, 2, \dots \quad (3.9)$$

where

$$Df = \frac{1}{\sin\theta} \frac{\delta}{\delta\theta} \left(\sin\theta \frac{\delta f}{\delta\theta} \right) + \frac{1}{\sin^2\theta} \frac{\delta^2 f}{\delta\phi^2} \quad (3.10)$$

is Beltrami's operator for the sphere. The radiation function $p(r)$ is therefore determined in the region $r > R$ by its radiation pattern.

In a similar way the two-dimensional radiation function can be written as [3.9]

$$p(kr) = H_0^{(2)}(kr) \sum_{n=0}^{\infty} \frac{F_n(\theta)}{(kr)^n} + H_1^{(2)}(kr) \sum_{n=0}^{\infty} \frac{G_n(\theta)}{(kr)^n} \quad (3.11)$$

or

$$p(kr) \sim \sqrt{\frac{2}{\pi kr}} e^{-i(kr - \frac{\pi}{2})} \sum_{n=0}^{\infty} \frac{f_n(\theta)}{(kr)^n} \quad (3.12)$$

using the asymptotic expansions for the Hankel functions of the second kind $H_n^{(2)}$. In the latter asymptotic expansion, the radiation patterns $F_n(\theta)$ and $G_n(\theta)$ are combined into

a complex radiation pattern $f_n(\theta)$.

It is observed that, in order to model the acoustic pressure field in an unbounded domain using a single layer of variable order infinite wave envelope elements (see Figure 3.1), sufficient degrees of freedom in the radial direction are needed to model the amplitude decay of the outgoing propagating waves. As well, satisfactory angular discretization is required for modelling the angular radiation pattern. The elements span over a radial slice of the acoustic medium and extend out to infinity. They have a defined acoustic source location and model the amplitude decay and the wavelike variation of the outgoing wave-forms [3.14,3.15]

The geometry mesh, used in modelling acoustic radiation and scattering problems, consists of a semi-circular layer of variable order infinite wave envelope elements, matched onto a conventional finite element mesh, modelling the acoustic near-field. The geometry of the elements is oriented according to the ray paths of the solution, i.e. radial edges perpendicular to the outgoing wave-fronts. In practice, this means that the source locations of the variable order infinite wave envelope elements should closely coincide with the actual physical acoustic source location. Reference [3.15] discusses the importance and the sensitivity of the method to this geometric orientation aspect.

The formulation of the variable order infinite wave envelope element involves three main aspects, i.e. the infinite geometry mapping, special shape and weighting functions, all of which are explained in detail in Reference [3.15] and summarized in the following sections.

3.2.3.1. Infinite geometry mapping

The infinite geometry mapping consists of a *one to one* mapping of a unit parent element onto a real element extending to infinity. This type of geometry mapping is obtained by introducing a singularity in the radial direction (at $t = 1$ or $r = \infty$) in the mapping functions, yielding an inverse mapping of the form

$$t = 1 - 2 \frac{a}{r} \quad (3.13)$$

where a and r respectively denote the distance from the source to the finite boundary and the source to an arbitrary point of the variable order infinite wave envelope element.

3.2.3.2. Shape functions

The special shape functions of the variable order infinite wave envelope element are chosen such that both the amplitude decay and the wavelike variation of the field variable p can be modelled.

An appropriate amplitude decay is obtained through the use of Lagrangian polynomials of order n in the radial direction of the parent element, which transform to $1/r^n$ expansions in the real element, due to the infinite geometry mapping. As such, an arbitrary number of degrees of freedom can be specified for representing the amplitude decay of the outgoing travelling waves. Since the amplitude decay for two-dimensional waves resembles that of a $1/\sqrt{r}$ expansion, a \sqrt{r} factor is added to the radial shape functions for two-dimensional modelling.

In previous implementations of this method, only linear shape functions have been used in modelling the pressure field in the angular direction, along with a discretization rule of thumb of seven acoustic degrees of freedom per wavelength. In this chapter, an angular quadratic and cubic discretization is introduced. The angular quadratic variable order infinite wave envelope element is implemented as an isoparametric element in the angular direction by also using quadratic mapping functions for the geometry mapping. The angular cubic element, on the other hand, is formulated as a subparametric element. This higher order modelling in the angular direction allows for a better modelling of the curved wave-fronts of the outgoing travelling waves.

The wavelike variation is taken into account using a periodic component in the form of a complex exponential given as

$$\exp(-ik\mu(s,t)) \quad (3.14)$$

where the phase function $\mu(s,t) = a(s)(1+t)/(1-t)$ uses an interpolated source location $a(s)$ in order to maintain phase compatibility of the shape functions with any conventional finite elements that may be used to model the near-field.

Finally, combining the different aspects discussed above, the shape function results in the following form

$$N^n(s,t) = T^n(t) S(s) e^{-ik\mu(s,t)} \quad (3.15)$$

where the radial part T^n is a Lagrangian polynomial of order n and the angular part S can be a linear, quadratic or cubic polynomial.

3.2.3.3. Weighting functions

The wave envelope approach involves the use of a modified Galerkin procedure [3.12-3.15]. The complex conjugate of the shape functions are used as weighting functions, combined with a $(a/r)^2$ geometric weighting function $G_w(t)$, given as

$$G_w(t) = \left(\frac{1-t}{2} \right)^2 \quad (3.16)$$

This results in a weighting function of the form

$$W^n(s,t) = G_w(t) N^{n*}(s,t) = G_w(t) T^n(t) S(s) e^{+ik\mu(s,t)} \quad (3.17)$$

such that the complex exponentials cancel out of the integrands of the system matrix formulation, allowing for regular Gauss quadrature integration. All harmonic spatial variations have thus been removed and only the modelling of the *envelope* of the outgoing travelling waves remains.

3.2.4. MODELLING OF IMPEDANCE PLANES

The modelling of sound radiation and scattering using variable order infinite wave envelope elements requires a discretization of the total acoustic field. The field variable, e.g. acoustic pressure, along an infinite half-plane is thus represented through the shape functions along the edges of the conventional finite elements and the infinite radial edges of the variable order infinite wave envelope elements that coincide with the infinite half-plane. It is therefore possible to directly apply impedance boundary conditions along such an infinite half-plane. The contribution of the infinite radial edges to the damping matrix A from Equation (3.6) can be written as

$$\begin{aligned} A_{ij} &= \int_{S_{\infty} \text{ edges}} \rho \overline{A_n} W_i N_j dS \\ &= \int_{-1}^1 \rho \overline{A_n} G_{w_i}(t) T^n_i(t) T^n_j(t) \|J\| dt \end{aligned} \quad (3.18)$$

where J denotes the Jacobian of the geometry transformation from global to local coordinates.

As such, the implementation of a finite impedance boundary condition along infinite boundaries is very easily accomplished, in comparison with boundary element methods where special kernels are required in the formulation [3.18,3.19].

3.2.5. APPLICATION OF SOURCES

Two methods for applying acoustic sources are investigated. The first method involves the superposition of the scattered and incident acoustic pressure fields, while the second method consists of a direct application of a source term at a nodal acoustic degree of freedom.

3.2.5.1. Superposition of scattered and incident acoustic pressure fields

The superposition procedure consists of modelling the scattered acoustic pressure field p_s , using boundary conditions obtained from the known incident pressure field p_i , due to the acoustic source. The boundary conditions are applied in the form of prescribed normal velocity boundary conditions, given as

$$\overline{v_{n_s}} = (\overline{A_n} \overline{p_i} - \overline{v_{n_i}}) + \overline{A_n} p_s \quad (3.19)$$

In order to obtain the total pressure field p_t , the known incident pressure field can be superimposed onto the scattered field. Note that for hard wall $\overline{A_n} = 0$ and the boundary condition $\overline{v_{n_t}} = \overline{v_{n_s}} + \overline{v_{n_i}} = 0$ is satisfied.

A problem arises when sources are to be modelled that are situated above, instead of on an infinite half-plane. Such source configurations require an adequate modelling of the normal velocity profile along the infinite edge of the variable order infinite wave envelope element, based on the normal velocities evaluated at the acoustic degrees of freedom and the element shape functions. This cannot be accurately imposed unless the prescribed acoustic source is in the near vicinity of the source of the variable order infinite wave envelope element, in which case the element shape function, with its amplitude decay and wavelike variation, can be used. For an acoustic source located elsewhere, the modelling of the imposed normal velocity boundary conditions will be poor.

When considering a source above a flat hard plane, i.e. a symmetry plane, an image source may be used as depicted in Figure 3.2. Using this method, it is only necessary to find the normal velocities due to the incident fields of the two sources on the scattering body, as the condition $\overline{v_n} = 0$, is automatically satisfied along the edge of the infinite half-plane, alleviating the above described problem.

3.2.5.2. Nodal source application

A spherical (3D) or cylindrical (2D) source can be applied to an acoustic degree

of freedom to directly yield the total acoustic pressure field. The acoustic pressure field generated by a point source (also referred to as acoustic monopole) can be written as [3.20,3.21]

$$p(r) = \frac{P_{amp}}{r} e^{-ikr} \quad (3.20)$$

where the monopole amplitude P_{amp} is the pressure at a sphere of unit radius and r the radial distance from the source.

The pressure field due to a radially vibrating sphere of radius R is given as [3.20,3.21]

$$p(r) = \frac{i \rho \omega R^2 \bar{V}_0}{r(1 + ikR)} e^{-ik(r-R)} \quad (3.21)$$

where \bar{V}_0 is the radial surface velocity of the sphere. If the radius can be considered small such that $kR \ll 1$, Equation (3.21) becomes

$$p(r) = \frac{i \rho \omega Q}{4 \pi r} e^{-ikr} \quad (3.22)$$

where the volume source-strength Q is defined as the area of the pulsating sphere times its surface velocity

$$Q = 4 \pi R^2 \bar{V}_0 \quad (3.23)$$

A point source can be considered as a limiting case of a radially vibrating sphere, where the radius R tends to zero, while simultaneously the radial surface velocity \bar{V}_0 becomes larger, such that the volume source-strength Q remains constant. In doing so, the radially pulsating sphere is being idealized as a point.

From Equations (3.20) and (3.21), the volume source-strength can then be written as

$$Q = \frac{4\pi P_{amp}}{i\rho\omega} \quad (3.24)$$

In the finite element model, a point source can therefore be applied at an acoustic degree of freedom i by considering an infinitesimal small pulsating sphere of radius ϵ at that location, as shown in Figure 3.3. The coefficient of the forcing vector F_i becomes

$$\begin{aligned} F_i &= \lim_{\epsilon \rightarrow 0} \left[i\rho\omega \int_{S_i} \overline{V}_{0i} dS \right] \\ &= i\rho\omega \lim_{\epsilon \rightarrow 0} (4\pi\epsilon^2 \overline{V}_{0i}) \\ &= i\rho\omega Q \\ &= 4\pi P_{amp} \end{aligned} \quad (3.25)$$

In a similar way, a pulsating cylinder of infinitesimal small radius ϵ can be considered for the two-dimensional modelling of a cylindrical source. The coefficient for the forcing vector becomes

$$F_i = 4P_{amp} \quad (3.26)$$

From the nature of the nodal source application, it is understood that only sources in the near-field can be modelled, i.e. in the conventional element region. A source application within the variable order infinite wave envelope element region will yield irregular results due to the inappropriate acoustic source location of the infinite elements with respect to the point source position.

If the point source does not coincide with an acoustic degree of freedom, the source strength is distributed among the acoustic degrees of freedom of the element, using the element shape functions, as in

$$F^e_i = 4P_{amp} N_i \quad (3.27)$$

for a two-dimensional cylindrical source.

3.2.6. POST-PROCESSING OF RESULTS

In order to obtain the field variables, i.e. the acoustic pressure and particle velocity, at an arbitrary point, two different methods can be used. One method involves determining the element within which the field point is located. Then a simple interpolation can be performed among the acoustic degrees of freedom of the element, using the element shape functions [3.15].

Another method makes use of the boundary element method formulation [3.5,3.6]. Using the calculated surface pressures $p(Q)$ and normal velocities $v_n(Q)$, the pressure $p(P)$ at an arbitrary point P in the acoustic field can be evaluated (see Figure 3.4).

In general, this relationship can be written as

$$p(P) = \int_{\Gamma} \left(p(Q) \frac{\delta G(P, Q)}{\delta n} + i \rho \omega G(P, Q) v_n(Q) \right) d\Gamma(Q) \quad (3.28)$$

with

$$\begin{aligned} G(P, Q) &= \frac{-i}{4} H_0^{(2)}(kr(P, Q)) & \text{for 2D} \\ G(P, Q) &= \frac{e^{-ikr(P, Q)}}{4\pi r(P, Q)} & \text{for 3D} \end{aligned} \quad (3.29)$$

where G is the free-space Green's function.

3.3. DISCUSSION OF RESULTS

3.3.1. LIMITATIONS OF THE VARIABLE ORDER INFINITE WAVE ENVELOPE ELEMENT MODELLING

From observation of the infinite series, outlined in Equations (3.8) and (3.12), two important aspects can be considered. First of all, the angular discretization has to be sufficient, such that the radiation patterns can adequately be modelled. Furthermore, it seems plausible that a quadratic trial function would be more effective in the angular

direction, in order to model the lobe-shaped radiation patterns, as opposed to the simple linear discretization.

A second aspect involves the radial discretization. The more terms are present in the $(1/r)$ expansion, i.e. higher order element, the better the radiation condition will be satisfied in general.

In order to assess the importance of the previous aspects, tests have been performed, both for axisymmetric three-dimensional and two-dimensional acoustic modelling, i.e. the radiating rigid sphere and the infinitely long radiating rigid cylinder respectively. The acoustic medium is air, with speed of sound $c = 340$ m/s and density $\rho = 1.21$ kg/m³. The computational mesh for such type of configuration can be ideally shaped, i.e. circular layer of variable order infinite wave envelope elements with a common source in the origin, thus avoiding possible additional errors due to the geometry sensitivity of the formulation, as discussed in Reference [3.15]. The variable order infinite wave envelope elements are directly matched onto the radiating body, as shown in Figure 3.5, in order to solely concentrate on the performance of the infinite element itself.

In the following sections the multi-pole radiation of the axisymmetric oscillating sphere and the oscillating infinitely long rigid cylinder are investigated. Before proceeding to the analysis of the modelling of the multi-poles, the important aspect of the critical wave number for multi-pole radiation from curved shells is introduced. This critical wave number constitutes the transition from a poor to a good radiator. The phenomenon can be explained as presented in Reference [3.22], for the case of an infinitely long oscillating cylinder. At the critical wave number, the circumferential wave number of the velocity distribution $k_c = n/R$, where n is the order of multi-pole, is equal to the acoustic wave number k . If the acoustic wave number is smaller than the critical wave number, i.e. $k < k_c$, destructive cancellation will occur from adjacent zones of positive and negative volume velocity distribution, rendering inefficient radiation. For acoustic wave numbers above the critical wave number, efficient radiation is obtained. The same reasoning can be made for spherical multi-poles.

3.3.1.1. Axisymmetric oscillating sphere

In general, the surface velocity of an axisymmetric oscillating sphere (radius = R) can be written as a sum of Legendre polynomials [3.20]

$$\overline{V}^0(\theta) = \overline{V}_0^0 + \overline{V}_1^0 P_1(\mu) + \overline{V}_2^0 P_2(\mu) + \dots + \overline{V}_n^0 P_n(\mu) + \dots \quad (3.30)$$

where $\mu = \cos\theta$, P_n is the Legendre polynomial of order n and

$$\overline{V}_n^0 = \left(n + \frac{1}{2}\right) \int_0^\pi \overline{V}^0(\theta) P_n(\mu) \sin\theta \, d\theta \quad (3.31)$$

The acoustic pressure, generated by the n^{th} component can then be written as

$$p_n(r, \theta) = i \rho c \overline{V}_n^0 P_n(\mu) \frac{k^2 R^2}{kr} \frac{S_n(kr) + i C_n(kr)}{U_n(kR) + i V_n(kR)} \quad (3.32)$$

where S_n , C_n , U_n and V_n are the Stenzel functions of order n defined by

$$\begin{aligned} S_n(kr) &= \sqrt{\frac{\pi kr}{2}} J_{n+\frac{1}{2}}(kr) \\ C_n(kr) &= -\sqrt{\frac{\pi kr}{2}} N_{n+\frac{1}{2}}(kr) \\ U_n(kr) &= kr S_{n+1}(kr) - n S_n(kr) \\ V_n(kr) &= kr C_{n+1}(kr) - n C_n(kr) \end{aligned} \quad (3.33)$$

with J_ν and N_ν the Bessel functions of the first and second kind respectively. The components, described in Equation (3.32), are the so-called *zonal spherical harmonics*. They form a complete system of orthogonal functions that can be used to describe any type of axisymmetric vibration of a spherical shell.

In the following presentation of results, spherical multi-poles of order n have been modelled. Results are presented in both polar plots and frequency response functions.

Figures 3.6 and 3.7 show a frequency response function of a spherical monopole

modelled by variable order infinite wave envelope models with linear (referred to as LWE) and quadratic (QWE) angular discretization. The angular quadratic elements are able to model the monopole exactly for all orders, while the angular linear elements show slight deviations from the analytical solution for the different orders. The angular quadratic elements therefore prove to be superior for modelling the curved wave-fronts of the outgoing waves. No further improvement was found by going to a cubic angular discretization.

In Figures 3.8 to 3.11, polar plots of different order multi-poles at an acoustic wave number of $kR = 20$ are shown. The geometry mesh for the numerical model consists of a single layer of seventy-five quadratic variable order wave envelope elements, directly matched onto the radiating body, as shown in Figure 3.5. Results are compared to analytical solutions, calculated from Equation (3.32). The low order multi-poles of order one and two can be modelled without any difficulty, since the acoustic wave number is well above the critical wave number of these multi-poles. When multi-poles of higher order have to be modelled, an increasingly higher number of acoustic degrees of freedom in the radial direction is needed, as shown in the modelling of the tenth order multi-pole. Finally, when modelling at the critical wave number, as is the case for the multi-pole of order twenty in Figure 3.11, even a wave envelope model of ninth order shows some discrepancy from the analytical solution. When considering variable order infinite wave envelope elements beyond order nine, tests have shown that the condition number of the system matrices increases drastically. Elements of order ≥ 10 (for double precision arithmetic) have shown to yield ill-conditioned system matrices, producing erratic results. It is seen that as the radiation efficiency decreases, the modelling performance of the variable order infinite wave envelope models diminishes.

To emphasize that the above shown limitation of the variable order infinite wave envelope modelling can be attributed to the lack of radial, rather than angular, discretization, tests were done with increased angular discretization. Figure 3.12 shows results of the limiting case, i.e. the oscillating sphere of order twenty ($kR = 20$), for geometry meshes of seventy-five angular quadratic, seventy-five angular cubic and hundred and fifty angular quadratic ninth order infinite wave envelope elements. All

models result into the same solution, showing no improvement for the higher angular discretization.

The frequency response functions in Figures 3.13 to 3.16, show how well the elements of different order perform in the various frequency ranges. The greatest errors occur for kR acoustic wave numbers around the critical wave number. The error decreases when models of higher order elements are used. At wave numbers above the critical wave number all variable order infinite wave envelope element approximations converge to the analytical solution. This can be explained by looking at the asymptotic expansion of Equation (3.32), which can be written as [3.21]

$$p_n(r, \theta) \sim \bar{P}_{const}(R) \frac{e^{-ikr}}{kr} \quad kr \rightarrow \infty \quad (3.34)$$

Thus as $kr \rightarrow \infty$, a simple $1/r$ modelling is sufficient for modelling the pressure amplitude decay. It can be observed from Figures 3.13 to 3.16 that the transition from a poor to a more efficient radiator occurs at the critical wave number $kR = n$, where n is the order of multi-pole.

From this it is important to note that the wave number at which the acoustic field is evaluated, is of great importance when determining the highest order of multi-pole that can be modelled by a particular variable order infinite wave envelope element model. Basically one can state that all multi-poles in their radiating mode can be modelled adequately, i.e. when the condition $k > k_c$ is satisfied. Intuitively this comes not as a surprise, since the formulation of the variable order infinite wave envelope is developed as a radiating element, with its built in amplitude decay and wavelike variation.

3.3.1.2. Infinitely long oscillating cylinder

In a similar way, the oscillating cylinder (radius = R) of order n is investigated, where [3.9]

$$p(r, \theta) = -i \rho c \bar{V}_n \frac{H_n^{(2)}(kr)}{H_n^{(2)'}(kR)} \cos(n\theta) \quad (3.35)$$

based on a prescribed radial surface velocity, given by

$$\bar{V}_n(\theta) = \bar{V}_n \cos(n\theta) \quad \bar{V}_n \ll R \quad (3.36)$$

The different multi-poles are studied in Figures 3.17 to 3.20 and 3.21 to 3.24, revealing identical observations for the axisymmetric oscillating sphere.

3.3.1.3. Scattering from a rigid body

In the following, the performance of the variable order infinite wave envelope elements for the modelling of acoustic fields, due to the scattering from a rigid body, is investigated. Again, ideally shaped bodies, i.e. an infinitely long rigid cylinder and a rigid sphere, are being used.

A frequency response function of the scattered acoustic pressure amplitude at $x = -5R$ and $y = 0$ for $1 < kR < 30$, due to the scattering of an acoustic plane wave of unit amplitude, travelling in the positive x -direction, from a rigid cylinder (*radius* = R) is now considered. Again, the geometry mesh for the numerical model consists of a single layer of seventy-five quadratic variable order infinite wave envelope elements. Results for wave envelope element modelling of orders seven to nine are compared to the analytical solution, given as [3.20]

$$p_s(r, \theta) = -P_0 \sum_{n=0}^{\infty} \epsilon_n i^n \frac{J_n'(kR) H_n^{(2)}(kr)}{H_n^{(2)'}(kR)} \cos n\theta \quad (3.37)$$

where ϵ_n is the Neumann function ($\epsilon_n = 1$ if $n = 0$ and $\epsilon_n = 2$ if $n > 0$).

Figure 3.25 shows how the frequency range of the numerical modelling gradually can be extended up to a limit of $kR = 20$, by moving to higher order variable order infinite wave envelope element modelling. This can be easily explained by examining the analytical solution from Equation (3.37). The scattered acoustic pressure field can be

interpreted as a superposition of an infinite series of multi-poles. The higher the frequency, the higher order of multi-poles, i.e. the more terms in the infinite series, are needed for convergence of the analytical expression. The ninth order infinite wave envelope element has been shown to be able to model multi-poles up to order twenty, which is about the number of multi-poles required for establishing the scattered pressure field for $kR = 20$, for convergence of the analytical series of Equation (3.37) within satisfactory accuracy. For modelling higher frequency scattering, superior modelling is necessary in order to be able to filter the higher order multi-poles. A polar plot of the scattered acoustic pressure amplitude at $r = 5R$, for the limiting case $kR = 20$, is shown in Figure 3.26.

In a similar way, axisymmetric modelling of the acoustic scattering of a plane wave, travelling in the negative z -direction, from a rigid sphere (*radius* = R) can be studied, as illustrated in Figures 3.27 and 3.28. The analytical solution in this case can be written as [3.20]

$$p_s(r, \theta) = -P_0 \sum_{n=0}^{\infty} \frac{(2n+1) i^n P_n(\cos \theta) U_n(kR)}{kr [U_n(kR) + i V_n(kR)]} [S_n(kr) + i C_n(kr)] \quad (3.38)$$

The results reveal identical limitations in analyzing acoustic scattering at higher wave numbers. Failure of modelling multi-poles of order higher than twenty leads to a frequency limitation, i.e. $kR < 20$, for scattering problems.

As indicated earlier, all of the above tests can be considered ideal cases for numerical modelling using variable order infinite wave envelope elements. For the modelling of acoustic radiation and scattering from bodies of arbitrary shape, performance can be expected to be poorer, mainly due to errors induced by the inability to generate a geometry mesh that closely reflects the nature of the problem. In general, the source location for the variable order infinite wave envelope elements is not known. It is understood that the performance of the variable order infinite wave envelope element can eventually be improved by adding conventional finite element layers for modelling the acoustic near-field. These conventional finite element regions have to extend *far enough* into the field, such that the variable order infinite wave envelope element layer can

properly match onto it, and thus, provide an adequate radiation condition for the unbounded acoustic domain. In practice that quickly results in a fairly large conventional finite element regions, yielding a large number of acoustic degrees of freedom. In this case, boundary integral type methods will prove to be more efficient.

3.3.2. MODELLING OF A COHERENT MONOFREQUENCY LINE SOURCE ABOVE A HOMOGENEOUS IMPEDANCE PLANE

In the following two-dimensional application, the acoustic pressure field due to a coherent monofrequency line source above a homogeneous impedance plane is calculated. This type of acoustic wave propagation problem has been thoroughly analyzed by S. N. Chandler-Wilde and D. C. Hothersall [3.18]. They derived an approximate analytical solution, $G_\beta(\mathbf{r}, \mathbf{r}_0)$, to the problem, outlined in Reference [3.18] and briefly summarized in Appendix 3-A.

The coherent monofrequency line source is located at $\mathbf{r}_0 = (x_0, y_0)$. The receiver at $\mathbf{r} = (x, y)$ is situated in the half-space S , $y > 0$, above the homogeneous impedance plane δS , $y = 0$, as shown in Figure 3.29.

Results, obtained by using variable order infinite wave envelope element models, are compared to the G_β -solution. The geometry mesh consists of a single layer of sixteen variable order infinite wave envelope elements with quadratic angular discretization (QWE), matched on to a circular near-field region (radius $r = 0.5$, centred around the origin $x = 0$; $y = 0$), filled with fifty-eight quadratic conventional elements. The source, applied by the direct nodal source application, is located at $x = 0$; $y = 0.25$.

Figures 3.30 to 3.32 show results for frequency response functions of the amplitude of the acoustic pressure for a receiver at $x = 10$; $y = 0.25$. Relative surface admittance varies from $\beta = 0.005$, $\beta = 0.1$ to $\beta = 0.5$. Higher order infinite wave envelope element modelling proves to be necessary to accommodate the increasing relative surface admittance.

As an illustration, contour fields of the acoustic pressure field ($k = 10$) of the modelling of a cylindrical source above a hard plane ($\beta = 0$) and an impedance plane

($\beta = 0.5$) are given in Figures 3.33 and 3.34, respectively. Again, results compare well with the G_B -solution. A second order infinite wave envelope element was used for the hard plane modelling, while a fifth order element was required for the impedance plane.

3.3.3. MODELLING OF ACOUSTIC SCATTERING OF A CYLINDRICAL SOURCE FROM A DOUBLE BARRIER CONFIGURATION

In this section, the two-dimensional scattering of a cylindrical source from a double barrier configuration is studied. Results obtained by applying the different acoustic source application methods are investigated, as well as the two post-processing methods, explained in the theoretical Sections 3.2.5. and 3.2.6. respectively. The geometry mesh for this problem is shown in Figure 3.35. The region between the two barriers is modelled by thirty quadratic conventional finite elements (referred to as CFE). A single layer of twenty variable order infinite wave envelope elements, with quadratic angular discretization, models the acoustic far-field. The source is located in the symmetry plane at $x = 0$ and $y = 0.2W$, with a the characteristic dimension of the problem.

Figures 3.36 and 3.37 show frequency response functions of the amplitude (dB) of the acoustic pressure for a receiver at $x = 5W$ and $y = 0.15W$, for respectively a rigid ($\beta = 0$) and a soft platform ($\beta = 0.5$). β is the complex relative surface admittance and the platform is the horizontal boundary between the two barriers. Three different eighth order infinite wave envelope models are shown. The first two models differ in the source application method, i.e. the direct source application at an acoustic degree of freedom and the superposition method, while the third model illustrates the alternative boundary element post-processing method. Results are compared to the boundary element method (collocation-procedure from SYSNOISE software [3.23]). The boundary element method mesh comprised fifty-eight, equally sized, linear elements.

Both source application methods yield virtually identical results over the whole frequency range. Each of the methods however has its advantages and limitations. The superposition of scattered and incident field method relies on the adequate modelling of velocity boundary conditions along the boundaries of the acoustic field, for calculating

the scattered acoustic field. As discussed before, problems can arise along the infinite edges of the variable order infinite wave envelope elements, i.e. when modelling infinite half planes. In general, the normal velocity profile can not be modelled accurately along the infinite edges of the element by using the shape functions of the element formulation. It is therefore recommended to only use the method of field superposition when the infinite half plane is also a symmetry plane, as is the case in the problem at hand. The method of image sources can then easily be applied, yielding normal velocity boundary conditions only on the radiating body.

The direct nodal source application relies on the availability of an acoustic degree of freedom in the *near* vicinity of the source. In practise, this means that only near-field sources can be modelled, i.e. at a node or distributed among the nodes of a conventional finite element. As such, the source can always be modelled within $\lambda/6$ of the actual source location, pending on adequate field discretization according to the rule of thumb of about seven acoustic degrees of freedom per wavelength. The method proves to be very efficient. A straightforward search technique is used in order to determine the acoustic degree of freedom associated to the source. The forcing vector is then modified accordingly, as outlined in the theoretical Section 3.2.5., and the total acoustic pressure field is promptly calculated.

The boundary element post-processing method is now investigated. Although slight deviations to the interpolation method are noticed at the higher frequencies, both methods yield virtually identical results over the whole frequency range. The boundary element based post-processing method relies strongly on the accuracy of the surface field variables, i.e. surface pressure and normal velocity. The accuracy of these values inherently depends on the quality of the modelling of the whole acoustic field, i.e. near-field as well as far-field. Therefore, if accurate surface field variables are obtained, the interpolated field variables will be of comparable accuracy.

The advantages or disadvantages of the two methods therefore largely lie in the practical implementation. The interpolation method requires a search strategy to determine within which element's limits the different post-processing field points lie. As soon as these elements are assigned, a simple interpolation among the nodal degrees of freedom,

using the element shape functions, yields the acoustic field variables, as outlined in Reference [3.15]. The boundary element based method demands an integration across the radiating boundary, according to Equation (3.28), for every single field point.

The efficiency of either method is very case dependent, i.e. number of degrees of freedom in the computational model and number of field points where the acoustic field variables have to be evaluated. In general, the interpolation method proves to be efficient when results at a large number of field points have to be evaluated, e.g. calculation of large pressure fields. While the boundary element based method is practical, when results are sought at a few distinct field points. In the latter case, the interpolation method again becomes more beneficial if frequency response functions are calculated. The identification of the element, associated to the field point, can be done before the frequency sweep. Then a simple interpolation after each frequency step renders the result at the field point.

3.4. CONCLUSIONS

Different modelling aspects and limitations of the variable order infinite wave envelope element modelling for acoustic radiation and scattering have been discussed. The emphasis in this chapter is on the analysis of the limitations of this finite element based modelling tool for wave propagation in unbounded acoustic fields.

The study of the limitations involves an investigation into how well the Sommerfeld radiation condition is satisfied. The formulation of the variable order infinite wave envelope element stems from the observation that any radiation function can be written as an infinite series of a $(1/r^n)$ expansion, for a region exterior to a given sphere of radius R [3.3]. This suggests that, in order to model the acoustic far-field using a single layer of variable order infinite wave envelope elements, sufficient degrees of freedom in the radial direction are needed to model the amplitude decay of the outgoing propagating waves. As well, satisfactory angular discretization is required for modelling the angular radiation pattern.

A systematic study of the modelling of the higher order multi-poles of the infinitely long radiating rigid cylinder and the axisymmetric pulsating rigid sphere,

revealed the importance of the critical wave number of the multi-pole, which constitutes the transition from a poor to a good radiator. Multi-poles can be modelled accurately as long as the acoustic wave number is greater than the critical wave number of the multi-pole. The modelling accuracy at wave numbers around the critical wave number can be improved by going to higher order wave envelope element modelling. The limit of ninth order modelling in the radial direction is due to numerical limitations for double precision arithmetic, as ill-conditioned system matrices are obtained for higher order modelling. Furthermore, the importance of quadratic trial functions in the angular direction can be attributed to the need for accurate modelling of the lobe-shaped radiation patterns of the multi-poles.

In general, the radiation function of an arbitrary radiating body can be interpreted as a superposition of a series of multi-poles. The apparent frequency limitation of $kR < 20$ for acoustic scattering from an infinitely long rigid cylinder or rigid sphere can therefore be explained by observing what order of multi-poles are present in the expansion for the scattered acoustic pressure field.

The acoustic wave propagation above an impedance plane due to a coherent monofrequency line source was also studied. A homogeneous impedance boundary condition was prescribed along the infinite radial edge of the variable order infinite wave envelope element. Results compared well to the approximate G_p -solution.

Two different methods of applying acoustic sources were analyzed. The standard approach involves the superposition of scattered and incident acoustic pressure fields. The calculation of the scattered acoustic field requires adequate modelling of the normal velocity boundary conditions along the boundary of the acoustic domain due to the incident pressure field of the acoustic source. In general, this can not be imposed accurately along the infinite edges of the variable order infinite wave envelope element, unless the prescribed acoustic source is located on the infinite half plane or, for sources above the plane, that the source closely coincides with the acoustic source of the infinite wave envelope element. For acoustic hard infinite planes this can be avoided through the use of image sources. The other method consists of a direct application of a source term at an acoustic degree of freedom. This method proves to be very efficient, but requires

an acoustic degree of freedom to closely coincide with the prescribed source location. Therefore only sources within the acoustic near-field can be modelled.

Since the total domain is discretized, for variable order infinite wave envelope element modelling, acoustic field variables at arbitrary field points can be calculated by interpolating among the degrees of freedom of the element. Another method is introduced, where the acoustic pressure at a field point is evaluated, based upon the acoustic pressure and normal velocity values on the boundary of the acoustic domain, using the boundary integral formulation. Both methods proved to be of similar accuracy and their advantages and disadvantages can solely be attributed to their practical implementation.

The study of the use of variable order infinite wave envelope elements for acoustic radiation and scattering, as an alternative for boundary element modelling, has revealed both advantages and limitations. These limitations become especially apparent in the modelling of high frequency scattering problems. It is believed that the limitations can be attributed to the *local* approach of applying the Sommerfeld radiation condition, as opposed to the *global* technique used in boundary integral type methods. The computational efficiency (i.e. compared to the boundary element method), due to the banded system matrices, seems to be paid for by a lack of generality in imposing the Sommerfeld radiation condition. It is desired to merge the advantages of both modelling strategies closer together, i.e. the precise application of the radiation condition in the boundary element method and the efficient computational scheme of the variable order infinite wave envelope element modelling. An extension of the boundary element method can be considered, by the development of a variable order infinite boundary element, that could be used for so-called boundary element subdomaining [3.24,3.25]. It would be desired to seek out an optimum degree of subdomaining to strike a balance between computational efficiency and the generality of the imposition of the Sommerfeld radiation condition.

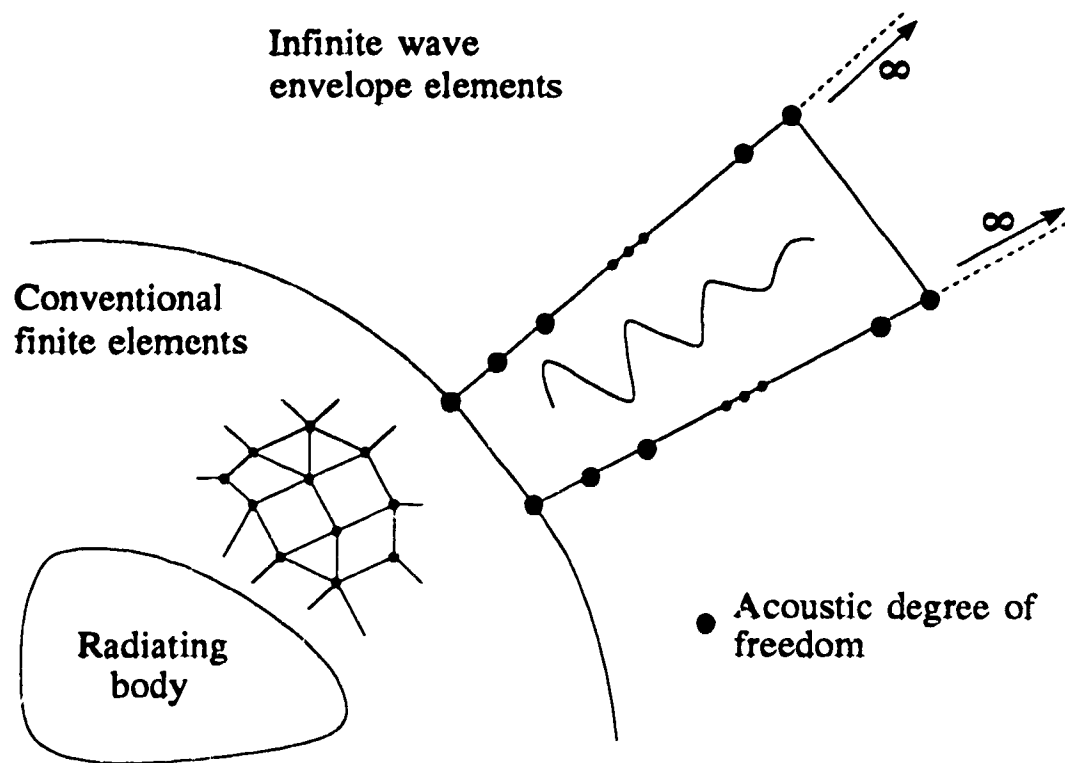


Figure 3.1 Modelling an infinite acoustic domain using conventional finite elements and variable order infinite wave envelope elements.

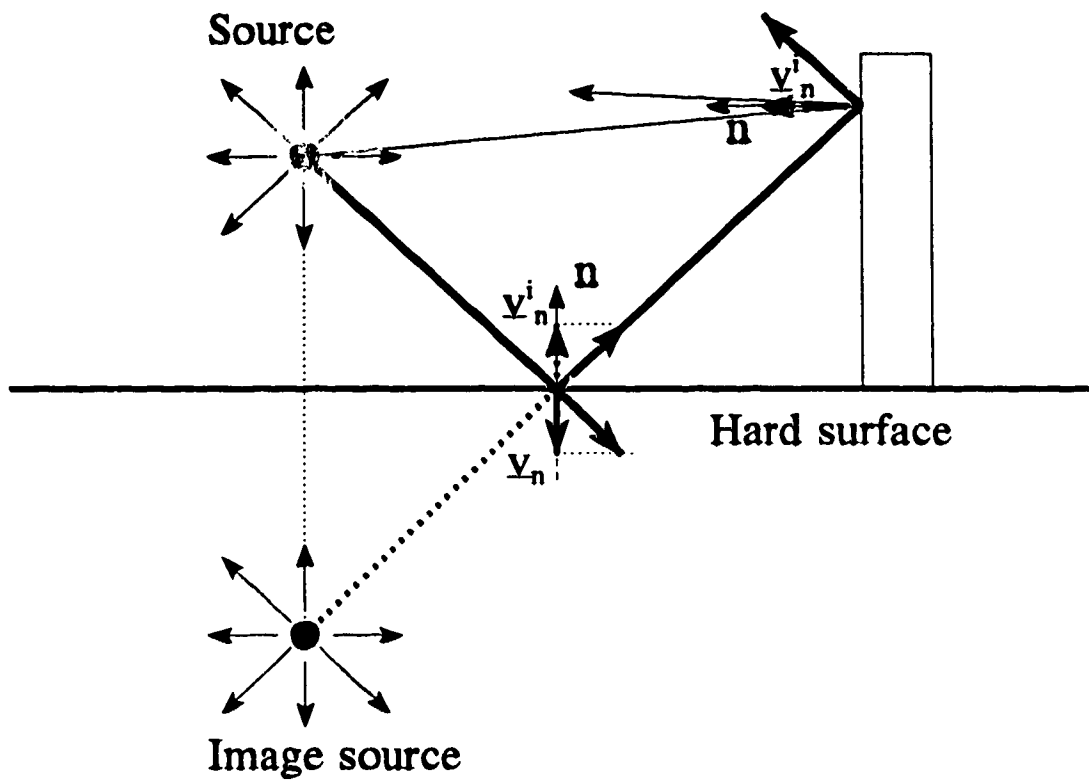


Figure 3.2 The use of image sources in acoustic scattering problems above a hard plane.

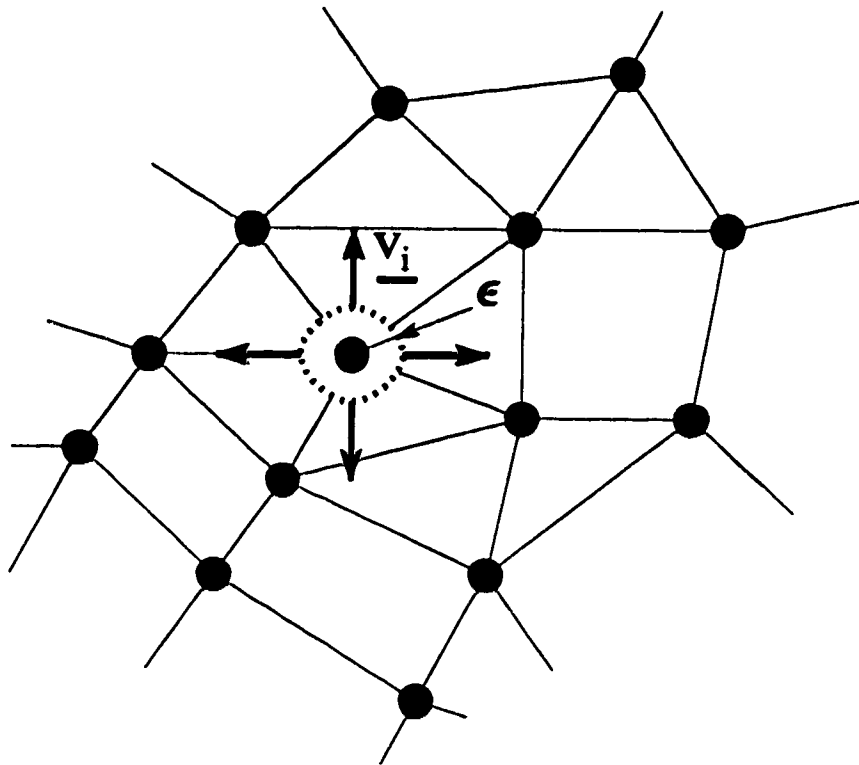


Figure 3.3 Applying a two-dimensional cylindrical source at an acoustic degree of freedom.

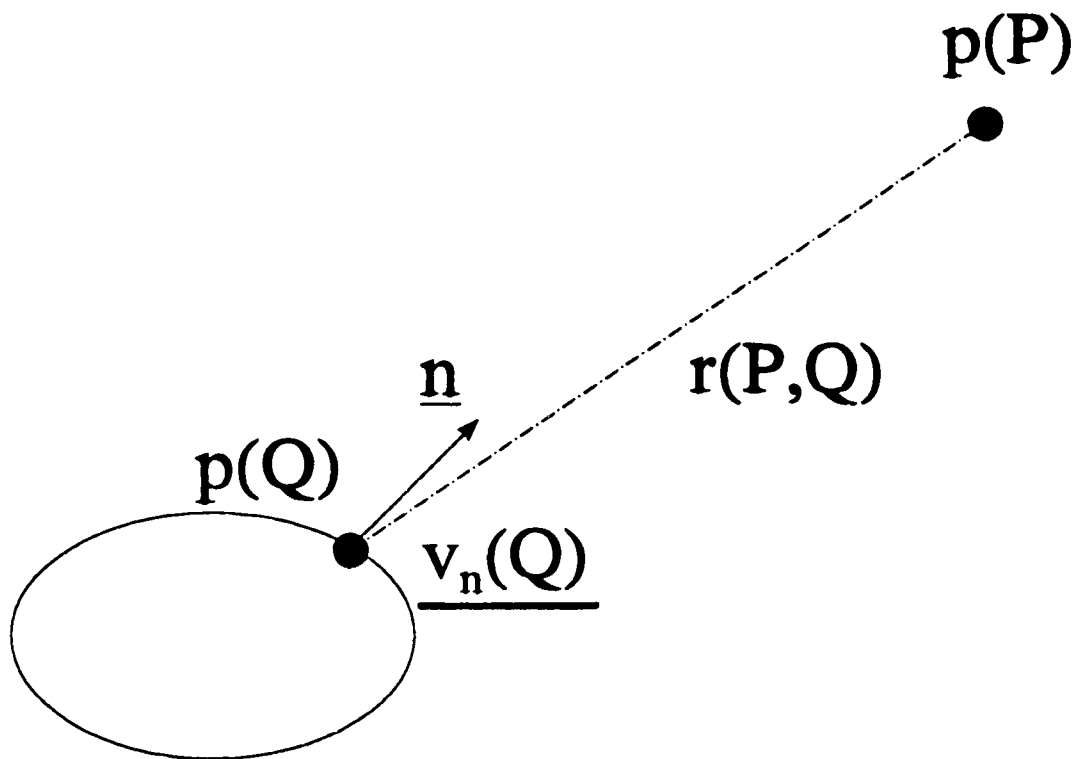


Figure 3.4 The boundary element post-processing concept.

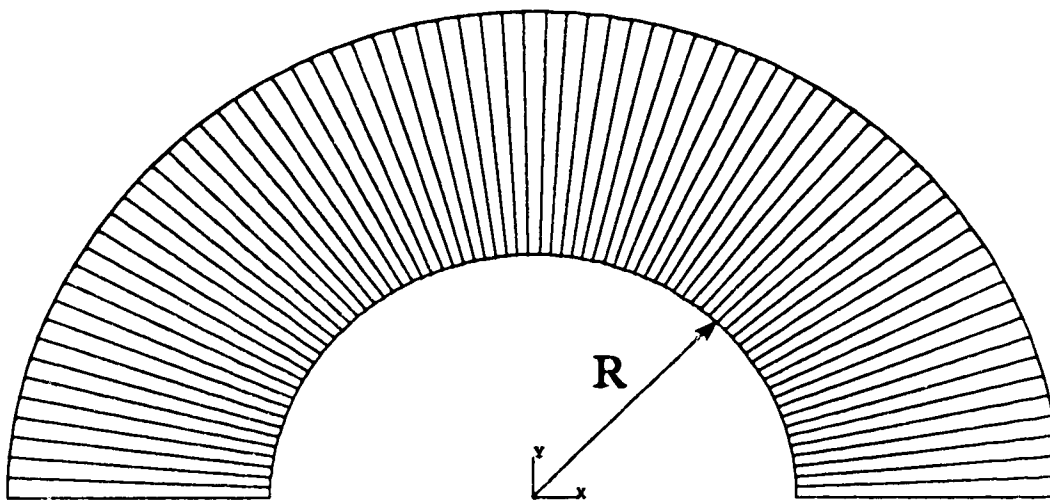


Figure 3.5 A single layer of 75 quadratic infinite wave envelope elements for two-dimensional modelling of acoustic radiation or scattering from a cylinder.

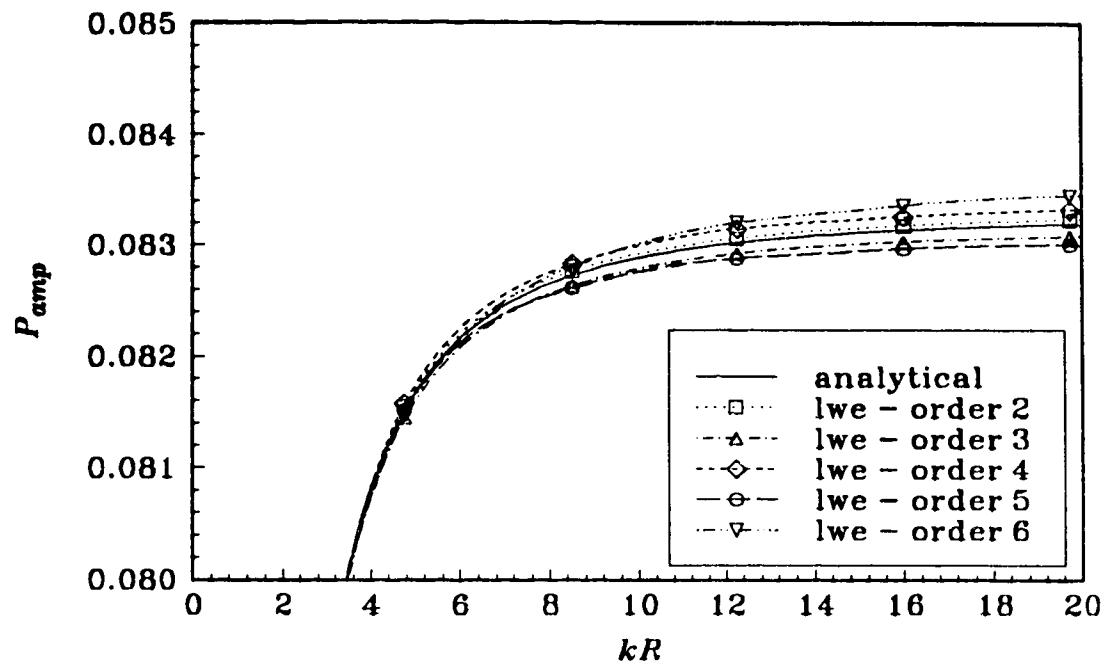


Figure 3.6 Acoustic radiation by a sphere - monopole.
 Geometry mesh used: 90 lwe.
 Frequency response function of the amplitude of the radiated acoustic pressure at $r = 5R$.

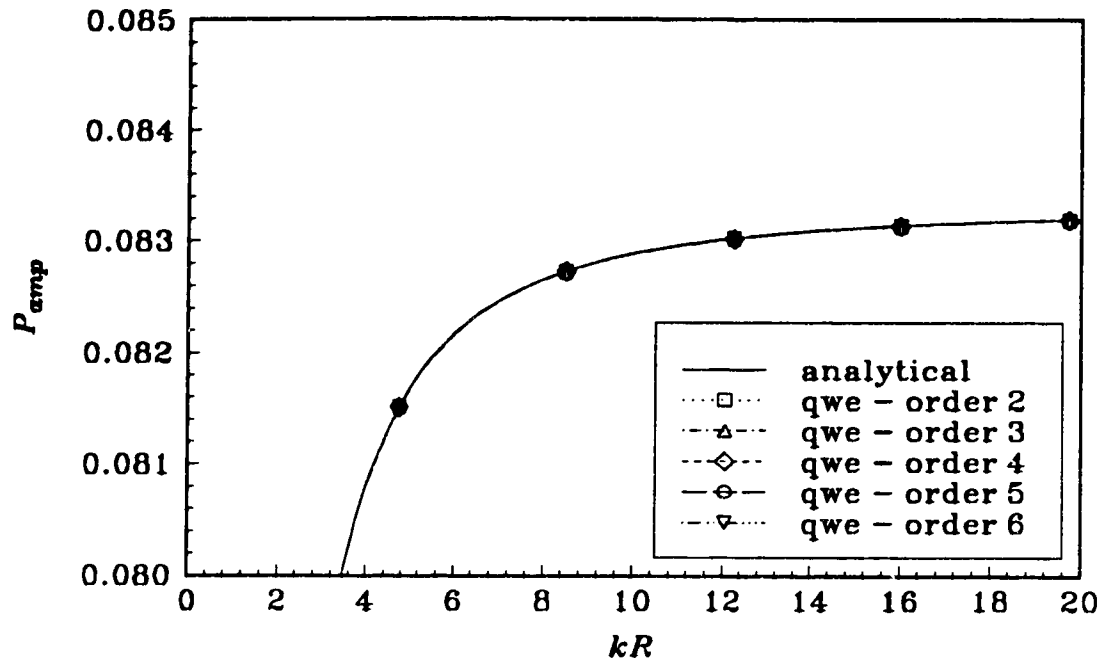


Figure 3.7 Acoustic radiation by a sphere - monopole.
 Geometry mesh used: 45 qwe.
 Frequency response function of the amplitude of the radiated acoustic pressure at $r = 5R$.

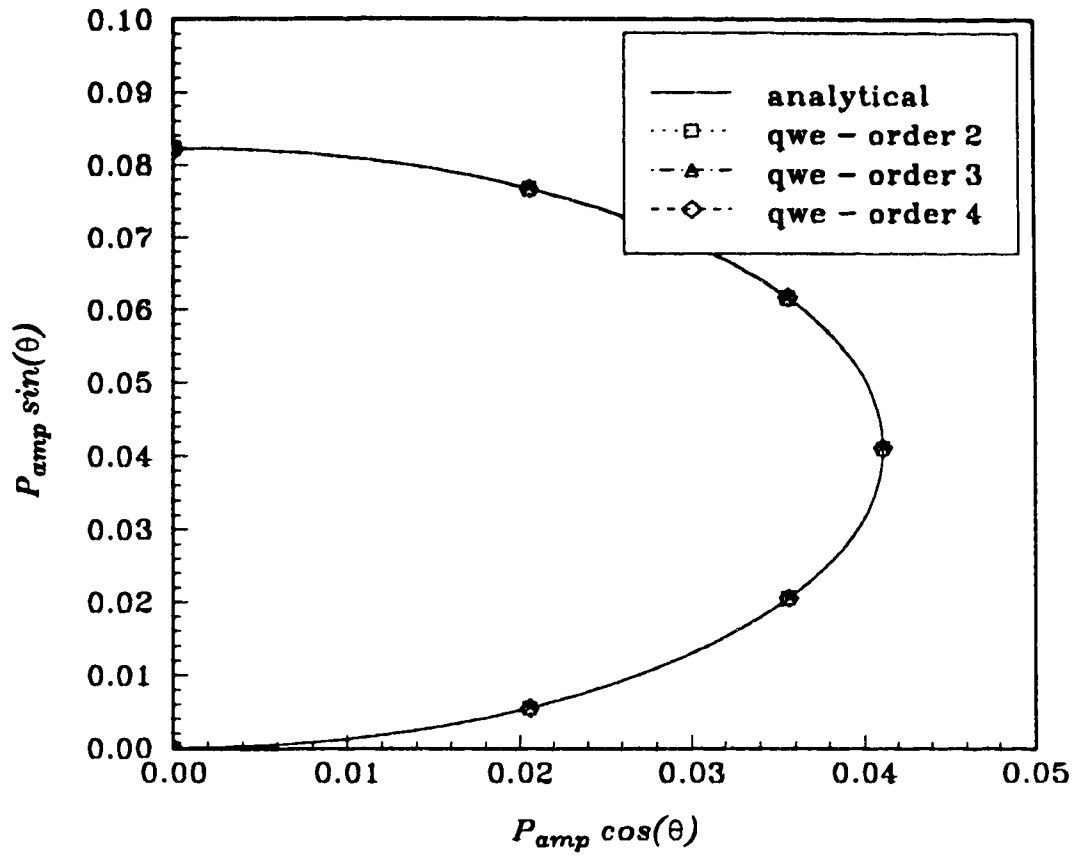


Figure 3.8 Spherical multi-pole of order 1.
 Geometry mesh used: 75 qwe.
 Polar plot ($0 < \theta < 90$) of the amplitude of the radiated acoustic pressure
 at $r = 5R$ for $kR = 20$.

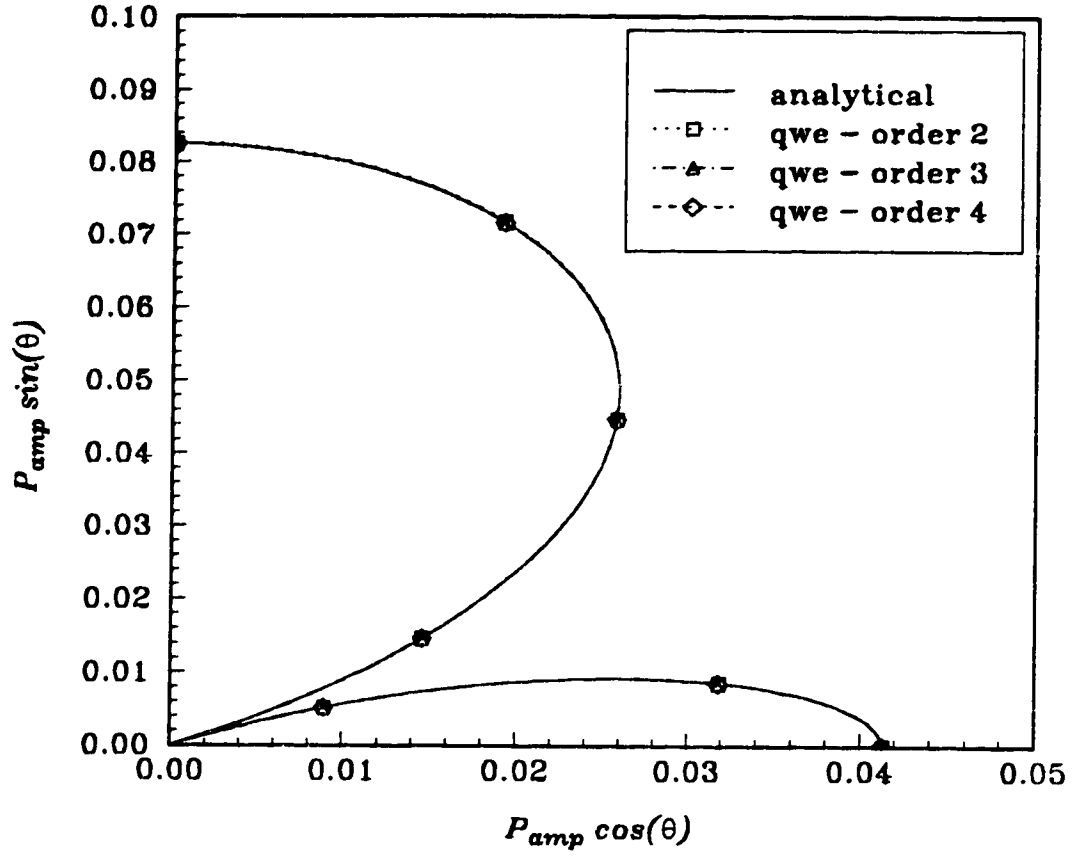


Figure 3.9 Spherical multi-pole of order 2.
 Geometry mesh used: 75 qwe.
 Polar plot ($0 < \theta < 90$) of the amplitude of the radiated acoustic pressure
 at $r = 5R$ for $kR = 20$.

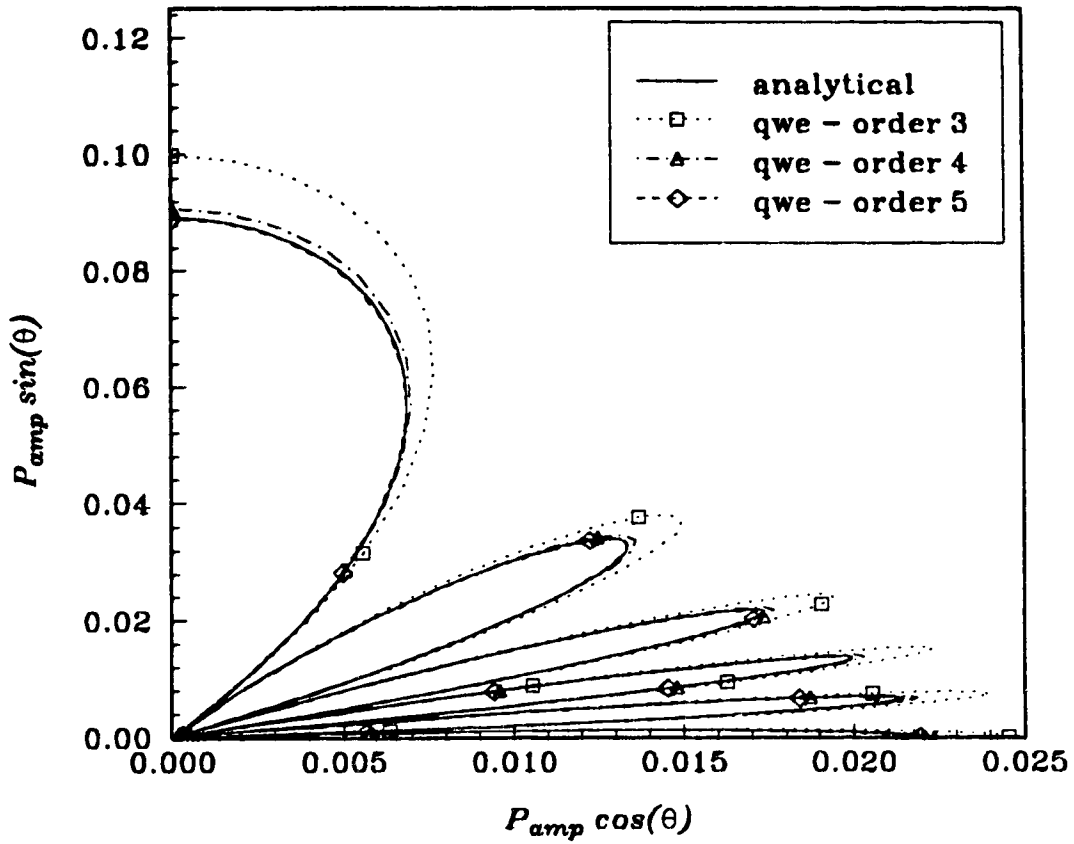


Figure 3.10 Spherical multi-pole of order 10.
 Geometry mesh used: 75 qwe.
 Polar plot ($0 < \theta < 90$) of the amplitude of the radiated acoustic pressure
 at $r = 5R$ for $kR = 20$.

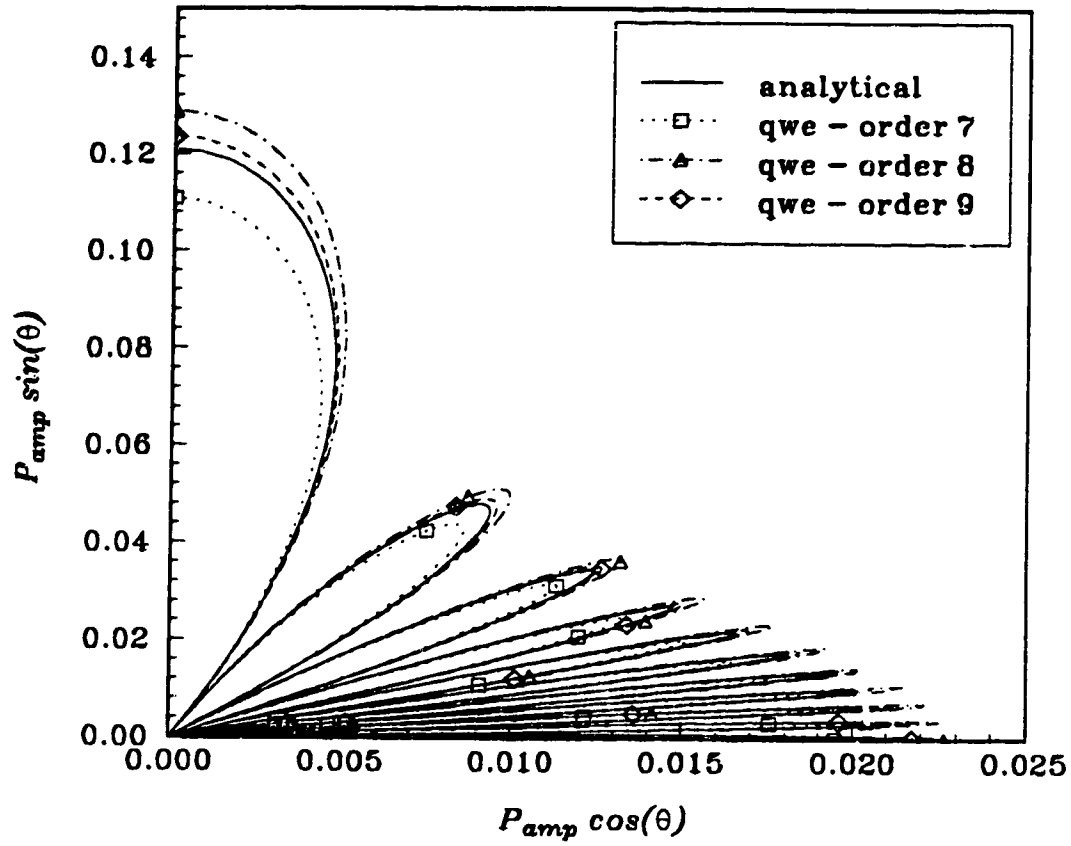


Figure 3.11 Spherical multi-pole of order 20.
 Geometry mesh used: 75 qwe.
 Polar plot ($0 < \theta < 90$) of the amplitude of the radiated acoustic pressure
 at $r = 5R$ for $kR = 20$.

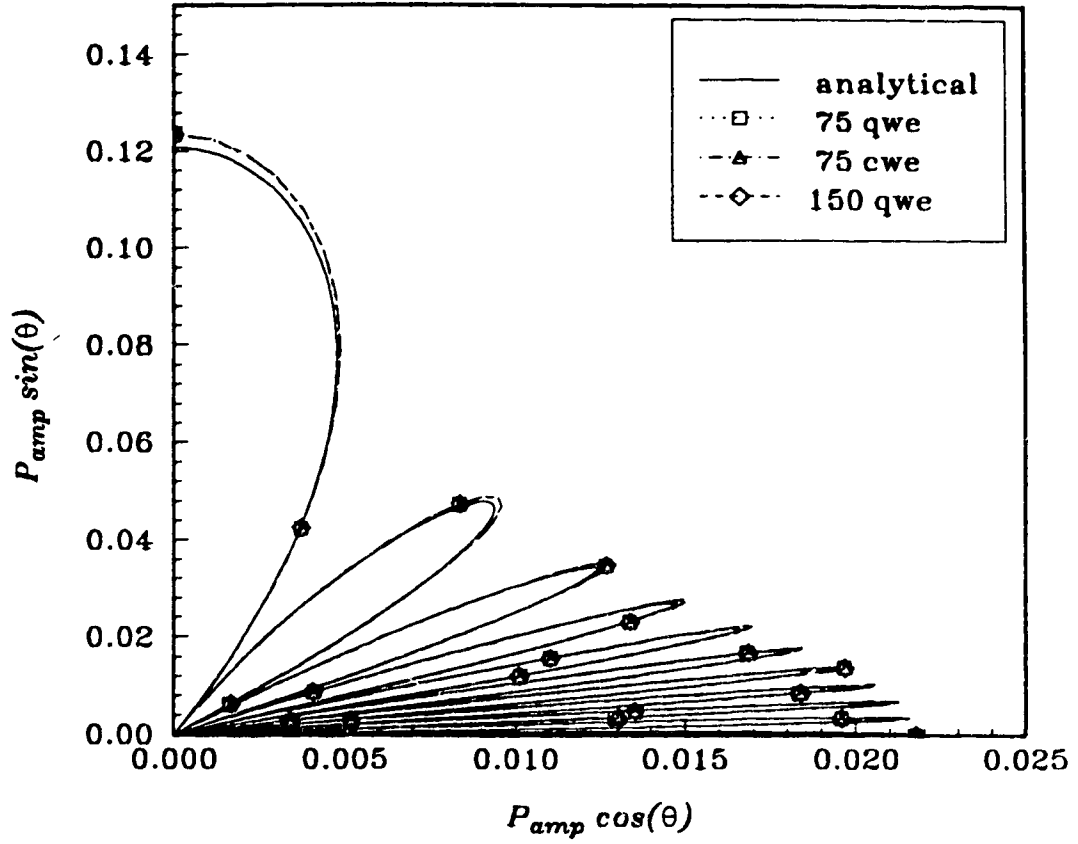


Figure 3.12 Spherical multi-pole of order 20.
Different angular discretization in geometry mesh.
Polar plot ($0 < \theta < 90$) of the amplitude of the radiated acoustic pressure
at $r = 5R$ for $kR = 20$.

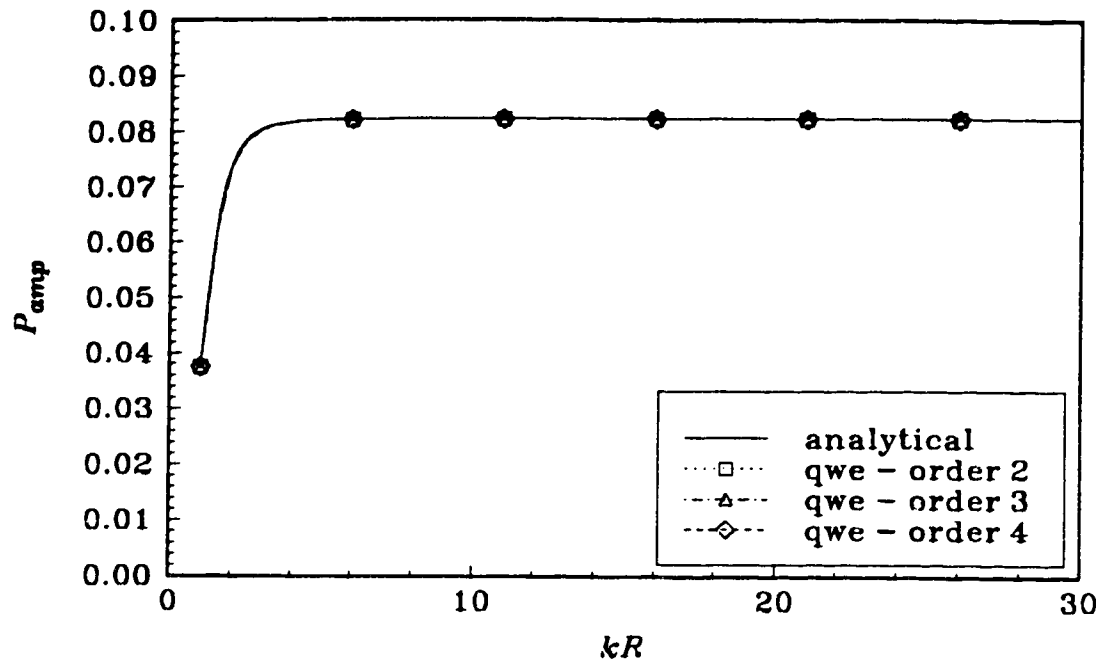


Figure 3.13 Spherical multi-pole of order 1.
 Geometry mesh used: 75 qwe.
 Frequency response function of the amplitude of the radiated acoustic pressure at $x = 0$; $y = 5R$.

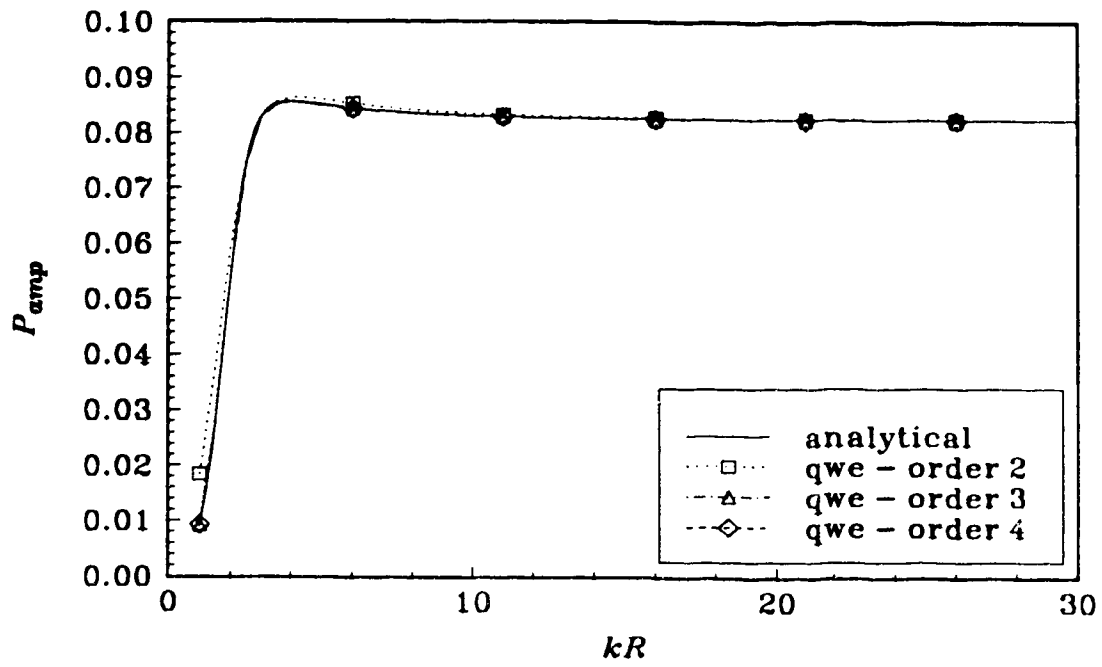


Figure 3.14 Spherical multi-pole of order 2.
 Geometry mesh used: 75 qwe.
 Frequency response function of the amplitude of the radiated acoustic pressure at $x = 0$; $y = 5R$.

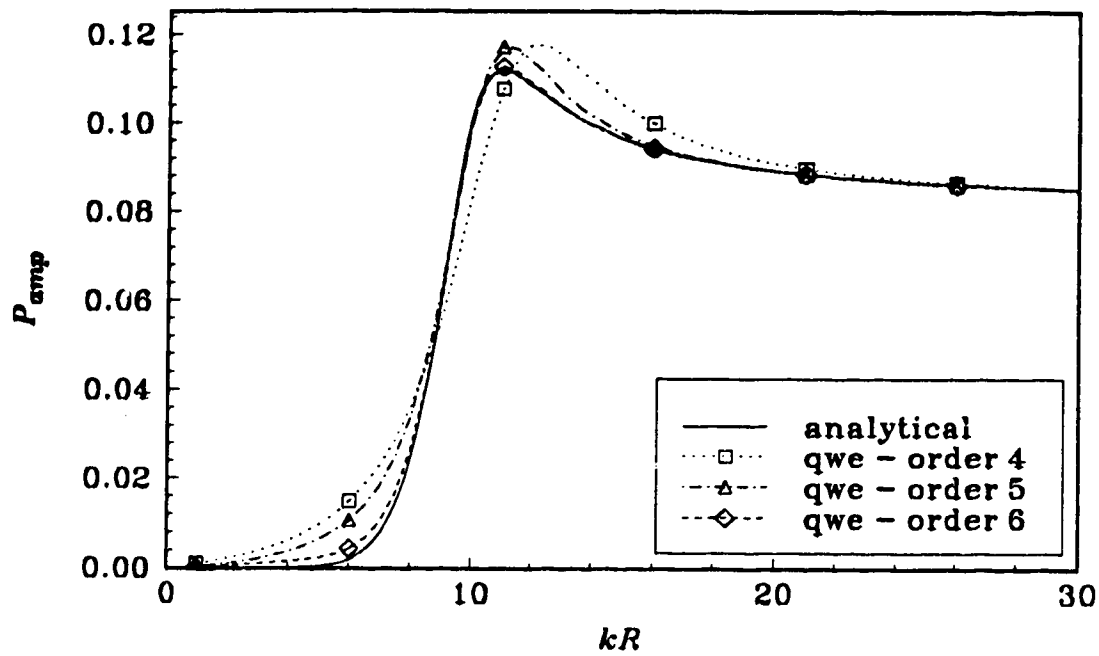


Figure 3.15 Spherical multi-pole of order 10.
 Geometry mesh used: 75 qwe.
 Frequency response function of the amplitude of the radiated acoustic pressure at $x = 0$; $y = 5R$.

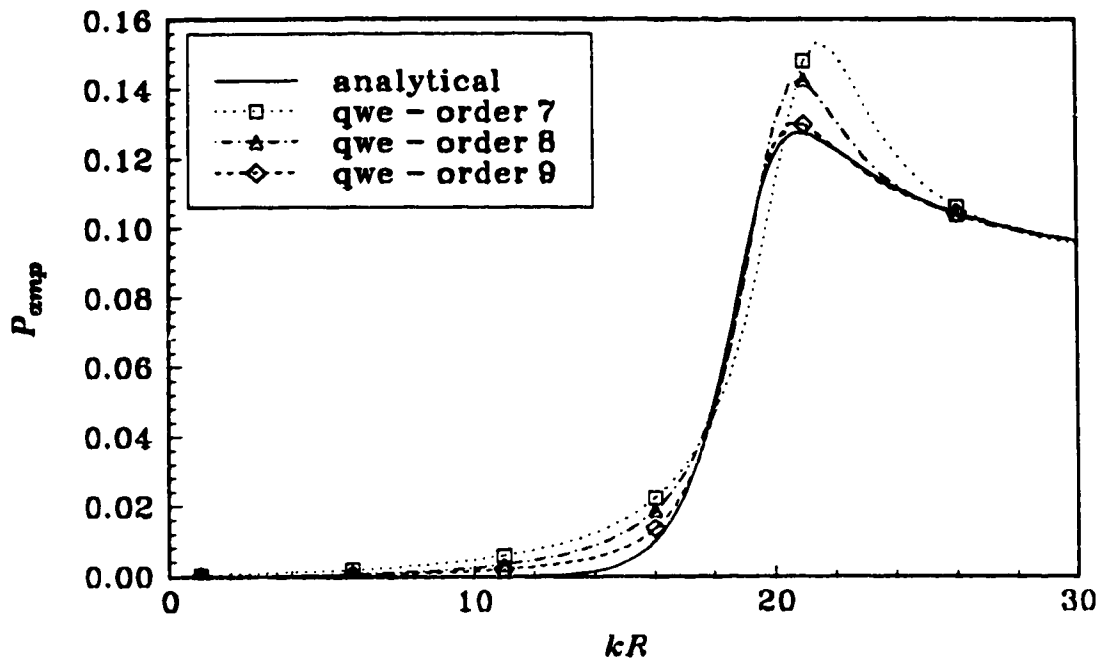


Figure 3.16 Spherical multi-pole of order 20.
 Geometry mesh used: 75 qwe.
 Frequency response function of the amplitude of the radiated acoustic pressure at $x = 0$; $y = 5R$.

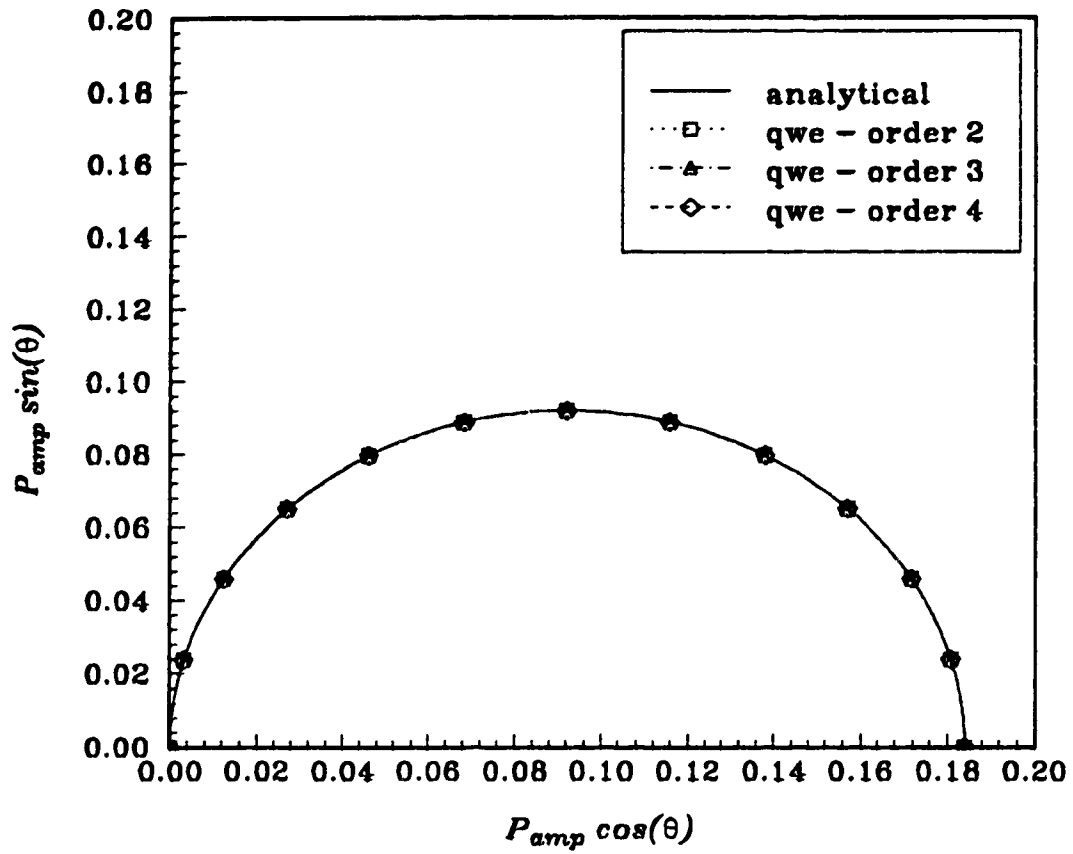


Figure 3.17 Cylindrical multi-pole of order 1.
 Geometry mesh used: 75 qwe.
 Polar plot ($0 < \theta < 90$) of the amplitude of the radiated acoustic pressure
 at $r = 5R$ for $kR = 20$.

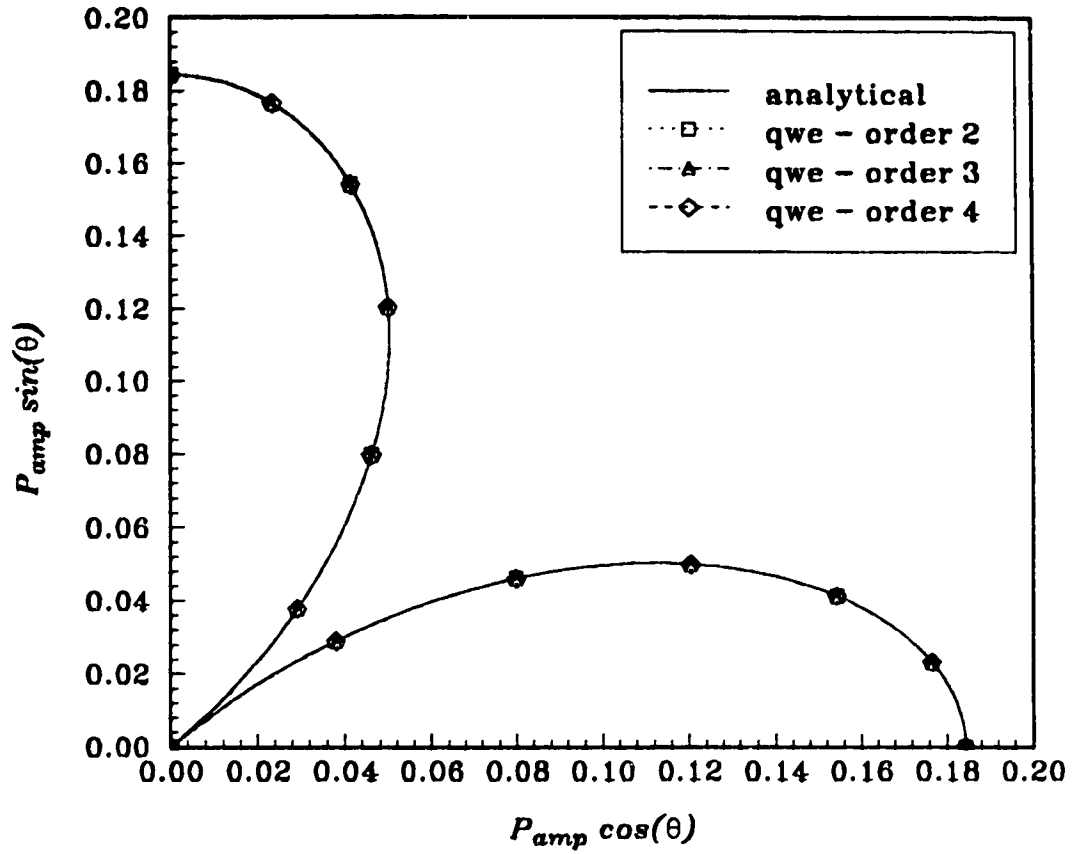


Figure 3.18 Cylindrical multi-pole of order 2.
 Geometry mesh used: 75 qwe.
 Polar plot ($0 < \theta < 90$) of the amplitude of the radiated acoustic pressure
 at $r = 5R$ for $kR = 20$.

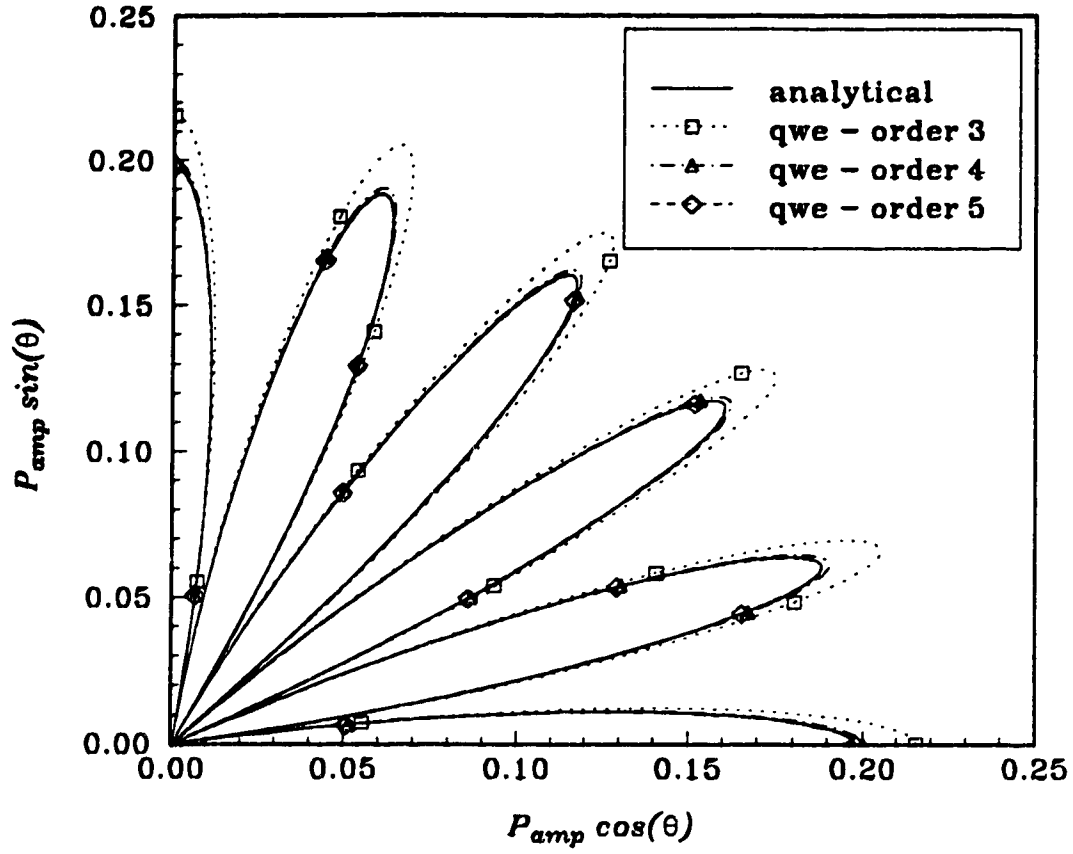


Figure 3.19 Cylindrical multi-pole of order 10.
 Geometry mesh used: 75 qwe.
 Polar plot ($0 < \theta < 90$) of the amplitude of the radiated acoustic pressure
 at $r = 5R$ for $kR = 20$.

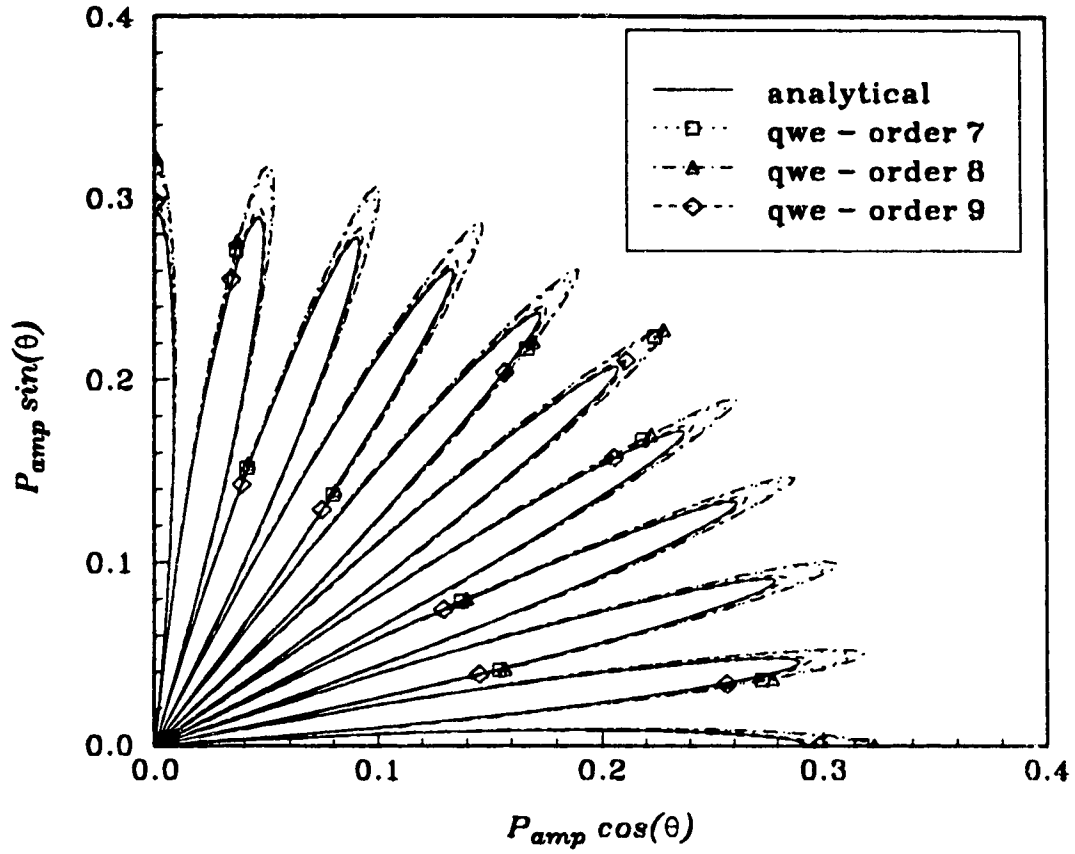


Figure 3.20 Cylindrical multi-pole of order 20.
 Geometry mesh used: 75 qwe.
 Polar plot ($0 < \theta < 90$) of the amplitude of the radiated acoustic pressure
 at $r = 5R$ for $kR = 20$.

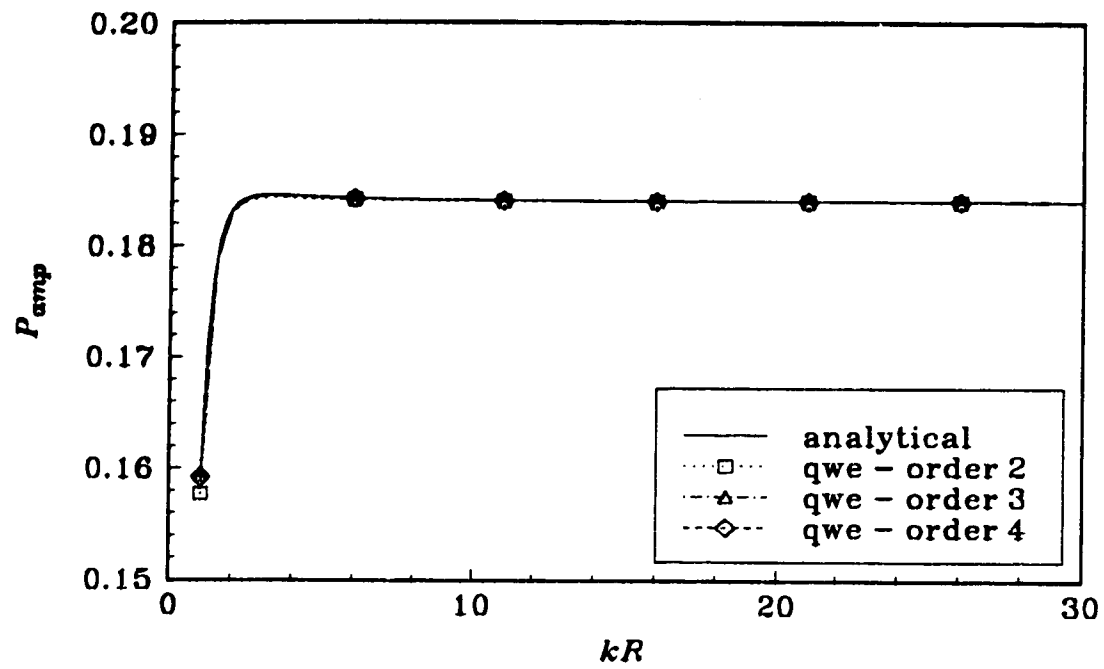


Figure 3.21 Cylindrical multi-pole of order 1.
 Geometry mesh used: 75 qwe.
 Frequency response function of the amplitude of the radiated acoustic pressure at $x = 5R$; $y = 0$.

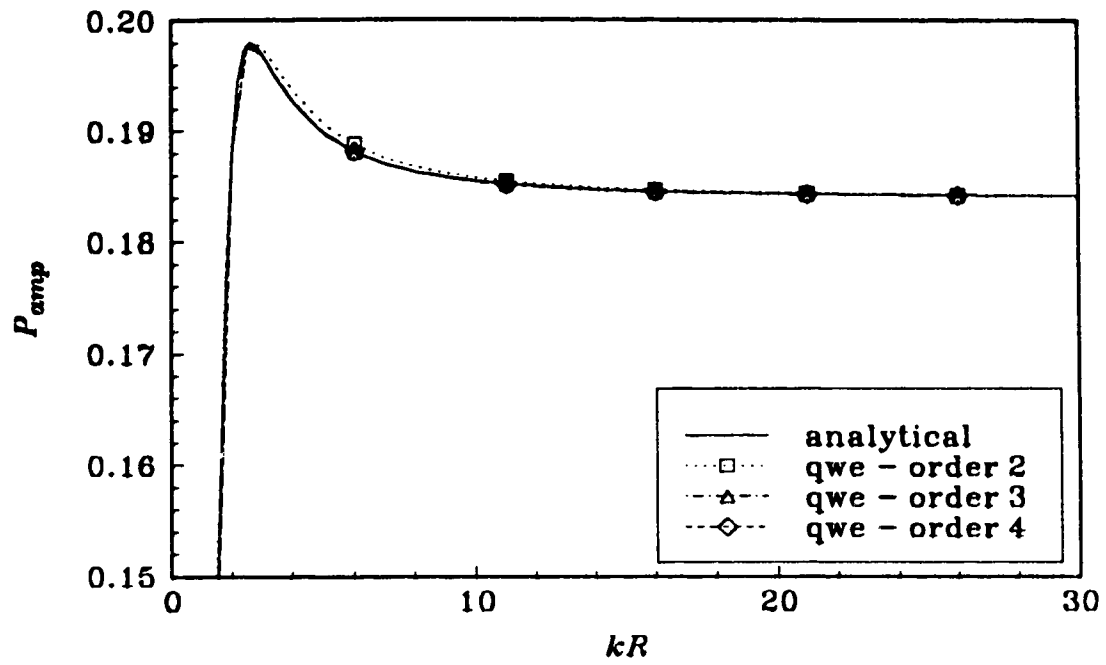


Figure 3.22 Cylindrical multi-pole of order 2.
 Geometry mesh used: 75 qwe.
 Frequency response function of the amplitude of the radiated acoustic pressure at $x = 5R$; $y = 0$.

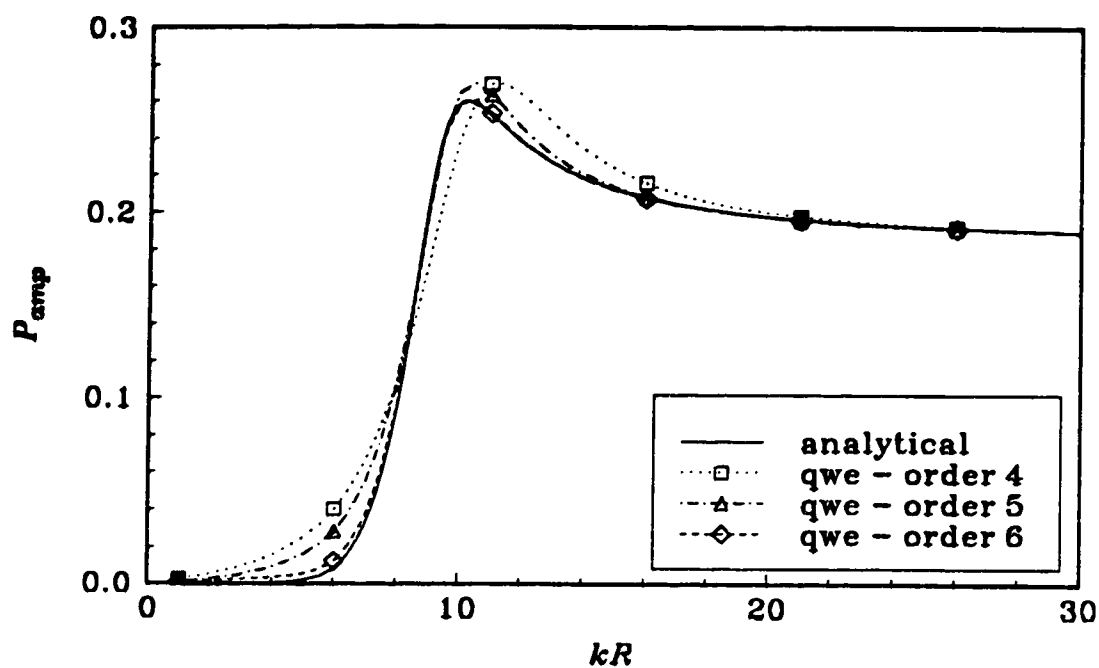


Figure 3.23 Cylindrical multi-pole of order 10.
 Geometry mesh used: 75 qwe.
 Frequency response function of the amplitude of the radiated acoustic pressure at $x = 5R$; $y = 0$.

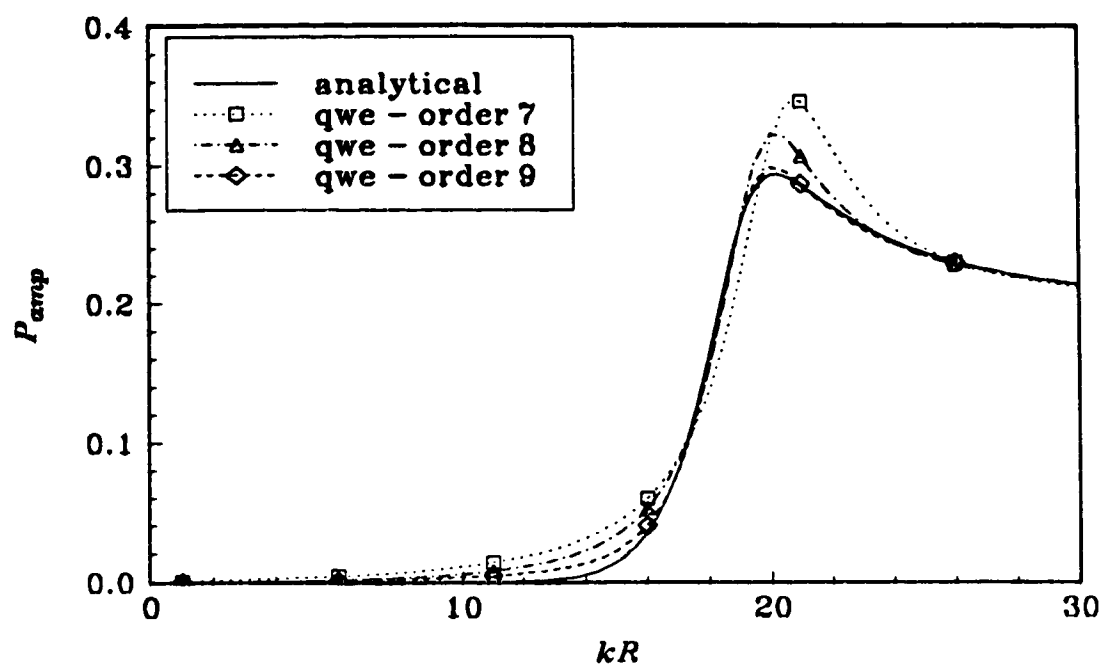


Figure 3.24 Cylindrical multi-pole of order 20.
 Geometry mesh used: 75 qwe.
 Frequency response function of the amplitude of the radiated acoustic pressure at $x = 5R$; $y = 0$.

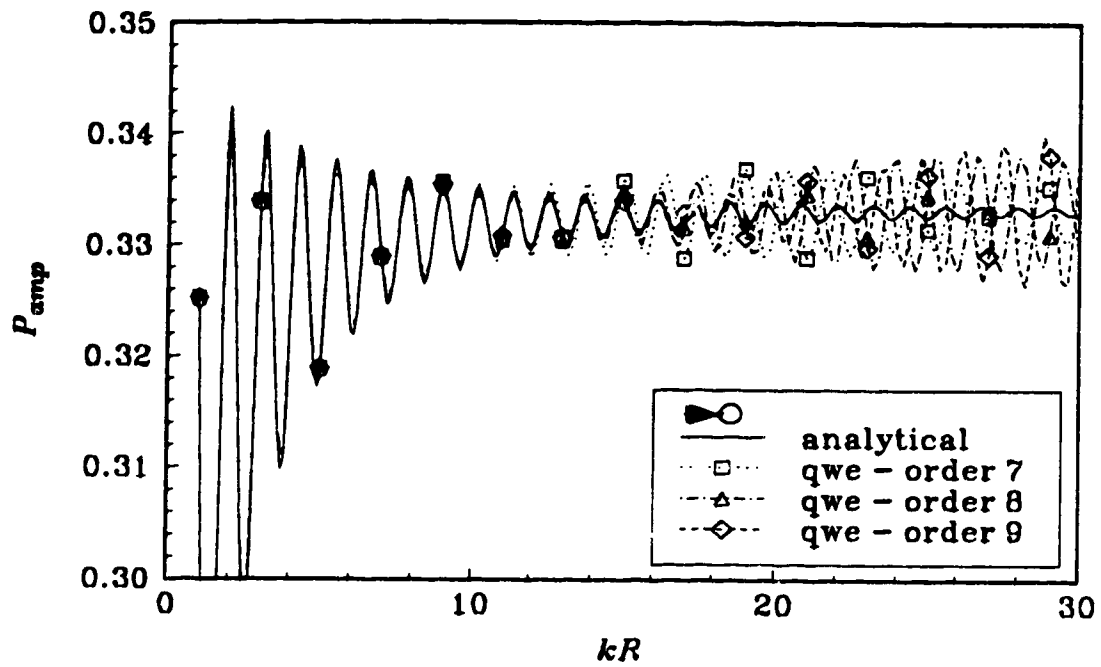


Figure 3.25 Scattering of an acoustic plane wave ($\rightarrow +x$) from a rigid cylinder.
 Geometry mesh used: 75 qwe.
 Frequency response function of the amplitude of the scattered acoustic pressure $|P_s|/|P_i|$ at $x = -5R$; $y = 0$.

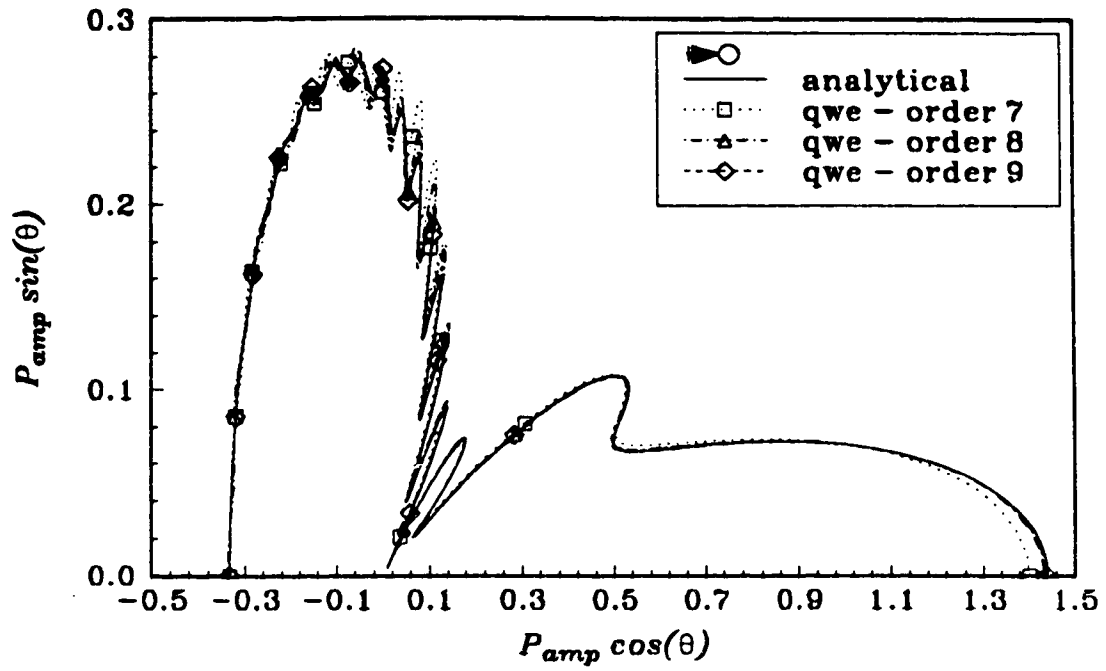


Figure 3.26 Scattering of an acoustic plane wave ($\rightarrow +x$) from a rigid cylinder. Geometry mesh used: 75 qwe. Polar plot ($0 < \theta < 180$) of the amplitude of the scattered acoustic pressure $|P_s|/|P_i|$ at $r = 5R$ for $kR = 20$.

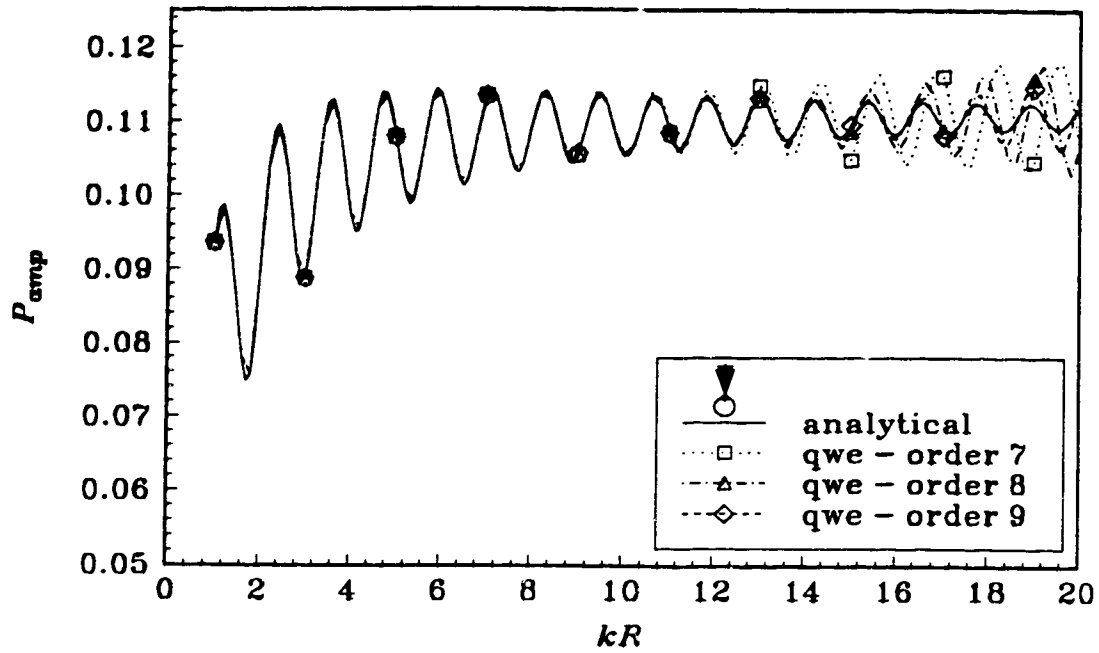


Figure 3.27 Scattering of an acoustic plane wave ($\downarrow -z$) from a rigid sphere.
 Geometry mesh used: 75 qwe.
 Frequency response function of the amplitude of the scattered acoustic pressure $|P_s|/|P_i|$ at $x = 0$; $y = 5R$.

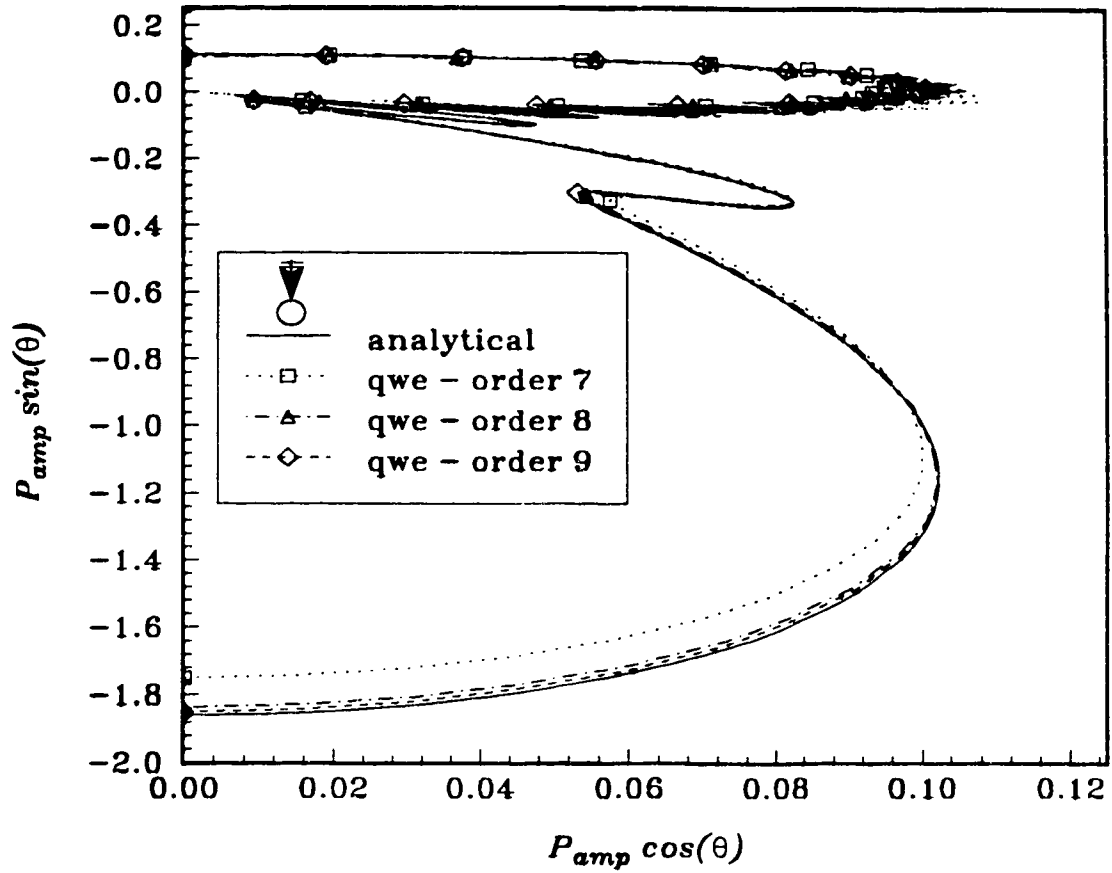


Figure 3.28 Scattering of an acoustic plane wave ($\downarrow -z$) from a rigid sphere. Geometry mesh used: 75 qwe. Polar plot ($-90 < \theta < 90$) of the amplitude of the scattered acoustic pressure $|P_s|/|P_i|$ at $r = 5R$ for $kR = 20$.

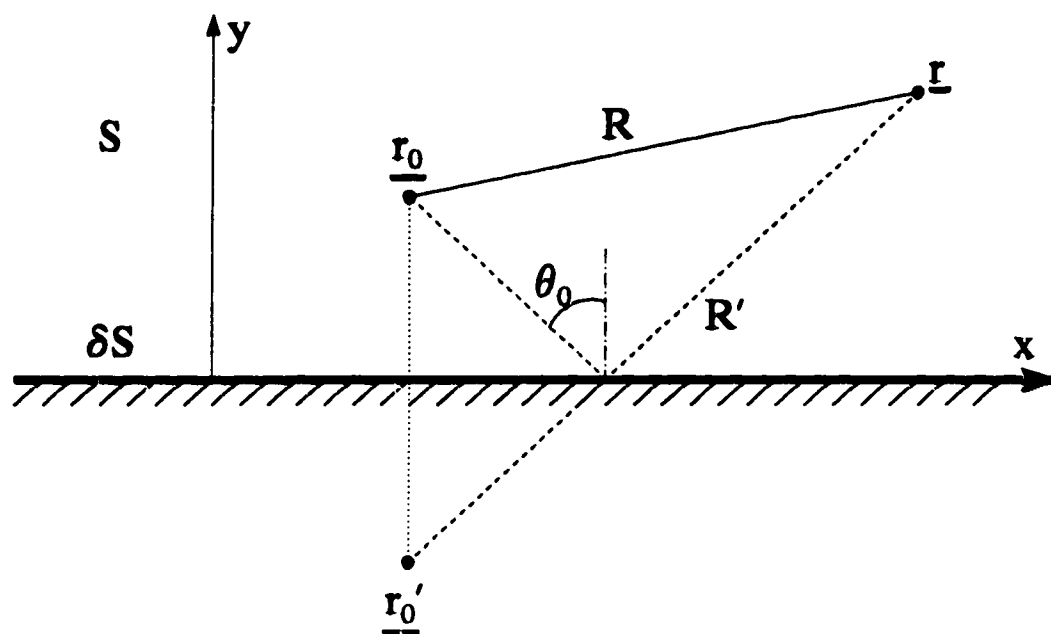


Figure 3.29 Cylindrical source above a homogeneous impedance plane: Configuration sketch.

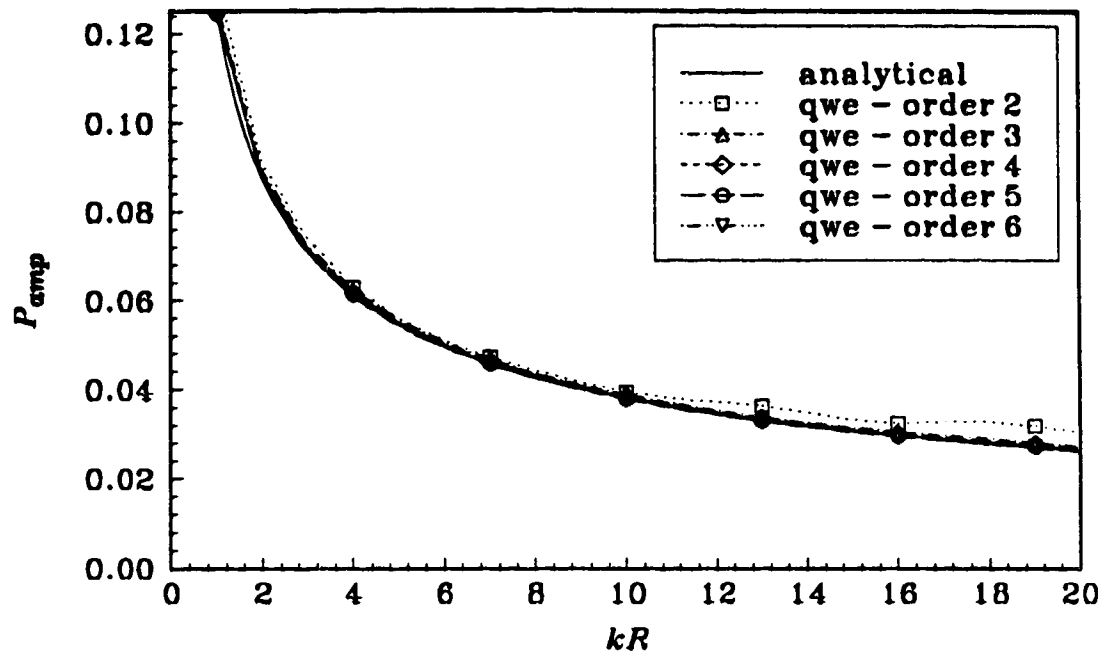


Figure 3.30 Modelling of a cylindrical source, at $x = 0$; $y = 0.25$, above a homogeneous impedance plane ($\beta = 0.005$).
 Geometry mesh used: 58 cfe and 16 qwe.
 Frequency response function of the amplitude of the acoustic pressure at $x = 10$; $y = 0.25$.

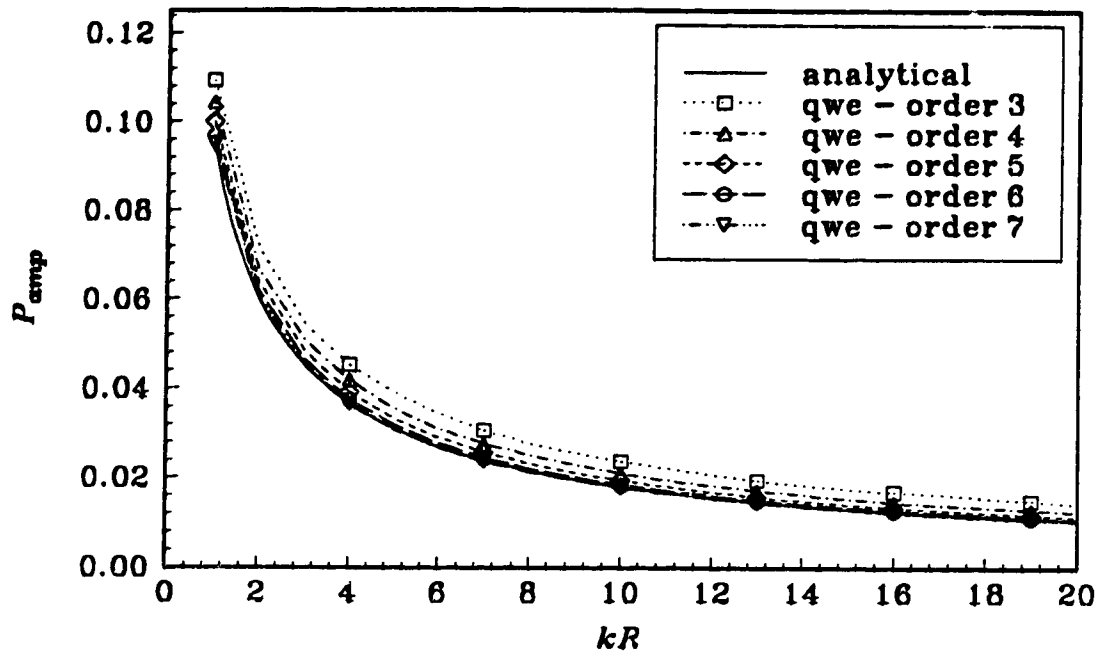


Figure 3.31 Modelling of a cylindrical source, at $x = 0$; $y = 0.25$, above a homogeneous impedance plane ($\beta = 0.1$). Geometry mesh used: 58 cfe and 16 qwe. Frequency response function of the amplitude of the acoustic pressure at $x = 10$; $y = 0.25$.

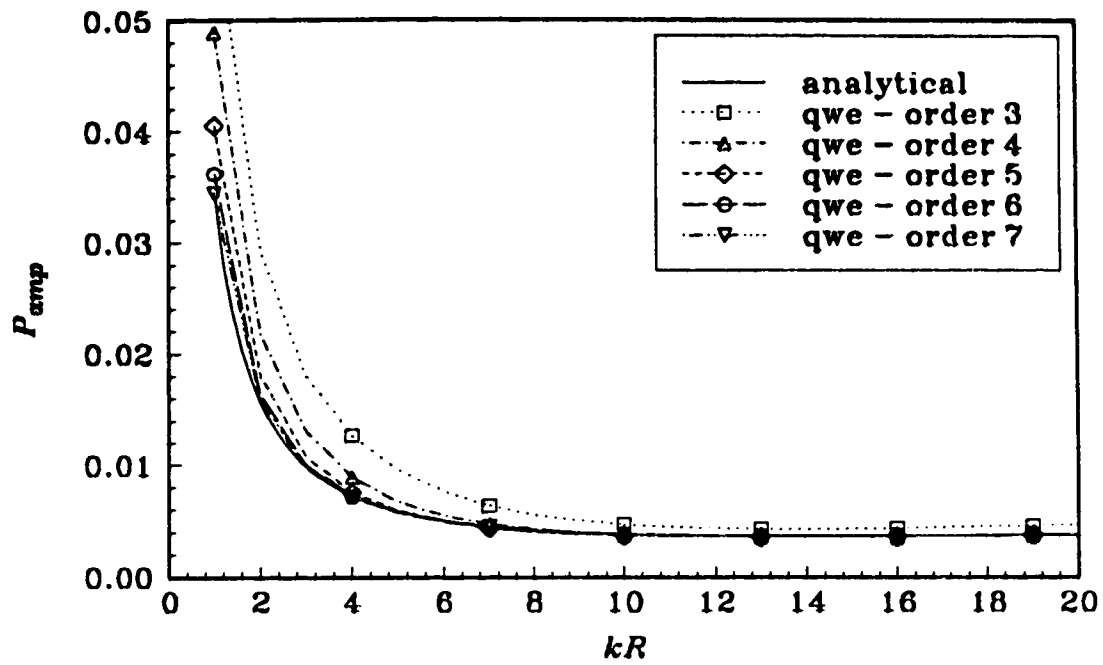


Figure 3.32 Modelling of a cylindrical source, at $x = 0$; $y = 0.25$, above a homogeneous impedance plane ($\beta = 0.5$).
 Geometry mesh used: 58 cfe and 16 qwe.
 Frequency response function of the amplitude of the acoustic pressure at $x = 10$; $y = 0.25$.

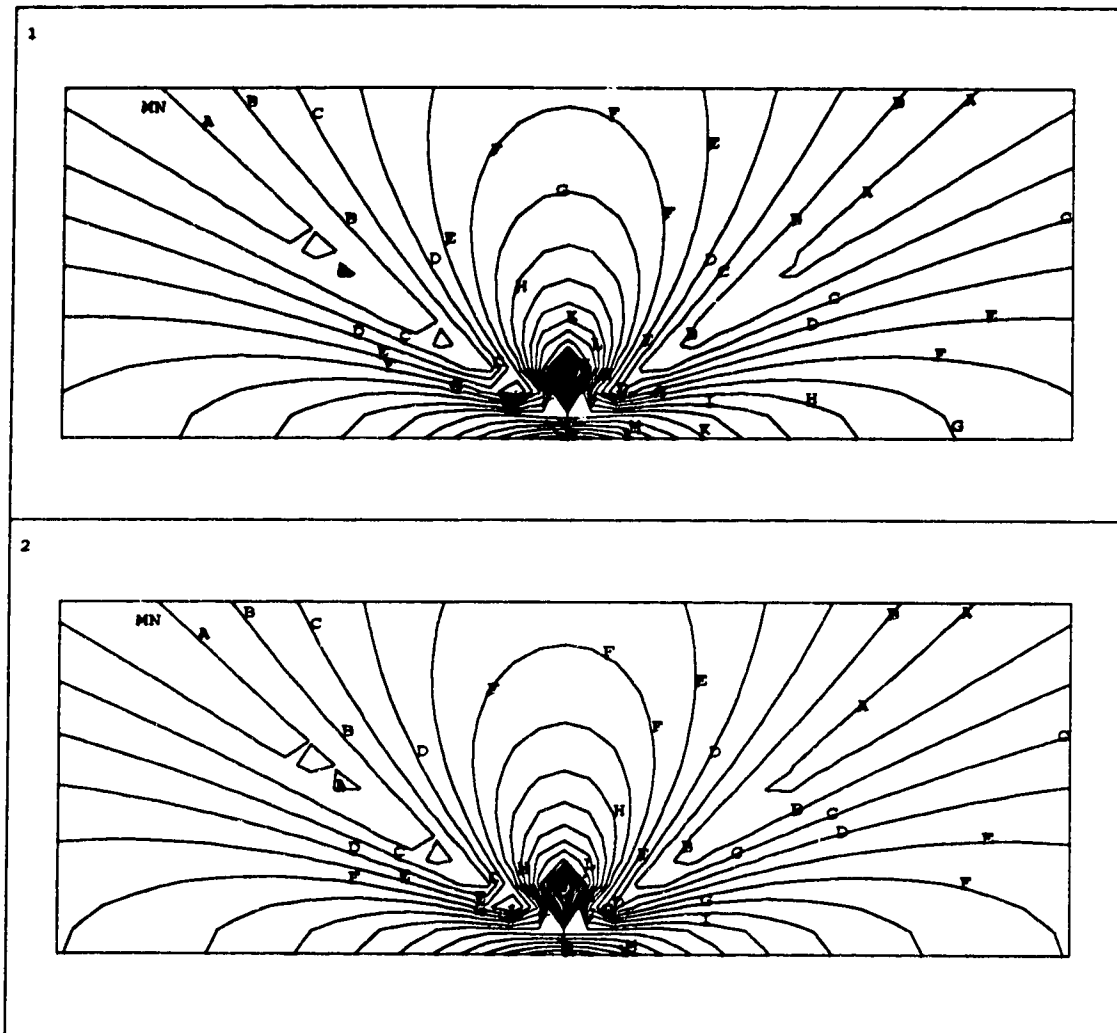


Figure 3.33 Modelling of a cylindrical source, at $x = 0$; $y = 0.25$, above a hard plane ($\beta = 0$). (1) G_β -solution; (2) 2nd order infinite wave envelope element modelling.
 Geometry mesh used: 58 cfe and 16 qwe.
 Contour plot of the amplitude of the acoustic pressure for $k = 10$.

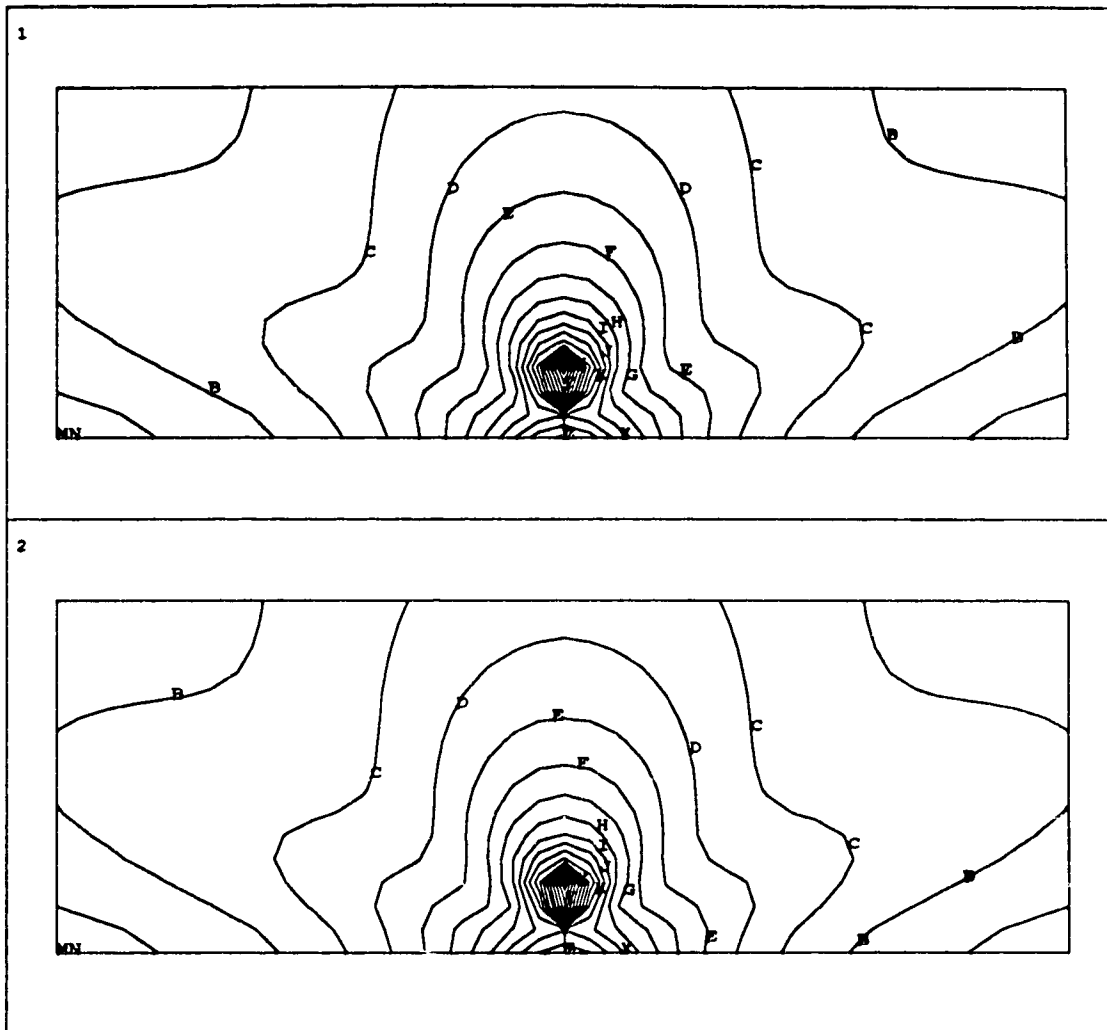


Figure 3.34 Modelling of a cylindrical source, at $x = 0$; $y = 0.25$, above a homogeneous impedance plane ($\beta = 0.5$).
 (1) G_β -solution; (2) 5th order infinite wave envelope element modelling.
 Geometry mesh used: 58 cfe and 16 qwe.
 Contour plot of the amplitude of the acoustic pressure for $k = 10$.

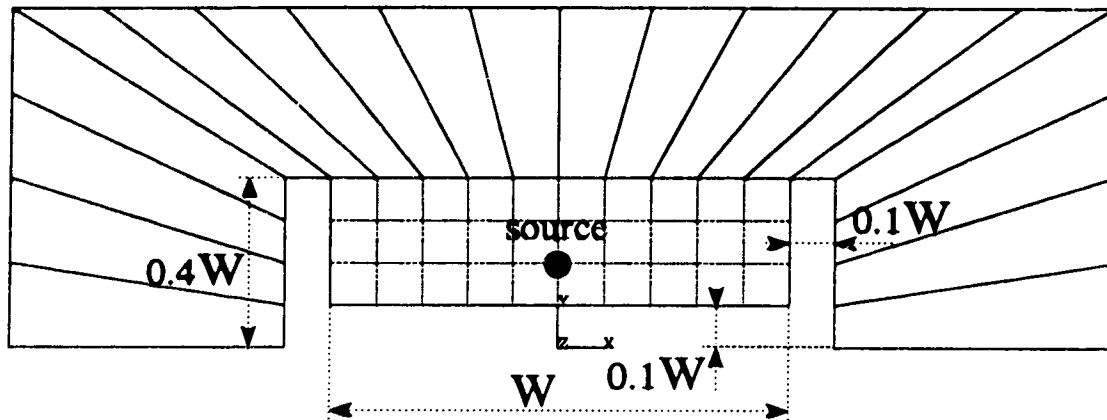


Figure 3.35 Geometry mesh for the modelling of a double barrier configuration: 30 conventional finite elements (cfe) and 20 qwe.

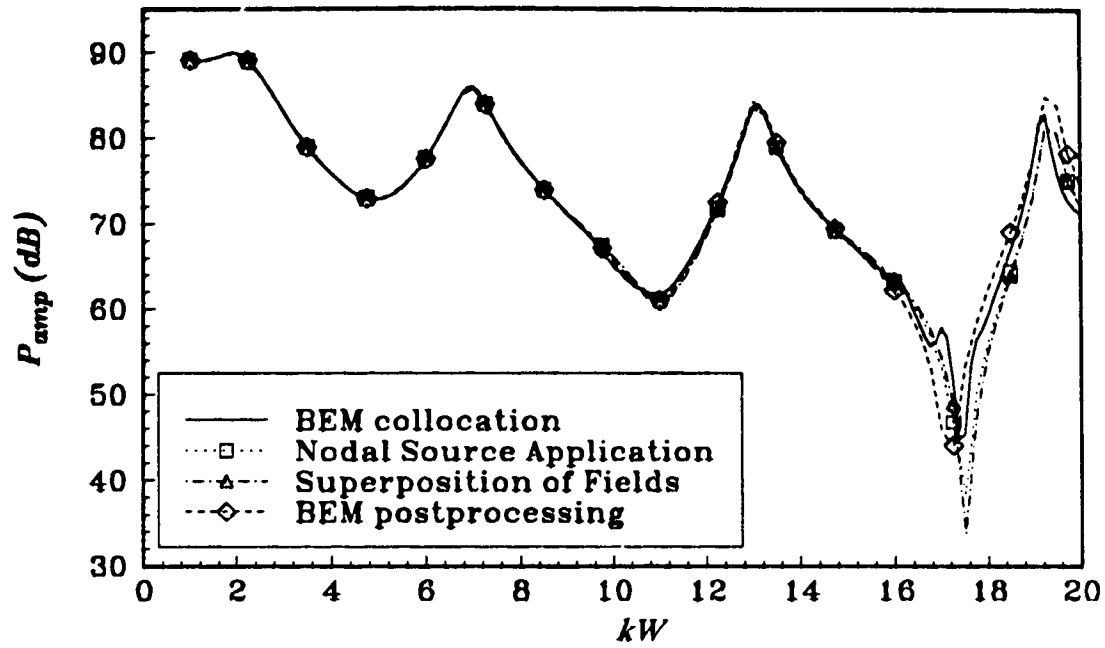


Figure 3.36 Scattering from a double barrier with rigid platform ($\beta = 0$).
 Cylindrical source at $x = 0$; $y = 0.2W$.
 Geometry mesh used: 30 cfe and 20 qwe (order 8).
 Frequency response function of the amplitude (dB) of the acoustic pressure
 at $x = 5W$; $y = 0.15W$.

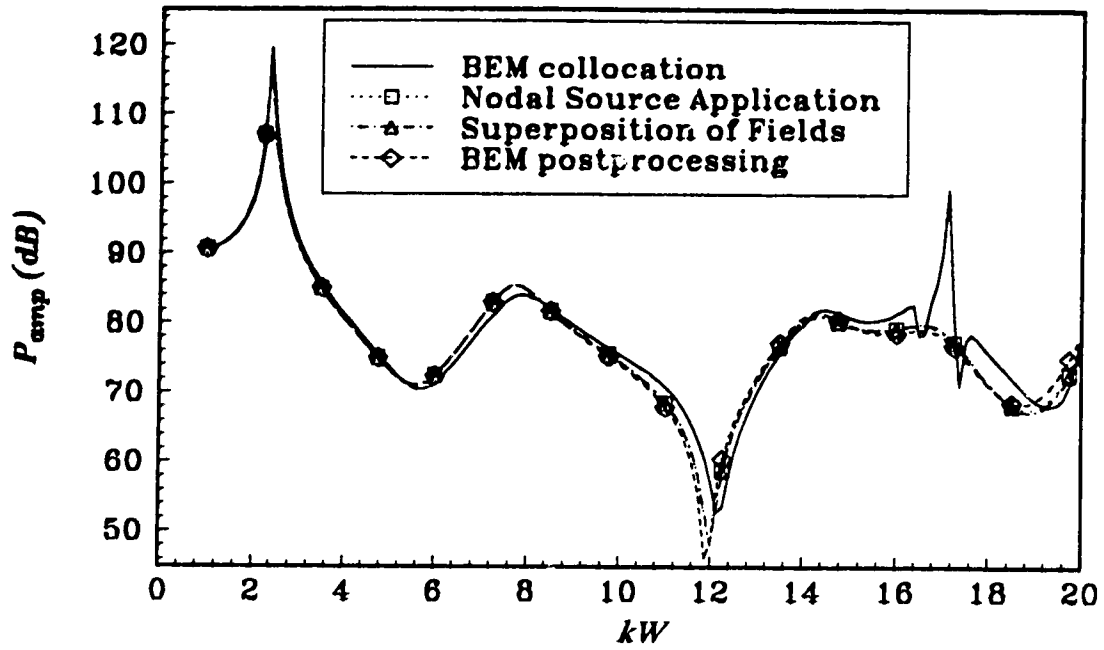


Figure 3.37 Scattering from a double barrier with soft platform ($\beta = 0.5$).
 Cylindrical source at $x = 0$; $y = 0.2W$.
 Geometry mesh used: 30 cfe and 20 qwe (order 8).
 Frequency response function of the amplitude (dB) of the acoustic pressure
 at $x = 5W$; $y = 0.15W$.

REFERENCES

- 3.1. F. V. ATKINSON, "On Sommerfeld's radiation condition," *The Philosophical Magazine* **40**, 645-651 (1949).
- 3.2. A. BAYLISS, M. GUNZBURGER and E. TURKEL, "Boundary conditions for the numerical solution of elliptic equations in exterior regions," ICASE Report No. 80/1, NASA Langley, (1980).
- 3.3. C. H. WILCOX, "A generalization of theorems of Rellich and Atkinson," *Proceedings of the American Mathematical Society*, 271-276 (1956).
- 3.4. O. C. ZIENKIEWICZ, D. W. KELLY and P. BETTESS, "The Sommerfeld (radiation) condition on infinite domains and its modelling in numerical procedures," *Computing Methods in Applied Sciences and Engineering, Third International Symposium, IRIA Laboria, Lect. In Math. V* **704**, 169-192 (1977).
- 3.5. A. F. SEYBERT, "Review of the boundary element method in acoustics," *Noise Control Foundation, New York, NY, USA* **2532**, 25-32 (1991).
- 3.6. K. R. FYFE and F. ISMAIL, "Investigation of the acoustic properties of vibrating finite cylinders," *Journal of Sound and Vibration* **128**, 361-376 (1989).
- 3.7. R. BOSSUT and J.-N. DECARPIGNY, "Finite element modelling of radiating structures using dipolar damping elements," *Journal of the Acoustical Society of America* **86**, 1234-1244 (1989).
- 3.8. P. M. PINSKY, L. L. THOMPSON and N. N. ABOUD, "Local high-order radiation boundary conditions for the two-dimensional time-dependent structural acoustics problem," *Journal of the Acoustical Society of America* **91**, 1320-1335 (1992).
- 3.9. J. ASSAAD, J.-N. DECARPIGNY, C. BRUNEEL, R. BOSSUT and B. HAMONIC, "Application of the finite element method to two-dimensional radiation problems," *Journal of the Acoustical Society of America* **94**, 562-573 (1993).
- 3.10. P. BETTESS and O. C. ZIENKIEWICZ, "Diffraction and refraction of surface waves using finite and infinite elements," *International Journal for Numerical*

- Methods in Engineering **11**, 1271-1290 (1977).
- 3.11. R. J. ASTLEY and W. EVERSMAN, "Finite element formulations for acoustical radiation," *Journal of Sound and Vibration* **88**(1), 47-64 (1983).
 - 3.12. R. J. ASTLEY, "Wave envelope and infinite elements for acoustical radiation," *International Journal for Numerical Methods in Fluids* **3**, 507-526 (1983).
 - 3.13. R. J. ASTLEY and W. EVERSMAN, "Wave envelope and infinite element schemes for fan noise radiation from turbofan inlets," *American Institute of Aeronautics and Astronautics Journal* **22**, 1719-1726 (1984).
 - 3.14. R. J. ASTLEY, J. P. COYETTE, G. J. MACAULAY, "Mapped wave envelope elements for acoustical radiation and scattering," *Journal of Sound and Vibration* **170**, 97-118 (1994).
 - 3.15. L. CREMERS, K. R. FYFE and J. P. COYETTE, "A variable order infinite acoustic wave envelope element," *Journal of Sound and Vibration* **171**(4), 483-508 (1992).
 - 3.16. J. P. COYETTE, "Modelling radiation from submerged structures, a comparison of boundary element and finite element techniques," *Second International Congress on Recent Developments in Air- and Structure-borne Sound and Vibration*, March 4-6, Auburn University, Eds. M. J. Crocker and P. K. Raju, **2**, 1027-1035 (1992).
 - 3.17. J. P. COYETTE, "Validation of a new wave envelope formulation for handling exterior acoustic and elasto-acoustic problems in the frequency domain," *DGLR/AIAA 14th Aeroacoustics Conference*, May 11-14, Aachen, **1**, 421-427 (1992).
 - 3.18. S. N. CHANDLER-WILDE and D. C. HOTHERSALL, "On the Green function for two-dimensional acoustic propagation above a homogeneous impedance plane," *Research report*, Department of Civil Engineering, University of Bradford, UK, (1991).
 - 3.19. D. C. HOTHERSALL, S. N. CHANDLER-WILDE and M. N. HAJMIRZAE, "Efficiency of single noise barriers," *Journal of Sound and Vibration* **146**(2), 303-322 (1991).
 - 3.20. E. SKUDRZYK, *The Foundations of Acoustics* (Springer-Verlag, Vienna, New-

York, 1971).

- 3.21. **A. D. PIERCE, *ACOUSTICS: An Introduction to its Physical Principles and Applications*** (Published by the Acoustical Society of America, New-York, 1991).
- 3.22. **F. FAHY, *Sound and Structural Vibration: Radiation, Transmission and Response***, (Academic Press, London, 1985)
- 3.23. **SYSNOISE User's Manual, Version 4.4A, Numerical Integration Technologies**, Leuven, Belgium, (1992).
- 3.24. **X. ZENG, L. F. KALLIVOKAS AND J. BIELAK**, "Stable localized symmetric integral equation method for acoustic scattering problems," *Journal of the Acoustical Society of America* **91**, 2510-2518 (1992).
- 3.25. **Y. KAGAWA, T. YAMABUCHI AND S. KITAGAMI**, "Infinite boundary element and its application to a combined finite-boundary element technique for unbounded field problem," in *Boundary Element Methods in Engineering*, edited by C. A. Brebbia (Springer-Verlag, Berlin), 1017-1026 (1983).

CHAPTER 4

A VARIABLE ORDER INFINITE ELEMENT FOR MULTI-DOMAIN BOUNDARY ELEMENT MODELLING OF ACOUSTIC RADIATION AND SCATTERING¹

4.1. INTRODUCTION

The modelling of acoustic radiation and scattering from arbitrary shaped bodies in an infinite domain is an inherent part of noise control engineering. Acoustic modelling involving jet engine noise, speaker and road noise barrier design, to name a few, have been widely investigated. In all these applications, the acoustic field variables at arbitrary field points, due to a vibrating body within the infinite acoustic domain, have to be determined.

The problem is governed by the Helmholtz equation, with appropriate boundary conditions on the radiating body, and the Sommerfeld radiation condition [4.1-4.4].

¹A version of this chapter will be submitted to *Journal of Sound and Vibration*.

Numerous numerical procedures have been developed for analyzing these type of wave propagation problems. Amongst all these methods, different boundary integral and finite element based methods have proven to be effective.

The boundary integral methods are very attractive from a theoretical point of view [4.5-4.9]. Through the use of the free-space Green's function, satisfying the Helmholtz equation and the radiation condition, and Green's second theorem, the problem can be reduced to solving a boundary integral equation. Therefore, only a discretization of the sound radiating surface is necessary. In a first stage, the field variables on the surface are solved for, whereafter the field variables at an arbitrary field point can be determined. The boundary element method reflects an accurate *global* application of the radiation condition. The global implementation implies that all acoustic degrees of freedom are interconnected. The resulting system of equations therefore includes full complex system matrices, quickly leading to computer data-storage problems, and in turn high calculation times, in spite of the reduced problem size, obtained from the limited discretization requirements. Another disadvantage is the non-uniqueness problem [4.10-4.13]. The boundary integral equation methods fail at critical frequencies, where no unique solution can be obtained. These critical frequencies are the eigenfrequencies of the complementary interior problem. Different methods have been developed for solving this singularity problem, most of which tend to be computationally costly.

A wide variety of finite element based methods have been developed, in an effort to incorporate the advantages of the finite element formulation. Although the whole acoustic domain has to be discretized, in general resulting in a large number of degrees of freedom, favourable computational efficiency can be obtained, due to banded system matrices. Methods range from truncation of conventional finite element schemes by analytical expansions [4.4,4.14], damping elements [4.15-4.17] or *pc*-impedance conditions [4.4,4.14], to infinite element formulations such as the infinite wave envelope element method [4.18-4.24]. The latter elements span to infinity and have an appropriate amplitude decay and wavelike variation incorporated for modelling the outgoing propagating waves. It has been shown that this local application of the radiation condition leads to modelling limitations [4.24]. In essence, only *good* radiators can be accurately

modelled, that is, those cases where the acoustic energy predominantly flows towards infinity along the infinite elements.

The multi-domain boundary element method aims at providing a compromise between the computational efficiency of the finite element based methods and the accurate global modelling of the Sommerfeld radiation condition. An indirect variational multi-domain element method has been successfully implemented by Zeng et al. [4.25]. A quadratic infinite boundary element is matched onto a number of conventional boundary elements for modelling the acoustic field variables along the infinite interfaces of adjacent subdomains. Along these infinite edges, continuity of the acoustic pressure and its normal gradient is enforced. The formulation results in banded symmetric system matrices, due to the chain assembly of the different boundary element subdomains. The method has been proven to accurately model acoustic radiation and scattering problems. A great advantage of the method is that no singularities are encountered due to the non-uniqueness problem of the conventional boundary integral methods.

In this chapter, a multi-domain boundary element scheme is presented using the direct collocation boundary element method. Special variable order infinite boundary elements are developed for accurate modelling of the acoustic field variables along the infinite interfaces. These variable order elements are based on the variable order wave envelope elements presented in Refs. [4.23,4.24]. An arbitrary number of acoustic degrees of freedom can be specified along the infinite edges, for proper modelling of the amplitude decay. In most applications, conventional boundary interface elements in the acoustic near field can therefore be omitted. Again, the set of linear boundary element equations results in banded system matrices and a unique solution can be obtained for all frequencies.

Numerous examples of two-dimensional and axisymmetric radiation and scattering problems have been investigated, exploring the performance of the present multi-domain concept. It will be shown that going to a high degree of subdomaining of the acoustic field, results in a more local application of the Sommerfeld radiation condition, and consequently reduced performance in modelling general radiation and scattering problems. Therefore, in general, a trade-off must be made between computational efficiency and

generality of the implementation of the Sommerfeld radiation condition.

4.2. THEORY

4.2.1. GOVERNING EQUATIONS AND BOUNDARY CONDITIONS

The acoustic pressure field, due to radiation or scattering from a rigid body into an unbounded inviscid domain, is governed by the classical wave equation, given as

$$\nabla^2 p(\mathbf{x}, t) = \frac{1}{c^2} \frac{\partial^2 p(\mathbf{x}, t)}{\partial t^2} \quad \mathbf{x} \in V \quad (4.1)$$

where $p(\mathbf{x}, t)$ denotes the acoustic pressure and c the speed of sound in the acoustic medium. When only harmonic steady-state conditions are considered, the classical wave Equation (4.1) reduces to the Helmholtz equation

$$\nabla^2 p(\mathbf{x}) + k^2 p(\mathbf{x}) = 0 \quad \mathbf{x} \in V \quad (4.2)$$

where $k = \omega / c$ is the acoustic wave number.

In general, three types of boundary conditions can be applied. These boundary conditions include prescribed acoustic pressure, velocity or acoustic impedance on the surface of the body, which are referred to as Dirichlet, Neumann and mixed or Robin boundary conditions respectively. A commonly applied prescribed velocity profile on the radiating body S_o is given as

$$\nabla p(\mathbf{x}) \cdot \mathbf{n}_o = -i \rho \omega \overline{v_n} \quad \mathbf{x} \in S_o \quad (4.3)$$

where \mathbf{n}_o is the unit normal on the surface S_o , ρ the density of the acoustic medium and $\overline{v_n}$ the prescribed normal surface velocity.

Furthermore, in order to obtain a well-posed problem, the pressure field must be constrained to vanish at infinity. This is accomplished by imposing a radiation condition at infinity. An appropriate radiation condition is given by the Sommerfeld radiation condition [4.1-4.4]

$$\lim_{r \rightarrow \infty} r^\alpha \left(\frac{\partial p}{\partial r} + i k p \right) = 0 \quad (4.4)$$

where $\alpha = 1$ for three-dimensional and $\alpha = 1/2$ for two-dimensional problems. This condition ensures that no sources at infinity contribute to the acoustic field. Only outgoing travelling waves are allowed, guaranteeing a net acoustic energy flow towards infinity.

4.2.2. THE DIRECT BOUNDARY ELEMENT METHOD

Different boundary integral methods have been developed for solving acoustic problems. These integral formulations typically consist of two phases. The first phase involves solving for the unknown acoustic field variable distributions on the boundary from a set of integral relations within the domain of the vibrating boundary S_o . In a second phase, the acoustic field exterior or interior to the vibrating surface can be determined from an explicit integral representation involving the previously calculated surface distributions.

The boundary integral methods can be classified, in general, based on their formulation approach, i.e. direct or indirect, and their solution method, i.e. collocation or variational. In the direct formulation, the field variables are the acoustic pressure and normal particle velocity, while the indirect approach uses the pressure and normal velocity jumps, also referred to as the double and single layer potentials respectively. In the collocation solution method, a set of equations is assembled by writing the Helmholtz surface integral equation for each unknown field variable on the boundary, which leads to a full non-symmetric complex system matrix. The variational solution method is based on the minimization of a functional equivalent to the boundary integral equation and leads to a full symmetric complex system matrix. In general, the direct formulation is combined with a collocation solution method, while a variational solution method is most suited for the indirect formulation. All these boundary element methods are well documented in the literature, i.e. References [4.5-4.9,4.26]. The direct collocation boundary element method, chosen for this work, will be explained in some detail in the following sections.

4.2.2.1. Surface Helmholtz integral equation

As outlined in Appendix 4-A, the equivalent integral equation for the Helmholtz equation (Equation (4.2)) can be reduced to a boundary integral equation, through the use of the free-space Green's function and Gauss' integral theorem. The dimension of the problem is therefore reduced by one, i.e. a volume integral becomes a surface integral.

The Helmholtz integral equation can be written as

$$C(P)p(P) = \int_{S_o} \left(p(Q) \frac{\delta G(P,Q)}{\delta n} - G(P,Q) \frac{\delta p(Q)}{\delta n} \right) dS(Q) \quad (4.5)$$

where

$$\begin{aligned} C(P) &= 1 & P \in V \\ &= \frac{1}{2} & P \in S \\ &= 0 & P \notin V \end{aligned} \quad (4.6)$$

This equation relates the acoustic pressure in a particular point P , to the acoustic pressure and normal particle velocity distribution on the radiating boundary. $G(P,Q) = G(|R_p - R_q|)$ is the free-space Green's function, given as

$$\begin{aligned} G(|R_p - R_q|) &= \frac{-i}{4} H_0^{(2)}(k|R_p - R_q|) & 2D \\ G(|R_p - R_q|) &= \frac{e^{-ik|R_p - R_q|}}{4\pi|R_p - R_q|} & 3D \end{aligned} \quad (4.7)$$

for two- and three-dimensional acoustic radiation and scattering, respectively. $H_0^{(2)}$ is the zeroth order Hankel function of the second kind and $|R_p - R_q|$ is the distance between the two field points P and Q , as depicted in Figure 4.1.

The essence of the direct collocation boundary element method is to relate the acoustic surface pressure at a particular point on the surface, to the acoustic pressure and normal particle velocity distribution of the rest of the radiating body. The key identity is therefore the surface Helmholtz integral equation. For this integral equation, the factor

$C(P)$ takes on the value $1/2$ in Equation (4.5). This is only valid for smooth surfaces, for which the surface normal takes on a unique value. For special cases, e.g. corners, where the surface normal is not unique, a more general expression for the factor is necessary, given as [4.8]

$$C(P) = 1 + \frac{1}{4\pi} \int_{S_o} \frac{\delta}{\delta n} \left(\frac{1}{|R_p - R_q|} \right) dS(Q) \quad (4.8)$$

The factor $C(P)$ can be interpreted as the exterior solid angle at point P on the surface S_o . In general, the surface Helmholtz integral can be written as

$$\begin{aligned} \left[1 + \frac{1}{4\pi} \int_{S_o} \frac{\delta}{\delta n} \left(\frac{1}{|R_p - R_q|} \right) dS(Q) \right] p(P) \\ = \int_{S_o} \left(p(Q) \frac{\delta G(P, Q)}{\delta n} - G(P, Q) \frac{\delta p(Q)}{\delta n} \right) dS(Q) \end{aligned} \quad (4.9)$$

4.2.2.2. Two-dimensional numerical implementation

The surface Helmholtz boundary integral equation for two-dimensional acoustic radiation can be expressed as

$$C(P) p(P) = \int_{\Gamma_o} \left(p(Q) \frac{\delta G(P, Q)}{\delta n} - G(P, Q) \frac{\delta p(Q)}{\delta n} \right) d\Gamma(Q) \quad (4.10)$$

where the solid angle factor is given by

$$C(P) = 1 + \frac{1}{4} \int_{\Gamma_o} \frac{\delta}{\delta n} \left(\frac{1}{|R_p - R_q|} \right) d\Gamma(Q) \quad (4.11)$$

and the free-space Green's function as in Equation (4.7).

The boundary element procedure now proceeds by discretizing the radiating boundary into M_e elements of length Γ_m , which yields

$$C(P) p(P) = \sum_{m=1}^{M_e} \left[\int_{\Gamma_m} \left(p_m(Q) \frac{\delta G(P,Q)}{\delta n} - G(P,Q) \frac{\delta p_m(Q)}{\delta n} \right) d\Gamma_m(Q) \right] \quad (4.12)$$

The elements are chosen to be isoparametric, where the geometry Γ_m is mapped onto a parent element $[-1, 1]$. Within each element the acoustic pressure p_m and the gradient of the acoustic pressure $\frac{\delta p_m}{\delta n}$ can be approximated using conventional shape functions $N_j(s)$, given as

$$\begin{aligned} p_m(s) &= \sum_{j=1}^{\alpha} N_j(s) p_{m_j} \\ \frac{\delta p_m(s)}{\delta n} &= \sum_{j=1}^{\alpha} N_j(s) \frac{\delta p_{m_j}}{\delta n} \end{aligned} \quad (4.13)$$

where s is the local coordinate, α is the number of acoustic degrees of freedom within the element and, p_{m_j} and $\frac{\delta p_{m_j}}{\delta n}$ are the values of the acoustic pressure and the gradient of the acoustic pressure at the node, respectively. The surface Helmholtz boundary integral equation for an arbitrary degree of freedom i on the surface, can then be written as

$$\begin{aligned} C_i p_i &= \sum_{m=1}^{M_e} \left[\int_{-1}^1 \left[\left(\sum_{j=1}^{\alpha} N_j(s) p_{m_j} \right) \frac{\delta G_i}{\delta n} \right] \|J\| ds \right] - \\ &\quad \sum_{m=1}^{M_e} \left[\int_{-1}^1 \left[G_i \left(\sum_{j=1}^{\alpha} N_j(s) \frac{\delta p_{m_j}}{\delta n} \right) \right] \|J\| ds \right] \end{aligned} \quad (4.14)$$

where G_i denotes the free-space Green's function between point i and an arbitrary point on the surface, and $\|J\|$ is the determinant of the Jacobian of the geometric transformation between the real element and the unit parent element. The equation can then be rearranged, yielding the following expression

$$\sum_{m=1}^{M_e} [a_{m_j}] \{p_{m_j}\} - C_i p_i = \sum_{m=1}^{M_e} [b_{m_j}] \left\{ \frac{\delta p_{m_j}}{\delta n} \right\} \quad (4.15)$$

with

$$\begin{aligned}
a_{m_j} &= \int_{-1}^1 N_j(s) \frac{\delta G_i}{\delta n} \|J\| ds \\
b_{m_j} &= \int_{-1}^1 N_j(s) G_i \|J\| ds
\end{aligned} \tag{4.16}$$

These integrals can be evaluated using standard Gauss-Legendre quadrature. Respectively two and three Gauss points are used for linear and quadratic boundary element formulations. A singularity problem occurs though, when evaluating the local contributions of the elements directly connected to the node i at hand. The integrand, i.e. the Green's kernel, becomes singular as the distance $|R_p - R_q|$ approaches zero. The approach of Telles [4.27] is adopted to deal with this singularity problem. The method consists of an additional transformation through which the quadrature points are shifted towards the singularity of the integrand, as explained in Appendix 4-B.

This equation can be expressed for all acoustic degrees of freedom of the radiating boundary. The assembled set of equations can therefore be written as

$$[A] - [J] [C] \{p\} = [B] \left\{ \frac{\delta p}{\delta n} \right\} \tag{4.17}$$

For a standard acoustic radiation problem, the normal velocity profile of the radiating body is given. The system of boundary element equations then yields

$$[A] \{p\} = -i \rho \omega [B] \{\bar{v}\} \tag{4.18}$$

where the solid angle terms, $C(p)$, are assumed to be incorporated within the matrix A . The array $\{p\}$ denotes the vector of the unknown nodal acoustic pressures, while $\{\bar{v}\}$ is the prescribed normal velocity vector. The acoustic surface pressure at the acoustic degrees of freedom can be solved for from this set of linear equations, after which the acoustic pressure at an arbitrary field point can be evaluated by means of the Helmholtz integral equation (Equation (4.5)).

4.2.2.3. Axisymmetric numerical implementation

For axisymmetric acoustic radiation, the surface Helmholtz boundary integral equation can be written in the form

$$C(P) p(P) = \int_{\Gamma_o} \left[p(Q) \left(\int_0^{2\pi} \frac{\delta G(P,Q)}{\delta n} d\theta \right) - \left(\int_0^{2\pi} G(P,Q) d\theta \right) \frac{\delta p(Q)}{\delta n} \right] d\Gamma(Q) \quad (4.19)$$

where the solid angle factor is given by

$$C(P) = 1 + \frac{1}{4\pi} \int_{\Gamma_o} \left[\int_0^{2\pi} \frac{\delta}{\delta n} \left(\frac{1}{|R_p - R_q|} \right) d\theta \right] d\Gamma(Q) \quad (4.20)$$

and the free-space Green's function as in Equation (4.7). In these equations, θ is the angular coordinate and Γ_o is the generator of the axisymmetric surface S_o of the radiating body. The only added difficulty for the axisymmetric boundary element formulation lies in the evaluation of the integrals in the angular θ -direction, given as

$$\begin{aligned} K^A(P,Q) &= \int_0^{2\pi} \frac{e^{-ik|R_p - R_q|}}{|R_p - R_q|} d\theta(Q) \\ K^B(P,Q) &= \int_0^{2\pi} \frac{\delta}{\delta n} \left(\frac{e^{-ik|R_p - R_q|}}{|R_p - R_q|} \right) d\theta(Q) \end{aligned} \quad (4.21)$$

These integrals can be evaluated in terms of elliptic integrals, as introduced by Soenarko [4.8]. His approach is to split the integrals into a non-singular and a singular part, as follows

$$\begin{aligned}
K^A(P,Q) &= K_1^A(P,Q) + K_2^A(P,Q) \\
&= \int_0^{2\pi} \left(\frac{e^{-ik|R_p-R_q|} - 1}{|R_p-R_q|} \right) d\theta(Q) + \int_0^{2\pi} \left(\frac{1}{|R_p-R_q|} \right) d\theta(Q) \\
K^B(P,Q) &= K_1^B(P,Q) + K_2^B(P,Q) \\
&= \int_0^{2\pi} \frac{\delta}{\delta n} \left(\frac{e^{-ik|R_p-R_q|} - 1}{|R_p-R_q|} \right) d\theta(Q) + \int_0^{2\pi} \frac{\delta}{\delta n} \left(\frac{1}{|R_p-R_q|} \right) d\theta(Q)
\end{aligned} \tag{4.22}$$

The non-singular parts K_1^A and K_1^B can then be evaluated by a conventional Gauss-quadrature scheme, while the remaining singular integrals K_2^A and K_2^B can be transformed into complete elliptic integrals of the first and second kind, as explained in detail in Reference [4.8]. The number of Gauss-quadrature points used for evaluating the non-singular integrals K_1^A and K_1^B depends on the acoustic wave number k of the problem and the distance R_o from the element to the axisymmetry axis. Tests have shown that accurate results can be obtained as long as the number of Gauss quadrature points along half the axisymmetric circumference is greater than $1.25 kR_o$. Note that, due to symmetry, only half the angular integral has to be evaluated numerically, i.e. $0 \leq \theta \leq \pi$.

4.2.3. THE MULTI-DOMAIN CONCEPT

The direct collocation boundary element method, as explained in the previous sections, renders a full complex system of linear equations, i.e. all acoustic degrees of freedom are interconnected. The fully populated system matrix can therefore quickly become very large. This causes computer data storage problems and in turn longer calculation times in the solution phase of the boundary element method. To reduce the interconnectivity of the acoustic degrees of freedom, the multi-domain concept of the boundary element method is introduced. This concept has been used in many different applications such as muffler design, non-homogeneous structures and fracture mechanics

[4.28,4.29].

For this procedure, the acoustic domain is divided into a number of subdomains. In general, each subdomain can have different material properties. For this study the total acoustic field is assumed to have a constant speed of sound c and density ρ . The different subdomains are separated by imaginary surfaces or interfaces. Each subdomain can separately be modelled by the direct collocation boundary element method. A global assembly of the boundary element subdomains is then performed by forcing continuity of the acoustic pressure and the normal gradient of the acoustic pressure at the subdomain interfaces.

For example, a two domain boundary element model is given for the acoustic modelling of an infinitely long rigid cylinder Γ^o , as depicted in Figure 4.2. The subdomains are separated by an infinite radial interface Γ^i , along which the continuity conditions are specified. Another special interface is introduced, i.e. Γ^h , modelling a hard infinite half plane or symmetry plane. Along these surfaces the gradient of the acoustic pressure is forced to zero.

First, each domain is treated separately. The Helmholtz equation is satisfied in both domains

$$\begin{aligned}\nabla^2 p_1(x_1) + k^2 p_1(x_1) &= 0 & x_1 \in S_1 \\ \nabla^2 p_2(x_2) + k^2 p_2(x_2) &= 0 & x_2 \in S_2\end{aligned}\tag{4.23}$$

The corresponding Helmholtz integral equations can then be written as

$$\begin{aligned}C_1(P_1) p_1(P_1) &= \int_{\Gamma_1 \cup \Gamma_1^h \cup \Gamma_1^o \cup \Gamma_1^i} \left(p_1(Q) \frac{\delta G(P_1, Q)}{\delta n_1} - G(P_1, Q) \frac{\delta p_1(Q)}{\delta n_1} \right) d\Gamma(Q) \\ C_2(P_2) p_2(P_2) &= \int_{\Gamma_2 \cup \Gamma_2^h \cup \Gamma_2^o \cup \Gamma_2^i} \left(p_2(Q) \frac{\delta G(P_2, Q)}{\delta n_2} - G(P_2, Q) \frac{\delta p_2(Q)}{\delta n_2} \right) d\Gamma(Q)\end{aligned}\tag{4.24}$$

After discretization into elements, two sets of equations are obtained, in the form

$$\begin{aligned}
\begin{bmatrix} A_1^h & A_1^o & A_1^i \end{bmatrix} \begin{bmatrix} p_1^h & p_1^o & p_1^i \end{bmatrix}^T &= \begin{bmatrix} B_1^h & B_1^o & B_1^i \end{bmatrix} \begin{bmatrix} \frac{\delta p_1^h}{\delta n_1} & \frac{\delta p_1^o}{\delta n_1} & \frac{\delta p_1^i}{\delta n_1} \end{bmatrix}^T \\
\begin{bmatrix} A_2^h & A_2^o & A_2^i \end{bmatrix} \begin{bmatrix} p_2^h & p_2^o & p_2^i \end{bmatrix}^T &= \begin{bmatrix} B_2^h & B_2^o & B_2^i \end{bmatrix} \begin{bmatrix} \frac{\delta p_2^h}{\delta n_2} & \frac{\delta p_2^o}{\delta n_2} & \frac{\delta p_2^i}{\delta n_2} \end{bmatrix}^T
\end{aligned} \tag{4.25}$$

Applying the continuity conditions along the domain interfaces and setting the normal acoustic pressure gradient to zero on the hard plane, leads to the following global set of equations

$$\begin{bmatrix} A_1^{h+o} & A_1^i & -B_1^i & 0 \\ 0 & A_2^i & B_2^i & A_2^{o+h} \end{bmatrix} \begin{Bmatrix} p_1^{h+o} \\ p_1^i \\ \frac{\delta p_1^i}{\delta n_1} \\ p_2^{o+h} \end{Bmatrix} = \begin{bmatrix} B_1^o & 0 \\ 0 & B_2^o \end{bmatrix} \begin{Bmatrix} \frac{\delta p_1^o}{\delta n_1} \\ \frac{\delta p_2^o}{\delta n_2} \end{Bmatrix} \tag{4.26}$$

The problem unknowns are therefore the acoustic pressure along *all* the boundaries and the gradient of the acoustic pressure along the subdomain interfaces. For a standard Neumann problem, with prescribed velocity profile along the radiating boundary, the global system can be expressed as

$$\begin{bmatrix} A_1 & A_1^i & -B_1^i & 0 \\ 0 & A_2^i & B_2^i & A_2 \end{bmatrix} \begin{Bmatrix} p_1 \\ p_1^i \\ \frac{\delta p_1^i}{\delta n_1} \\ p_2 \end{Bmatrix} = -i \rho \omega \begin{bmatrix} B_1^o & 0 \\ 0 & B_2^o \end{bmatrix} \begin{Bmatrix} \overline{v_1} \\ \overline{v_2} \end{Bmatrix} \tag{4.27}$$

where the superscripts *h+o* are dropped for convenience.

The concept can now easily be expanded to an arbitrary number of subdomains. The global assembled system reduces to a banded form, given as

$$\begin{bmatrix}
A_1 & A_1^{1,2} & -B_1^{1,2} & 0 & 0 & 0 & 0 & \dots & 0 & 0 & 0 & 0 & \dots & 0 & 0 & 0 & 0 \\
0 & A_2^{1,2} & B_2^{1,2} & A_2 & A_2^{2,3} & -B_2^{2,3} & 0 & \dots & 0 & 0 & 0 & 0 & \dots & 0 & 0 & 0 & 0 \\
0 & 0 & 0 & 0 & A_3^{2,3} & B_3^{2,3} & A_3 & \dots & 0 & 0 & 0 & 0 & \dots & 0 & 0 & 0 & 0 \\
\vdots & \vdots & \vdots & \vdots & \vdots & \vdots & \vdots & \ddots & \vdots & \vdots & \vdots & \vdots & \ddots & \vdots & \vdots & \vdots & \vdots \\
0 & 0 & 0 & 0 & 0 & 0 & 0 & \dots & A_j & A_j^{j,j+1} & -B_j^{j,j+1} & 0 & \dots & 0 & 0 & 0 & 0 \\
0 & 0 & 0 & 0 & 0 & 0 & 0 & \dots & 0 & A_{j+1}^{j,j+1} & B_{j+1}^{j,j+1} & A_{j+1} & \dots & 0 & 0 & 0 & 0 \\
\vdots & \vdots & \vdots & \vdots & \vdots & \vdots & \vdots & \ddots & \vdots & \vdots & \vdots & \vdots & \ddots & \vdots & \vdots & \vdots & \vdots \\
0 & 0 & 0 & 0 & 0 & 0 & 0 & \dots & 0 & 0 & 0 & 0 & \dots & A_{N-1} & A_{N-1}^{N-1,N} & -B_{N-1}^{N-1,N} & 0 \\
0 & 0 & 0 & 0 & 0 & 0 & 0 & \dots & 0 & 0 & 0 & 0 & \dots & 0 & A_N^{N-1,N} & B_N^{N-1,N} & A_N
\end{bmatrix}
\begin{bmatrix}
P_1 \\
P_1^{1,2} \\
\frac{\partial P_1^{1,2}}{\partial n_1} \\
P_2 \\
P_2^{2,3} \\
\frac{\partial P_2^{2,3}}{\partial n_2} \\
P_3 \\
\vdots \\
P_j \\
P_j^{j,j+1} \\
\frac{\partial P_j^{j,j+1}}{\partial n_j} \\
P_{j+1} \\
\vdots \\
P_{N-1} \\
P_{N-1}^{N-1,N} \\
\frac{\partial P_{N-1}^{N-1,N}}{\partial n_{N-1}} \\
P_N
\end{bmatrix} = \quad (4.28)$$

$$-i\rho\omega \begin{bmatrix}
B_1^o & 0 & \dots & 0 & 0 & \dots & 0 & 0 \\
0 & B_2^o & \dots & 0 & 0 & \dots & 0 & 0 \\
\vdots & \vdots & \ddots & \vdots & \vdots & \ddots & \vdots & \vdots \\
0 & 0 & \dots & B_j^o & 0 & \dots & 0 & 0 \\
0 & 0 & \dots & 0 & B_{j+1}^o & \dots & 0 & 0 \\
\vdots & \vdots & \ddots & \vdots & \vdots & \ddots & \vdots & \vdots \\
0 & 0 & \dots & 0 & 0 & \dots & B_{N-1}^o & 0 \\
0 & 0 & \dots & 0 & 0 & \dots & 0 & B_N^o
\end{bmatrix} \begin{bmatrix}
\overline{v_1} \\
\overline{v_2} \\
\vdots \\
\overline{v_j} \\
\overline{v_{j+1}} \\
\vdots \\
\overline{v_{N-1}} \\
\overline{v_N}
\end{bmatrix}$$

where the superscripts of type $j,j+1$ denote the interface between subdomain j and $j+1$. A chain assembly of N subdomains results therefore into a banded non-symmetric system matrix, which can be stored in banded form. This, notwithstanding the increased number of acoustic degrees of freedom, results in considerable data storage reduction and enhances computational efficiency of the solution phase.

4.2.4. VARIABLE ORDER INFINITE BOUNDARY ELEMENT

The added difficulty in applying the multi-domain concept to acoustic radiation problems in unbounded domains is that the interfaces between the different subdomains are of infinite extent. An efficient way of modelling these infinite interfaces is of crucial

importance. The added number of acoustic degrees of freedom has to be held to a minimum in order to be able to take full advantage of the banded structure of the system matrices. In the variational multi-domain approach developed by Zeng et al. [4.25], the acoustic field variables along the infinite interfaces are modelled by a limited number of conventional boundary elements, followed by a special infinite boundary element to extent the solution to infinity. This infinite boundary element is based upon the *finite element based* infinite elements, introduced by the group of Zienkiewicz et al. [4.14]. The later element was also the basis for the infinite wave envelope element formulation, as explained in ref. [4.22-4.24].

An infinite geometry mapping is used to map the infinite element region on to a finite parent element $[-1, 1)$. Due to this geometry mapping a polynomial shape function in the parent element renders a $(1/r)$ -expansion in the real infinite element, which is well suited for modelling the amplitude decay of the field variables. A complex exponential is added to model the wavelike variation of the outgoing waves.

In this chapter, an infinite element of variable order is proposed. It was seen from the formulation of the variable order infinite wave envelope element [4.23,4.24], that a higher order element was able to more accurately model the outgoing travelling waves and that in many cases the need for conventional elements in the near field was eliminated. The important aspects of the variable order infinite boundary element are explained in more detail in the following sections.

4.2.4.1. Infinite geometry mapping

The infinite geometry mapping is illustrated in Figure 4.3. The one-to-one transformation is completely defined by the positions of node 1, $\underline{x}_I (x_I, y_I)$, at the finite boundary of the infinite element, and node 2, $\underline{x}_{II} (x_{II}, y_{II})$, a distance a away from node 1. The parameter a denotes the distance from the pole of the inverse transformation $\underline{x}_0 (x_0, y_0)$ to the finite boundary at node 1, given as

$$a = |\underline{x}_I - \underline{x}_0| = |\underline{x}_{II} - \underline{x}_I| \quad (4.29)$$

The mapping from local to global coordinates can thus be written as

$$\begin{aligned}x(t) &= \sum_{i=I}^{II} M_i(t) x_i \\y(t) &= \sum_{i=I}^{II} M_i(t) y_i\end{aligned}\tag{4.30}$$

where the mapping functions are defined as

$$\begin{aligned}M_I(t) &= \frac{-2t}{1-t} \\M_{II}(t) &= \frac{1+t}{1-t}\end{aligned}\tag{4.31}$$

The inverse geometry mapping can be found by solving for t in Equation (4.31), which yields

$$t = 1 - 2 \frac{a}{r}\tag{4.32}$$

In this equation, r is a radial coordinate along the infinite element with the origin at the pole \underline{x}_0 . From inspection of the mapping relationships, it is seen that the local coordinates $t = -1, 0, 1$ correspond to the global coordinates $\underline{x} = \underline{x}_I, \underline{x}_{II}, \infty$, respectively.

4.2.4.2. Shape function

The shape function used for modelling the acoustic field variables along the infinite boundary element, are based on the shape functions used in the formulation of the variable order infinite wave envelope element as in Reference [4.23]. These functions combine a suitable amplitude decay and a wavelike variation for modelling outgoing travelling waves. In the following, both aspects are explained in more detail.

A. Amplitude decay

The infinite geometry mapping, discussed in section 4.2.4.1., transforms a polynomial function in the parent finite element into a $(1/r)$ -expansion in the real infinite element. This can easily be verified by considering a one-dimensional example, as presented in detail in Reference [4.23]. The asymptotic value for the field variable at

infinity is set to zero, according to the radiation boundary condition. This can be accomplished by forcing the value of the acoustic degree of freedom at infinity to zero. Therefore, in case of an n^{th} order infinite boundary element, only the n finite acoustic degrees of freedom of the infinite element contribute, through their respective shape functions, to the modelling of the acoustic field variable at an arbitrary point in the infinite element. The shape functions are of the form

$$\begin{aligned} & a_0 + a_1 t + a_2 t^2 + \dots + a_n t^n \\ & \quad \quad \quad \uparrow \\ & b_1 \left(\frac{1}{r} \right) + b_2 \left(\frac{1}{r} \right)^2 + \dots + b_n \left(\frac{1}{r} \right)^n \end{aligned} \quad (4.33)$$

which are very suitable for modelling a decaying travelling wave.

The use of Lagrangian polynomials once again ensures full flexibility in the choice of the order of the polynomial for modelling the amplitude decay. The Lagrangian polynomial is fully determined by the choice of n acoustic nodes within the element and the $n+1^{\text{th}}$ node at infinity. The position of these n acoustic nodes are in essence arbitrary. In case of the variable order wave envelope element, they are equally spaced between the first two geometry nodes, as shown in Reference [4.23]. For the variable order infinite boundary element at hand, they will be chosen to suit the numerical integration scheme, as explained later in Section 4.2.4.3.

In general, the decaying factor of the shape function can be written as

$$T_i^n(t) = \frac{\pi(t)}{\pi'(t_i) (t - t_i)} \quad 1 \leq i \leq n \quad (4.34)$$

with

$$\pi(t) = \prod_{i=1}^{n+1} (t - t_i) \quad (4.35)$$

The amplitude of a propagating wave in a two-dimensional domain decays approximately as a $(1/\sqrt{r})$ -expansion. To accommodate the shape functions for modelling two-dimensional acoustic radiation problems, a \sqrt{r} factor can be premultiplied. In local coordinates this leads to a factor given as [4.23]

$$R^n_i(t) = \sqrt{\frac{1-t_i}{1-t}} \quad (4.36)$$

B. Wavelike variation

The wavelike variation consists of a periodic component in the form of a complex exponential $\exp(-ikr)$. In order to maintain compatibility with the shape functions of the conventional boundary elements in the acoustic near field, the phase of this periodic component must be adjusted at the finite-infinite element interface ($t = -1$), i.e. set to zero. The wavelike variation component therefore results into the following form in local coordinates

$$e^{-ik(r-a)} = e^{-ik\mu(t)} = e^{-ika \frac{1+t}{1-t}} \quad (4.37)$$

The phase function $\mu(t)$ simply represents the radial distance to the finite-infinite element interface along the infinite element.

Finally, the shape functions for the n acoustic degrees of freedom of the variable order infinite element can be expressed as a combination of the amplitude decay and the wavelike variation, as in

$$\begin{aligned} N^n_i(t) &= R^n_i(t) T^n_i(t) e^{-ik\mu(t)} & 2D \\ N^n_i(t) &= T^n_i(t) e^{-ik\mu(t)} & 3D \text{ (axisymmetric)} \end{aligned} \quad (4.38)$$

The field variables p and $\frac{\delta p}{\delta n}$ along the variable order infinite boundary element can now be approximated, as in Equation (4.13), yielding

$$\begin{aligned} p(t) &= \sum_{j=1}^n N^n_j(t) p^*_j \\ \frac{\delta p(t)}{\delta n} &= \sum_{j=1}^n N^n_j(t) \frac{\delta p^*_j}{\delta n} \end{aligned} \quad (4.39)$$

Here the nodal quantities are marked with a star $*$ since they do not exactly denote the acoustic pressure or the normal gradient of the acoustic pressure, respectively, at the

acoustic degree of freedom at hand. To obtain the proper values of the acoustic field variables, the phase correction $e^{-ik\mu(t)}$, incorporated in the shape functions, must be applied.

Two different types of variable order infinite boundary elements will be used. A first type, denoted as a variable order infinite interface boundary element, is applied for modelling the acoustic field variables along the infinite interfaces that separate the individual subdomains. Along these elements both the acoustic pressure as well as the normal gradient of the acoustic pressure are considered acoustic degrees of freedom. For the other type, referred to as a variable order infinite rigid half plane boundary element, only the acoustic pressure is considered as an acoustic degree of freedom, while the normal gradient of the acoustic pressure is forced to zero. The latter element is used for modelling symmetry planes or infinite rigid half planes.

4.2.4.3. Numerical integration

The contribution of the variable order infinite elements to the surface Helmholtz equation involves integrals along an infinite domain. The integrals in local coordinates, involved in the formation of the system matrix for two-dimensional analysis, are of the form

$$\begin{aligned} a_j &= \int_{-1}^1 R^n_j(t) T^n_j(t) e^{-ik\mu(t)} \frac{\delta G_i}{\delta n} \|J\| dt \\ b_j &= \int_{-1}^1 R^n_j(t) T^n_j(t) e^{-ik\mu(t)} G_i \|J\| dt \end{aligned} \quad (4.40)$$

where $\|J\|$ is the determinant of the Jacobian for the infinite geometry transformation. In the following an approximate integration method for this type of integral will be explained.

The integrals of Equation (4.40) are evaluated according to the scheme developed by Zeng et al. [4.25]. The method consists of truncating the infinite element region at a

finite distance r_{∞} , as shown in Figure 4.3. This semi-infinite boundary is set to be at $r_{\infty} = a + 15\lambda$, or fifteen wavelengths away from the finite-infinite boundary. The contribution to the integral of the region beyond this boundary has proven to be negligible for the applications considered in this chapter. The truncated integral can be evaluated by dividing the semi-infinite domain of the real element into a number of finite subelements of equal length, as illustrated in Figure 4.4. Each of these subelements can then subsequently be integrated by conventional Gauss-Legendre quadrature. Convergence tests suggest a scheme of thirty-two subelements and four quadrature points, respectively, to be adequate. Each subelement therefore spans about half a wavelength in this integration scheme.

The truncation of the infinite integral has consequences on the position of the acoustic degrees of freedom within the element. The fact that the contribution beyond r_{∞} is negligible, means that in practise the acoustic pressure can be forced to vanish at the semi-infinite boundary. The $n+1^{\text{th}}$ acoustic degree of freedom of the n^{th} order infinite boundary element is therefore assumed to be zero at this position r_{∞} . The first acoustic degree of freedom is located at the finite-infinite interface for obvious compatibility reasons with the conventional boundary elements of the acoustic near field. The position of the remaining $n-1$ acoustic degrees of freedom are chosen as depicted in Figure 4.4 for a fourth order infinite boundary element. The acoustic degrees of freedom are positioned as the end-nodes of the first $n-1$ subelements. This particular choice has a practical advantage, in that the integration singularities can be easily dealt with on the subelement level. For each subelement, a check can be performed to detect whether or not a singularity occurs. In case of a singularity, the approach of Telles [4.27], as outlined in Appendix 4-B, can be adopted for integrating the subelement in the same way as for the integration of conventional boundary elements.

It should be noted that the numerical integration of the variable order infinite boundary element becomes very costly in terms of computation time for the axisymmetric formulation. For each Gauss-quadrature point in the radial direction, the non-singular integrals in the angular direction, i.e. K_1^A and K_1^B from Equation (4.22), have to be evaluated. Depending on the acoustic wave number this involves a considerable number

of Gauss-quadrature points, as indicated in Section 4.2.2.3.

4.2.5. Post-processing of results

After solving the set of complex linear equations of the boundary element method, the acoustic pressure and the normal surface velocity are known. The value of the acoustic field variable at an arbitrary point in the field can then be evaluated by applying the Helmholtz integral equation (Equation (4.5)). For the multi-domain boundary element method, this can be done in two ways. One method consists of applying the Helmholtz integral equation only for the subdomain within which the particular field point lies. Each field point therefore has to be assigned to its subdomain. Another method, which has been used for the work in this chapter, is to use the global Helmholtz integral equation along the real boundary Γ_0 , as in the conventional boundary element method.

4.3. DISCUSSION OF RESULTS

4.3.1. SIMPLE ACOUSTIC RADIATION AND SCATTERING EXAMPLES

To illustrate the use and performance of the multi-domain boundary element method, different examples of acoustic radiation and scattering from a rigid body are presented in the following sections.

In the first two sections, acoustic radiation models of the infinitely long rigid cylinder and the axisymmetric sphere are chosen to thoroughly test the two-dimensional and axisymmetric implementation of the multi-domain direct collocation boundary element method, respectively. Results are compared to conventional direct collocation boundary element models and analytical solutions.

A typical boundary element mesh of an infinite acoustic subdomain is shown in Figure 4.5. The boundary of the radiating object is discretized using conventional linear or quadratic boundary elements, according to the rule of thumb of seven acoustic degrees of freedom per acoustic wavelength. The different subdomains are separated by means of

interface boundary elements, along which the continuity of the acoustic field variables is prescribed. A single variable order infinite interface boundary element can be combined with a number of conventional interface boundary elements in the acoustic near field of the infinite interface. The computational meshes for the test cases at hand are chosen as depicted in Figures 4.6 and 4.7. In order to thoroughly explore the performance of the higher order infinite boundary element, the conventional interface boundary elements are omitted in most test cases. The symmetry planes in the two-dimensional models are enforced by implementing variable order infinite rigid half plane boundary elements. In all examples, the acoustic medium is air at ambient conditions, with density $\rho = 1.21 \text{ kg/m}^3$ and speed of sound $c = 340 \text{ m/s}$.

4.3.1.1. Acoustic monopole radiation by an infinitely long rigid cylinder

Figure 4.8 shows the frequency response function, within a frequency range of $0 < kR < 40$, for a uniformly pulsating infinitely long rigid cylinder of radius R . Results are compared with the direct collocation boundary element solution and the analytical solution, given as [4.30]

$$p(r) = -i\rho c \overline{V}_0 \frac{H_0^{(2)}(kr)}{H_0^{(2)'}(kR)} \quad (4.41)$$

where $H_0^{(2)}$ is the zeroth order cylindrical Hankel function of the second kind and \overline{V}_0 is the velocity amplitude of the vibrating cylinder. A boundary element discretization of one hundred and twenty linear boundary elements is chosen for modelling the radiating boundary of the cylinder, for both the conventional and the multi-domain boundary element calculation mesh. As a first test, only two subdomains are created at this stage. In the figure legends, the multi-domain boundary element methods are labelled with the number of subdomains and the order of the infinite boundary element, e.g. 2 dom - order 1 indicates two domains and an infinite element of order one. A single infinite interface boundary element of order one is used for modelling the infinite radial interfaces between the subdomains. Note that this simple multi-domain mesh has the same number

of acoustic degrees of freedom as the conventional boundary element mesh.

As shown in Figure 4.8, the multi-domain solution models the monopole radiation accurately for all frequencies. It doesn't share the non-uniqueness problem of solution at certain critical frequencies, as found in most boundary element formulations. The direct collocation boundary element method does reflect non-uniqueness problems at these critical frequencies. The occurrence of the singularities at critical frequencies is a purely mathematical problem arising from properties of the boundary integral equation. No physical meaning for the exterior radiation problem can be attributed to this phenomenon, since an exterior boundary value problem has a unique solution for all frequencies. As explained in Reference [4.12], the critical frequencies for an exterior Neumann boundary value problem are the eigenfrequencies of the complementary interior homogeneous Dirichlet problem.

The monopole radiation problem of the infinitely long rigid cylinder is formulated as a Neumann boundary value problem with uniform velocity boundary conditions $\bar{v}_n = \bar{V}_o$. The critical frequencies are therefore the resonant frequencies of the interior standing modes of the infinitely long cylinder, subject to pressure-release boundary conditions $\bar{p} = 0$, given as [4.7,4.34]

$$k_{0q}R = \alpha_{B_{0q}} \quad (4.42)$$

where $\alpha_{B_{0q}}$ is the q^{th} root of the zeroth order Bessel function of the first kind, which can be found from

$$J_0(\alpha_{B_{0q}}) = 0 \quad (4.43)$$

In general, it can be shown, that the critical wave numbers, $k_{nq}R$, for a cylindrical multipole of order n can be solved from [4.7,4.34]

$$J_n(\alpha_{B_{nq}}) = 0 \quad n = 0, 1, 2, \dots \quad (4.44)$$

From tables, as in Reference [4.35], the first four critical wave numbers are therefore given as $k_{01}R = 2.405$, $k_{02}R = 5.520$, $k_{03}R = 8.654$ and $k_{04}R = 11.792$.

For acoustic radiators of arbitrary shape, these critical frequencies can not readily

be determined. A good indication of their occurrence, however, is the condition number of the system matrix A . Around critical frequencies the condition number increases rapidly.

Different methods to overcome this non-uniqueness problem for boundary element formulations have been developed. All these methods have been documented in the literature as in References [4.10-4.13]. The most popular method consists of combining the surface and the interior integral equations, the so-called CHIEF-method as formulated by Schenck [4.10]. The idea is to over-determine the systems with equations from the interior Helmholtz integral. The over-determined system is then solved by a least squares procedure. The problem for this method lies in the choice of the interior collocation points, as points chosen on the nodal lines of the interior standing modes do not aid in reducing this problem. For high frequencies this can quickly become a problem. Numerous over-determination points may have to be chosen for certain frequency ranges in order to effectively solve the non-uniqueness problem. Dealing with singularities can thus become very costly in terms of calculation time.

As mentioned before, the multi-domain boundary element method doesn't reflect non-uniqueness problems. From the previous discussion, this can intuitively be explained from the observation that the complementary Dirichlet problem of each subdomain boundary value problem has no eigenfrequencies, simply, because the complementary domain is of infinite extent as well. No standing modes can exist in the complementary problem, as it too is an exterior boundary value problem. The multi-domain boundary element method can therefore be used to avoid singularities caused by the non-uniqueness problem of the boundary integral equation.

4.3.1.2. Acoustic monopole radiation by an axisymmetric rigid sphere

A similar test is conducted for the axisymmetric monopole radiation due to a uniformly pulsating rigid sphere of radius R . Figure 4.9 shows the frequency response function, again within a frequency range of $0 < kR < 40$. Results are compared with the direct collocation boundary element solution and the analytical solution, given as

[4.30]

$$p(r) = \rho c \overline{V}_0 \left(\frac{R}{r} \right) \frac{ikR}{1 + ikR} e^{-ik(r-R)} \quad (4.45)$$

where \overline{V}_0 is the velocity amplitude of the pulsating sphere. The computational mesh for the multi-domain boundary element method consists of two domains separated by a single infinite interface boundary element of order one. Figure 4.9 shows excellent agreement between the multi-domain and the analytical solution. The direct collocation boundary element method is again subject to the non-uniqueness problem. Similarly, for the pulsating sphere, these critical frequencies are the eigenfrequencies of the standing modes within the sphere subject to pressure-release boundary condition. These critical frequencies can be found from the solution of [4.7,4.8]

$$j_0(k_{0q}R) = 0 \quad (4.46)$$

and therefore are

$$k_{0q}R = q\pi \quad q = 1, 2, 3, \dots \quad (4.47)$$

where j_0 is the zeroth order spherical Bessel function of the first kind.

As noted earlier, the axisymmetric multi-domain boundary element method quickly becomes very costly in terms of calculation time for higher frequencies, due to the expensive numerical integration of the infinite interface elements. As mentioned earlier in Sections 4.2.2.3. and 4.2.4.3., each evaluation of the free-space Green's function involves a numerical integration in the angular direction, requiring a considerable number of Gauss-quadrature points as the frequency and the distance from the symmetry axis increases. The multi-domain boundary element method is therefore less attractive for axisymmetric radiation models.

4.3.1.3. Acoustic plane wave scattering from an infinitely long rigid cylinder

In the following, the acoustic plane wave scattering from an infinitely long rigid cylinder of radius R is modelled using the multi-domain boundary element method. The scattering problem is reformulated as an equivalent radiation problem through the application of the superposition method [4.24]. The normal velocity boundary conditions for the calculation of the scattered acoustic pressure field p_s are obtained from the known incident pressure field p_i , in the form $\overline{v_{n_s}} = -\overline{v_{n_i}}$ for a rigid scatterer. Results are compared to the analytical solution, given as [4.30]

$$p_s(r, \theta) = -P_0 \sum_{n=0}^{\infty} \epsilon_n i^n \frac{J'_n(kR) H_n^{(2)}(kr)}{H_n^{(2)}(kR)} \cos(n\theta) \quad (4.48)$$

where J_n is an n^{th} order Bessel function of the first kind, ϵ_n is the Neumann function ($\epsilon_n = 1$ if $n = 0$ and $\epsilon_n = 2$ if $n > 0$), P_0 is the amplitude of the incident plane wave $p_i(x) = P_0 \exp(-ikx)$, travelling along the symmetry axis (x -axis), and θ is measured from the direction of the incoming plane wave. The infinite series converges rapidly and can be truncated according to a suitable convergence criterium.

In Figures 4.10 and 4.11, polar plots are shown of the scattered acoustic pressure field at a radius of $r = 5R$ for a wave number of $kR = 2.405$ and $kR = 8.654$ respectively (i.e. the first and third critical wave numbers). These specific wave numbers are chosen, since they constitute critical frequencies for the problem at hand. A simple two subdomain boundary element model is used for modelling the scattered acoustic field. Results for infinite interface elements of order one, two and three are compared with the analytical solution. In both cases good agreement is observed, even for the low first order boundary element modelling. The results for the modelling of order two and three are virtually indistinguishable, with a slight edge for the third order modelling of the side-scattering region, i.e. around $\theta = 90^\circ$. Again, no singularity problems are observed for the multi-domain boundary element modelling at these critical frequencies.

Next, the forward, sideward and backward scattered acoustic pressure is observed in the frequency range $0 < kR < 30$, for both the near ($r = 1.1R$) and far

($r = 100R$) field. These tests give an overall view of the performance of the simple two subdomain boundary element model in the whole frequency range of interest. Figures 4.12 to 4.14 show the results for the near field, while the far field results are presented in Figures 4.15 to 4.17. As in the previous polar plots, at least a second order infinite boundary element model is needed for accurate modelling of the acoustic pressure field within the frequency range. One should also note that the results for the far field appear to be better than those of the near field. This can be explained following the reasoning in the next section. It will be shown that a scattered pressure field can be interpreted as a superposition of multi-poles. In order to model the local scattering phenomenon in the vicinity of the scatterer at increasing wave numbers, higher order multi-poles are necessary. The multi-domain boundary element method will reveal limitations in modelling these higher order multi-poles, resulting in reduced accuracy for those scattering fields that require a contribution of these multi-poles.

4.3.2. LIMITATIONS OF THE MULTI-DOMAIN BOUNDARY ELEMENT MODELLING

In all the examples studied up to now, only a simple multi-domain model with two subdomains has been used. For this low degree of subdomaining, the infinite interface can be adequately modelled by a single infinite boundary element of order two in the frequency range of interest, i.e. $0 < kR < 30$. In the following, multi-domain models of higher degree of subdomaining will be studied. The higher the degree of subdomaining, the more banded the system matrices will be, resulting in data-storage advantages and computational efficiency. On the other hand, from the discussion of the variable order infinite wave envelope element in Reference [4.24], one can expect that a high degree of subdomaining inevitably will lead to a more local implementation of the radiation condition, and thus a limitation in the modelling capability of arbitrary radiation patterns.

The sideward plane wave scattering from an infinitely long rigid cylinder of radius R is chosen as test case to explore the limitations of the multi-domain boundary element modelling. The frequency range is selected as $0 < kR < 20$, since results in this range

already reflect the modelling problems for the multi-domain models under investigation. The boundary of the cylinder is modelled using sixty quadratic conventional boundary elements. Models of two, four, twelve and twenty subdomains are used, while the order of the variable order infinite elements varies from one up to five. Again, in most cases the infinite interface is modelled by a single variable order infinite element, to fully concentrate on the performance of the new element.

Figures 4.18 to 4.21 show the scattered acoustic pressure amplitude for a field point at $x = 0$ and $y = 5R$, for first, second, third and fourth order multi-domain modelling respectively. For each particular order, results for respectively two, four, twelve and twenty subdomain models are presented and compared to the analytical solution. On the other hand, Figures 4.22 to 4.25 present the same results, grouped per individual multi-domain model, while varying the order of the infinite boundary element.

Overall, one can state that for a given order of the infinite boundary element the performance of the multi-domain boundary element modelling decreases when going to a higher degree of subdomaining. While for a given level of subdomaining, the modelling accuracy improves when the order of the infinite boundary element is increased. The effect becomes more apparent at higher wave numbers. It should be noted here that the modelling problems at low wave numbers, for a high degree of subdomaining combined with a high order boundary element modelling, can be attributed to another phenomenon, that will be explained later at the end of this section.

The fact that more acoustic degrees of freedom are needed along the infinite interfaces, when the level of subdomaining of the acoustic domain and the acoustic wave number of the scattering problem increases, can be explained according to the same reasoning presented in Reference [4.24] for the variable order infinite wave envelope element method. The scattered field from a rigid infinitely long cylinder can be considered as a superposition of multi-poles of different order, which are of the form [4.30]

$$p(r, \theta) = -i \rho c \bar{V}_n \frac{H_n^{(2)}(kr)}{H_n^{(2)'}(kR)} \cos(n\theta) \quad (4.49)$$

where the prescribed radial surface velocity is given by

$$\overline{V}_n(\theta) = \overline{V}_n \cos(n\theta) \quad \overline{V}_n \ll R \quad (4.50)$$

As is the case for the variable order infinite wave envelope element modelling, the ability for modelling higher order multi-poles requires not only satisfactory angular discretization for modelling the lobe-shaped pressure patterns, but moreover, a sufficient number of acoustic degrees of freedom along the infinite interfaces are needed, for modelling the amplitude decay. This reasoning is based on the observation of the asymptotic infinite expansion of an arbitrary two-dimensional pressure field within a region $r > R$ [4.17]

$$p(kr) \sim \sqrt{\frac{2}{\pi kr}} e^{-i(kr - \frac{\pi}{2})} \sum_{n=0}^{\infty} \frac{f_n(\theta)}{(kr)^n} \quad (4.51)$$

where $f_n(\theta)$ is a complex radiation pattern.

It was found, from the study of the limitations of the variable order infinite wave envelope element, that only the radiation patterns that constitute a good radiator can be modelled accurately. This means that the multi-poles of different order can be modelled as long as the acoustic wave number k is greater than the critical wave number $k_c = n/R$, as indicated in Reference [4.24,4.31]. Furthermore, it was observed that the error in modelling radiation patterns with acoustic wave numbers around and below the critical wave number, can be reduced by going to a higher order element modelling.

In case of the multi-domain boundary element modelling, a similar behaviour is expected when the acoustic domain is subdivided into a fair number of subdomains, rendering a local application of the radiation condition. In Figures 4.26 to 4.28, polar plots of the acoustic pressure amplitude of the cylindrical multi-pole radiation of order five, fifteen and twenty-five are presented. The acoustic response was taken at a radius $r = 5R$ for an acoustic wave number of $kR = 20$. The multi-domain mesh consists of twenty subdomains, with a single infinite interface boundary element of order one to four, and

has a boundary element discretization of sixty quadratic conventional boundary elements along the radiating boundary of the cylinder.

In Figure 4.26 the radiation pattern of a multi-pole of order five is shown. Since the acoustic wave number $kR = 20$ is well above the critical wave number $kR = 5$, no problems are expected for this case. The results of the multi-domain models of order one to four correspond perfectly to the analytical solution. A cylindrical multi-pole of order fifteen is then considered in Figure 4.27. For this case the acoustic wave number is fairly close to the critical wave number $kR = 15$. Some problems are now detected for the lower order multi-domain modelling. The fourth order infinite boundary element reflects the best performance in this case. Finally a poor radiator configuration is investigated in Figure 4.28. The acoustic wave number is now lower than the critical wave number $kR = 25$ of this cylindrical multi-pole of order twenty five. As can be seen from the figure, all multi-domain models fail. In the following figure (Figure 4.29), an attempt to model the same multi-pole, using infinite boundary elements of order five, is shown. Some improvement can be detected due to the fact that at least the pattern of the different lobes are being modelled. The amplitude of the different lobes though still reflect major discrepancies. The same figure also reveals that even a multi-domain model of only four subdomains fails in a similar way.

From the above tests of the multi-domain boundary element modelling with interfaces modelled by a single variable order infinite boundary element, one can conclude that only good radiators can be modelled. Figures 4.30 and 4.31 show contour plots of the amplitude of the radiated acoustic pressure field for a cylindrical multi-pole of order ten, evaluated using the analytical expression of Equation (4.49). The field in Figure 4.30 is calculated at an acoustic wave number of $kR = 5$, which is below the critical wave number of $kR = 10$. The pressure pattern obtained consequently reflects a poor radiator. The acoustic energy flows back and forth within the acoustic near field, the so-called short circuiting phenomenon. On the other hand, the pressure pattern shown in Figure 4.31 is calculated at a wave number of $kR = 15$, above the critical wave number of the cylindrical multi-pole. The pressure pattern now reveals the characteristic field of a good radiator, where the acoustic energy predominantly flows towards infinity. From

the observation of these pressure patterns, the limitations of the multi-domain boundary element modelling with interfaces of single variable order boundary elements come as no surprise. Due to the nature of the infinite boundary elements, i.e. outgoing wavelike variation and prescribed amplitude decay, little transfer of acoustic energy from one subdomain into the other is possible.

The observation presented above suggests that, for modelling poor radiators below the critical wave number, it can be beneficial to model the interface in the near field with conventional interface boundary elements. These elements can be seen as a window for acoustic energy transfer between the different subdomains. Figure 4.32 shows a polar plot of the previously modelled cylindrical multi-pole of order twenty five at an acoustic wave number of $kR = 20$. Very good agreement is obtained for the results obtained from a multi-domain model where the near field of the infinite interface is modelled by four quadratic conventional interface boundary elements, confirming the above reasoning.

Finally, another aspect of the multi-domain boundary element modelling should be re-addressed. It was noted earlier in this section, that modelling problems occur when calculating scattered pressure fields at very low wave numbers, using multi-domain models with a high number of acoustic degrees of freedom along the infinite interface. The scattered field at these low wave numbers consists predominantly of a superposition of the contribution of the multi-poles of low order, i.e. the monopole, dipole, etc.. From the discussion in this section, these low order multi-poles can be modelled accurately by very simple multi-domain models. A first order infinite interface boundary element has proven to be sufficient. Therefore, when using more *flexible* multi-domain boundary element models, i.e. with more acoustic degrees of freedom, a numerically unstable system can be obtained. The likelihood of this numerical instability is confirmed by a high condition number for the system matrices, indicating an ill-conditioned set of boundary element equations for these multi-domain models.

4.3.3. CYLINDRICAL SOURCE SCATTERING FROM A SINGLE RIGID BARRIER

In a last example, a two-dimensional cylindrical source scattering from a single

rigid barrier is studied. The barrier is of height $H = 1$ and width $W = 0.2H$. The cylindrical acoustic source is located at $x = -1.5H$ and $y = 0.15H$, as shown in Figure 4.33. The computational meshes used for this problem have a boundary element discretization of eighty-eight linear conventional boundary elements along the radiating boundary of the barrier. The multi-domain meshes employ the variable order infinite rigid hard plane boundary elements along the plane $y = 0$. The single subdomain mesh spans the whole region from the one infinite rigid half plane boundary element to the other, while the two subdomain mesh reveals a variable order infinite interface element along the symmetry plane $x = 0$. All infinite elements used are of order one in order to add the least number of acoustic degrees of freedom.

Figure 4.33 shows a contour plot of the pressure amplitude of the total acoustic field at a wave number of $kH = 5$, obtained from the two subdomain model. The total acoustic pressure field is obtained from superposition of the calculated scattered pressure field and the incident field due to the cylindrical source. The standing wave patterns in front and the acoustic shadow zone in the region behind the barrier can be observed.

Frequency response functions of the amplitude of the total acoustic pressure at a field point located at $x = 5H$ and $y = 0.1H$ are given in Figures 4.34 and 4.35. The results are compared with calculations obtained from direct collocation boundary element methods. The conventional boundary element methods reflect singularity problems at wave numbers around $k = 16$ and $k = 32$. These singularities can be drastically reduced by applying the over-determination procedure. Figure 4.34 reflects the result when using ten randomly spaced over-determination points within the barrier geometry. The two subdomain boundary element model shows no signs of singularities and proves once again to be a convenient method for completely excluding the non-uniqueness problem. The multi-domain method is not only efficient, in that no extra degrees of freedom are added, but it also avoids the need for finding the appropriate number and, especially, the location for the interior over-determination points. The latter is not an easy task for arbitrary geometry configurations.

Figure 4.35 reveals an interesting aspect. When the acoustic domain is modelled by a single subdomain, weak singularities appear at similar wave numbers as detected for

the conventional direct collocation boundary element method. This can be explained by the fact that the domain of the complementary problem allows for local resonances. In this case, the interior of the single barrier can act as a local resonator. As soon as two subdomains are defined the possibility of a local resonator is removed.

A great advantage of the multi-domain boundary element modelling is thus the fact that one can always make sure that the different acoustic subdomains are well defined. In doing so, not only the singularities can be removed, but moreover the well-known difficulties with boundaries folding back onto each other, as in thin slender structures, can be avoided [4.28].

Finally Figure 4.36 shows a plot of the insertion loss in dB of the single barrier for the same source-receiver configuration. The insertion loss is defined as

$$IL (dB) = - 20 \log \left| \frac{p}{p_h} \right| \quad (4.52)$$

where p_h is the acoustic pressure at the receiver location due to the source above a rigid half plane, without the barrier in place. The results produced by the multi-domain model show a characteristic insertion loss curve for this type of barrier, while the conventional boundary element method obviously shows problems due to the non-uniqueness problem.

4.4. CONCLUSIONS

A new variable order infinite boundary element for direct collocation multi-domain boundary element modelling of acoustic radiation and scattering problems has been presented. The special aspects of the finite to infinite geometry mapping, the variable order Lagrangian shape functions and the wavelike variation have been adopted from the formulation of the variable order infinite wave envelope element.

The main difficulty for the implementation of the element lies in the integration within the infinite domain. In a first attempt, the approach of Zeng et al. [4.25] is used. The integral is truncated at a finite distance and divided into a number of subelements, which are integrated separately by conventional Gauss quadrature. Singularities are taken

care of by the method of Telles [4.27] within each subelement. The integration scheme is therefore quite costly in terms of calculation time, especially, in case of axisymmetric modelling, where each evaluation of the free-space Green's kernel involves an integration in the angular direction. In future research, different integration schemes can be investigated for more efficient evaluation of the infinite integral.

Due to costly integration of the axisymmetric formulation, test cases have been focussed on the two-dimensional multi-domain boundary element modelling. The acoustic modelling of radiation and scattering from an infinitely long rigid cylinder is investigated to evaluate the performance of the direct collocation multi-domain boundary element method. A great advantage is the fact that no singularities are present due to the non-uniqueness problem, common for conventional boundary element formulations. However slight singularity problems manifest themselves, when local resonances in the complementary *interior* problem can be established. The latter can always be avoided by a proper choice of subdomain geometry. In fact, through an adequate selection of subdomains, the boundary of each subdomain can be well defined, in a way that problems of near-singular behaviour, involved with thin slender structures, can be avoided.

Tests have been performed with different computational meshes, where the degree of subdomaining and the order of the infinite boundary element has been varied. It was found that going to a higher order of subdomaining results in a more *local* application of the Sommerfeld radiation condition and thus limitations in modelling general radiation and scattering problems. In fact, at a high degree of subdomaining similar behaviour is noticed as in the case of the variable order infinite wave envelope element [4.24]. It is seen that in general *good* radiators, where the acoustic energy predominantly flows towards infinity, can be modelled without any problem. For *poor* radiators, where energy flows within the acoustic near field, adequate transfer of acoustic energy is necessary across the subdomain interfaces. This can be accomplished to some degree by going to higher order infinite interface elements, but eventually, a so-called acoustic window of conventional interface boundary elements is necessary to allow for sufficient acoustic energy exchange from one subdomain into the other.

The multi-domain boundary element method has great promise to be an adequate

tool for modelling scattering problems from arbitrary barrier configurations. Even with a minimal degree of subdomaining, the great advantage of avoiding the non-uniqueness problem is prominent. Furthermore, the fact that infinite half planes can be modelled by means of the variable order infinite boundary elements, opens up a whole new class of barrier configurations. Barrier configurations with half planes elevated at different heights can now be modelled. One can also think of applying a uniform impedance along these infinite edges. These infinite impedance planes have been modelled before to some extent by the implementation of special Green's kernels in the boundary element formulation, as in Reference [4.31]. In the latter formulation, only a single infinite impedance plane can be considered, while by using the multi-domain approach different impedance plane configurations, e.g. again at different heights, can be analyzed. Scattering models of this type can prove very useful in the study of road noise barriers.

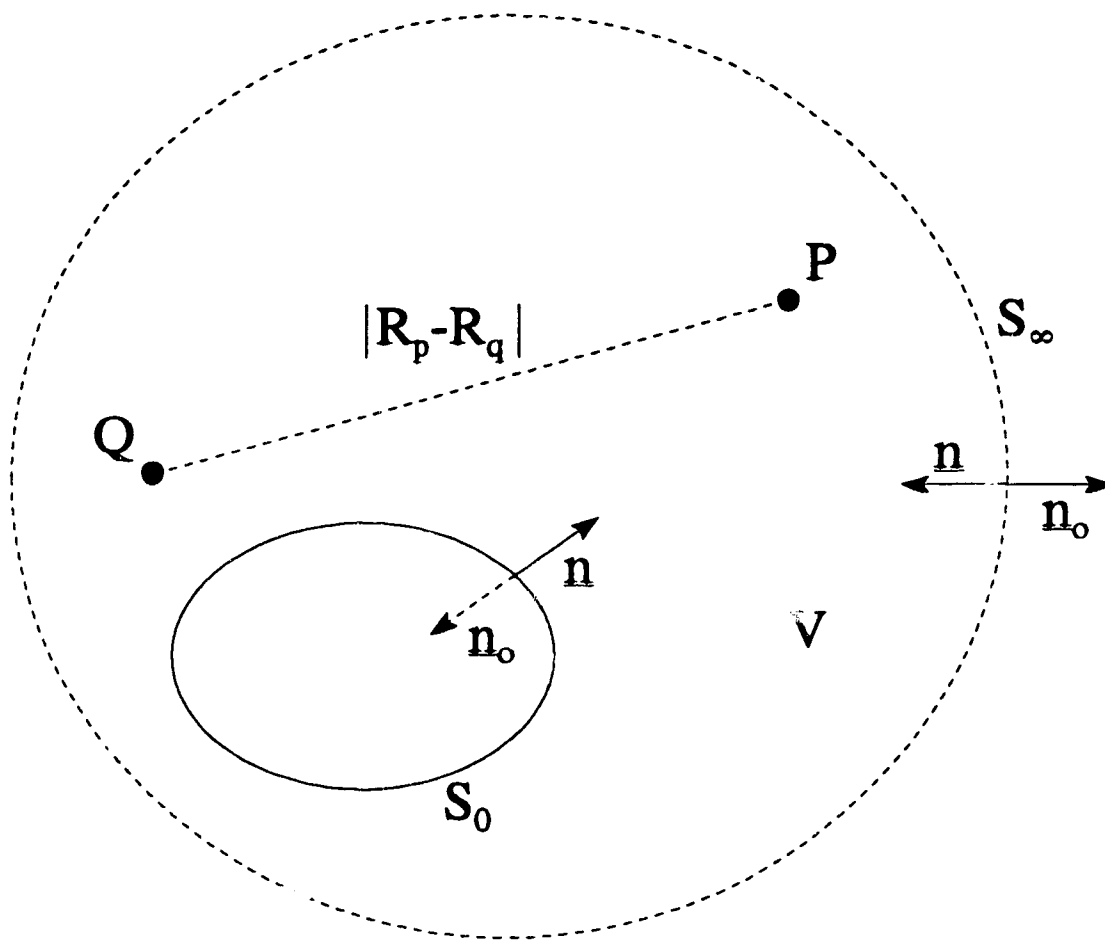


Figure 4.1 Radiating body in an infinite domain: geometric configuration for boundary integral formulations.

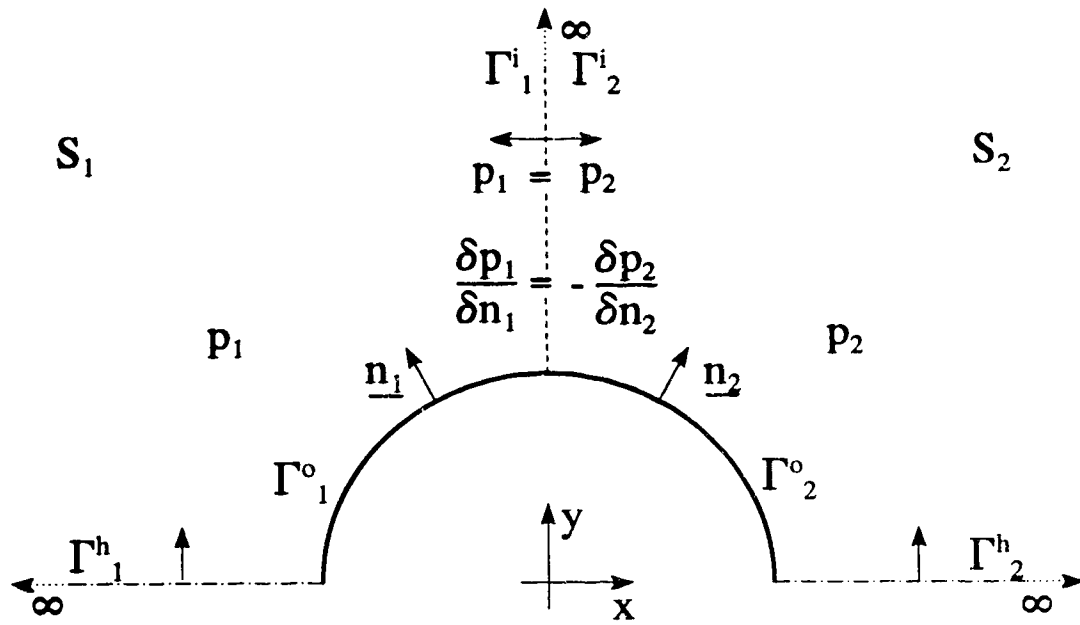


Figure 4.2 Multi-domain boundary element configuration.

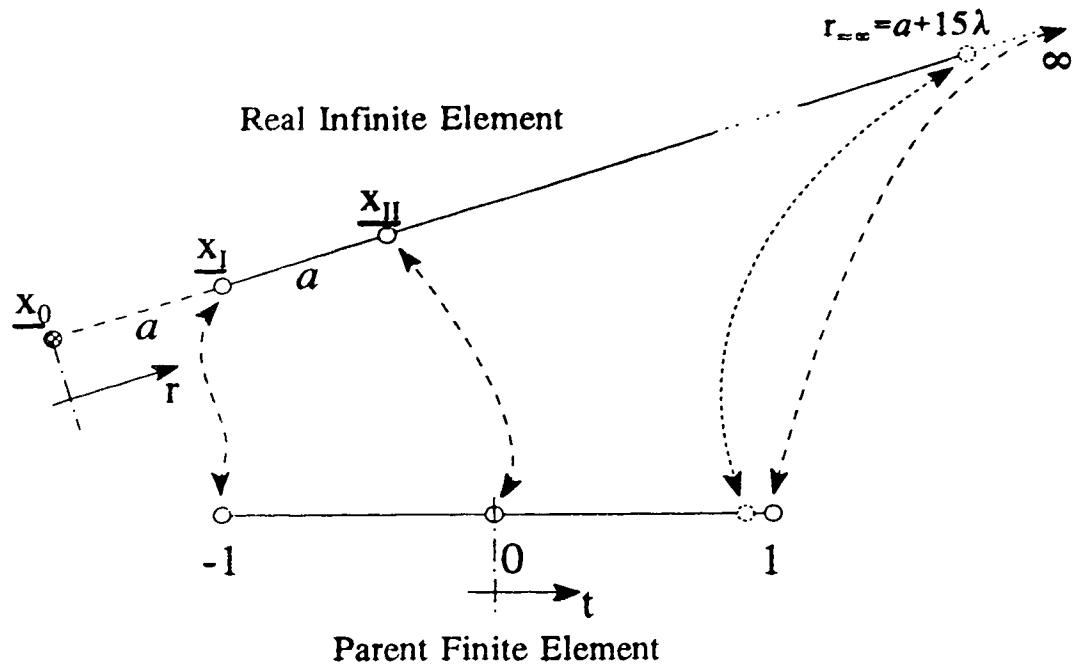


Figure 4.3 Infinite boundary element geometry mapping.

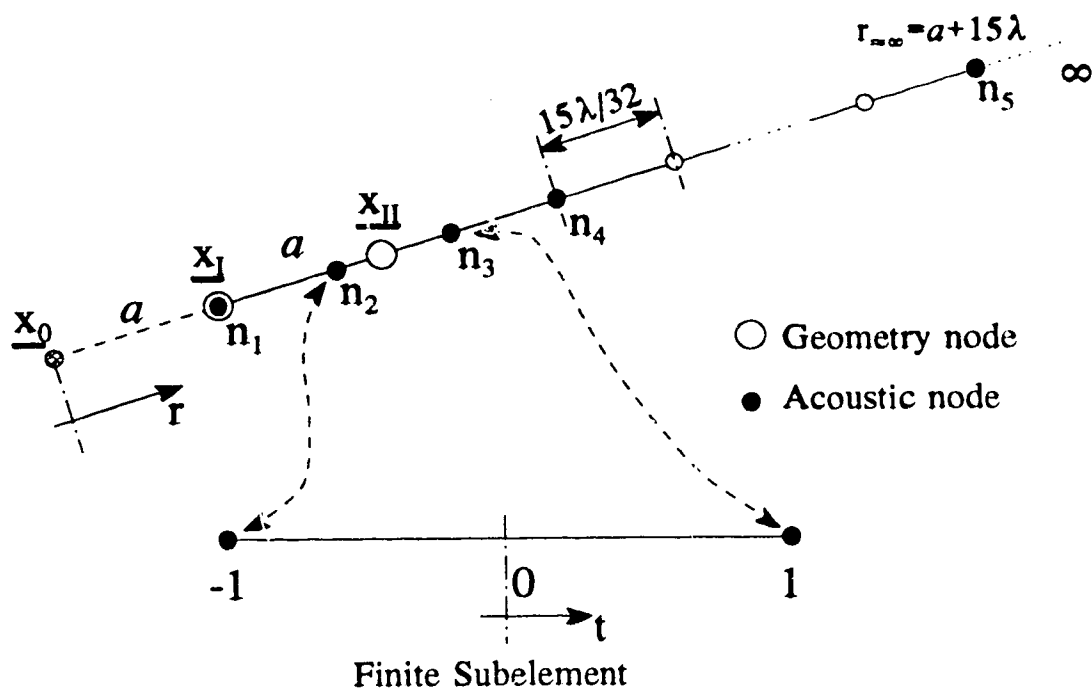


Figure 4.4 Variable order infinite boundary element.

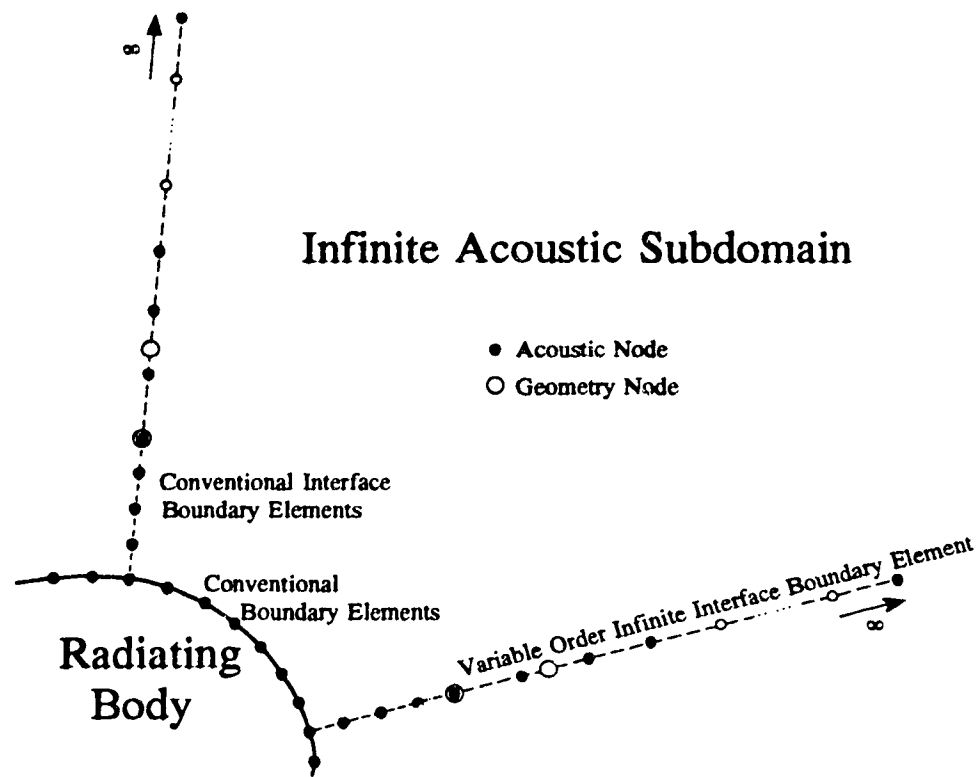


Figure 4.5 Sample subdomain boundary element discretisation.

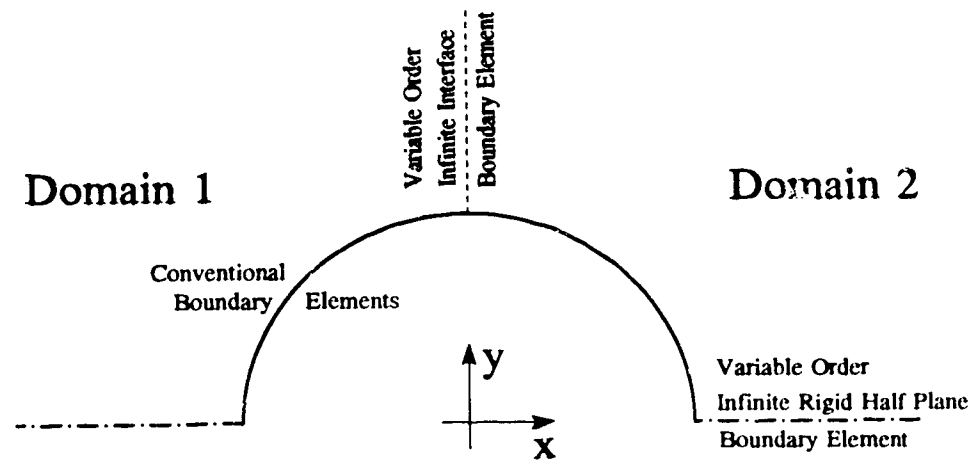


Figure 4.6 Sample two-dimensional multi-domain mesh for an infinitely long rigid cylinder.

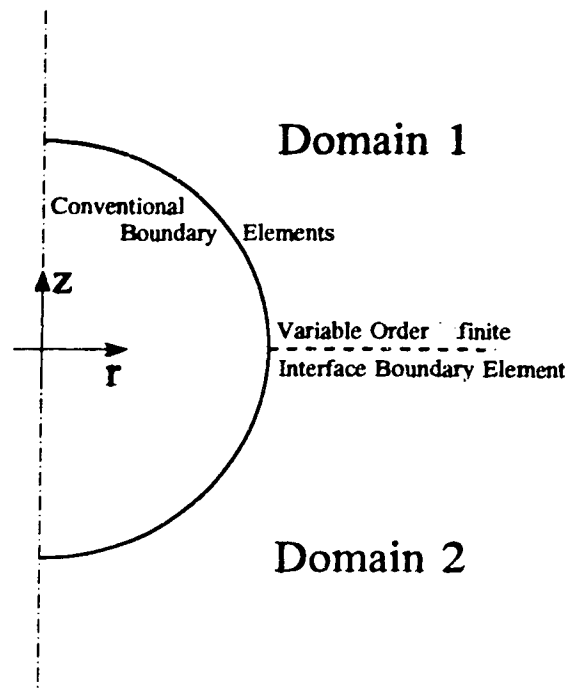


Figure 4.7 Sample axisymmetric multi-domain mesh for a rigid sphere.

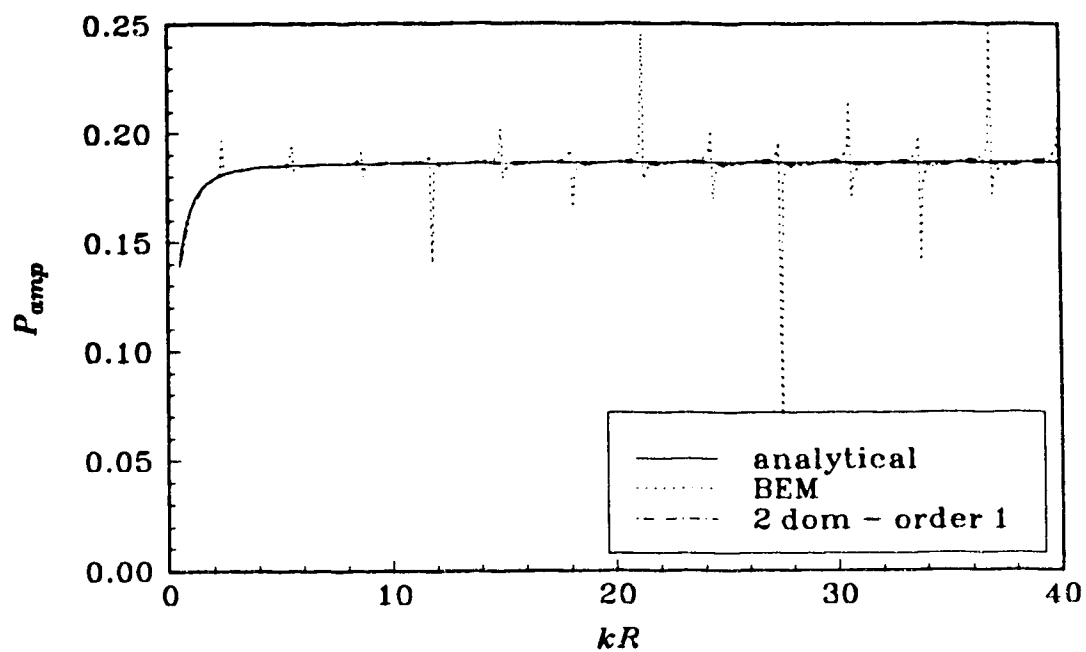


Figure 4.8 Acoustic radiation by a rigid cylinder - monopole.
Frequency response function of the amplitude of the radiated acoustic pressure at $r = 5R$.

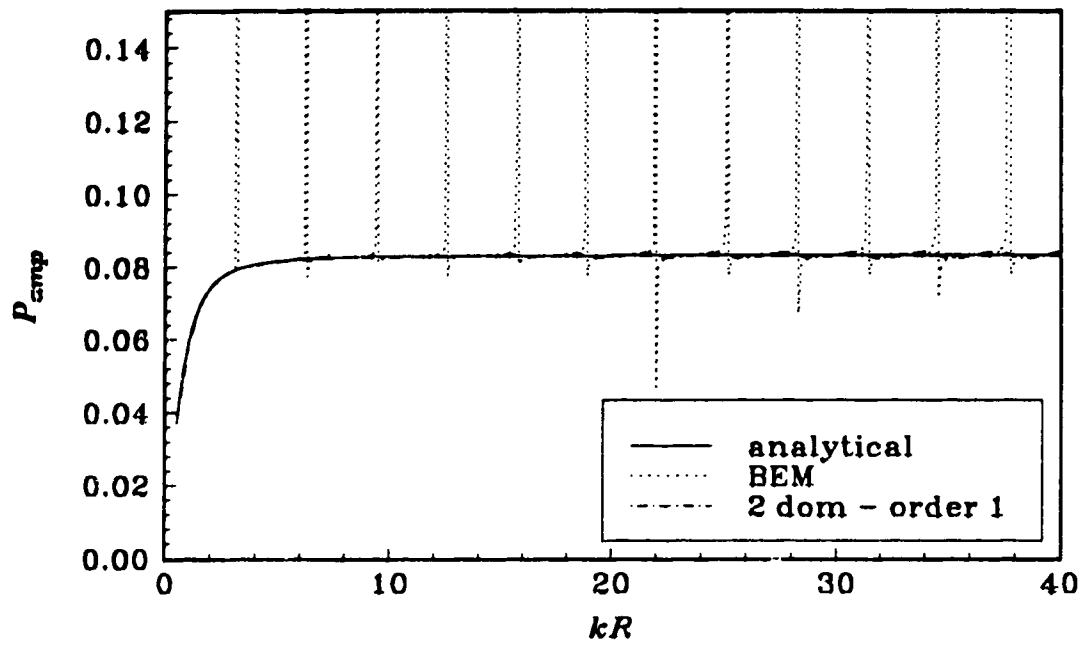


Figure 4.9 Acoustic radiation by a rigid sphere - monopole.
Frequency response function of the amplitude of the radiated acoustic pressure at $r = 5R$.

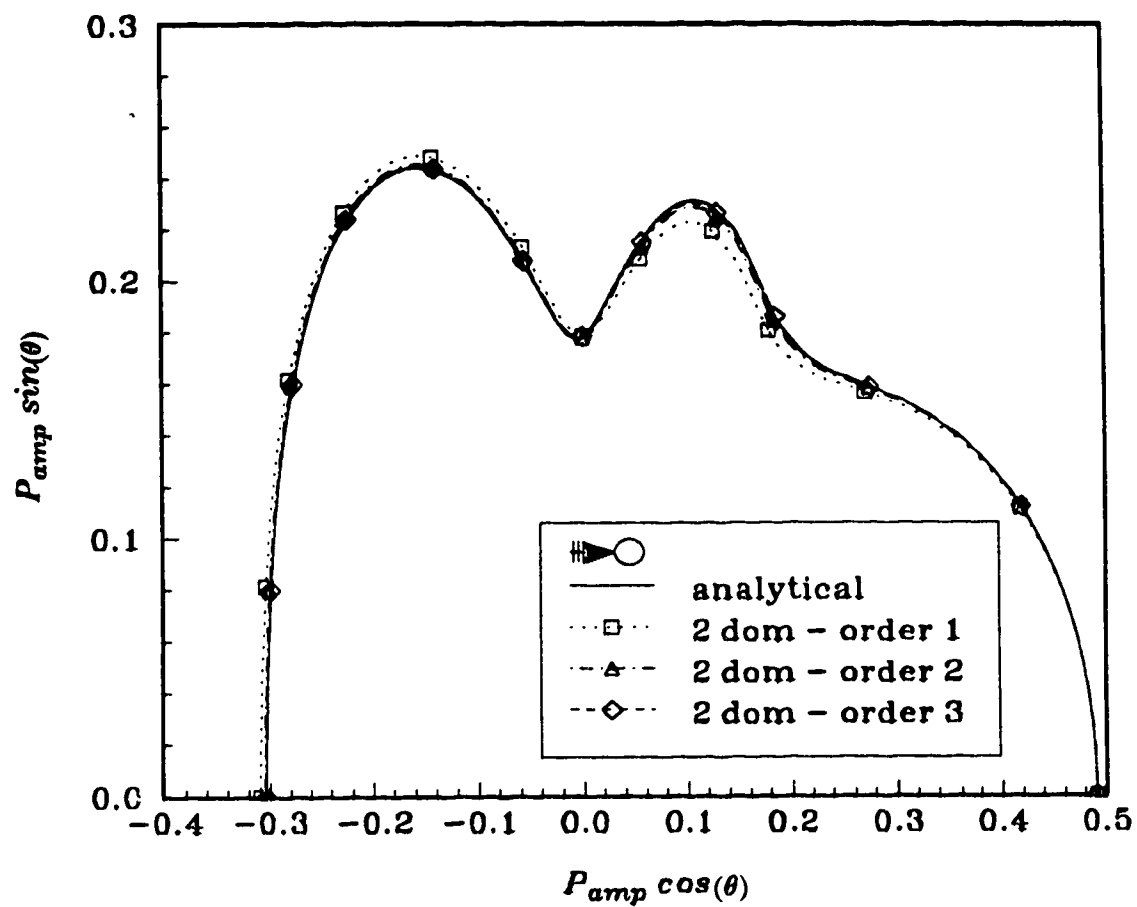


Figure 4.10 Scattering of an acoustic plane wave ($\rightarrow +x$) from a rigid cylinder. Polar plot ($0 < \theta < 180$) of the amplitude of the scattered acoustic pressure $|P_s|/|P_i|$ at $r = 5R$ for $kR = 2.405$.

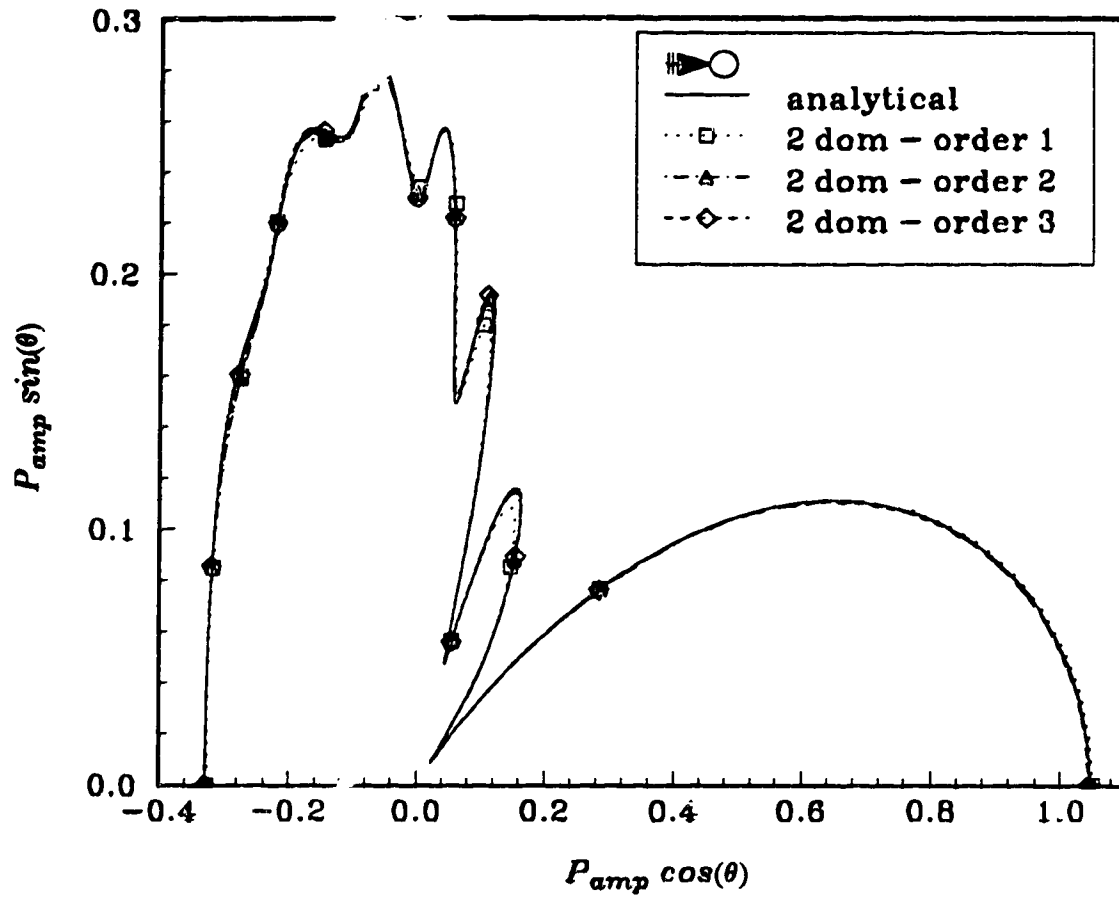


Figure 4.11 Scattering of an acoustic plane wave ($\rightarrow +x$) from a rigid cylinder. Polar plot ($0 < \theta < 180$) of the amplitude of the scattered acoustic pressure $|P_s|/|P_i|$ at $r = 5R$ for $kR = 8.654$.

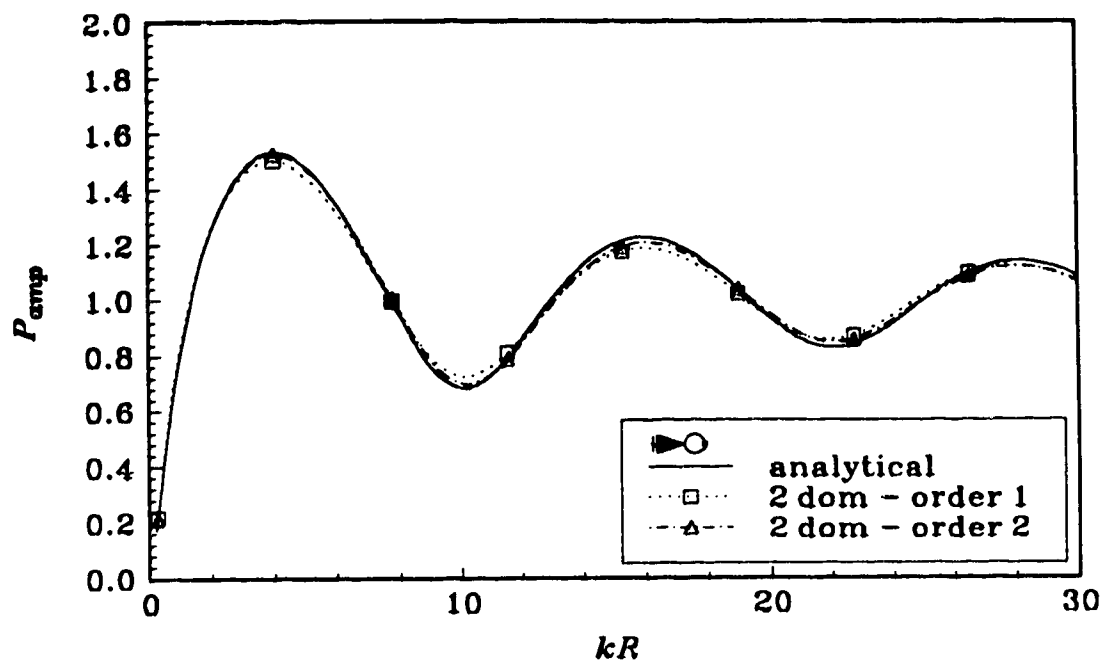


Figure 4.12 Scattering of an acoustic plane wave ($\rightarrow +x$) from a rigid cylinder. Frequency response function of the amplitude of the scattered acoustic pressure $|P_s|/|P_i|$ at $x = 1.1R$; $y = 0$ (Near field - forward scattering).

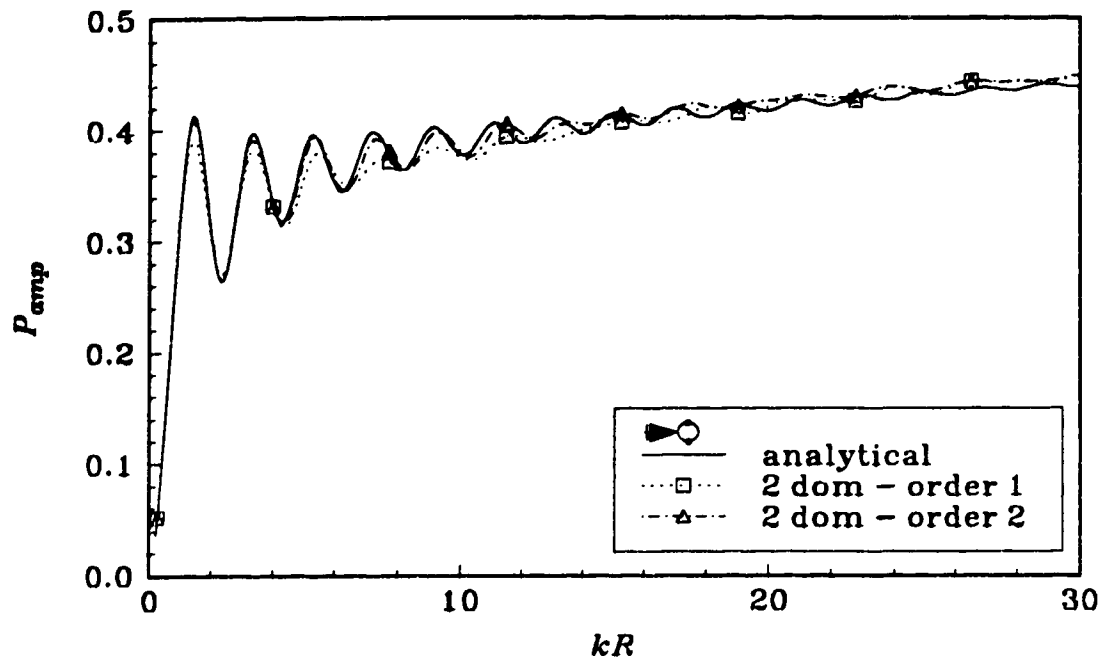


Figure 4.13 Scattering of an acoustic plane wave ($\rightarrow +x$) from a rigid cylinder. Frequency response function of the amplitude of the scattered acoustic pressure $|P_s|/|P_i|$ at $x = 0$; $y = 1.1R$ (Near field - sideward scattering).

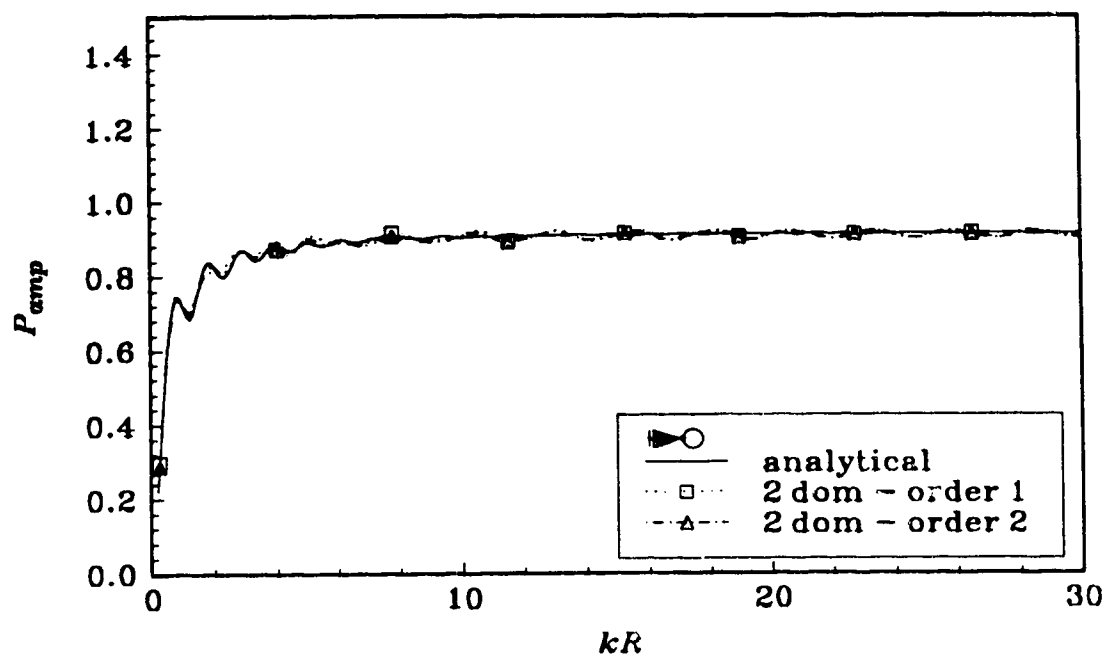


Figure 4.14 Scattering of an acoustic plane wave ($\rightarrow +x$) from a rigid cylinder. Frequency response function of the amplitude of the scattered acoustic pressure $|P_s|/|P_i|$ at $x = -1.1R$; $y = 0$ (Near field - backward scattering).

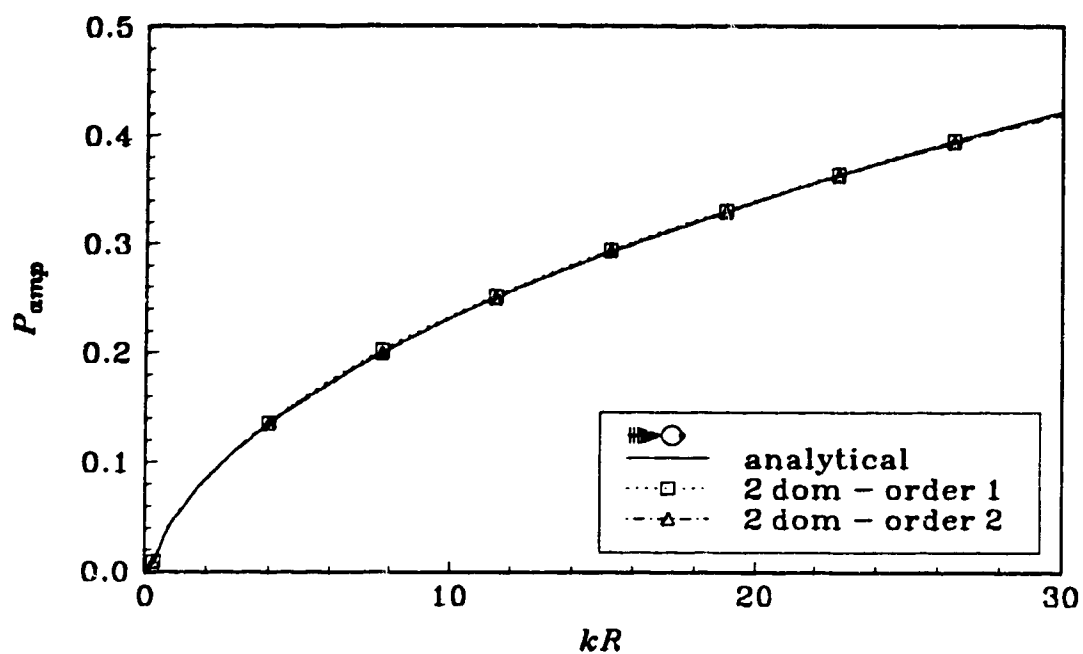


Figure 4.15 Scattering of an acoustic plane wave ($\rightarrow +x$) from a rigid cylinder. Frequency response function of the amplitude of the scattered acoustic pressure $|P_s|/|P_i|$ at $x = 100R$; $y = 0$ (Far field - forward scattering).

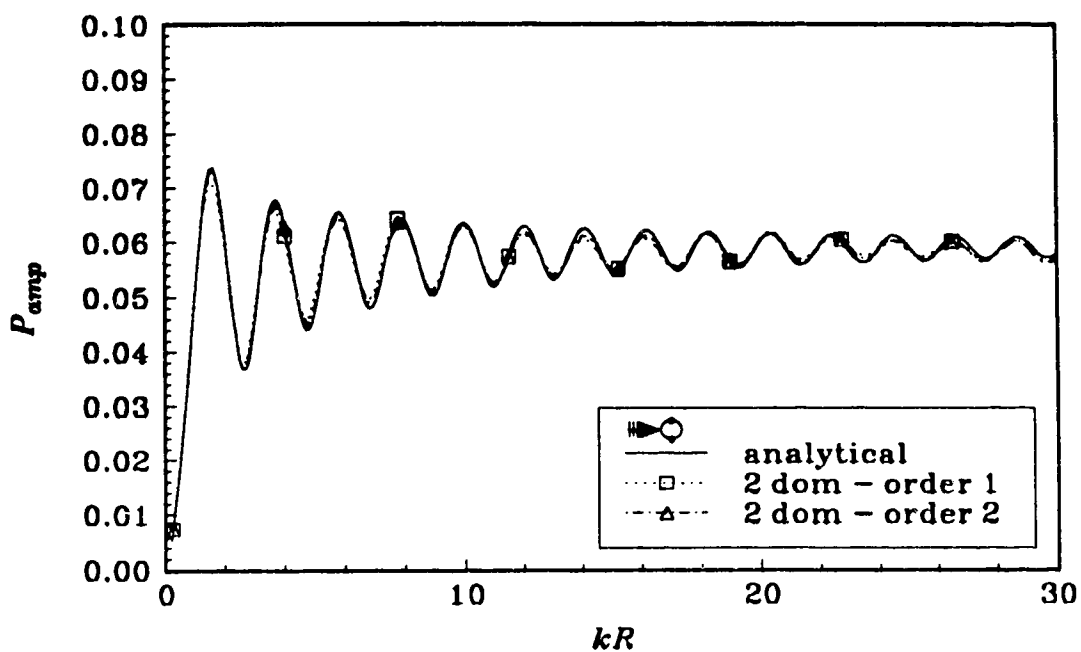


Figure 4.16 Scattering of an acoustic plane wave ($\rightarrow +x$) from a rigid cylinder. Frequency response function of the amplitude of the scattered acoustic pressure $|P_s|/|P_i|$ at $x = 0$; $y = 100R$ (Far field - sideward scattering).

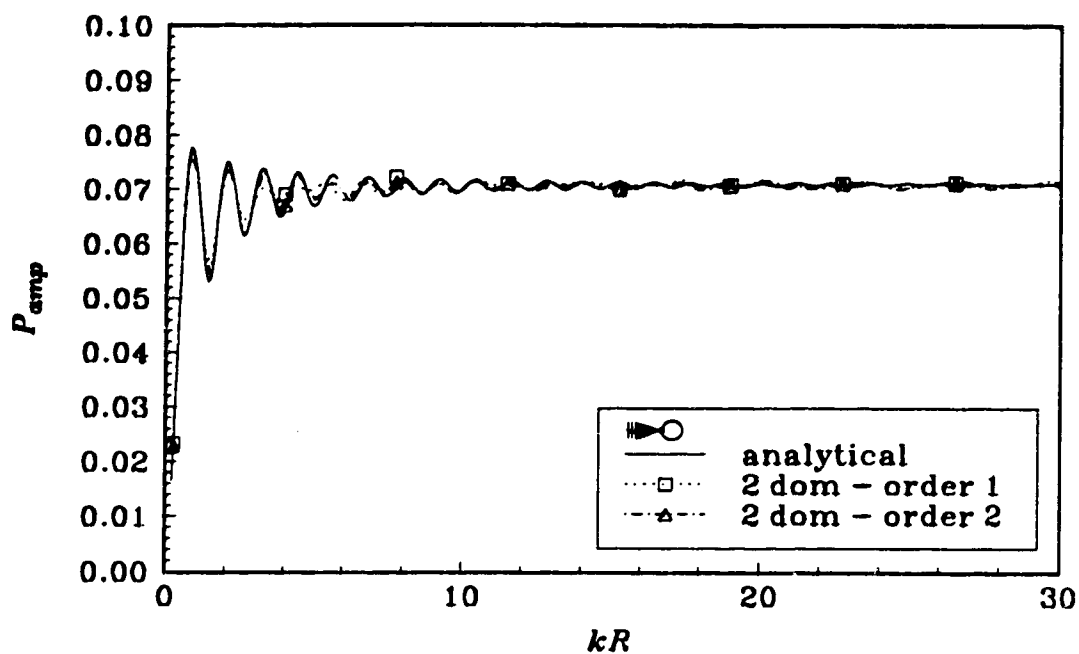


Figure 4.17 Scattering of an acoustic plane wave ($\rightarrow +x$) from a rigid cylinder. Frequency response function of the amplitude of the scattered acoustic pressure $|P_s|/|P_i|$ at $x = -100R$; $y = 0$ (Far field - backward scattering).

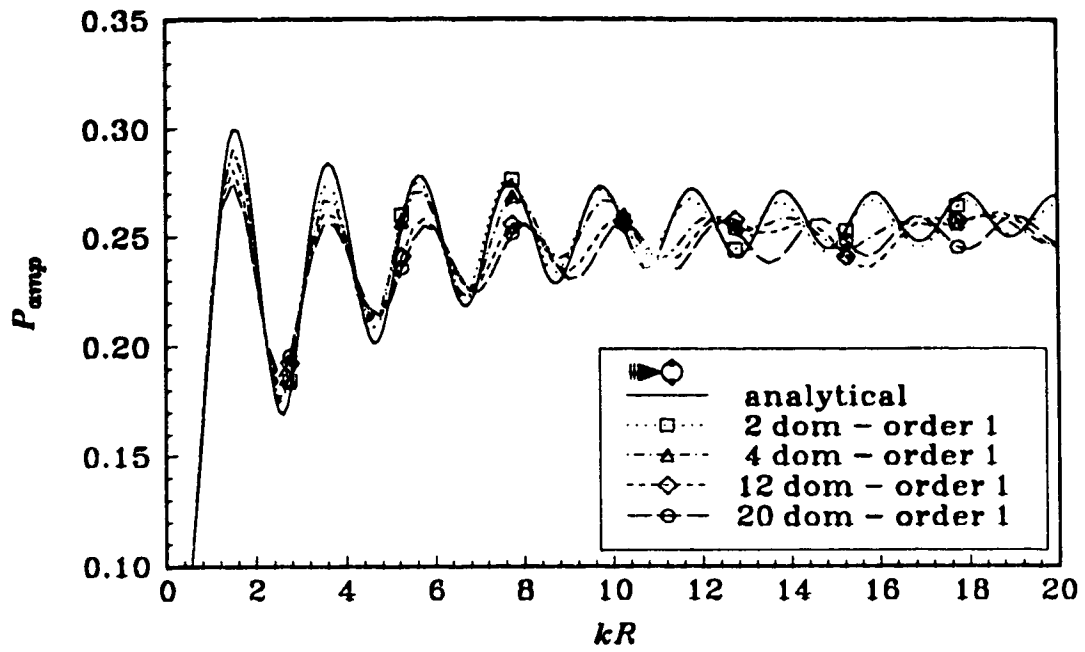


Figure 4.18 Scattering of an acoustic plane wave ($\rightarrow +x$) from a rigid cylinder. Frequency response function of the amplitude of the scattered acoustic pressure $|P_s|/|P_i|$ at $x = 0$; $y = 5R$. Results obtained for infinite boundary elements of order 1, while varying the degree of subdomaining.

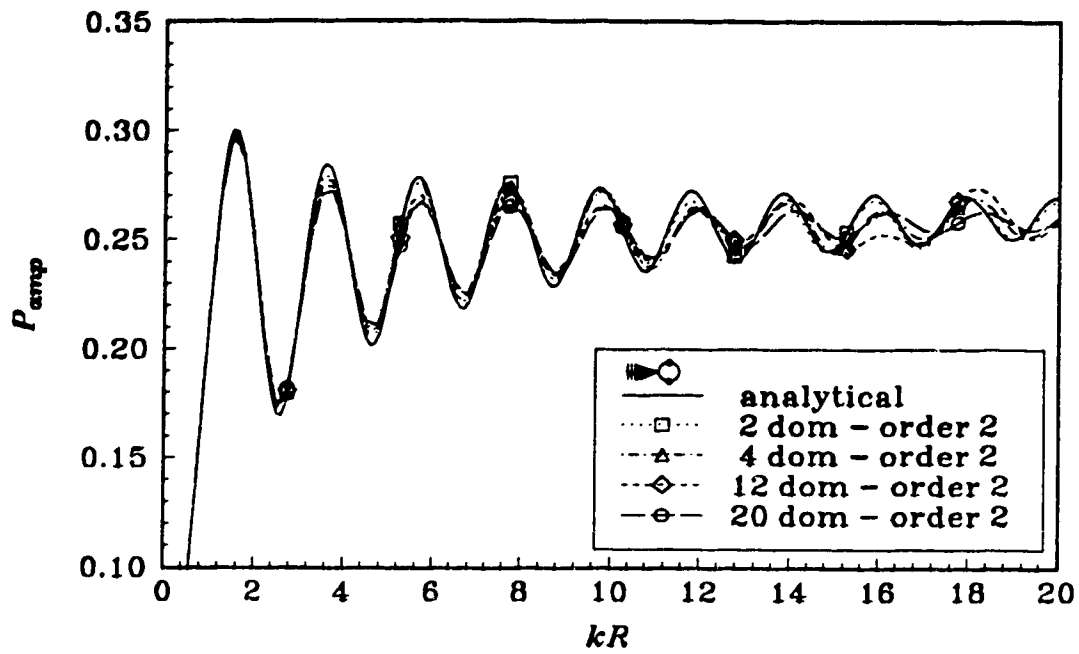


Figure 4.19 Scattering of an acoustic plane wave ($\rightarrow +x$) from a rigid cylinder. Frequency response function of the amplitude of the scattered acoustic pressure $|P_s|/|P_i|$ at $x = 0$; $y = 5R$. Results obtained for infinite boundary elements of order 2, while varying the degree of subdomaining.

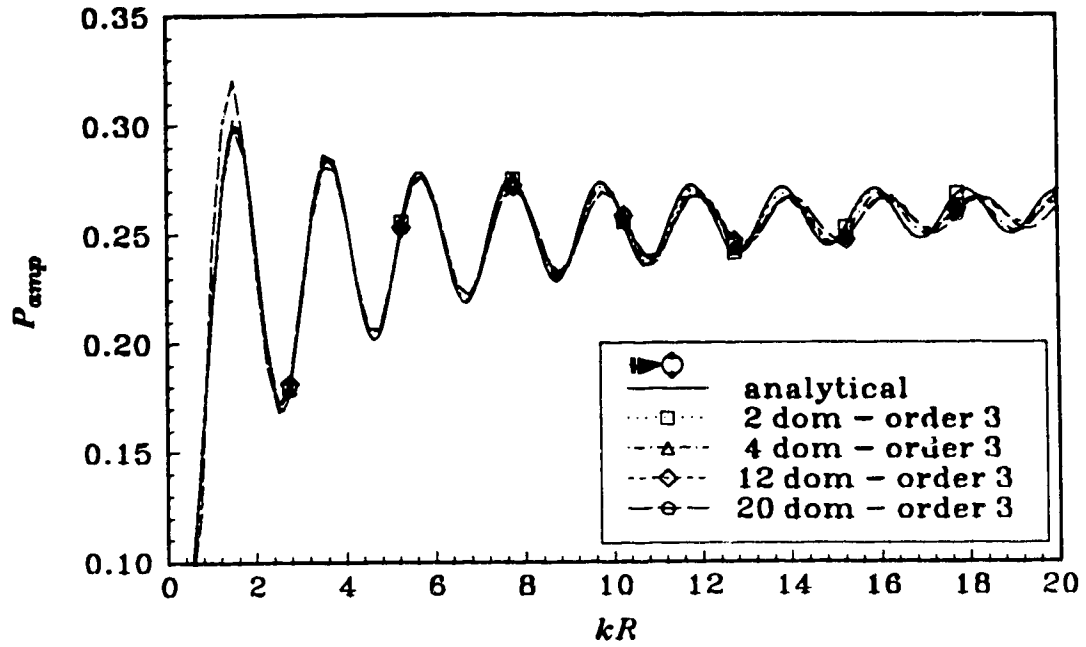


Figure 4.20 Scattering of an acoustic plane wave ($\rightarrow +x$) from a rigid cylinder. Frequency response function of the amplitude of the scattered acoustic pressure $|P_s|/|P_i|$ at $x = 0$; $y = 5R$. Results obtained for infinite boundary elements of order 3, while varying the degree of subdomaining.

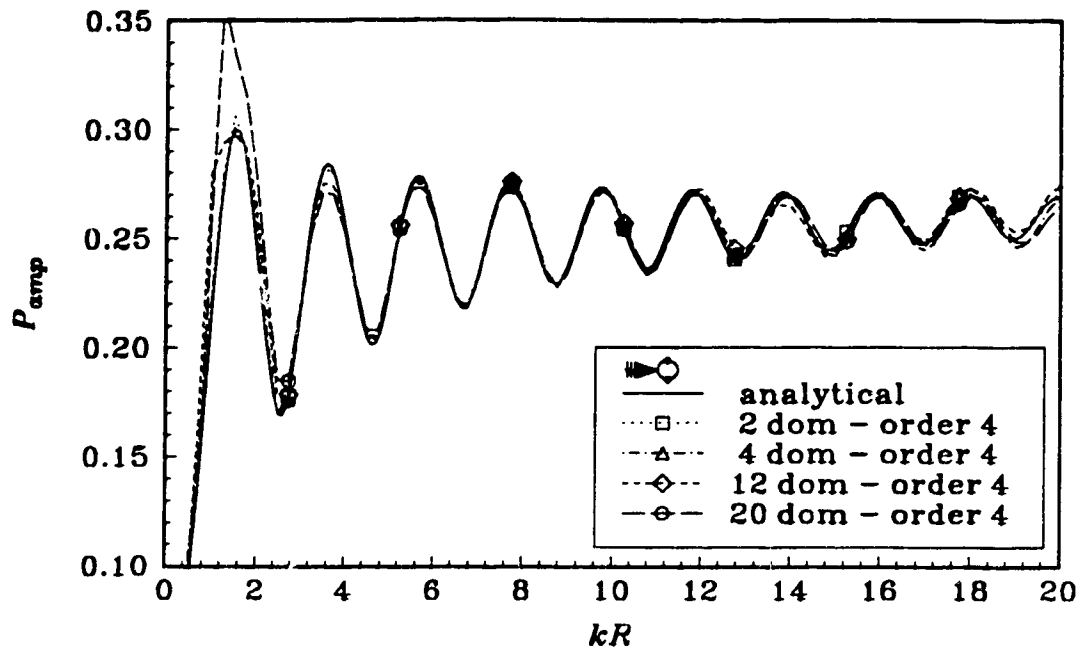


Figure 4.21 Scattering of an acoustic plane wave ($\rightarrow +x$) from a rigid cylinder. Frequency response function of the amplitude of the scattered acoustic pressure $|P_s|/|P_i|$ at $x = 0$; $y = 5R$. Results obtained for infinite boundary elements of order 4, while varying the degree of subdomaining.

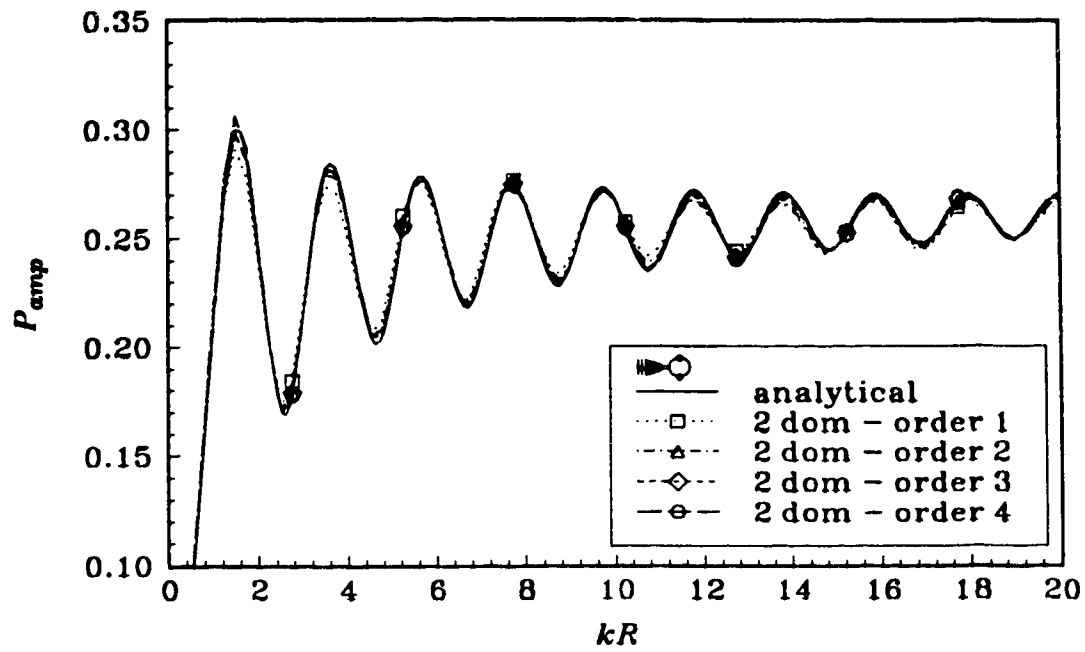


Figure 4.22 Scattering of an acoustic plane wave ($\rightarrow +x$) from a rigid cylinder. Frequency response function of the amplitude of the scattered acoustic pressure $|P_s|/|P_i|$ at $x = 0$; $y = 5R$. Results obtained for a mesh with 2 subdomains, while varying the order of the infinite boundary element.

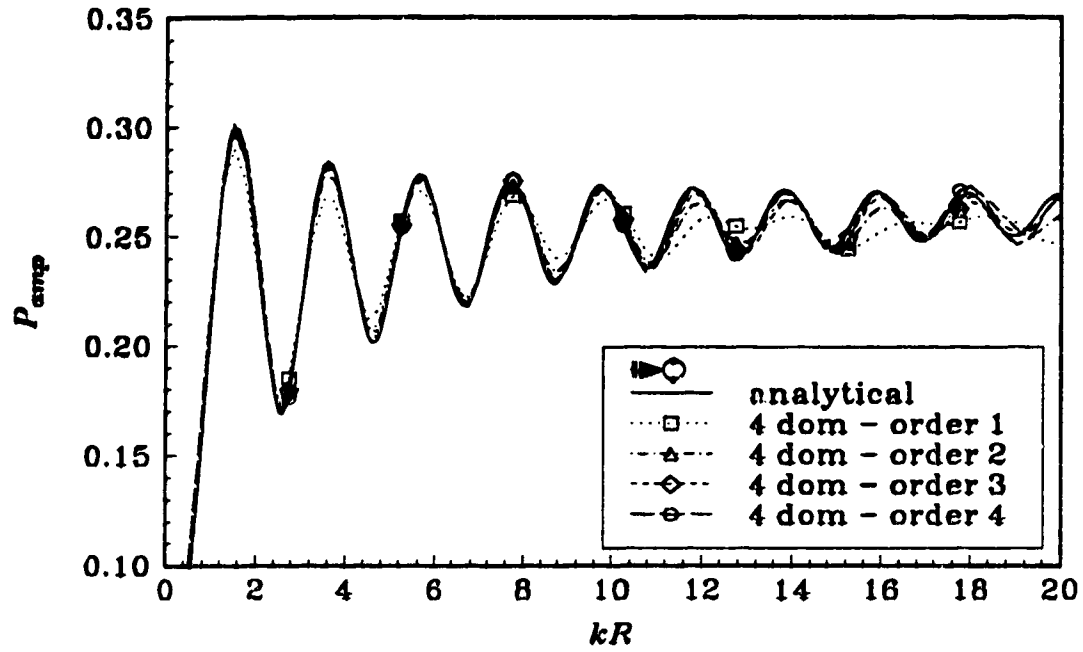


Figure 4.23 Scattering of an acoustic plane wave ($\rightarrow +x$) from a rigid cylinder. Frequency response function of the amplitude of the scattered acoustic pressure $|P_s|/|P_i|$ at $x = 0$; $y = 5R$. Results obtained for a mesh with 4 subdomains, while varying the order of the infinite boundary element.

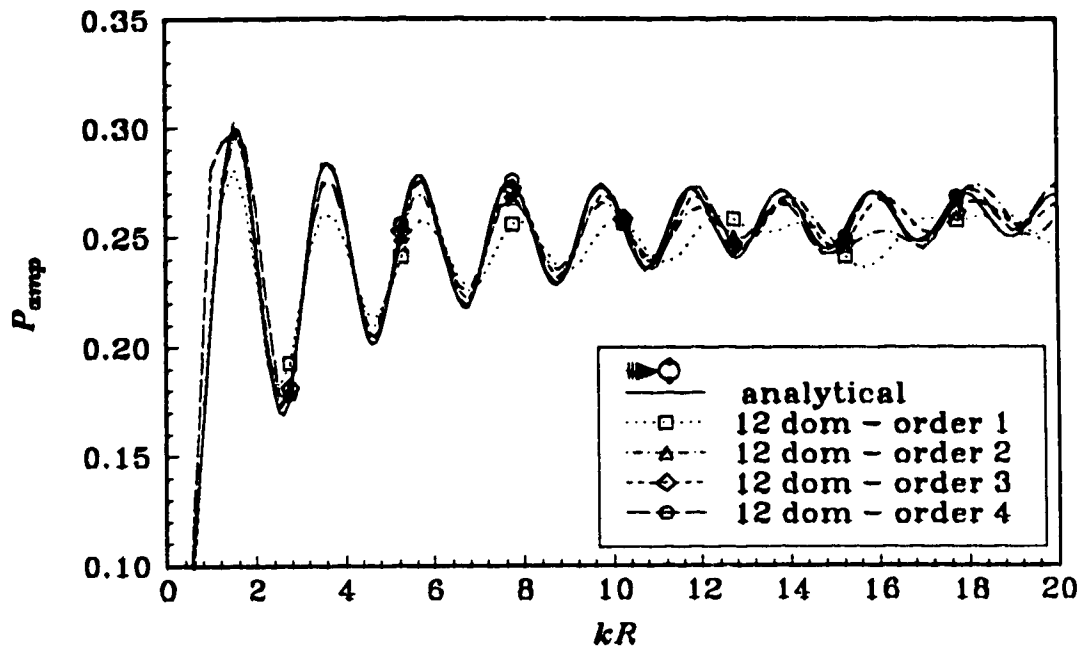


Figure 4.24 Scattering of an acoustic plane wave ($\rightarrow +x$) from a rigid cylinder. Frequency response function of the amplitude of the scattered acoustic pressure $|P_s|/|P_i|$ at $x = 0$; $y = 5R$. Results obtained for a mesh with 12 subdomains, while varying the order of the infinite boundary element.

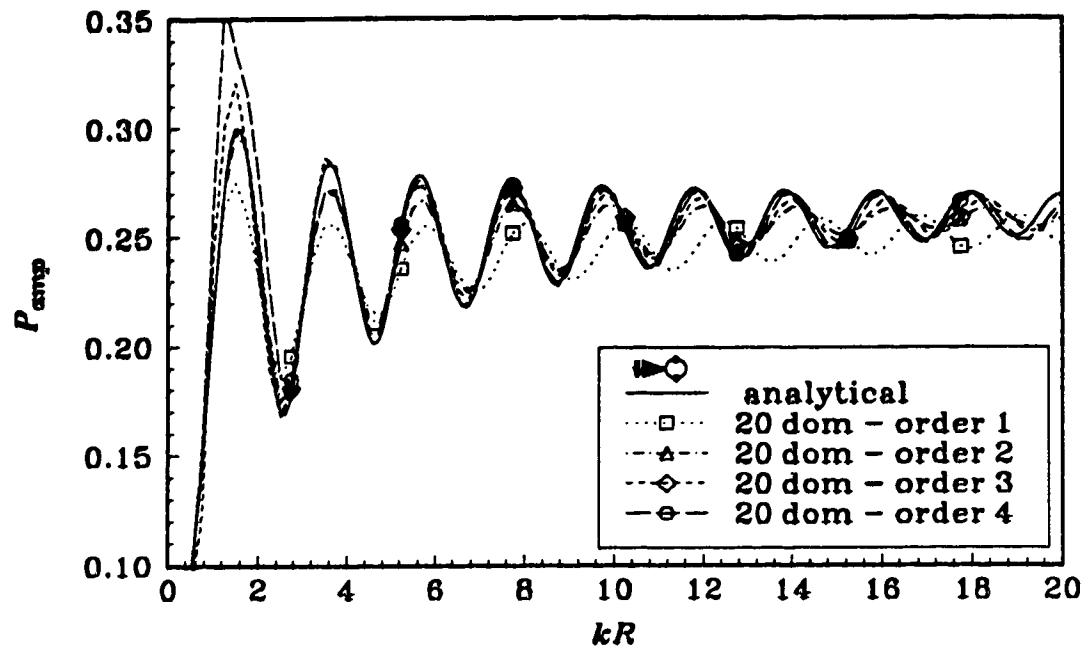


Figure 4.25 Scattering of an acoustic plane wave ($\rightarrow +x$) from a rigid cylinder. Frequency response function of the amplitude of the scattered acoustic pressure $|P_s|/|P_i|$ at $x = 0$; $y = 5R$. Results obtained for a mesh with 20 subdomains, while varying the order of the infinite boundary element.

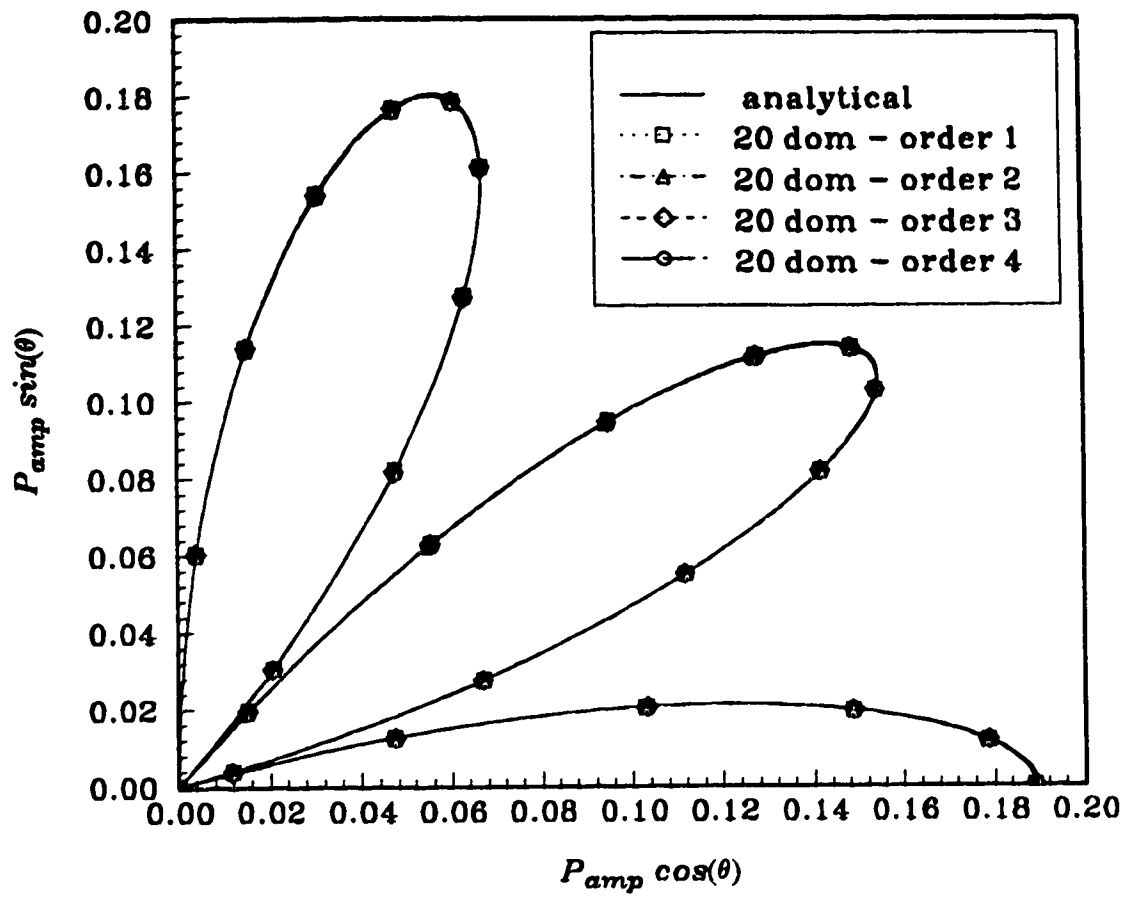


Figure 4.26 Cylindrical multi-pole of order 5.
Polar plot ($0 < \theta < 90$) of the amplitude of the radiated acoustic pressure at $r = 5R$ for $kR = 20$.

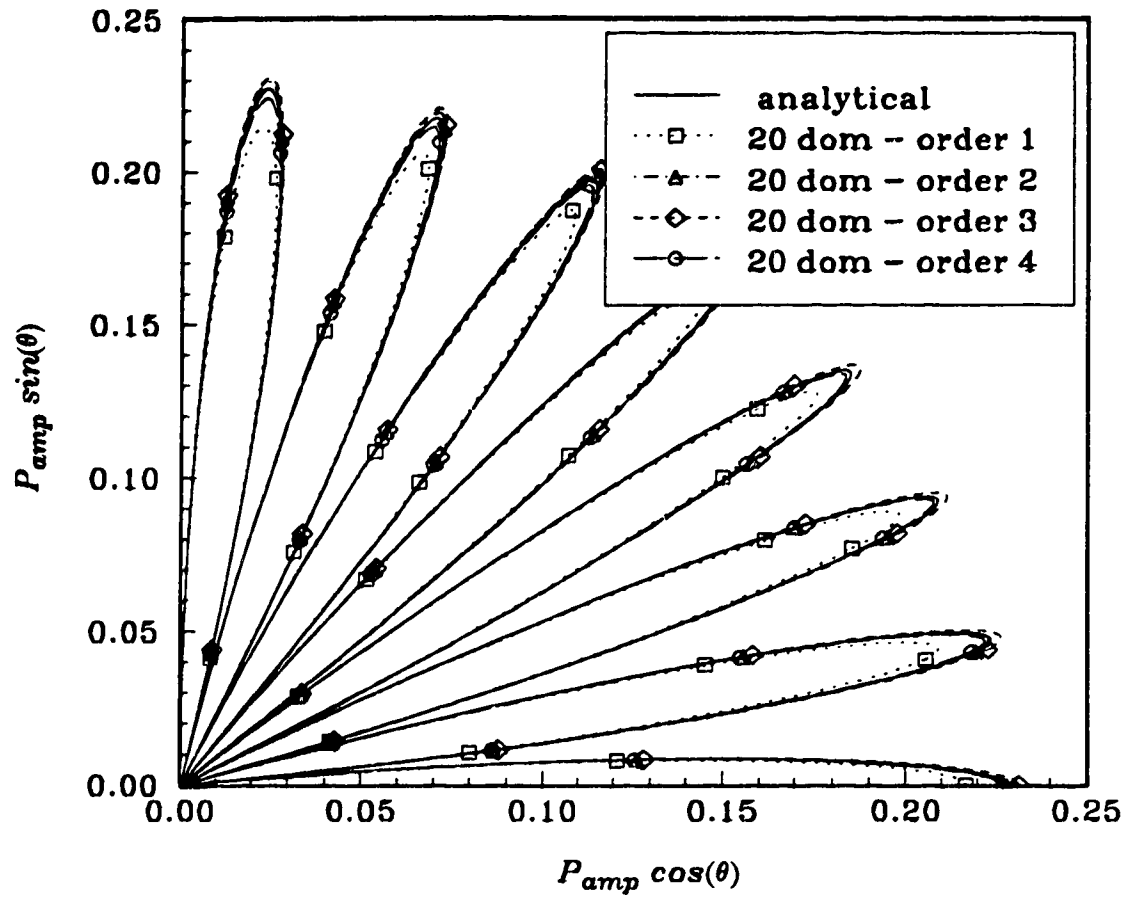


Figure 4.27 Cylindrical multi-pole of order 15.
Polar plot ($0 < \theta < 90$) of the amplitude of the radiated acoustic pressure at $r = 5R$ for $kR = 20$.

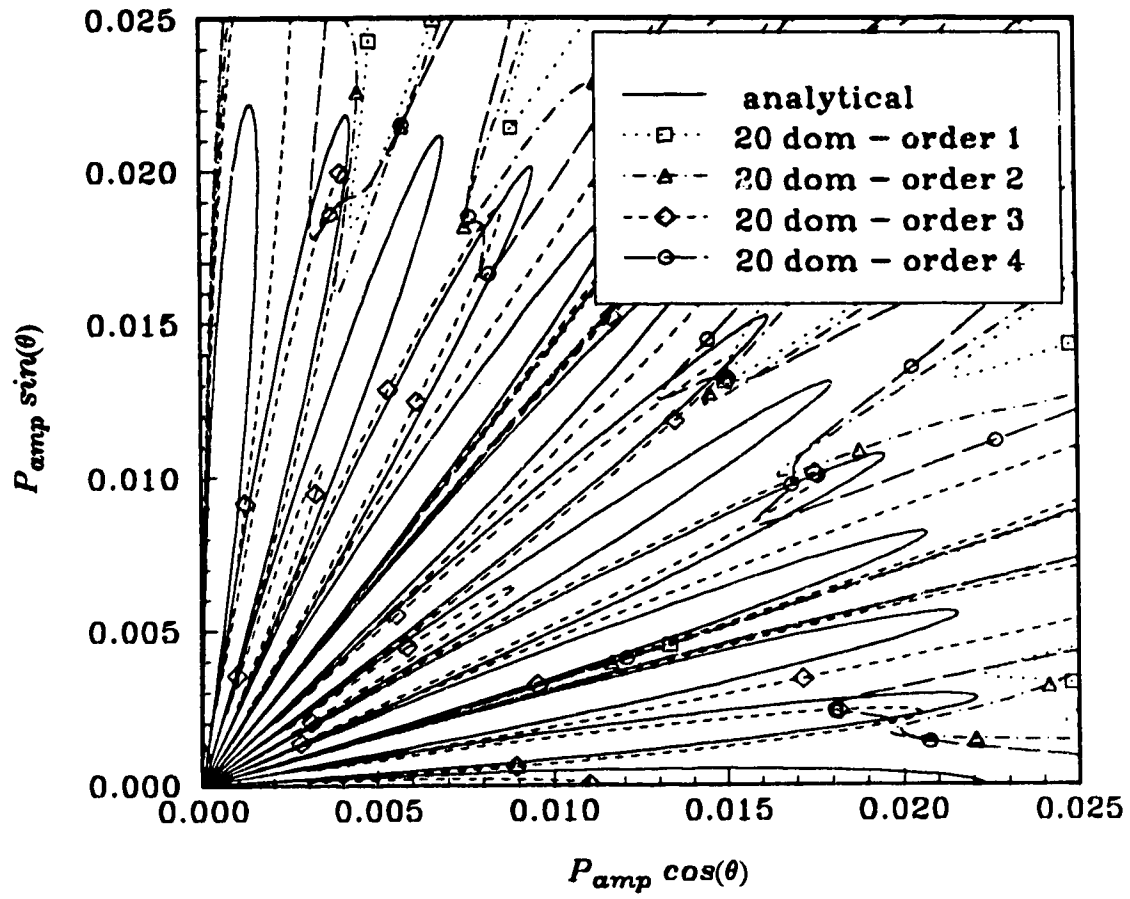


Figure 4.28 Cylindrical multi-pole of order 25.

Polar plot ($0 < \theta < 90$) of the amplitude of the radiated acoustic pressure at $r = 5R$ for $kR = 20$.

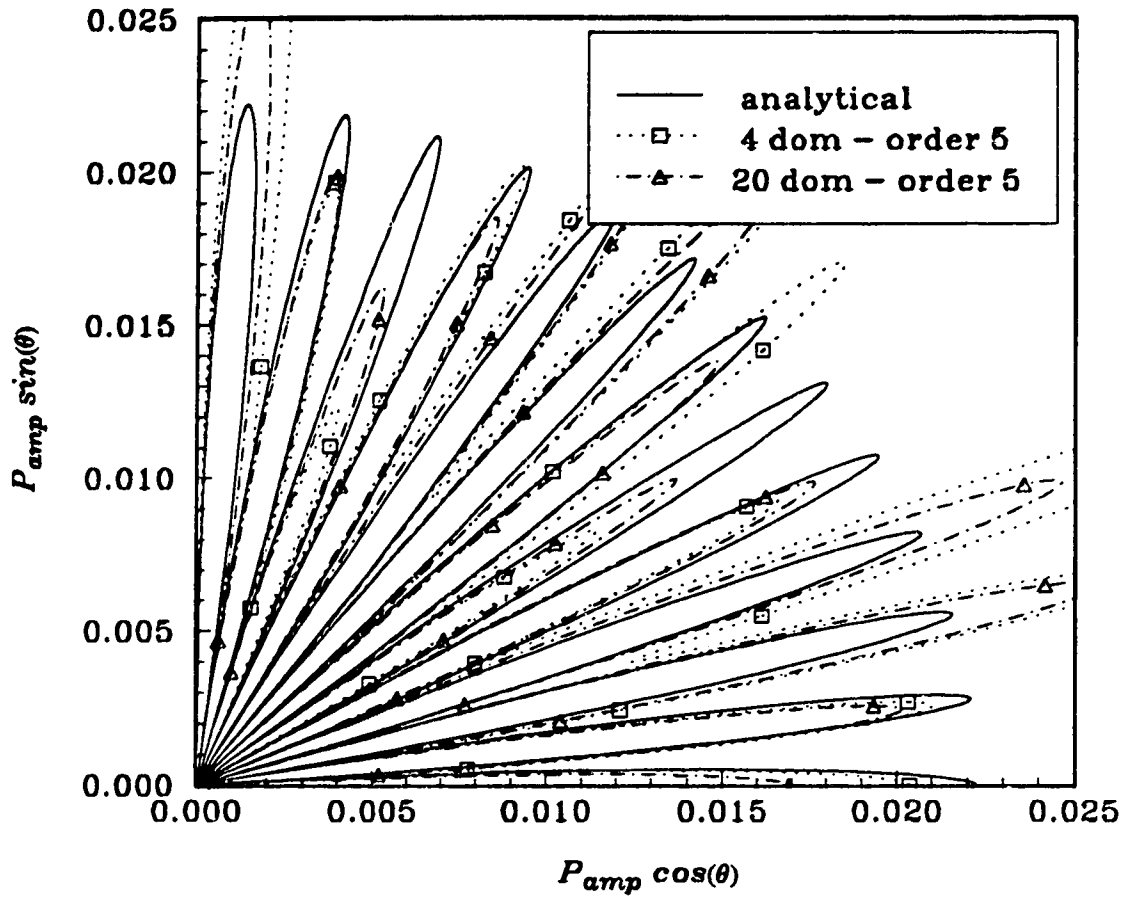


Figure 4.29 Cylindrical multi-pole of order 25.

Polar plot ($0 < \theta < 90$) of the amplitude of the radiated acoustic pressure at $r = 5R$ for $kR = 20$.

Effect of degree of subdomaining.

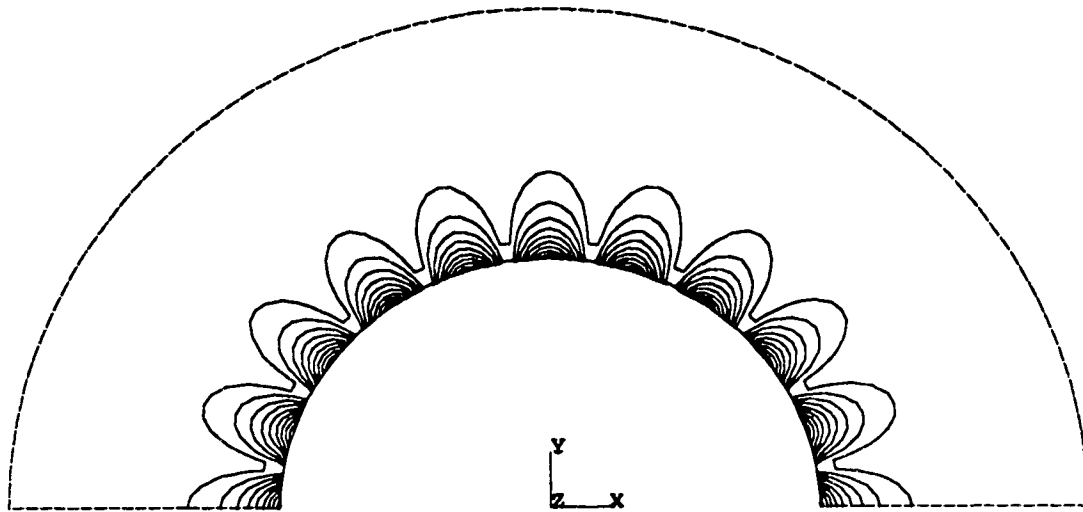


Figure 4.30 Cylindrical multi-pole of order 10.
Contour plot of the amplitude of the acoustic pressure for $kR = 5$.
Example of a poor radiator.

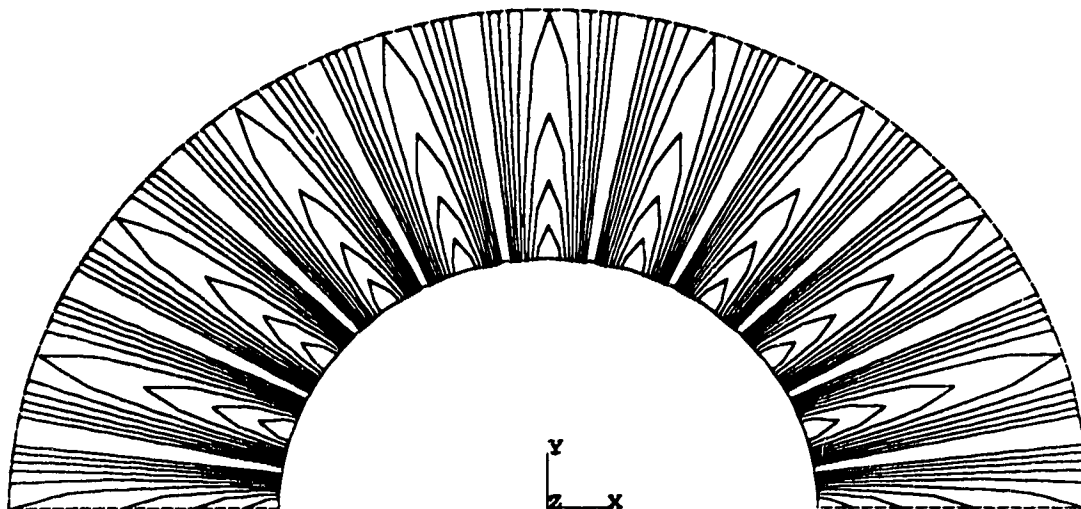


Figure 4.31 Cylindrical multi-pole of order 10.
Contour plot of the amplitude of the acoustic pressure for $kR = 15$.
Example of a good radiator.

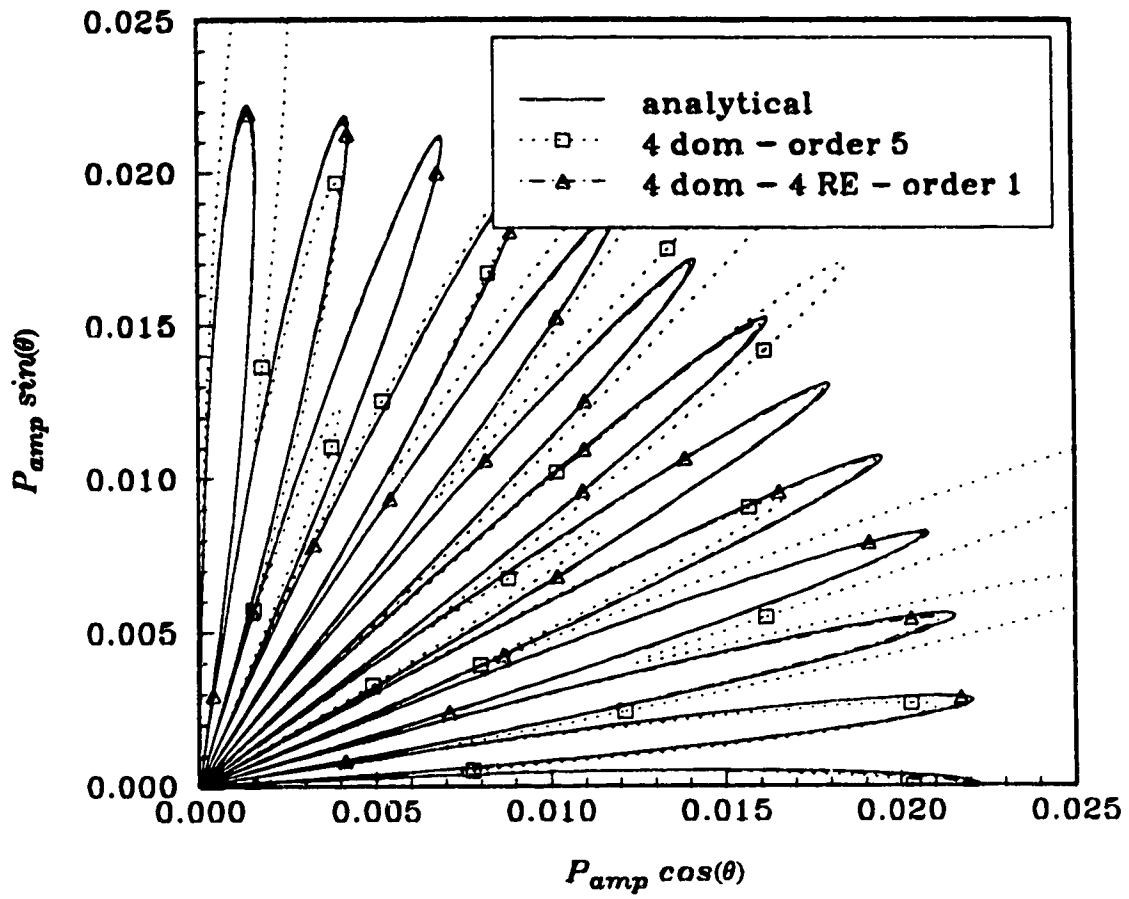


Figure 4.32 Cylindrical multi-pole of order 25.

Polar plot ($0 < \theta < 90$) of the amplitude of the radiated acoustic pressure at $r = 5R$ for $kR = 20$.

Effect of the use of conventional interface boundary elements in the acoustic near field.

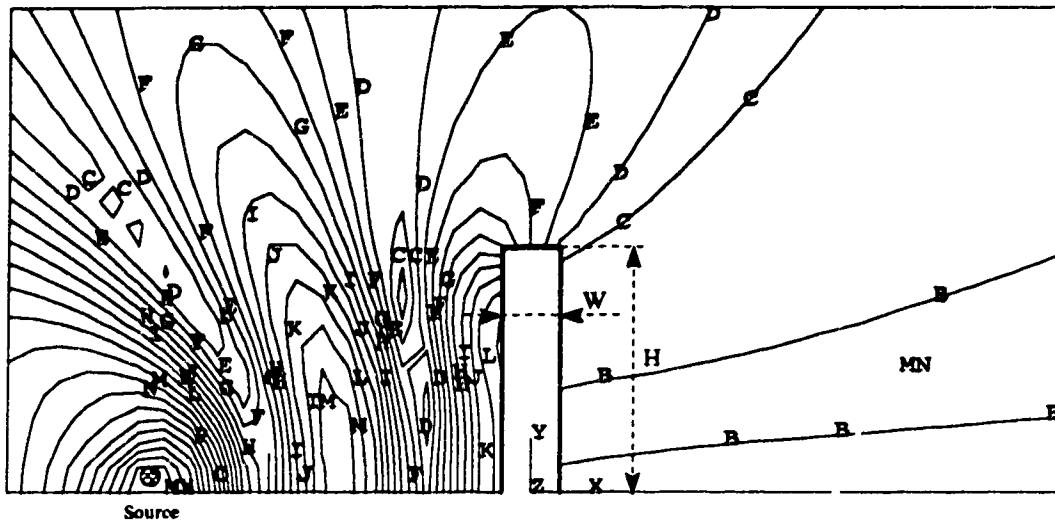


Figure 4.33 Scattering of a two-dimensional cylindrical source from a single rigid barrier (source @ $x = -1.5H$; $y = 0.15$).
Contour plot of the amplitude of the total acoustic pressure for $kH = 5$.
(Contour levels ranging from 0 to 2.0 with a step of 0.1)

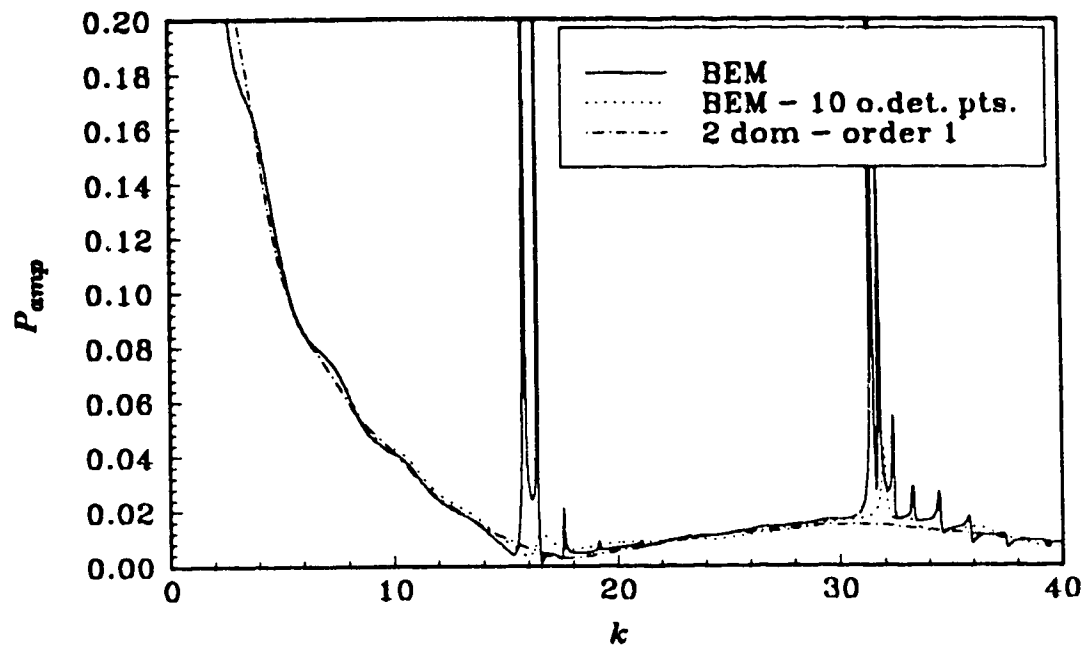


Figure 4.34 Scattering of a two-dimensional cylindrical source from a single rigid barrier (source @ $x = -1.5H$; $y = 0.15$).
Frequency response function of the amplitude of the total acoustic pressure at $x = 5H$; $y = 0.1H$.

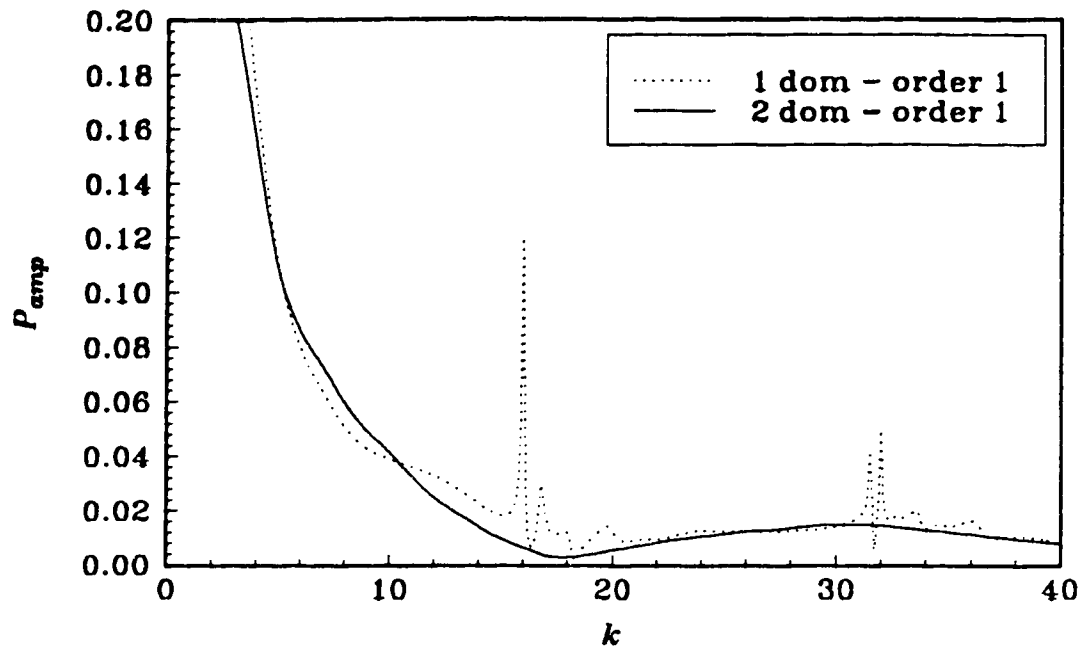


Figure 4.35 Scattering of a two-dimensional cylindrical source from a single rigid barrier (source @ $x = -1.5H$; $y = 0.15$).
Frequency response function of the amplitude of the total acoustic pressure at $x = 5H$; $y = 0.1H$.
Effect of local resonances.

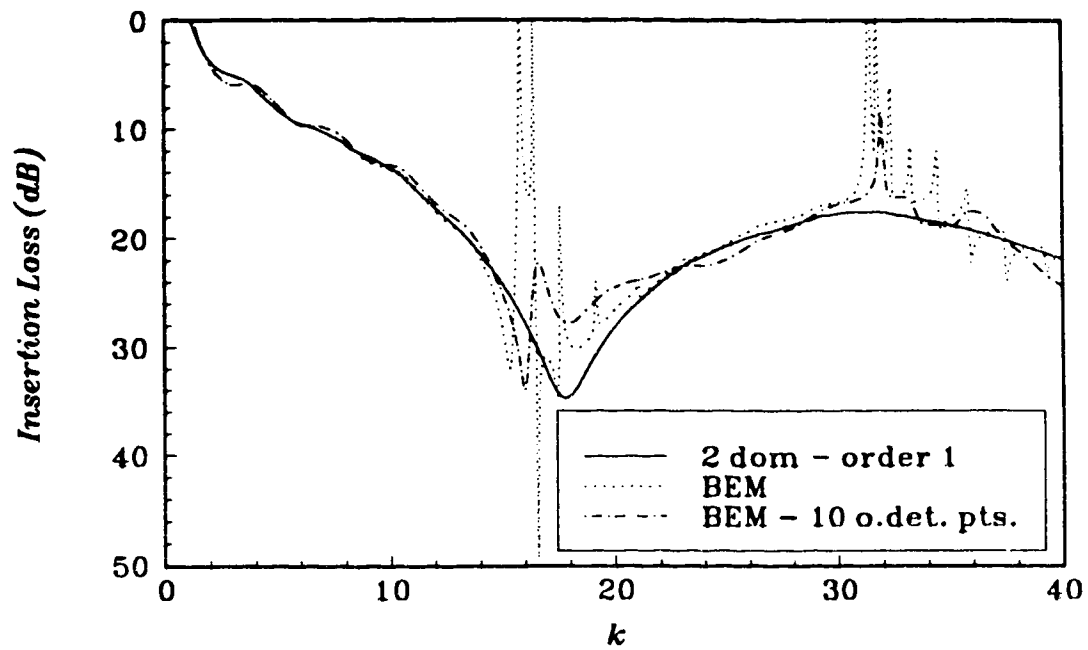


Figure 4.36 Scattering of a two-dimensional cylindrical source from a single rigid barrier (source @ $x = -1.5H$; $y = 0.15$).
Frequency response function of the insertion loss at $x = 5H$; $y = 0.1H$.

REFERENCES

- 4.1. F. V. ATKINSON, "On Sommerfeld's radiation condition," *The Philosophical Magazine* **40**, 645-651 (1949).
- 4.2. A. BAYLISS, M. GUNZBURGER and E. TURKEL, "Boundary conditions for the numerical solution of elliptic equations in exterior regions," ICASE Report No. 80/1, NASA Langley, (1980).
- 4.3. C. H. WILCOX, "A generalization of theorems of Rellich and Atkinson," *Proceedings of the American Mathematical Society*, 271-276 (1956).
- 4.4. O. C. ZIENKIEWICZ, D. W. KELLY and P. BETTESS, "The Sommerfeld (radiation) condition on infinite domains and its modelling in numerical procedures," *Computing Methods in Applied Sciences and Engineering, Third International Symposium, IRIA Laboria, Lect. in Math. V 704*, 169-192 (1977).
- 4.5. "Boundary element methods in acoustics", Eds. R. D. Ciskowski and C. A. Brebbia, Boston, Computational Mechanics Publications (1991).
- 4.6. A. F. SEYBERT, "Review of the boundary element method in acoustics," Noise Control Foundation, New York, NY, USA 2532, 25-32 (1991).
- 4.7. K. R. FYFE, "An Investigation of the acoustic properties of vibrating finite cylinders using the boundary element method," Ph.D dissertation, University of Waterloo (1986).
- 4.8. B. SOENARKO, "An advanced boundary element formulation for acoustic radiation and scattering in three dimensions", Ph.D. dissertation, University of Kentucky (1983).
- 4.9. S. AMINI and P. J. HARRIS, "A comparison between various boundary integral formulations of the exterior acoustic problem", *Computer methods in applied mechanics and engineering* **84**, 59-75 (1990).
- 4.10. H. A. SCHENCK, "Improved integral formulation for acoustic radiation problems", *Journal of the Acoustical Society of America* **44**, 41-58 (1967).
- 4.11. A. J. BURTON and G. F. MILLER, "The application of integral equation methods to the numerical solution of some exterior boundary value problems", *Proceedings*

- of the Royal Society of London **A323**, 201-210 (1971).
- 4.12. L. G. COPLEY, "Fundamental results concerning integral representations in acoustic radiation", *Journal of the Acoustical Society of America* **44**, 28-32 (1968).
 - 4.13. E. DOKUMACI, "A study of the failure of numerical solutions in boundary element analysis of acoustic radiation problems", *Journal of Sound and Vibration* **139**, 83-97 (1990).
 - 4.14. O. C. ZIENKIEWICZ, P. BETTESS, T. C. CHIAM and C. EMSON, "Numerical methods for unbounded field problems and a new infinite element formulation", *Computational Methods for Infinite Domain Media-Structure Interaction* **AMD 46**, 115-147 (1981).
 - 4.15. R. BOSSUT and J.-N. DECARPIGNY, "Finite element modelling of radiating structures using dipolar damping elements," *Journal of the Acoustical Society of America* **86**, 1234-1244 (1989).
 - 4.16. P. M. PINSKY, L. L. THOMPSON and N. N. ABOUD, "Local high-order radiation boundary conditions for the two-dimensional time-dependent structural acoustics problem," *Journal of the Acoustical Society of America* **91**, 1320-1335 (1992).
 - 4.17. J. ASSAAD, J.-N. DECARPIGNY, C. BRUNEEL, R. BOSSUT and B. HAMONIC, "Application of the finite element method to two-dimensional radiation problems", *Journal of the Acoustical Society of America* **94**, 562-573 (1993).
 - 4.18. P. BETTESS and O. C. ZIENKIEWICZ, "Diffraction and refraction of surface waves using finite and infinite elements," *International Journal for Numerical Methods in Engineering* **11**, 1271-1290 (1977).
 - 4.19. R. J. ASTLEY and W. EVERSMAN, "Finite element formulations for acoustical radiation," *Journal of Sound and Vibration* **98**(1), 47-64 (1983).
 - 4.20. R. J. ASTLEY, "Wave envelope and infinite elements for acoustical radiation," *International Journal for Numerical Methods in Fluids* **3**, 507-526 (1983).
 - 4.21. R. J. ASTLEY and W. EVERSMAN, "Wave envelope and infinite element schemes for fan noise radiation from turbofan inlets," *American Institute of*

- Aeronautics and Astronautics Journal **22**, 1719-1726 (1984).
- 4.22. R. J. ASTLEY, J. P. COYETTE, G. J. MACAULAY, "Mapped wave envelope elements for acoustical radiation and scattering," Journal of Sound and Vibration **170**, 97-118 (1994).
 - 4.23. L. CREMERS, K. R. FYFE and J. P. COYETTE, "A variable order infinite acoustic wave envelope element," Journal of Sound and Vibration **171**(4), 483-508 (1994).
 - 4.24. L. CREMERS and K. R. FYFE, "On the use of variable order infinite acoustic wave envelope elements for acoustic radiation and scattering," Journal of the Acoustical Society of America (submitted for publication).
 - 4.25. X. ZENG, L. F. KALLIVOKAS AND J. BIELAK, "Stable localized symmetric integral equation method for acoustic scattering problems," Journal of the Acoustical Society of America **91**, 2510-2518 (1992).
 - 4.26. SYSNOISE Theoretical Manual, Version 5.0, Numerical Integration Technologies, Leuven, Belgium, 1993.
 - 4.27. J. C. F. TELLES, "A self-adaptive co-ordinate transformation for efficient numerical evaluation of general boundary element integrals," International Journal of Numerical Methods in Engineering **24**, 959-973 (1987).
 - 4.28. C. Y. R. CHENG, A. F. SEYBERT and T. W. WU, "A multidomain boundary element solution for silencer and muffler performance prediction," Journal of Sound and Vibration **151**(1), 119-129 (1991).
 - 4.29. M. REZAYAT, "A general boundary-integral formulation for zoned three-dimensional media," International Journal for Numerical Methods in Engineering **36**, 1563-1572 (1993).
 - 4.30. E. SKUDRZYK, *The Foundations of Acoustics* (Springer-Verlag, Vienna, New-York, 1971).
 - 4.31. F. FAHY, *Sound and Structural Vibration: Radiation, Transmission and Response*, (Academic Press, London, 1985)
 - 4.32. S. N. CHANDLER-WILDE and D. C. HOTHERSALL, "On the Green function for two-dimensional acoustic propagation above a homogeneous impedance plane,"

**Research Report, Department of Civil Engineering, University of Bradford (UK)
(1991).**

- 4.33. "Sound, Structures, and their Interaction", M. C. Junger and D. Feit, The MIT Press, Cambridge, Massachusetts, (1972).**
- 4.34. J. VAN BLADEL, Electromagnetic Fields, McGraw-Hill, (1964).**
- 4.35. "Handbook of mathematical functions", Eds. M. Abramowitz and I. A. Stegun, Dover Publications, Inc., New York (1972).**

CHAPTER 5

CONCLUSIONS AND FUTURE RESEARCH

5.1. SUMMARY

The numerical modelling of the acoustic pressure field generated by an arbitrary vibrating body in an infinite domain is a challenging task. The major difficulty lies in the adequate application of the Sommerfeld radiation condition. In theory, this radiation condition has to be satisfied at an imaginary surface at infinity, prescribing local outgoing travelling plane waves.

The boundary element formulations satisfy this condition exactly through the use of the free-space Green's function, and are therefore suitable for modelling this type of wave propagation problem. From a practical point of view however, in general, two major problems are encountered in the use of these boundary element methods. One problem is the fact that the boundary element method is in essence a *global* acoustic numerical modelling tool. This means that all acoustic degrees of freedom are directly coupled to all other acoustic degrees of freedom of the model, leading to fully-populated complex system matrices as compared to the banded symmetric matrices resulting from finite

element analysis. This necessitates very large computation times and memory requirements, rendering large-scale problems unsolvable. The other problem is the well-known non-uniqueness problem at certain critical frequencies. Modified boundary element methods, that have been developed to reduce these singularity problems, have proven to be impractical, i.e. adequate choice of interior over-determination points, and can be costly in terms of computation time.

The finite element based methods for acoustic radiation and scattering administer a *local* application of the Sommerfeld radiation condition. Through an adequate choice of element connectivity, computationally efficient banded system matrices can be obtained for this class of methods. The recent developments in this area involve the higher order boundary dampers and a special class of infinite elements, the so-called infinite wave envelope elements. These infinite elements are matched onto a conventional finite element mesh, modelling the acoustic near-field. The near-field mesh has to extend sufficiently into the acoustic domain to avoid spurious reflections of the outgoing waves at the finite-infinite element interface.

The objective of this thesis was to enhance the formulation of the infinite wave envelope element for two-dimensional and axisymmetric acoustic modelling. A variable order infinite wave envelope element was developed, allowing for the specification of an arbitrary number of acoustic degrees of freedom in the radial direction of the element, going out to infinity. The element is capable of modelling the outgoing waves more accurately, and can therefore be moved towards the radiating body, minimizing the need for conventional finite elements in the acoustic near-field.

The different aspects of the formulation of the variable order infinite wave envelope element have been discussed in Chapter 2. The flexible choice of acoustic degrees of freedom has been implemented by using Lagrangian type element shape functions for modelling the amplitude decay. An inverse geometry mapping was developed for post-processing results at arbitrary field points within the acoustic domain. Preliminary tests have shown the improving ability of modelling general radiation and scattering problems by going to higher order elements. The sensitivity to acoustic source location of the variable order infinite wave envelope elements has been investigated. It

was shown that the higher order elements can reduce the geometry mesh sensitivity of the method.

Chapter 3 was devoted to an investigation into the performance of the variable order infinite wave envelope element modelling. The formulation of the variable order infinite wave envelope element was enhanced by providing quadratic and cubic trial functions in the angular direction, for better modelling of the curved wave-fronts of the outgoing acoustic waves. Special modelling techniques, such as nodal acoustic source application and boundary element integral based post-processing, were introduced and tested. A very interesting application involved the modelling of acoustic scattering above a homogeneous impedance plane. In the past this has only been possible by means of very specialized boundary element methods with complicated Green's kernels, while the impedance condition along the infinite edges of the variable order infinite wave envelope elements can be readily incorporated into the finite element based modelling scheme.

A wide range of tests of radiation and scattering problems from an infinite rigid cylinder and an axisymmetric sphere were setup to explore the modelling limitations of the variable order infinite wave envelope element. In all models, the geometry mesh consisted of a single layer of infinite elements, directly matched onto the radiating body, to thoroughly test the performance of the element itself. A systematic investigation of the modelling of the different higher order multi-poles revealed that, although performance increased by going to higher order infinite wave envelope elements, in essence only *good radiators* can be modelled within the variable order infinite wave envelope element layer. The transition from *poor* to *good* radiator occurs at the critical wave numbers of the different order multi-poles. These same tests showed the importance of quadratic trial functions in the angular direction of the element, for modelling the lobe-shaped radiation patterns of the multi-poles.

The study of the variable order infinite wave envelope element indicated the limitations of a local application of the Sommerfeld radiation condition. The local application within the infinite element is only satisfactory when the acoustic energy indeed predominantly flows along the edges of the element. This only occurs when the vibrating body is radiating efficiently. The computational efficiency of the banded system

matrices has a trade-off of a limited generality in modelling the radiation condition.

In an effort to merge the accuracy of boundary element methods and the computational efficiency of the variable order infinite wave envelope element models, a multi-domain boundary element method was then developed. The method is based on the variational multi-domain boundary element method by Zeng et al.. A special variable order infinite interface boundary element was incorporated in a direct collocation multi-domain boundary element scheme, as outlined in Chapter 4. The trial functions of the infinite interface element are based on the shape functions of the variable order infinite wave envelope element, again in an effort to minimize the need for conventional interface boundary elements in the acoustic near-field.

The main difficulty encountered in this multi-domain boundary element implementation is the numerical integration of the infinite element contributions to the system matrices. The integral was truncated at a finite distance and divided into a number of subelements. Integration singularities are dealt with in each subelement separately by the approach of Telles. In future research, different integration schemes should be investigated for more efficient evaluation of these infinite integrals.

The great advantage of this multi-domain boundary element method is the fact that no singularities occur due to the well-known non-uniqueness problem of conventional boundary element methods. However it was shown that minor singularity problems can occur when local resonances in the complementary problem are possible. But, in general, these problems can be avoided by a proper choice of subdomain geometry.

A similar set of tests were performed to test the performance of the multi-domain boundary element method. The interfaces between the different subdomains were modelled by a single variable order infinite interface boundary element. Models of increasing degree of subdomaining were investigated. It was found that going to a high degree of subdomaining, and thus a more local application of the Sommerfeld radiation condition, revealed similar limitations as compared to the variable order infinite wave envelope element modelling. In order to properly model the acoustic field variables along the infinite interfaces, a higher order element is needed as the degree of subdomaining increases. In the case of very poor radiators, a so-called acoustic window of conventional

interface boundary elements is needed for proper acoustic energy transfer between the different subdomains.

The multi-domain boundary element method has proven to be a very attractive method for modelling acoustic radiation and scattering in infinite domains. The formulation is very flexible due to the fact that the degree of subdomaining can be chosen depending on whether or not computational efficiency, i.e. computer data-storage, or accuracy in the application of the Sommerfeld radiation condition, is important. The method shows a great advantage, even with a minimal degree of subdomaining, due to the fact that the non-uniqueness problem is completely eliminated.

The fact that infinite faces can be modelled with a single variable order infinite boundary element, opens up the possibility of modelling different types of half planes. It was shown how infinite rigid half planes can be modelled very easily. In future research the possibility of applying impedance conditions along these infinite edges can be considered. This would give the ability of modelling a whole new class of scattering and radiation problems. For example, scattering from barrier configurations with elevated impedance planes at different heights, important in the study of road noise barriers, would become possible. These barrier configurations cannot be modelled with conventional boundary element methods.

Finally, it should be noted that, in general, the finite element based variable order infinite wave envelope element method, as well as the direct collocation multi-domain boundary element method can be easily incorporated in existing elasto-acoustic coupling schemes for modelling the full interaction between the radiating structure and the acoustic pressure field.

5.2. CONCLUSIONS

The major conclusions of this thesis are as follows.

A variable order infinite wave envelope element for modelling acoustic radiation and scattering problems has been developed.

- the infinite wave element formulation was enhanced by providing the flexibility of specifying an arbitrary number of acoustic degrees of freedom in the radial direction, for adequate modelling of the outgoing sound waves. The element minimizes the need for conventional finite elements in the acoustic near-field.
- the finite element based formulation yields complex *banded* system matrices, allowing for efficient computer data storage and computation time requirements.
- the performance of the variable order infinite wave envelope is shown to be sensitive to the acoustic source location of the element. This element geometry sensitivity can be reduced by using higher order elements.
- two alternative post-processing methods were implemented, i.e. interpolation among the element acoustic degrees of freedom and the BEM-based method. Both methods were shown to be of comparable accuracy. As well, two methods of applying acoustic sources were introduced. A part from the familiar superposition of incident and scattered fields, a direct acoustic source application at an acoustic degree of freedom was developed.
- an impedance boundary condition can be applied along the infinite edges of the variable order infinite wave envelope element for modelling homogeneous infinite impedance planes. In the past, this type of modelling has only been realized in some specific cases by means of very specialized boundary element methods.
- a systematic study of the modelling of cylindrical and spherical higher order multi-pole radiation revealed limitations of the variable order infinite wave envelope element modelling, due to the *local* imposition of the Sommerfeld radiation.
 - quadratic shape functions in the angular direction of the element prove superior to the linear shape functions for modelling the lobe-shaped radiation patterns of the higher order multi-poles.

- in essence only *good* radiators can be modelled, i.e. where the acoustic energy predominantly flows towards infinity.
- the performance of the variable order infinite element improves by going to higher order elements.
- the order of the variable order infinite wave envelope element is limited to order nine. Higher order elements yield ill-conditioned system matrices.

A variable order infinite boundary element was developed to be used in a direct collocation multi-domain boundary element method, in an effort to merge the accuracy of boundary element methods and the computational efficiency of the variable order infinite wave envelope element models.

■ the variable order infinite boundary element was developed based on the variable order infinite wave envelope element, again to minimize the need for conventional boundary elements in the acoustic near-field along the infinite interfaces between the subdomains.

■ the main difficulty in the implementation of this method lies in the numerical integration of the contributions by the infinite elements to the system matrices. The method of simple truncation and the division into subelements proved to be adequate but costly in terms of computation time.

■ a similar study of the cylindrical and spherical higher order multi-poles was performed to test the performance of the multi-domain boundary element method.

- models of increasing degree of subdomaining reveal similar limitations as those of the variable order infinite wave envelope element modelling.
- for modelling *poor* radiators the use of a so-called acoustic window of conventional interface boundary elements proved to be necessary.

■ the great advantage of the multi-domain boundary element method is the fact that there are no singularities due to the non-uniqueness problem of conventional boundary element

methods.

- the multi-domain boundary element method allows for a flexible choice of degree of subdomaining, depending on whether computational efficiency or accuracy in the application of the Sommerfeld radiation condition is important.

5.3. RECOMMENDATIONS FOR FUTURE RESEARCH

Topics for future research, stemming from the completed work in this thesis, are mainly focussed upon the improvement of the multi-domain boundary element method, as listed below.

- alternative numerical integration methods can be investigated to evaluate the contributions by the infinite boundary elements to the system matrices more efficiently.
- a method for post-processing acoustic field variables at an arbitrary field point using the boundary values within a specific subdomain, rather than based on the surface values of the whole radiating body, can be implemented.
- homogeneous impedance conditions can be applied along the infinite boundary elements for efficient modelling of impedance half planes. Scattering problems from a special class of barrier configurations, e.g. with infinite impedance planes at different heights, can then be modelled.
- a multi-domain boundary element method with different material properties in the subdomains can be developed.
- both the variable order infinite wave envelope element and the multi-domain boundary element method can be incorporated in an elasto-acoustic coupling scheme.

APPENDIX 2-A

Finite Element Weighted Residual Formulation for Exterior Radiation

As in all finite element analysis, the residual formulation starts with the choice of a trial solution of the form

$$p'(x) = [N_i(x)] \{p_i\} \quad (2.A.1)$$

where the acoustic pressure $p'(x)$ is approximated by interpolating among the n nodal values p_i by means of interpolation (or shape) functions $N_i(x)$. This approximated pressure field $p'(x)$ no longer satisfies the Helmholtz equation exactly, but leads to a residual $R(x)$, defined as

$$\nabla^2 p'(x) + k^2 p'(x) = R(x) \quad x \in V \quad (2.A.2)$$

The objective is now to optimize the trial solution. Therefore the residual is orthogonalised over the entire domain V by means of a series of weighting functions $W_i(x)$. We get an integrated weighted residual, given as

$$\int_V W_i R \, dV = 0 \quad (2.A.3)$$

and, using Equation (2.A.2)

$$\int_V W_i \nabla^2 p' \, dV + k^2 \int_V W_i p' \, dV = 0 \quad (2.A.4)$$

Then Green's first theorem is applied to this integral equation, yielding,

$$\int_V \nabla W_i \cdot \nabla p' dV - k^2 \int_V W_i p' dV - \int_S W_i \frac{\partial p'}{\partial n} dS = 0 \quad (2.A.5)$$

In general, the surface integral in Equation (2.A.5) consists of two parts, one on the radiating body and one on a surface at infinity. This is depicted as

$$\int_S W_i \frac{\partial p'}{\partial n} dS = \int_{S_0} W_i \frac{\partial p'}{\partial n} dS + \int_{S_\infty} W_i \frac{\partial p'}{\partial n} dS \quad (2.A.6)$$

By applying normal velocity boundary conditions on the radiating body S_0 and the Sommerfeld radiation condition on the boundary at infinity S_∞ , we can write

$$\int_S W_i \frac{\partial p'}{\partial n} dS = -i\rho kc \int_{S_0} W_i \bar{v} dS - ik \int_{S_\infty} W_i p' dS \quad (2.A.7)$$

Since $p' \rightarrow 0$ as $S_\infty \rightarrow \infty$ will be prescribed by a suitable choice of shape functions, the damping term in Equation (2.A.7) at S_∞ will vanish. As a result, a set of simultaneous equations can be formulated in the form

$$[[K] - \omega^2 [M]] \{p\} = \{F\} \quad (2.A.8)$$

where related coefficients result from substitution of Equation (2.A.1) into Equation (2.A.5)

$$K_{ij} = \int_V \nabla W_i \cdot \nabla N_j dV \quad (2.A.9)$$

$$M_{ij} = \int_V \frac{1}{c^2} W_i N_j dV \quad (2.A.10)$$

$$F_i = -i\rho\omega \int_{S_0} W_i \bar{v} dS \quad (2.A.11)$$

In Equation (2.A.8), $[K]$ and $[M]$ are the acoustic stiffness and mass matrix. $\{F\}$ is the acoustic forcing vector corresponding to the prescribed velocity input on the sound radiating body, while $\{p\}$ are the unknown nodal pressure values to be solved for.

APPENDIX 2-B

Derivative of the Radial Shape Function

All local derivatives of the shape functions in Equation (2.42) to (2.45) are easy to evaluate. The derivative of the radial shape functions however, is somewhat more involved and can be written as follows

$$\begin{aligned}
 \frac{dT_i^n}{dt} &= \frac{dT_i^n}{d\tau} \frac{d\tau}{dt} \\
 &= (n-1) \frac{dT_i^n}{d\tau} \\
 &= (n-1) C_i^n \frac{d}{d\tau} \left[\left(\prod_{\substack{j=0 \\ j \neq i-1}}^{n-1} (\tau-j) \right) (\tau - 2(n-1)) \right] \\
 &= (n-1) C_i^n \left\{ \sum_{\substack{k=0 \\ k \neq i-1}}^{n-1} \left[\left(\prod_{\substack{j=0 \\ j \neq i-1}}^{k-1} (\tau-j) \right) \left(\prod_{\substack{j=k \\ j \neq i-1}}^{n-1} (\tau-j) \right) (\tau - 2(n-1)) \right] + \prod_{\substack{j=0 \\ j \neq i-1}}^{n-1} (\tau-j) \right\}
 \end{aligned} \tag{2.B.1}$$

Note that the $R_i^n(\tau)$ factor has to be considered in case of two-dimensional shape functions.

APPENDIX 2-C

Inverse Geometry Mapping

To determine whether or not a field point is situated within a certain element, the inverse geometry mapping is performed on the global coordinates of the field point. If the field point lies in the element, the local coordinates will fall within the unit limits of the parent element (*i.e.* $-1 \leq s \leq 1$ and $-1 \leq t \leq 1$).

Unfortunately the inverse of the element geometry mappings, used in the acoustic finite element modelling, are not easily obtainable in general, yielding a set of two non-linear equations in the local coordinates s and t . For the infinite geometry mapping used in the formulation of the n^{th} order infinite wave envelope element given in Equation (2.20), this set of non-linear equations can be written as

$$\begin{aligned} f(s,t) &= X_0 + X_1 s + X_2 t + X_3 s t = 0 \\ g(s,t) &= Y_0 + Y_1 s + Y_2 t + Y_3 s t = 0 \end{aligned} \quad (2.C.1)$$

where

$$\begin{aligned} X_0 &= -2x + x_3 + x_4 \\ X_1 &= -x_3 + x_4 \\ X_2 &= 2x - 2x_1 - 2x_2 + x_3 + x_4 \\ X_3 &= -2x_1 + 2x_2 - x_3 + x_4 \end{aligned} \quad (2.C.2)$$

and similarly

$$\begin{aligned} Y_0 &= -2y + y_3 + y_4 \\ Y_1 &= -y_3 + y_4 \\ Y_2 &= 2y - 2y_1 - 2y_2 + y_3 + y_4 \\ Y_3 &= -2y_1 + 2y_2 - y_3 + y_4 \end{aligned} \quad (2.C.3)$$

In the above equations, x and y are the global coordinates for the field point under investigation, while x_i and y_i are the global coordinates of the geometry nodes of the element at hand.

The set of non-linear equations, given in (2.C.1), can iteratively be solved for by the Newton-Raphson method, as follows

$$\begin{bmatrix} \frac{\partial f}{\partial s} & \frac{\partial f}{\partial t} \\ \frac{\partial g}{\partial s} & \frac{\partial g}{\partial t} \end{bmatrix} \begin{Bmatrix} \Delta s \\ \Delta t \end{Bmatrix} = - \begin{Bmatrix} f \\ g \end{Bmatrix} \quad (2.C.4)$$

An obvious initial guess is the local origin, i.e. $s = 0$ and $t = 0$. The functions f and g are very well behaved within the unit domain of the parent element. When the field point is within the element, the method converges to the local coordinates of the field point within a few iterations. Whereas when the node lies outside the element, the solution immediately jumps outside the unit area of the parent element. Therefore, the current values of s and t are checked with the unit element limits after each iteration. As soon as $|s| > 1$ or $|t| > 1$, the routine is aborted with the conclusion that the field point does not lie within the element. When convergence is obtained, a flag is set showing that the field point is situated within the limits of the element and the local coordinates are past through for use in the interpolation of the results among the acoustic degrees of freedom of the element.

APPENDIX 2-D

Effect of Source Shift

A one-dimensional example is used to show the effect of a source shift on numerical modelling of an amplitude decay, using variable order infinite wave envelope elements. For convenience, the spatial wavelike variation is omitted. The differential equation to be solved is

$$\frac{d^2 p(x)}{dx^2} - \frac{2p(x)}{x^2} = 0 \quad (2.D.1)$$

with the boundary condition,

$$\frac{dp}{dx} = \frac{-1}{x^2} \quad (2.D.2)$$

The exact solution to this problem is a simple reciprocal decay. It can, therefore, be modelled exactly using a variable order infinite wave envelope element with its source at the origin $x = 0$.

In order to assess the power of higher order elements, the source location is now shifted to $x = 1$, yielding the following infinite element configuration

$$x_0 = 1 \quad x_I = 2 \quad x_{II} = 3$$

The infinite geometry mapping is now given by

$$\iota = 1 - \frac{2a}{x} = 1 - \frac{2}{x} \quad (2.D.3)$$

From the results in Table (2.D.1), the effect of the source shift is substantial for the first order infinite element modelling. Going to higher order elements drastically

reduces the error introduced by the improper source location. This indicates that a higher order element may possibly account for the poor location of the acoustic source.

x	p(x)							
	Exact	Infinite element order						
		1 st	2 nd	3 rd	4 th	5 th	6 th	7 th
2	0.50000	0.44788	0.49841	0.49998	0.50000	0.50000	0.50000	0.50000
3	0.33333	0.22394	0.32392	0.33403	0.33350	0.33332	0.33333	0.33333
4	0.25000	0.14929	0.23255	0.24859	0.25013	0.25005	0.25000	0.25000
5	0.20000	0.11197	0.18064	0.19717	0.19983	0.20003	0.20001	0.20000
10	0.10000	0.04976	0.08490	0.09624	0.09923	0.09987	0.09998	0.10000
100	0.01000	0.00452	0.00802	0.00937	0.00982	0.00995	0.00999	0.01000

Table 2.D.1

APPENDIX 3-A

Modelling of a Coherent Monofrequency Line Source above a Homogeneous Impedance Plane.

The coherent monofrequency line source is located at $\mathbf{r}_0 = (x_0, y_0)$. The receiver at $\mathbf{r} = (x, y)$ is situated in the half-space S , $y > 0$, above the homogeneous impedance plane δS , $y = 0$, as shown in Figure 3.29.

Consider $G_\beta(\mathbf{r}, \mathbf{r}_0)$ as the acoustic pressure at a receiver point \mathbf{r} , due to a unit line source at \mathbf{r}_0 , above an impedance plane with normalised surface admittance β . As discussed in Reference [3.18], $G_\beta(\mathbf{r}, \mathbf{r}_0)$, further referred to as the G_β -solution, can then be written as a sum of G_0 and a correction term P_β

$$G_\beta(\mathbf{r}, \mathbf{r}_0) = G_0(\mathbf{r}, \mathbf{r}_0) + P_\beta(\mathbf{r}, \mathbf{r}_0) \quad (3.A.1)$$

where G_0 is the acoustic pressure above a rigid plane, $\beta = 0$. G_0 can easily be calculated by superimposing the contribution of the line source at \mathbf{r}_0 and its image source at \mathbf{r}'_0 , given as

$$G_0(\mathbf{r}, \mathbf{r}_0) = -\frac{i}{4} H_0^{(2)}(kR) - \frac{i}{4} H_0^{(2)}(kR') \quad (3.A.2)$$

where $R = |\mathbf{r} - \mathbf{r}_0|$ and $R' = |\mathbf{r} - \mathbf{r}'_0|$ are the distance from the receiver to the source and image source respectively.

The correction term P_β can be written as a Laplace-type integral representation, as outlined in Reference [3.18]. For $\beta \approx 1$ this results in

$$P_{\beta}(z, r_0) = \frac{\beta e^{i\rho}}{\pi\sqrt{\rho}} \int_0^{\infty} s^{-\frac{1}{2}} e^{-s} f\left(\frac{s}{\rho}\right) ds, \quad \text{Im}\beta \geq 0 \quad (3.A.3)$$

while for $\beta \neq 1$

$$P_{\beta}(z, r_0) = \frac{\beta e^{i\rho}}{\pi\sqrt{\rho}} \int_0^{\infty} s^{-\frac{1}{2}} e^{-s} g\left(\frac{s}{\rho}\right) ds + \frac{\beta e^{i\rho(1-a_+)}}{2\sqrt{1-\beta^2}} \operatorname{erfc}\left(e^{\frac{-i\pi}{4}} \sqrt{\rho a_+}\right) \quad (3.A.4)$$

with $\rho = kR'$ and $\operatorname{erfc}(x)$, the complementary error-function. The functions $f(t)$ and $g(t)$ are defined as

$$\begin{aligned} f(t) &= -\frac{\beta + \gamma(1+it)}{\sqrt{t-2i}(t-ia_+)(t-ia_-)}, \quad \operatorname{Re}\sqrt{t-2i} > 0 \\ g(t) &= f(t) - \frac{e^{\frac{-i\pi}{4}} \sqrt{a_+}}{2\sqrt{1-\beta^2}(t-ia_+)}, \quad \operatorname{Re}\sqrt{1-\beta^2} \geq 0 \end{aligned} \quad (3.A.5)$$

where

$$a_{\pm} = 1 + \beta\gamma \mp \sqrt{1-\beta^2} \sqrt{1-\gamma^2}, \quad \operatorname{Re}\sqrt{1-\beta^2} \geq 0 \quad (3.A.6)$$

with $\gamma = \cos\theta_0$ and θ_0 the angle of incidence (see Figure 3.29).

Equations (3.A.3) and (3.A.4) are well suited for numerical approximation by Gauss-Laguerre quadrature, resulting in the following expressions [3.18]

$$P_{\beta} = P^1_{n,m} = \frac{\beta e^{i\rho}}{\pi \sqrt{\rho}} \sum_{j=1}^m w_{j,n} f\left(\frac{x_{j,n}}{\rho}\right) \quad (3.A.7)$$

$$P_{\beta} = P^2_{n,m} = \frac{\beta e^{i\rho}}{\pi \sqrt{\rho}} \sum_{j=1}^m w_{j,n} g\left(\frac{x_{j,n}}{\rho}\right) + \frac{\beta e^{i\rho(1-a.)}}{2\sqrt{1-\beta^2}} \operatorname{erfc}\left(e^{-\frac{i\pi}{4}} \sqrt{\rho a.}\right)$$

respectively. As discussed in Reference [3.18], optimal results, with respect to computational efficiency and accuracy, are obtained using a $(n = 40, m = 22)$ -rule, neglecting the weights for $j > 22$.

APPENDIX 4-A

The Helmholtz Integral Equation.

It is desired to obtain the pressure field $p(\mathbf{x})$ in terms of an integral equation that satisfies the Helmholtz equation in the domain V and the velocity boundary conditions at the boundary. The equivalent integral equation for the Helmholtz equation can be written as

$$\int_V \phi(\mathbf{x}) [\nabla^2 p(\mathbf{x}) + k^2 p(\mathbf{x})] dV = 0 \quad \mathbf{x} \in V \quad (4.A.1)$$

where ϕ is an arbitrary function, single valued and bounded within the domain V . Through the use of the free-space Green's function and Gauss' integral theorem, this integral equation can be simplified to a boundary integral equation, reducing the dimension of the problem by one. Next, the free-space Green's function is introduced and the boundary integral equations are derived.

Green's function

The free-space Green's function $G(P, Q) = G(|R_p - R_q|)$ is constructed by imposing two mathematical conditions, which also have apparent physical meaning. $|R_p - R_q|$ is the distance between the two field points P and Q .

Primarily, the Green's function is defined as the solution of the inhomogeneous Helmholtz equation, formulated as [4.33]

$$(\nabla^2 + k^2) G(|R_p - R_q|) = -\delta(|R_p - R_q|) \quad (4.A.2)$$

The right hand side denotes the three-dimensional Dirac delta function defined as

$$\begin{aligned} \int_V \phi(R_q) \delta(|R_q - R_p|) dV &= \phi(R_p) & R_p \in V \\ &= \frac{\phi(R_p)}{2} & R_p \in S \\ &= 0 & R_p \notin V \end{aligned} \quad (4.A.3)$$

The free-space Green's function thus constitutes the response in field point P , due to an acoustic point source of unit strength in field point Q . Note the symmetry in this definition, in that point P and Q are interchangeable.

Secondly, the free-space Green's function has to satisfy the Sommerfeld radiation condition. This can be written as

$$\lim_{|R_p - R_q| \rightarrow \infty} \left[|R_p - R_q|^\alpha \left(\frac{\delta G(|R_p - R_q|)}{\delta |R_p - R_q|} + ikG(|R_p - R_q|) \right) \right] = 0 \quad (4.A.4)$$

This radiation condition ensures that only outgoing travelling waves are present in the boundary integral equation for the acoustic pressure field.

Based on these two mathematical conditions, the free-space Green's function for the Helmholtz equation can be determined as [4.33]

$$\begin{aligned} G(|R_p - R_q|) &= \frac{-i}{4} H_0^{(2)}(k|R_p - R_q|) & 2D \\ G(|R_p - R_q|) &= \frac{e^{-ik|R_p - R_q|}}{4\pi|R_p - R_q|} & 3D \end{aligned} \quad (4.A.5)$$

for two- and three-dimensional acoustic radiation and scattering, respectively. In equation (4.A.5), $H_0^{(2)}$ is the zeroth order Hankel function of the second kind.

Boundary integral equation

Gauss' integral theorem, given as

$$\int_V \nabla \cdot \mathbf{E} dV = \int_S \mathbf{E} \cdot \underline{n}_a dS \quad (4.A.6)$$

relates the volume integral of a vector field \mathbf{E} to the surface integral of the outer normal component of \mathbf{E} . If one considers the vector field defined as

$$\mathbf{E} \equiv p(\mathbf{Q}) \nabla G(\mathbf{P}, \mathbf{Q}) - G(\mathbf{P}, \mathbf{Q}) \nabla p(\mathbf{Q}) \quad (4.A.7)$$

the identity of equation (4.A.6) results into the following expression,

$$\int_V (p \nabla^2 G - G \nabla^2 p) dV = - \int_{S = S_o + S_\infty} \left(p \frac{\delta G}{\delta n} - G \frac{\delta p}{\delta n} \right) dS \quad (4.A.8)$$

known as Green's second formula, where \underline{n} is the unit normal pointing towards the domain V . The surface integral is taken over the surface of the radiating body S_o and the surface at infinity S_∞ . The volume integral on the left hand side can be evaluated by solving for $\nabla^2 p$ and $\nabla^2 G$ from the Helmholtz equation and the inhomogeneous Helmholtz equation (4.A.2), respectively. After substitution into equation (4.A.8), the integrand of the volume integral reduces to $p(R_q) \delta(R_p - R_q)$. Therefore, referring to the definition of the Dirac delta function, stated in equation (4.A.3), the boundary integral equation becomes

$$C(\mathbf{P})p(\mathbf{P}) = \int_{S_o + S_\infty} \left(p(\mathbf{Q}) \frac{\delta G(\mathbf{P}, \mathbf{Q})}{\delta n} - G(\mathbf{P}, \mathbf{Q}) \frac{\delta p(\mathbf{Q})}{\delta n} \right) dS(\mathbf{Q}) \quad (4.A.9)$$

where

$$\begin{aligned}
C(P) &= 1 & P \in V \\
&= \frac{1}{2} & P \in S \\
&= 0 & P \notin V
\end{aligned} \tag{4.A.10}$$

Helmholtz integral equation

The boundary integral equation (4.A.9) shows a contribution by the surface at infinity to the acoustic pressure in an arbitrary field point P . It can be shown that this contribution vanishes [4.7], due to the Sommerfeld radiation condition. The Helmholtz integral equation then becomes

$$C(P)p(P) = \int_{S_0} \left(p(Q) \frac{\delta G(P,Q)}{\delta n} - G(P,Q) \frac{\delta p(Q)}{\delta n} \right) dS(Q) \tag{4.A.11}$$

The acoustic energy can therefore only flow from the vibrating body towards infinity. From a physical point of view, equation (4.A.11) states that the acoustic pressure at a field point P is equal to the response due to a distribution of forces, weighted according to the acoustic surface pressure, and a distribution of point sources, weighted by the surface normal velocity, respectively. If the surface acoustic pressure and normal particle velocity distribution on the radiating body is known, the acoustic pressure at an arbitrary field point can be evaluated by means of the Helmholtz integral equation.

Surface Helmholtz integral equation

The key identity, used in the direct collocation boundary element method, is the so-called Helmholtz surface integral equation. This equation relates the surface pressure in a particular point P on the surface, to the acoustic pressure and normal particle velocity

distribution of the rest of the radiating boundary. As shown before, this means that the factor $C(P)$ takes on the value $1/2$ in equation (4.A.11). This is only valid for smooth surfaces, for which the surface normal takes on a unique value. For special cases, e.g. corners, where the surface normal is not unique, a more general expression for the factor $C(P)$ is necessary, given as [4.8]

$$C(P) = 1 + \frac{1}{4\pi} \int_{S_o} \frac{\delta}{\delta n} \left(\frac{1}{|R_p - R_q|} \right) dS(Q) \quad (4.A.12)$$

The factor $C(P)$ can be interpreted as the exterior solid angle at point P on the surface S_o . In general, the surface Helmholtz integral can therefore be written as

$$\begin{aligned} & \left[1 + \frac{1}{4\pi} \int_{S_o} \frac{\delta}{\delta n} \left(\frac{1}{|R_p - R_q|} \right) dS(Q) \right] p(P) \\ & = \int_{S_o} \left(p(Q) \frac{\delta G(P, Q)}{\delta n} - G(P, Q) \frac{\delta p(Q)}{\delta n} \right) dS(Q) \end{aligned} \quad (4.A.13)$$

APPENDIX 4-B

Efficient Numerical Integration of the Singular Boundary Element Integrals

A singularity occurs when the field points P and Q coincide in evaluating the boundary integrals. As the distance $|R_p - R_q|$ approaches zero, the free-space Green's function becomes singular. Although the total integral remains finite, special integration methods have to be adopted to accurately integrate the rapidly changing function around the singularity.

The approach by Telles [4.27] is an efficient method to deal with this type of singularities for two-dimensional and axisymmetric analysis. The method consists of an additional co-ordinate transformation whereby the Gauss-Legendre quadrature points are shifted towards the location of the singularity.

Let the singular integral in local co-ordinates be as follows

$$I = \int_{-1}^1 f(s) ds \quad (4.B.1)$$

and let the location of the singularity be at \bar{s} . In case of linear conventional boundary elements, the singularity occurs at $\bar{s} = -1$ or $\bar{s} = 1$, i.e. the corner nodes of the element. The quadratic element has an additional singularity at the midside node $\bar{s} = 0$.

A new variable $\bar{\gamma}$ is defined as

$$\bar{\gamma} = \sqrt[3]{\bar{s}s^* + |s^*|} + \sqrt[3]{\bar{s}s^* - |s^*|} + \bar{s} \quad (4.B.2)$$

where $s^* = \bar{s}^2 - 1$. The integral can now be written as

$$I = \int_{-1}^1 f \left(\frac{(\gamma - \bar{\gamma})^3 + \bar{\gamma} (\bar{\gamma}^2 + 3)}{1 + 3\bar{\gamma}^2} \right) \frac{3(\gamma - \bar{\gamma})^2}{1 + 3\bar{\gamma}^2} d\gamma \quad (4.B.3)$$

The integral is then integrated in the local co-ordinate γ , using ten Gauss-Legendre quadrature points.